TiO_2 SEMICONDUCTOR PHOTODEGRADATION OF SUBSTITUTED RESORCINOLS: KINETIC AND MECHANISTIC STUDIES

By

AYŞE NEREN ÖKTE

BS.in Chem. Boğaziçi University, 1992

MS.in Chem., Boğaziçi University, 1994

Submitted to the Institute for Graduate Studies in
Science and Engineering in partial fulfillment of
The requirements for the degree of

Doctor

of

Philosophy

Boğaziçi University

1999

"Eğitim ve öğretimde uygulanacak yol, bilgiyi insan için fazla süs, bir zorbalık aracı yahut medeni bir zevkden ziyade maddi hayatta başarılı olmayı sağlayan pratik ve kullanılması mümkün bir cihaz haline getirmektir..."

Mustafa Kemal ATATÜRK

(1923)

To my family

ACKNOWLEDGEMENTS

I would like to mention my gratitude to my thesis supervisor Prof. Dr. Yüksel İnel for his invaluable guidence, patience, suggestions and long-term encouragement throughout this study. I want to thank him for all the energy and time he put into this work.

I am also indepted to my friend Marianne Sowa Reşat. It is an honour for me to work with her. Her endless support, valuable discussions and guiding comments overcome the difficulties on the preparation of this work. I can never thank her enough.

I thank to my jury members, Assoc. Prof. Dr. Zeynep Atay, Prof. Dr. Dilek Çalgan, Prof. Dr. İzzet Tor and Prof. Dr. Tereza Varnalı for their critics and discussions to the manuscript.

I also wish to thank Prof. Dr. Hadi Özbal and my friend Bilge Gedik, for their help in using atomic absorption spectrophotometer. I wish to mention the help of Dr. İnci İşli for measuring the BET surface areas of my samples. I also thank to Recep Koç for his technical assistance throughout the laboratory work of this study.

Hearty thanks go to our research students without them this work could have never been completed. My thanks also go to all my friends for their help during long periods of this work. Deepest thanks are for Hülya Metiner, Feyza Kolcu, Parisa Deljouie and Funda Oğuz for their endless encouragement. I also especially thank to my laboratory partners, Nurcan Şenyurt and Şaron Çatak for sharing with me my laboratory work despite their demanding work schedule and for their kindly support.

Finally, it is a great pleasure for me to express my appeciation to my father, my mother, and my brother Sezai for their endless love, patience and support throughout my life. It is also a welcome opportunity to thank to my brother Savaş, who sent almost all the references from Japan, and never leave me alone throughout my life and this study.

ABSTRACT

The photocatalytic degradation of 1,3-dihydroxybenzene (1,3-DHB) (resorcinol) and the substituted resorcinols, 3,5-dihydroxytoluene (3,5-DHT), 1,3-dihydroxy-5-methoxybenzene (1,3-DHMB) and 3,5-dihydroxybenzoic acid (3,5-DHBA) in the presence of aqueous suspensions of TiO_2 are investigated kinetically and mechanistically.

The effects of initial concentrations of the reactants, the pH of the medium, temperature, incident photon flux, and irradiation time are examined in detail. It is found that 1,3-DHB and 3,5-DHT obey pseudo-first order kinetics whereas 1,3-DHMB and 3,5-DHBA obey zero order kinetics. The Langmuir type of plot confirms that reactions take place on the surface of TiO_2. 1,3-DHB, 3,5-DHT, and 1,3-DHMB are found to be most efficient at pH 9.0 while 3,5-DHBA had highest efficiency at its natural pH 4.4. The activation energy is found as 11.2 kJ/mol, 17.4 kJ/mol, 17.1 kJ/mol, and 10.3 kJ/mol for 1,3- DHB, 3,5-DHT, 1,3-DHMB, and 3,5-DHBA, respectively. Based on the relative photonic efficiency concept, the quantum yield is found as 0.34, 0.22, 0.35, and 0.38 for 1,3- DHB, 3,5-DHT, 1,3-DHMB, and 3,5-DHBA, respectively.

Deposition of Fe^{3+}, Ni^{2+}, Zn^{2+}, Nb^{5+}, Ta^{5+}, Co^{2+}, Mn^{2+}, Al^{3+}, Cr^{3+} and V^{4+} on the surface of TiO_2 affects the photocatalytic degradation of reactant molecules. Differences in energy levels, electronic configurations, and reactions of charge trapping, charge release and migration as well as recombination and interfacial charge transfer are found to be effective in the photoactivities of the metals. Fe^{3+} showed the highest efficiency.

ÖZET

1,3- dihidroksibenzen (1,3-DHB) (resorsinol) ve takılandırılmış resorsinoller, 3,5-dihidroksitoluen (3,5-DHT), 1,3-dihidroksi-5-metoksibenzen (1,3-DHMB) ve 3,5-dihidroksibenzoik asit (3,5-DHBA)'in TiO_2 içeren sulu çözeltilerdeki fotokatalitik degradasyonu, kinetik ve mekanistik olarak inceledi.

Reaktanların başlangıç konsantrasyonları, ortamın pH'sı, sıcaklık, foton akısı ve ışıklandırılma süresinin etkileri detaylı olarak belirlendi. 1,3-DHMB ve 3,5-DHBA sıfırıncı dereceden kinetiğe uyarken, 1,3-DHB ve 3,5-DHT'in ise yalancı birinci dereceden kinetiğe uyum sağladığı bulundu. Langmuir türünden elde edilen grafik reaksiyonların TiO_2 yüzeyinde oluştuğunu onayladı. 3,5-DHBA en yüksek verimliliği doğal pH değerinde (pH=4.4) verirken 1,3-DHB, 3,5-DHT ve 1,3-DHMB en yüksek verimliliği pH 9.0'da verdiler. 1,3-DHB, 3,5-DHT, 1,3-DHMB ve 3,5-DHBA için aktivasyon enerjileri sırasıyla 11.2 kJ/mol, 17.4 kJ/mol, 17.1 kJ/mol ve 10.3 kJ/mol olarak bulundu. Bağıl nicem verimliliği fikrine göre 1,3-DHB, 3,5-DHT, 1,3-DHMB ve 3,5-DHBA nicem verimlilikleri sırasıyla 0.34, 0.22, 0.35 ve 0.38 olarak saptandı.

TiO_2 yüzeyinin Fe^{3+}, Ni^{2+}, Zn^{2+}, Nb^{5+}, Ta^{5+}, Co^{2+}, Mn^{2+}, Al^{3+}, Cr^{3+} ve V^{4+} iyonları ile katkılandırılmasının reaktan moleküllerinin fotokatalitik degradasyonunu etkilediği belirlendi. Metallerin fotoaktivitelerinde enerji düzeylerindeki farklılıkların, elektronik konfigürasyonlarının, yük tutma ve yük bırakma reaksiyonlarının, yük göçmesi ile yük birleşmesinin ve yüzey alanındaki yük aktarımının etken olduğu saptandı. Fe^{3+} iyonu en yüksek verimliliği gösterdi.

TABLE OF CONTENTS

LIST OF FIGURES

LIST OF TABLES

LIST OF SYMBOLS

A	Electron acceptor
AOP	Advanced oxidation processes
BET	Brauner-Emette-Teller
D	Electron donor
e^-	Electron
e_g	Degenerate dz^2 and dx^2-y^2 orabitals
E	Static dielectric constant of semiconductor
E_{bg}	Band gap energy
E_0	Static dielectric constant of vacuum
f	Fraction of light absorption
GC	Gas chromatography
h^+	Hole
HPLC	High performance liquid chromatography
I_a	Photon flux by homogeneous solution
I_0	Incident photon flux
k'	Appearent reaction rate constant
K	Adsorption constant
n_0	Refractive index of homogeneous solution
n_1	Refractive index of catalyst
N_d	Number of deposited metal atoms
M^{n+}	Metal ion
pzc	Zero point charge
P	Pairing energy
R	Reaction rate
R_i	Initial reaction rate
S	Substrate
t_{2g}	Degenerate dxy, dyz, and dzx orbitals
V^0	Standard electrode potential

V_s	Surface potential
W	Thickness of space charge layer
Δ_0	Energy difference between e_g and t_{2g}
ζ	Photonic efficiency
ζ_r	Relative photonic efficiency
ϕ	Quantum yield

1. INTRODUCTION

Advanced oxidation processes (AOP) have recently been studied. AOP's generate hydroxyl radicals, one of the most powerful oxidants known which are used to degrade unwanted organic contaminants. Most AOP's use various combinations of hydrogen peroxide, ozone, and ultraviolet light to generate hydroxyl radicals, and are thus quite energy intensive. One emerging technology utilizes illuminated semiconductors and is commonly referred to as photocatalysis. Photocatalysis has been extensively studied over the past two decades. Recent reviews are provided by Ollis and Al-Ekabi [1], Fox and Dulay [2], Legrini *et. al.* [3], Hoffmann *et. al.* [4], and Mills and Hunte [5].

The literature reports a variety of photocatalytic reactions involving, TiO_2, ZnO, Fe_2O_3, WO_3, CdS as commonly used photocatalysts for a variety of organic contaminants. These materials have the advantage of an absorption spectrum reaching through the UV and extending the near the visible spectral domain. Thus, one of the distinct advantages of photocatalysis over other AOP's is photocatalysts's ability to utilize solar energy and then to drive the production of hydroxyl radicals. Once hydroxyl radicals are formed, they readily attack organic molecules eventually degrading them to CO_2 and H_2O. When factors concerning photostability, toxicity, cost, availability, and redox efficiencies are all considered TiO_2 has turned out to be the photocatalyst of choice.

TiO_2 is active for light reduced redox processes due to its electronic structure, which is characterized by a filled valence band and an empty conduction band. When a photon with an energy of hv exceeds the bandgap energy, E_{bg}, of TiO_2 (3.2 eV), an electron is promoted from the valence band into the conduction band, leaving a hole behind. Excited state conduction band electrons and valence band holes can recombine and dissipate the input energy as heat, get trapped in surface states, or react with electron

donors and electron acceptors adsorbed on TiO_2 surface or within the surrounding layer of the charged particles.

Photocatalytic efficiency is controlled by the effectiveness of suppression of electron-hole recombination. This is also affected by reaction conditions, such as pH of the medium, concentration of the substrate molecule, temperature of the photocatalytic system, incident photon absorption, sorption of electron donors and acceptors, presence of electron or hole scavengers, and deposition of metals on the catalyst surface.

The deposition of metals on the TiO_2 surface significantly influences photoreactivity, charge carrier recombination rates, and interfacial electron-transfer rates. The photoreactivity in metal deposited TiO_2 suspensions appears to be a complex function of the metal concentration, the energy level of metal ions within the TiO_2 lattice, and their d electronic configuration (for transition metals), the distibution of metals, and the light intensity.

In this study, we present the photocatalytic degradation of 1,3-dihydroxybenzene (resorcinol), and the substituted resorcinols, 3,5-dihydroxytoluene, 1,3-dihydroxy-5-methoxybenzene and 3,5-dihydroxybenzoic acid in the presence of aqueous suspensions of metal deposited and undeposited TiO_2. Chapter 2 gives a brief summary of advanced oxidation technologies. Chapter 3 summarizes the theoretical background of heterogeneous photocatalysis and TiO_2. Factors which can affect the photocatalysis preceeds a review of phenol degradation in the presence of TiO_2 in chapter 3. Experimental set-ups, reagents used in the experiments, procedures, and instruments used in the analysis are given in Chapter 4. Chapters 5, 6, 7, and 8 present detailed investigation of the probe molecules in the presence of undeposited TiO_2. Photoinduced degradation of these molecules are followed by monitoring the decrease in their concentrations and resulting the increase in the amount of CO_2 evolved. The effect of metal deposition on the catalyst surface for the degradation of each substrate is discussed

in Chapter 9. A review of transition metals and the photocatalytic properties of metal deposited TiO_2 precedes the experimental results concerning degradation of organics in the presence and in the absence of a hole scavenger, methanol. More extensive studies of the effects of a metal on the photocatalyst using Fe^{3+} are given at the end of the chapter. Chapter 10 presents a discussion on the effectiveness of the photocatalyst on the degradation of the various compounds and the effects of parameters; pH, concentration of the reactants, irradiation time, temperature, and the incident photon flux in the degradation process. Chapter 11 gives a brief conclusion of the experimental results.

2. ADVANCED OXIDATION PROCESSES

In water and wastewater treatment, oxidation is used for the chemical conversion of a contaminant to more oxygenated forms by means of reactions with oxidizing agents, such as oxygen (O_2), ozone (O_3), or hydrogen peroxide (H_2O_2). However, the reaction times for complete oxidation are so long that their application for wastewater treatment is impractical. For this reason there is a need to develop effective methods for the degradation of organic pollutants, either to less harmful compounds or to their completely mineralized products, CO_2 and H_2O. Recent developments in applying catalytic and photochemical methods for chemical water treatment have led to improvements in oxidative degradation procedures for organic compounds dissolved or dispersed in aquatic media. They are generally referred to as advanced oxidation processes (AOP) [3].

The most effective way of oxidizing organics is to use chemical reactants with high oxidation potentials. As shown in Table 2.1, the most powerful oxidizing species available after fluorine is the hydroxyl radical. For this reason, most advanced oxidation processes for waste treatment are based on the generation of hydroxyl radicals as the reaction initiators.

TABLE 2.1. Oxidation potentials of some oxidants [3].

Oxidant	Oxidative Potential (V)
Fluorine	3.03
Hydroxyl Radical	2.80
Ozone	2.07
Hydrogen Peroxide	1.78
Perhydroxyl Radical	1.70
Permanganate ion	1.68
Chlorine dioxide	1.50
Chlorine	1.36

The hydroxyl radical is a short-lived, extremely potent oxidizing agent, capable of oxidizing organic compounds mostly by hydrogen atom abstraction (equation 2.1). This reaction generates organic radicals which, by addition of molecular oxygen, yield peroxyl radicals (equation 2.2). These intermediates initiate chain reactions of oxidative degradation, leading finally to carbon dioxide, water and inorganic salts. Besides hydrogen abstraction, electron transfer to hydroxyl radicals (equation 2.3) constitutes another mechanism of oxidative degradation.

$$^{\bullet}OH + RH \rightarrow R^{\bullet} + H_2O \qquad (2.1)$$

$$R^{\bullet} + O_2 \rightarrow RO^{\bullet}_2 \qquad (2.2)$$

$$^{\bullet}OH + RX \rightarrow RX^{\bullet +} + HO^{-} \qquad (2.3)$$

For both these pathways, the hydroxyl radical functions as the initiator. These hydroxyl radicals can be generated by both photochemical and non-photochemical methods. In non-photochemical oxidation, ozone at high pH (equation 2.4), ozone and hydrogen peroxide (equation 2.5), and Fenton's reaction (equation 2.6) all generate hydroxyl radicals in the absence of UV light.

$$2O_3 + H_2O \rightarrow {}^{\bullet}OH + 2O_2 + HO_2 \qquad (2.4)$$

$$O_3 + H_2O_2 \rightarrow {}^{\bullet}OH + O_2 + HO_2 \qquad (2.5)$$

$$Fe^{+2} + H_2O_2 \rightarrow Fe^{+3} + {}^{\bullet}OH + HO^{-} \qquad (2.6)$$
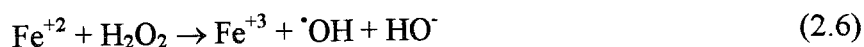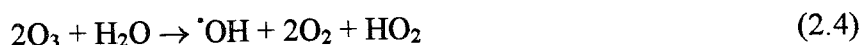
2.1. UV Photolysis

Photooxidation reactions occur following electronic excitation of organic contaminants. Upon photon absorption by the organic molecule (R-X), an electronically excited organic molecule (R-X)* is formed (equation 2.7). The electronically excited molecule can produce radical species either directly (equation 2.8) or by an electron transfer to molecular O_2 (equation 2.9). Radical species then react with oxygen (equation 2.10).

$$(\text{R-X}) + h\nu \longrightarrow (\text{R-X})^* \tag{2.7}$$

$$(\text{R-X})^* + h\nu \longrightarrow \text{R}^\bullet + \text{X}^\bullet \tag{2.8}$$

$$(\text{R-X})^* + O_2 \longrightarrow (\text{R-X})^{\bullet+} + O_2^{\bullet-} \tag{2.8}$$

$$\text{R}^\bullet + O_2 \longrightarrow \text{RO}_2 \tag{2.10}$$
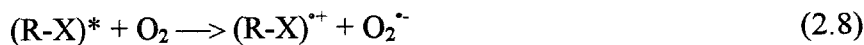
The rate of such a photooxidation depends on the absorption cross section of the medium, the quantum yield of the process, the photon rate at the wavelength of excitation, and the concentration of dissolved molecular oxygen. This process is usually practical only for treatment of a single compound in water [3].

2.2. H₂O₂/UV Photolysis

The simplest process available for the generation of hydroxyl radical is the photochemical cleavage of H_2O_2 (equation 2.11).

$$H_2O_2 + h\nu \rightarrow 2 \; {}^\bullet OH \qquad (2.11)$$

Reactions of hydroxyl radicals in the presence of an organic substrate may be differentiated by their mechanisms into four different classes; hydrogen abstraction, radical-radical reactions, electrophilic addition, and electron-transfer reactions.

Hydrogen Abstraction: The sequence of reactions occuring during the H_2O_2/UV process is shown in Figure 2.2.1. Hydroxyl radicals generated by hydrogen peroxide photolysis (a) react with organic compounds (HRH) primarily by hydrogen abstraction to produce an organic radical (RH$^\bullet$) (b). This radical reacts quickly with dissolved oxygen to yield an organic peroxyl radical (RHO$_2$$^\bullet$) (c), initiating subsequent thermal oxidation reactions. Then, there are three reaction paths that can be followed by either peroxyl radicals or their tetraoxide dimers: (1) Heterolysis and generation of organic cations as well as superoxide anion (d), (2) 1,3-hydrogen shift and homolysis into hydroxyl radicals and carbonyl compounds (e), and (3) back reaction to RH$^\bullet$ and O_2 (f). Hydrogen abstraction by RHO$_2$$^\bullet$ (g) and reaction of superoxide anion with H_2O to yield H_2O_2 (i) are the other paths for the reaction system in the H_2O_2/UV process. If insufficient oxygen is present in the system, formation of higher molecular weight products is possible in the reaction system (h).
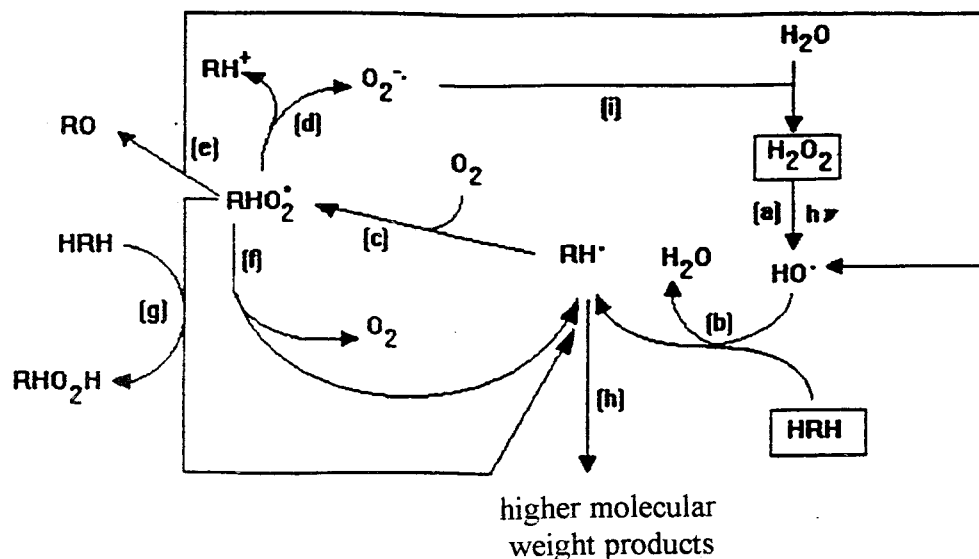
Figure 2.2.1. Reaction system for the H_2O_2/UV process [3].

Radical-Radical Reactions: Hydroxyl radicals will readily dimerize to H_2O_2 when generated at high concentrations (equation 2.12).   If an excess of H_2O_2 is used, $^{\bullet}OH$ radicals will produce hydroperoxyl radicals (equation 2.13) which are much less reactive and do not appear to contribute to the oxidative degradation of organic substrates.

$$^{\bullet}OH + {^{\bullet}OH} \rightarrow H_2O_2 \tag{2.12}$$

$$H_2O_2 + {^{\bullet}OH} \rightarrow H_2O + HO_2^{\bullet} \tag{2.13}$$

Electrophilic Addition: Electrophilic addition of $^{\bullet}OH$ radicals to organic π-systems results in the formation of organic radicals (equation 2.14).

$$\cdot OH + RX \rightarrow HORX^{\cdot} \qquad (2.14)$$

Electron-Transfer Reactions: When hydrogen abstraction or electrophilic addition reactions are disfavored due to multiple halogen substitution or steric hindrance, electron transfer reactions which result in the of reduction of hydroxyl radicals to hydroxide anions by an organic substrate (equation 2.15) become important.

$$\cdot OH + RX \rightarrow HO^- + RX^{\cdot +} \qquad (2.15)$$

2.2.1. Advantages and Disadvantages of H_2O_2/UV Process

The use of hydrogen peroxide as an oxidant has several advantages in comparison to other methods of chemical or photochemical water treatment. These advantages include commercial availability of the oxidant, on-site storage, and infinite solubility in water. There are, however, also disadvantages encountered with the H_2O_2/UV process such as; the small adsorption cross section of H_2O_2 at 254 nm and the trapping of $\cdot OH$ radicals by HCO_3^- and CO_3^{2-} ions which may be present in solution (equation 2.16 and 2.17). Although, the generated carbonate radical anion has been shown to be an oxidant itself, its oxidation potential is less positive than that of the $\cdot OH$ radical, therefore decreasing the efficiency of the organic decomposition.

$$\cdot OH + HCO_3^- \rightarrow H_2O + CO_3^{\cdot -} \qquad (2.16)$$
$$\cdot OH + CO_3^{2-} \rightarrow HO^- + CO_3^{\cdot -} \qquad (2.17)$$

2.2.2. Degradation of Phenolic Compounds by H_2O_2/UV Radiation

Various groups have examined the effectiveness of H_2O_2//UV radiation in degrading phenolic compounds. Castrantas *et. al.*. [6] studied the oxidation of phenol, 2-chlorophenol, 2,5-dimethylphenol and 2,5-dichlorophenol by using a low pressure Hg lamp. The effects of pH, UV power, initial concentration of the compound and H_2O_2 were investigated. Phenol was oxidized to 94 per cent of its original concentration in 16 minutes at a pH of 4. 2-chlorophenol, 2,5-dimethylphenol and 2,5-dichlorophenol were oxidized to 99 per cent of their original concentrations in 40, 30 and 30 minutes respectively at a pH of 8.

Lipczynska-Kochany and Bolton [7] investigated the oxidation of 4-chlorophenol in the presence of 0.07 M H_2O_2 in a quartz cell reactor by using Xe flash lamps. They found that 4-chlorophenol was oxidized to 80 per cent of its original concentration at a pH of 4.7.

In Legrini's review [3], 2×10^{-4} M phenol was irradiated with a 5.3 W low pressure Hg lamp with added H_2O_2 1.4×10^{-3} M in a 3.3 L recirculating flow reactor at a pH of 6.8. About 98 per cent oxidation was achieved in 50 minutes.

It can be seen that differing experimental conditions give widely varying times for completion of phenol mineralization, but it is evident from these studies that this system presents an acceptable as a route for degradation.

2.3. Ozone/UV Process

There are two steps involving the light induced homolysis of O_3 and the subsequent production of ${}^{\bullet}OH$ radicals by the reaction of atomic oxygen with water (equation 2.18 and 2.19). The overall photolysis of ozone in solution leads to the production of hydrogen peroxide in a sequence of reactions (equation 2.20) [8].

$$O_3 + h\nu \rightarrow O_2 + O \tag{2.18}$$

$$O + H_2O \rightarrow {}^{\bullet}OH + {}^{\bullet}OH \tag{2.19}$$

$$O_3 + H_2O + h\nu \rightarrow H_2O_2 + O_2 \tag{2.20}$$

Figure 2.3.1 is a summary of the chemistry involved in the generation of ${}^{\bullet}OH$ radicals by O_3/UV process.
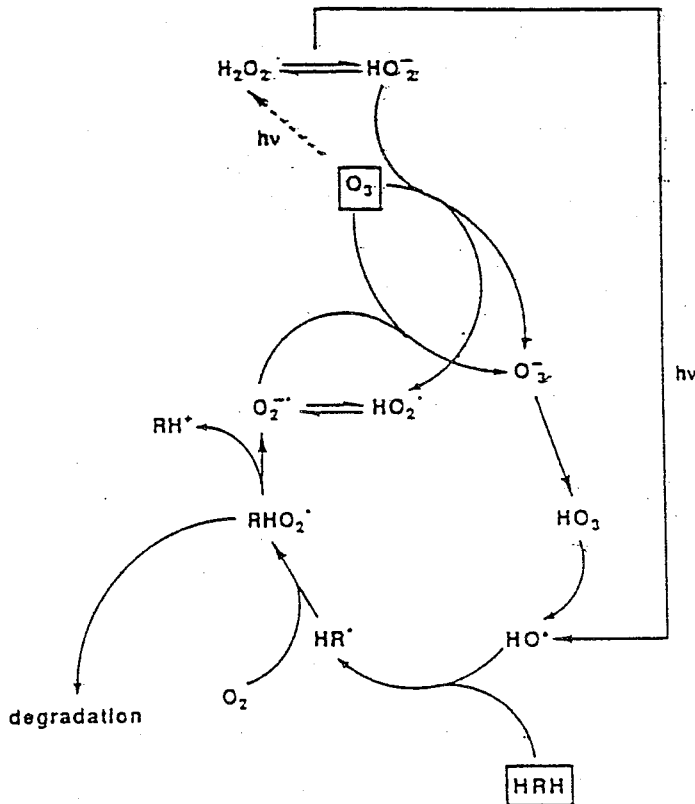
Figure 2.3.1. Reaction pathways in the ozone/UV and ozone/peroxide systems [3].

Initiation can occur by the reaction of ozone with HO^- or HO_2^-, or by photolysis of hydrogen peroxide. The latter is formed by ozone photolysis as well as from the reaction of ozone with many unsaturated organic compounds. $^{\cdot}OH$ radicals react with organic substrates to produce organic radicals, which efficiently add molecular oxygen to yield organic peroxyl radicals. These peroxyl radicals are the propagators of chain reactions of oxidative substrate degradation.

2.3.1. Advantages and Disadvantages of O_3/UV Process

Ozonation is a well known procedure in water technology and therefore, ozonizers are in most cases readily available. From the photochemist's point of view, the absorption spectrum of ozone provides a much higher absorption cross section at 254 nm than H_2O_2. However, there remains questions related to the mechanisms of free radical production and subsequent oxidation of organic substrates. In fact, there are mechanistic problems of dissolving and photolyzing ozone with high efficiency. In heterogeneous media, determination of the quantum efficiencies of reactivity of ozone toward most unsaturated organic compounds is related to the problem of quantifying rates of absorbed photons and still remains to be worked out.

2.3.2. Degradation of Phenolic Compounds by O_3/UV Radiation

Gurol et. al.. [9] studied the oxidative degradation of mixtures of phenolic compounds by the O_3/UV procedure using a 16 W low pressure Hg lamp. They reported that complete substrate removal (>99.5 per cent) for mixtures of phenol, p-cresol, 3,4-xylenol, and catechol (50 mg/l) occurred within 140 minutes. Authors also reported the effect of pH on the rates of oxidation of the organic compounds investigated. The improvement in the removal rates of phenols at higher pH was due to the higher ozone

absorption efficiency caused by the fast decomposition of ozone accelerated by phenolate ions.

Takahashi [10] studied the degradation of several groups of organic compounds, including phenols. Degradation of phenol was shown to be enhanced by the simultaneous use of ozone and UV light, however, a decrease in the rate was observed as the concentration of phenol increased. This result was interpreted as a consequence of competitive light absorption. Takahashi also found that the O_3/UV method was more efficient in phenol degradation than either the O_3 or UV methods alone.

When H_2O_2/UV and O_3/UV processes are compared to each other, it is observed that O_3/UV system is only effective for degrading phenolic species in alkaline media and requires relatively long irradiation times. In the H_2O_2/UV system, higher degradation percentages can be achieved both in the acidic and alkaline media. Also, complete mineralization requires shorter irradiation times for in the H_2O_2/UV system. Thus, we can conclude that H_2O_2/UV is a better process compared to the O_3/UV for the degradation of phenol.

3. HETEROGENEOUS PHOTOCATALYSIS

Heterogeneous photocatalysis occurs over irradiated semiconductors. These photocatalysis generate charge carriers (e⁻ and h⁺) that are ultimately positioned at the surface and can undergo a variety of events (recombination, trapping) in competition with other processes (redox chemistry). These charge carriers have been implicated in photocatalytic reductions of metals (Au, Pt, Ag, Hg, Pd........) and in various photocatalytic oxidations of halogenated and non-halogenated aromatics/aliphatics, surfactants, pesticides and herbicides. In the case of organics, total mineralization to CO_2 was demonstrated [11].
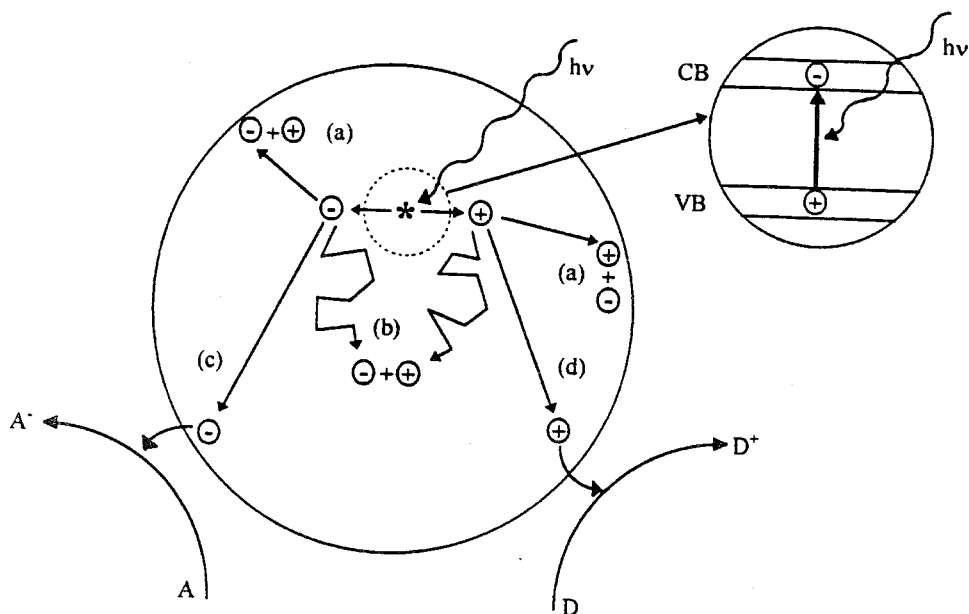
Figure 3.1. Major processes occuring on a semiconductor particle following electronic excitation. Electron-hole recombination can occur at the surface (reaction (a)) or in the bulk (reaction (b)) of the semiconductor. At the surface of the particle, photogenerated electrons can reduce an electron acceptor A (reaction (c)) and photogenerated holes can oxidize an electron donor D (reaction (d)) [5].

Electron and hole pairs can be generated in a semiconductor by the absorption of light of energy greater or equal to band-gap energy (E_{bg}) of the semiconductor (Figure 3.1). In an n-type semiconductor immersed in solution, an electric field forms spontaneously at the semiconductor-electrolyte interface; e^--h^+ pairs generated in the region of the electric field, i.e. the space charge region, are seperated efficiently, rather than undergoing recombination. As a consequence, in an n-type semiconductor, the photogenerated electron moves into the bulk of the semiconductor, where it can be transferred either to non-photoactive electrode (such as Pt) or through a surface site to a point where an electron acceptor, A, can be reduced, i.e. $A + e^- \rightarrow A^-$. In the mean time, the photogenerated hole, under the influence of the electric field, migrates towards the surface of the semiconductor to a surface site where it can oxidize a suitable electron donor, D, i.e. $D + h^+ \rightarrow D^+$. The energetics associated with a typical photoelectrochemical cell are illustrated in Figure 3.2 [5].
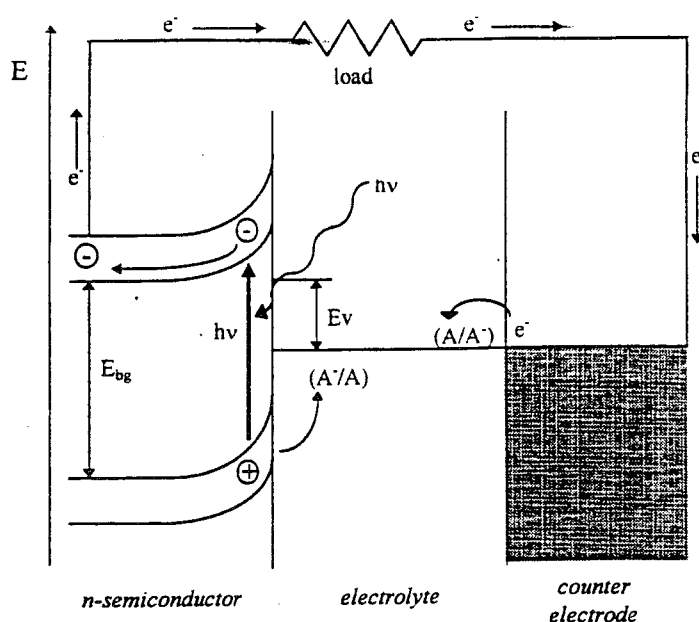
Figure 3.2. Energetics of a general photoelectrochemical cell for an n-type semiconductor [5].

The efficiency of photoelectrochemical cells can be improved by diffusing or co-adsorbing metal ions. It has been suggesting that the presence of metal ions makes the surface recombination states less deep and therefore less likely to mediate the efficiency lowering process of e^--h^+ recombination.

The semiconductor must be photoactive, able to utilize UV light, biologically and chemically inert, photostable and inexpensive [11]. The semiconductor TiO_2 satisfies all these criteria and is one of the best n-type semiconductors. It occurs naturally in three crystalline modifications, rutile, anatase and brookite. The most important ones are rutile and anatase. Brookite is the rarest and least important modification. Anatase and rutile differ in their bandgap energy, surface area, surface hydroxylation, surface charge caused by an excess of cations or anions on the surface, and the presence of dopants and impurities. On heating above 600 K, anatase transformation to rutile occurs.

3.1. Titanium Dioxide

Hoffmann *et. al.* proposed a general mechanism for heterogeneous photocatalysis on TiO_2 (Figure 3.1.1, Table 3.1.1) [4].

In the table TiOH represents the primary hydrated surface functionality of TiO_2, e^- is the conduction band electron, h^+ is a valence band hole, Red is an electron donor (i.e. reductant), Ox is an electron acceptor (i.e. oxidant), $Ti^{IV}OH^{\cdot+}$ is the surface trapped valence band hole (i.e. surface bound hydroxyl radical), and $Ti^{III}OH$ is the surface trapped conduction band electron. It is reported that there is always competition between charge carrier recombination and trapping which follows the competition between trapped carrier recombination and interfacial charge transfer.
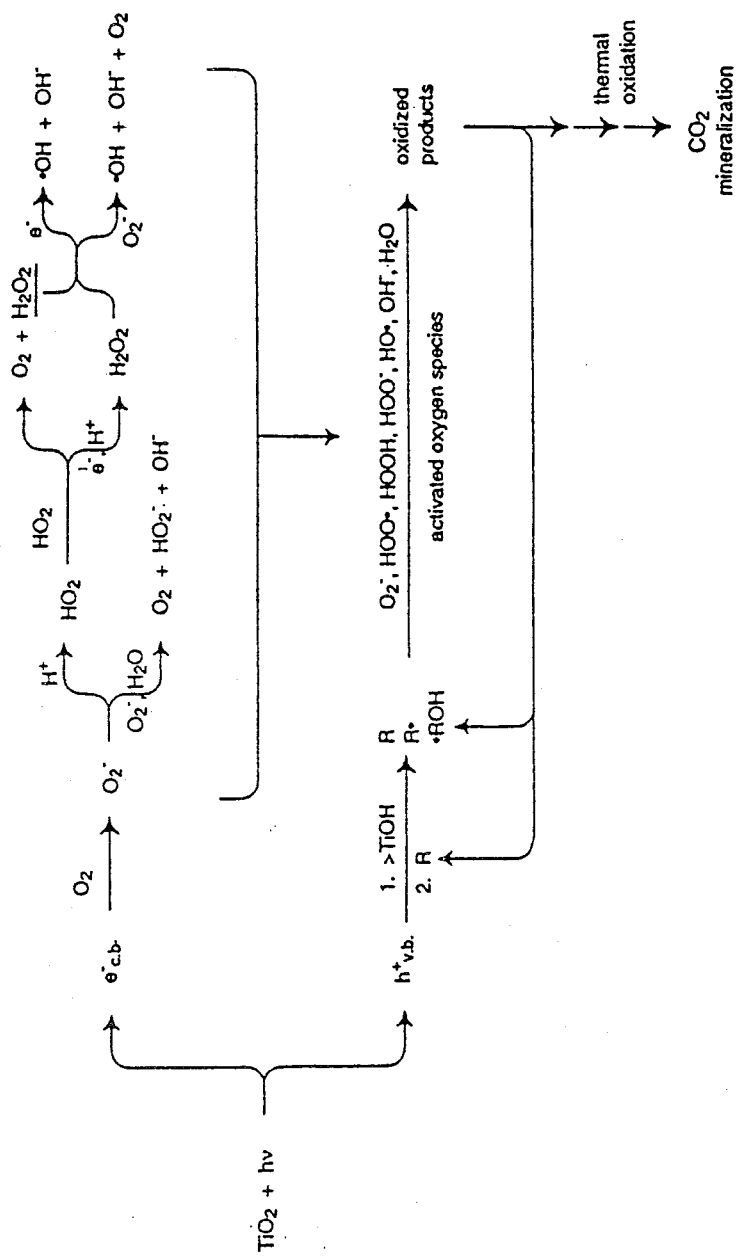
Figure 3.1.1. Reactions with activated oxygen species in the photoelectrochemical mechanism [4].

3.2. Surface Chemistry of TiO_2

Most metal oxides are hydroxylated under normal conditions, i.e. at room temperature and when water or its vapor has had access to the surface [12]. The reason for this hydroxylation is that the surface of an ionic crystal is more stable when it preserves its electroneutrality (Figure 3.2.1). The TiO_2 surface is covered with surface hydroxyls of an amphoteric character. Chemisorption of water molecules on the Ti^{4+} ions is expected since vacant coordination sites would be filled. However, proton transfer to neighbouring oxide ions should result in better charge neutralization. Two types of hydroxyl groups can be identified; terminal, in which the OH is bonded to a single Ti atom, and bridging, in which the OH is shared by two Ti atoms. The doubly coordinated OH groups should be strongly polarized by the cations, thus loosening the bond to hydrogen and resulting in acidic character. The acidic character should be much weaker with the singly coordinated OH groups, and one would expect a tendency for dissociation as hydroxide ions. These groups should be predominantly basic in character and might be exchangeable for other anions.

(a) (b)
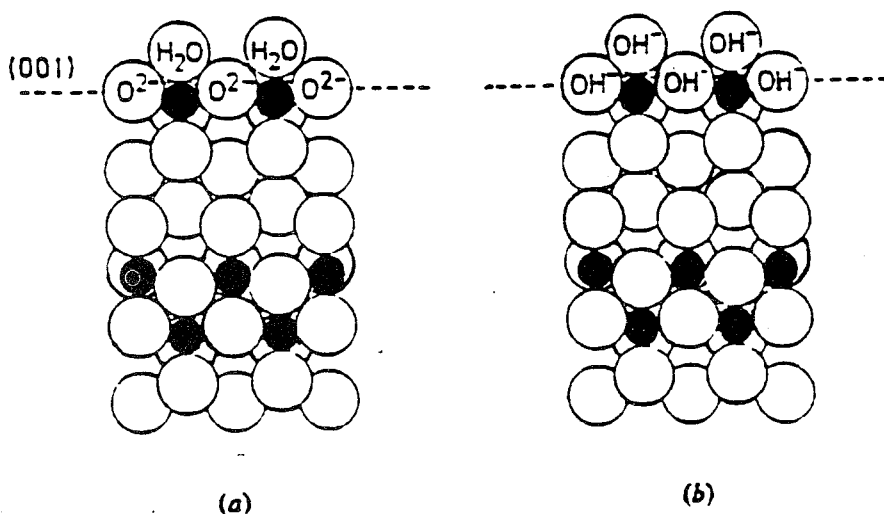
Figure 3.2.1. Formation of surface hydroxyls on the TiO_2 surface. (a) Surface adsorption of water. (b) Form of terminal and bridging hydroxyl groups maintain surface electroneutrality [12].

3.3. Metal Deposition on TiO$_2$ Surface

TiO$_2$ may provide both the oxidizing and reducing sites for the reaction, where the reduction is the "dark site" reaction (Figure 3.3.1). Since the dark site reactions may not occur with a high efficiency on a metallic or electrocatalytic site, higher efficiencies can be obtained by deposition of a metal on TiO$_2$ surface. It is reported that depositing a film of Pt onto the surface of TiO$_2$ greatly influences the number of surface states which promote electron transfer reactions at the interface (Figure 3.3.2) [13]. The concentration of reduced species Ti(III) was detected as a function of Pt loading of the catalyst. Figure 3.1.2.2 is a schematic diagram of the role of Pt loading on the TiO$_2$ surface in a photoredox reaction [13]. The role of metal deposited on the surface is to trap the photo injected electron and to intercept the rapid back reaction between electron and hole pairs.
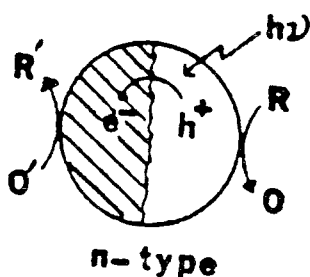
Figure 3.3.1. Schematic representation of a photocatalytic reaction [13].
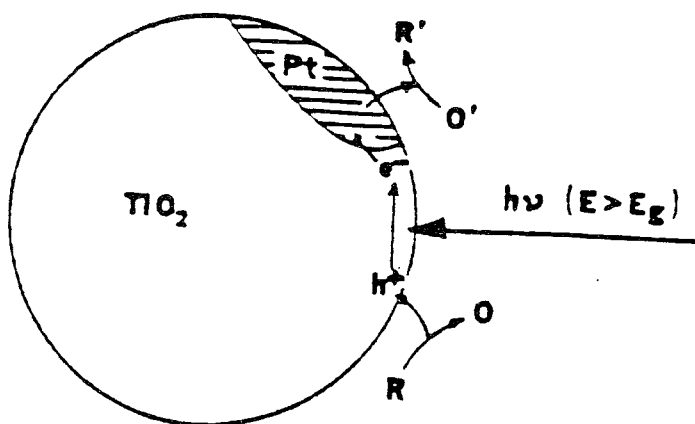
Figure 3.3.2. Representation of a photocatalytic reaction on a platinized TiO$_2$ [13].

Moser *et. al.* [14] in the Fe(III)-TiO$_2$ system observed both positive and negative mobile charge carriers are rapidly immobilized on trapping sites (Figure 3.3.3). The two trapping sites are locally seperated. The electrons are localized at the surface whereas the trapped hole states, i.e. the Fe(IV) centers, are randomly distributed over the whole volume of the TiO$_2$ particles.
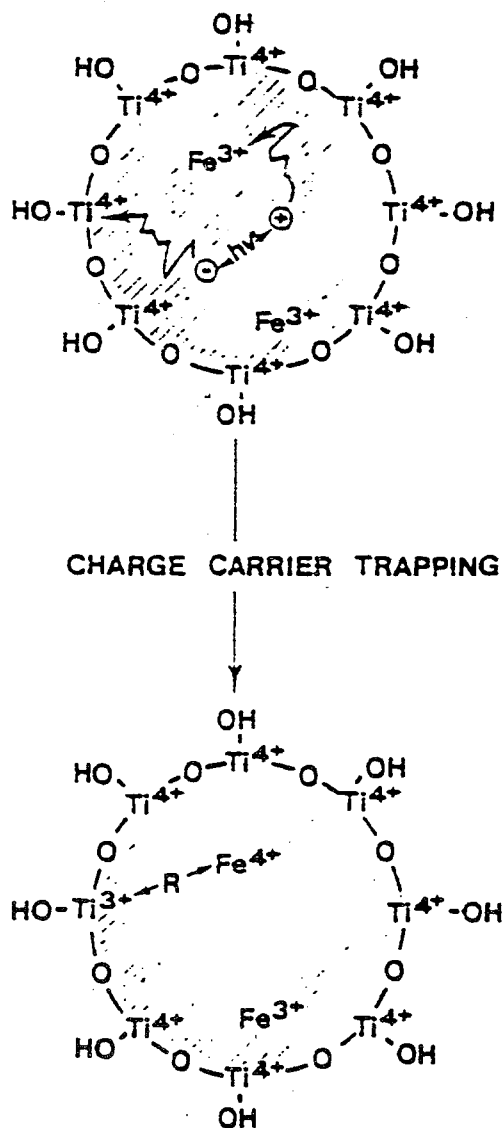
Figure 3.3.3. Schematic illustration of the mechanism proposed for light induced charge seperation in Fe(III) deposited TiO$_2$ [14].

3.4. Factors Affecting Photocatalytic Activity

Langmuir-Hinshelwood Kinetics: In general, the kinetics of photomineralization of organic substrates by oxygen, sensitized by TiO_2, fit a Langmuir-Hinshelwood kinetic scheme, i.e.

$$R_i = -\frac{[dS]_i}{dt} = \frac{k(S)K(S)[S]_i}{1+K(S)[S]_i} \qquad (3.1)$$

where R_i is the initial rate of substrate removal, $[S]_i$ is the initial concentration of the organic substrate, $K(S)$ is the Langmuir adsorption constant and equal to the ratio between k_a and k_d for the equilibrium reaction (S + TiO_2 (surface) $\leftrightarrow$ S-TiO_2) where k_a is the reaction rate constant for adsorption and k_d is for desorption. $k(S)$ is the reaction rate constant which provides a measure of reactivity of the photoactivated surface with S. The linearity of a plot of $1/R_i$ versus $1/[S]_i$, where $1/k(S)$ indicates the validity of the model for the system. It is also found that $k(S)$ is proportional to the fraction of O_2 adsorbed on TiO_2, i.e. $f(O_2)$

$$f(O_2) = \frac{K_{O2}[O_2]}{1+K_{O2}[O_2]} \qquad (3.2)$$

Assumptions of the model are [2]: At equilibrium, the number of surface active sites is fixed, only one substrate may bind at each surface site, there is no interaction between adjacent adsorbed molecules, the rate of surface adsorption of the substrate is greater

than the rate of any subsequent chemical reaction, and no irreversible blocking of active sites by binding to product occurs.

Effect of pH: The pH of an aqueous solution significantly affects all oxide semiconductors, including the surface charge on the semiconductor particles, the size of the aggregates formed and the energies of the conductance and valence bands. Higher reaction rates for various TiO_2 sensitized photomineralizations have been reported at both low and high pH [4].

TiO_2 possesses both acidic and basic properties. Hydroxyl groups on the TiO_2 surface are known to undergo the following acid-base equilibria:

$$TiOH^{2+} \leftrightarrow TiOH + H^+ \qquad pK_{a1} \qquad (3.3)$$

$$TiOH \leftrightarrow TiO^- \qquad pK_{a2} \qquad (3.4)$$

The pH of the zero point charge (pH_{zpc}) is;

$$pH_{zpc} = \frac{1}{2}(pK_{a1} + pK_{a2}) \qquad (3.5)$$

The reported point of zero charge for TiO_2 Degussa P25 is ~ 5.0. The surface is positively charged at pH's below the pH_{zpc} and favors adsorption of negatively charged species. On the other hand, the surface is negatively charged at pH's above the pH_{zpc} and favors adsorption of positively charged species.

Effect of Temperature: The overall process of semiconductor photocatalysis is not usually found to be particularly temperature sensitive. Reported activation energies usually lie in the range 5-16 kJ/mol. Increasing the temperature may increase the rate of oxidation of the organic substrate at the interface. However, it will also have the effect of lowering the adsorption isotherms associated with the substrate and O_2, and lowering the concentration of O_2. Most photocatalyst experiments are carried out under conditions in which the fraction of O_2, $f(O_2)$, is around one (i.e. $P_{O2}=1$ atm) and initial substrate concentration is low. Under these conditions, the effect of an increase in temperature on the kinetics of the oxidation process will be dominated by the effect on the rate of oxidation of the organic substrate at the interface [5].

Quantum Yield: Quantum yield (ϕ) expresses the number of molecules, N_{mol}, undergoing a reaction relative to the number of quanta, N_{photon}, absorbed by the photocatalyst (equation. 3.6).

$$\phi = \frac{N_{mol}(mol/s)}{N_{photon}(einstein/s)} = \frac{rate \quad of \quad reaction}{rate \quad of \quad absorption \quad of \quad photons} \qquad (3.6)$$

In heterogeneous semiconductor photocatalysis, the measurement of quantum yield is very difficult. The reason is that the rate of absorption of photons is very difficult to assess, since semiconductor particles will absorb, scatter, and transmit light. TiO_2 particulates are not capable of absorbing all the incident photon flux from a given source due to the light scattering off the particle surface. The intensity of light scattered by the suspension depends on the refractive indices of the scattering molecule/particle (n_1) and the surrounding medium (n_0) (Figure 3.4.1). For the materials making up a typical photocatalytic system in heterogeneous photocatalysis, n_0 is 1.33 for H_2O and n_1 is 1.5-1.7 for glass, 3.87 for rutile TiO_2, and ~2.5-3 for anatase TiO_2 all at 365 nm [15]. When $n_0 \approx n_1$, the extent of scattered light is negligible. When $n_1 > n_0$, light is expected to

be highly scattered, with losses of ~5-10 per cent of the light flux occurring. The percentage of photons absorbable appear to be in the range of ~50-65 per cent [15].

I_0 molecule/particle

detector

I_{SC} (light scattered)
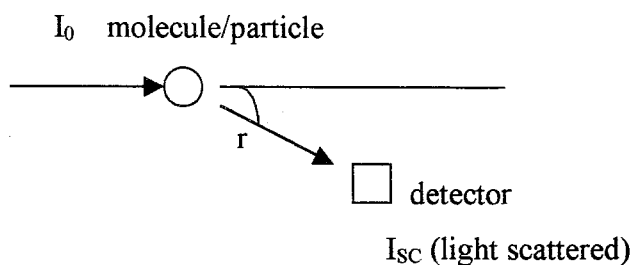
Figure 3.4.1. Light scattering by TiO_2 suspensions.

In defining (equation 3.6), properties of the catalyst surface are important since the course of reactions depends on the characteristics of the surface upon light activation. Also, light activated steps play major roles in defining the quantum yield. These steps include photon absorption, the formation of the hydroxyl radicals on the catalyst surface, and catalytic steps including adsorption/desorption events and reaction of the hydroxyl radicals with the adsorbed substrate [16]. However, all the surface sites occupied by OH⁻ groups are not catalytically active. Also, depending on the reactor geometry, particle aggregation, and stirring, not all of the BET catalyst surface is accessible to the substrate being oxidized.

A more useful term, photonic efficiency; ζ, has been proposed by Serpone and coworkers to compare process efficiencies and to avoid the confusion with quantum yields reported in the literature [17]. Photonic efficiency (ζ) describes the number of reactant molecules transformed or product molecules formed divided by the number of photons at a given wavelenght.

$$\zeta = \frac{N_{molecules} \, (mol/s) \quad produced}{N_{photons} \, (einstein/s) \quad incident \quad inside \quad reactor \quad cell} \qquad (3.7)$$

The relative photonic efficiency, ζ_r, is related to a standard photocatalyst and a standard secondary actinometer in photocatalyzed processes. Extensive studies have confirmed the usefulness of ζ_r [17]. The initial photodegradation of phenol was chosen as the standard process and Degussa P25 TiO_2 as the standard photocatalyst, and ζ_r is defined as:

$$\zeta_r = \frac{\text{rate of disappearance of substrate}}{\text{rate of disappearance of phenol}} \qquad (3.8)$$

where both initial rates are obtained under exactly the same conditions. Ultimately, ζ_r can be converted into the quantum yield, ϕ, once a quantum yield, $\phi_{standard}$, for a given photocatalyst and a given substrate has been determined (equation 3.9).

$$\phi = \zeta_r \phi_{standard} \qquad (3.9)$$

Sorption of Electron Donors and Acceptors: Sorption of electron donors and acceptors to the semiconductor surface is a critical step in photodegradation. The summation of chemical and electrostatic forces that bring substrates into contact with photoactive semiconductor surfaces include: inner sphere ligand substitution for metal ions and conventional organic and inorganic ligands, van der Waals forces, induced dipole-dipole interactions, dipole-dipole interactions, hydrogen bonding, outer sphere complexation, ion exchange, surface organic matter partitioning and sorbate hydrophobicity [4]. In general, all of these surface interactions yield sorption isotherms of a Langmurian nature.

Effect of Scavengers: The presence of O_2 is essential for the photomineralization of organic compounds. Adsorbed oxygen traps electrons, thereby delaying the electron-hole recombination. Like O_2, H_2O_2 can scavenge photogenerated electrons and be reduced either to water or to another hydroxyl radical. Thus, electron-hole recombination decreases, which in turn increases the rate of organic degradation. Oxidation of H_2O_2 by a hydroxyl radical or a photogenerated hole is also possible. This results in a decrease in the rate of organic degradation, by the competition between H_2O_2 and organics, for either hydroxyl radicals or photogenerated holes. Likewise, alcohols being efficient hole scavengers decrease the rate of degradation process [18].

Effect of Ionic Species: The adsorption of various anions and cations on the surface can influence the photocatalytic activity. It is found that perchlorate and nitrate anions have little effect on the degradation reactions whereas sulphate, chloride and phosphate ions can reduce the rate by 20 per cent-70 per cent due to competitive adsorption at the photoactivated reaction sites [19].

Reaction Stoichiometry: In general, the rates of change of a chemical substrate undergoing photocatalytic oxidation can be treated empirically without consideration of detailed mechanistic steps. For a hypothetical reaction (equation 3.10), equation 3.11 can be written as a standard kinetic relationship.

$$C_xH_yO_z + pO_2 \rightarrow x\ CO_2 + r\ H_2O \qquad (3.10)$$

$$-\frac{d[C_xH_yO_z]}{dt} = \frac{1}{x}\frac{d[CO_2]}{dt} \qquad (3.11)$$

3.5. Degradation of Phenolic Compounds by TiO_2

There are a number of recent publications concerning destruction of phenol and substituted phenols by photocatalytic oxidation using suspensions of TiO_2 semiconductor.

Okamoto *et. al.* [20] studied the heterogeneous photocatalytic decomposition of phenol over TiO_2 powder. They observed that the hydroxyl radicals are real reactive species and they are formed not only by the reaction of holes with adsorbed H_2O or OH^-, but also via H_2O_2 from superoxide radical formed by electron trapping of adsorbed O_2. The same group [21] studied the effects of several parameters, such as, pH, O_2 partial pressure, initial phenol concentration, concentration of TiO_2, incident light intensity, and temperature on the reaction rate of phenol degradation. Results indicated that the photocatalytic decomposition of phenol over anatase TiO_2 powder followed first order kinetics, up to high conversions, of which the apparent rate constant depended on the initial concentration of phenol, concentration of TiO_2, light intensity, and O_2 partial pressure. The activation energy was found as 10 kJ/mol.

Another study [22] based on the concept of combined adsorption and photocatalytic oxidation. The adsorbent/photocatalyst was titanium dioxide supported on silica gel. The illumination sources were 40 W and 20 W near UV fluorescent tubes. In closed system recirculation mode at a flow rate of 120 ml/min, 500 ml of 10 μM phenol solution was destroyed with an apparent first order rate constant of 0.141±0.002 1/min. In open system single pass mode, using 20 W lamp reactor and TiO_2 photocatalyst 99.9 per cent destruction of 940 mg/l phenol influent stream was achieved at a flow rate of 20 ml/min.

Matthews and McEvoy [23] used TiO_2 as a free suspension sand attached to sand for the photocatalytic oxidation of phenol. It was found that under identical illumination conditions the degradation rate with free suspension was approximately 2.6 times faster than with immobilized catalyst. The quantum yield from a 100μM solution in 0.1 per cent TiO_2 suspension was approximately 0.6 per cent. The disappearance of phenol and the formation of CO_2 was based on Langmuir-Hishelwood kinetics. The solution pH between 3.5 and 8.5 did not have a great effect on the degradation rates. The adsorption equilibrium constant was found to be dependent on the reciprocal of the initial phenol concentration.

Trillas *et. al.* [24] studied photodegradation of phenol conducted in a flow system, in which TiO_2 remains fixed onto glass pearls. The use of this system gave a high yields of degradation for phenol. It was also found that photodegradation depends on the pH of the solution, the point of zero charge of TiO_2 and pK_a of phenol. The main aromatic intermediates detected were hydroquinone, paraquinone, and hydrohydroquinone. Some long term irradiations were also performed, showing high degrees of photodegradation.

In 1998, Byrne *et. al.* [25] compared the photocatalytic efficiency of TiO_2 coatings using degradation of phenol in aqueous solution as a standard test system. The use of TiO_2 in suspension was efficient due to the large surface area of catalyst available for reaction. But, when TiO_2 was used in a suspension reactor, the catalyst should be removed following the treatment. Alternatively, the catalyst may be immobilised onto a suitable solid support matrix that would eliminate the need for post-treatment removal. Thus, authors used immobilised TiO_2 powder on solid support substrates such as stainless steel. The coated substrates were annealed in air at elevated temperatures to improve the adhesion of the catalyst to the supporting substrates. It was found that photocatalytic efficiency was not to be markedly dependent upon either the substrate used or the annealing temperature employed in the coating process. Surface analysis of the immobilised TiO_2 showed no significant differences in the elemental composition or in band gap energies.

Auguliaro *et. al.* [26] investigated the influence of hydrogen peroxide on the phenol degradation rate under near UV irradiation in homogeneous and heterogeneous systems. They found that the contemporary presence of oxygen and hydrogen peroxide strongly improves the phenol photodegradation rate in the heterogeneous system. The adsorption of phenol onto titanium dioxide was not affected by the presence of oxygen and hydrogen peroxide, however oxygen and hydrogen peroxide both compete for the adsorption onto the titanium dioxide surface and for the charge transfer process. It was also reported that phenol photodegradation follows second order kinetics according to mechanisms which involve radical species produced from oxygen photoreduction and hydrogen peroxide photodecomposition.

In 1992, Wei and Wan [27] proposed a theoretical model for photocatalytic oxidation of phenol, based on the generation of hydroxyl radicals as the rate determining step. The model fit well with the experimental results. They found that pseudo-first order reaction rate equation can be derived from the theoretical model and the apparent rate constant demonstrates the inverse dependence on initial phenol concentration. The competitive adsorption between OH^- and ArO^- can be used to explain the minimum initial reaction rate in the region near pH 10. This study also determined the enhanced effect of addition of H_2O_2 with ferric ions on the degradation rate of phenol.

The effect of hydrogen peroxide on the photocatalytic oxidation of phenol on illuminated TiO_2 surfaces was also studied by Wei *et. al.* [28]. Their results indicated that transition metal ions, such as Fe^{3+} and Cu^{2+}, affect the photocatalytic oxidation of phenol. In the absence of added H_2O_2, the ferric ions induce the occurrence of the photo-Fenton type reaction so that phenol removal was enhanced from 23 to 33 per cent within 8 hours. However, cupric ions show a negative effect. In the presence of H_2O_2, both ferric and cupric ions enhanced the phenol oxidation rate drastically.

Wei and Wan [29] studied factors that influence the photocatalytic oxidation of phenol in oxygenated solution with suspensions of titanium dioxide powders. It was reported that there was an optimum value for the TiO_2 content. The optimum amount was found as 1-3g/l solution, and excess TiO_2 causes a shielding effect of light. They also found that phenol oxidation was light intensity dependent. Sufficient O_2 supply was needed, but a too high gas flow rate induces large bubbles that eliminate the gas residence time and the gas/liquid contact interface. The pseudo-first order reaction rate constant was found to be inversely proportional to the initial concentration of phenol. A mechanism of the phenoxide ions being adsorbed on the TiO_2 surface has been proposed to account for this inverse effect. Moreover, when pH effect was analyzed, the competitive adsorption between phenoxide ions and OH⁻ ions on the TiO_2 surface was explained.

The influence of Fe^{3+}, Fe^{2+}, and Ag^+ on the phenol photodegradation in the presence of aqueous TiO_2 (anatase) and TiO_2 (rutile) dispersions was investigated by Sclafani *et. al.* [30]. It was reported that these ions can react very easily with peroxo species produced on the catalyst surface and/or in the solution. In the absence of oxygen, photooxidation rate was negligible in both anatase and rutile. The highest rate was achieved in the presence of Fe^{3+} (5×10^{-4} M) and oxygen. The photoactivity of rutile in similar conditions was negligible. They reported that the behaviour of Fe^{2+} was similar to Fe^{3+} for the same experimental conditions. The Ag^+/Ag redox couple enhanced the photooxidation rate of phenol in the presence of oxygen and anatase, but it was ineffective in the case of rutile. Finally, authors concluded that the decomposition of the peroxo species is an important kinetic step in the photocatalytic degradation of phenol.

Trillas *et. al.* [31] observed that the photocatalytic oxidation of phenol over TiO_2 takes place with high yields for dilute solutions, i.e, for phenol concentrations lower than 2×10^{-4} M. They also reported that the yield of the phenol photooxidation depends strongly on the pH of the solution. Maximum yields were obtained at pH 8 and also in very alkaline media. These

results were explained considering the processes that take place at surface of the semiconductor, in which OH radicals is about 4×10^4 times greater than the constant rate of direct reaction between phenol and photogenerated holes in the TiO_2 particles. From HPLC analysis, hydroquinone, paraquinone and 1,2,4-benzenetriol have been detected as intermediate products prior to the total phenol mineralization.

Palmisano *et. al.* [32] followed the phenol photodegradation in the presence of TiO_2 by using Fourier Transform Infrared technique. By this method, the catalyst surface was characterized and the photoprocess was investigated in a gas-solid regime, simulating the aqueous liquid-solid regime. Surface hydroxylation of the catalyst was followed, and the presence of some intermediates were analyzed

Al-Sayyed *et. al.* [33] determined the kinetics of disappearance of 4-chlorophenol in the presence of TiO_2, ZnO_2, and MoO_3 in water under illumination at $\lambda \geq 340nm$ and 293K. The TiO_2 sample was found to be the most active with an initial quantum yield of 0.01 in the pH range 3-6. The effects of the catalyst mass, radiant flux, temperature, concentration of 4-chlorophenol and substitutional doping of TiO_2 with Cr^{3+} ions were all investigated. It was reported that the rate of disappearance of 4-chlorophenol increased linearly with the amount of catalyst up to a level corresponding to complete absorption of the incident light. The rate also increased upon increasing 4-chlorophenol concentration up to 1.55×10^{-4} M but levelled off at higher values. This behaviour has been treated according to Langmuir-Hishelwood type relationship. The activation energy was found as 5.5 kJ/mol, which indicates that adsorption/desorption processes were almost temperature independent. At higher radiant flux, a levelling off occurred in the rate of disappearance of 4-chlorophenol which indicates the predominance of the recombination of photoproduced charges. It was also found that Cr^{3+}-doped TiO_2 is much less active than undoped TiO_2. Hydroquinone was obtained as the main intermediate in the degradation. 1,4-benzoquinone, and 4-chloro-1,2-

dihydroxybenzene were also detected. None of the toxic biphenly derivatives was found in the presence of TiO_2. Complete mineralization of 4-chlorophenol was eventually obtained.

The kinetics of photomineralization of 4-chlorophenol sensitized by Degussa P25 TiO_2 in O_2-saturated solution was studied by Mills and Morris [34]. Effect of different experimental parameters; pH, concentration of TiO_2, concentration of 4-chlorophenol, concentration of O_2, temperature, light intensity, concentration of KNO_3 were followed. At pH 2 and T= 30°C the initial relative rate of CO_2 photogeneration conforms to a Langmuir-Hinshelwood type kinetic scheme. The overall activation energy for this photosystem was determined as 16±2 kJ/mol.

The photocatalytic mineralisation of 4-chlorophenol to CO_2 in aqueous suspensions of TiO_2 was also investigated by Balcıoğlu and İnel [35]. The photomineralization was found to be pH dependent and the highest photoreactivity was observed in the neutral region. It was reported that evolution of CO_2 occurs via apparent zero order kinetics and was complete after approximately one hour irradiation. The activation energy was found to be 18 kJ/mol. Addition of small amounts of H_2O_2 (5×10^{-3} M) increased the rate of CO_2 formation and decreased the time needed for the degradation of 4-chlorophenol by a factor of 1/3.

Mills et. al. [36] reported detailed examination of intermediates in the photomineralization of 4-chlorophenol sensitized by Degussa P-25 TiO_2. Major intermediates were found as; 4-chlorocatechol, hydroquinone, benzoquinone, and 4-chlororesorcinol. The observed variations in the concentrations of 4-chlorophenol, 4-chlorocatechol, hydroquinone and CO_2 fit the predicted Langmuir-Hinshelwood kinetic equations. Authors also assumed three major possible routes in which the photogenerated hydroxyl radicals can react with 4-chlorophenol, i.e, 4-chlorophenol→4-chlorocatechol, 4-chlorophenol→hydroquinone,

4-chlorophenol→unstable intermediate→CO_2, with probabilities of occurring: 48 per cent, 10 per cent, and 42 per cent, respectively.

Mills and Morris [37] studied the photocatalytic activity of TiO_2 as a function of temperature to photomineralize 4-chlorophenol. They reported that heat treatment of the TiO_2 leads to a marked decrease in its photocatalytic activity at temperatures above 600°C. This result was associated with a decrease in the specific surface area of TiO_2, due to particle sintering, rather than the anatase to rutile transformation which occurs at temperatures above 700°C.

In 1996 [38], in a gas recycling reactor, the photocatalytic oxidation of aqueous solutions of phenol and 4-chlorophenol had been studied utilizing TiO_2 as photocatalyst in the presence and absence of hydrogen peroxide. The rate of oxidation to CO_2 was measured. It was found that the disappearance of phenol and 4-chlorophenol obeys pseudo first order kinetics whereas the rate of mineralisation is zeroth order. Addition of small amounts of H_2O_2 significantly enhanced the photomineralization rate. The complete mineralisation for 1×10^{-4} M phenol and 4-chlorophenol resulted in approximately 50-110 min whereas this period was shortened to 6-28 min by the addition of an optimum amount of H_2O_2.

Stafford *et. al.* [39] studied the mineralisation of 4-chlorophenol in aqueous TiO_2 suspension when the suspension was illuminated with long wavelength UV light ($300nm < \lambda < 400nm$). They observed that increased TiO_2 loading did not enhance the initial rate of 4-chlorophenol degradation in photocatalysis, however rate of mineralisation of 4-chlorophenol increased with higher TiO_2 loading. This was due to significant adsorption of 4-chlorocatechol (a primary photodegradation product) to the surface and to the increased importance of surface oxidation reactions. The quantum yield of mineralization also increased. It was also reported that the rate of mineralisation enhanced at lower light intensities. The quantum

yield of reaction of 4-chlorophenol increased with decreasing wavelength of light from $\phi=0.01$ at $\lambda=360$ nm to $\phi=0.07$ at $\lambda=300$ nm.

In the study of D'Oliveira *et. al.* [40], 2- and 3-chlorophenol were chosen as models of chlorinated aromatic pollutants. Effects of radiant flux, wavelength, initial concentration and pH were examined on the photocatalytic degradation of these compounds in TiO_2 aqueous suspensions. It was found that degradation at $\lambda>340$ nm was faster than direct photolysis at $\lambda>290$ nm. The deco.nposition rate was not much effected by the pH over a wide range. Complete mineralisation was achieved but it requires a much longer time than dechlorination and dearomatization. Parahydroxylation was the main pathway, so formation of chlorohydroquinone was expected for both 2- and 3-chlorophenol as an intermediate product. Further hydroxylation resulted in the formation of hydroxyhydroquinone, which rapidly decomposes to carboxylic acids and carbonly compounds, and then to CO_2 and H_2O.

In 1990, Matthews [41] determined the rates of CO_2 formation from a number of common organic compounds, including phenol, 2-chlorophenol, 3-chlorophenol and 4-chlorophenol. The dependence of their rates of oxidation obey Langmuir-Hishelwood kinetics. The effect of suspension loading was studied in detail for 4-chlorophenol and it was shown that loadings up to 0.1 per cent had little effect on the oxidation rate when 4-chlorophenol concentration was <1.2 mg/l. At higher concentrations, increased rates were obtained with increased suspension loading. When results compared with that of using immobilized form, little difference in oxidation rates were observed with high concentrations of solutes (50 mg/l). At low concentrations (1 mg/l) the oxidation rates using free suspensions were approximately a factor of two faster than those obtained with immobilized catalyst.

In 1985, Barbeni *et. al.* [42] studied the heterogeneous photocatalytic degradation of pentachlorophenol in aqueous solutions containing a suspension of TiO_2. They reported that the degradation rate is slightly influenced by the increased halogen content of pentachlorophenol with respect to 4-chlorophenol. Oxygen and water were essential in the complete mineralisation of this compound. It was also found that the decrease in pentachlorophenol concentration resulted in an increase in Cl^- ion concentration.

Matthews [43] studied twenty one organic compounds, known to be possible contaminants of water, with UV illuminated titanium dioxide powder in aqueous suspension. Rate of CO_2 formation from illuminated suspensions of 0.2 g TiO_2 in 400 ml of 1×10^{-3} M solutions under irradiation of medium pressure Hg lamp was followed. It was found that rate of formation of CO_2 for dihydroxyphenols was significantly greater than for phenol. Amongst the isomers, the para form was marginally greater in both dihydroxyphenols and chlorophenols.

In another study, Matthews [44] determined the rate of photocatalytic oxidation of a number of aromatic compounds in aqueous solutions over UV illuminated thin films of TiO_2 in a flow through reactor. According to this study, the destruction rate of each solute obeyed approximately first order kinetics. The reaction rate constant decreased with increasing solute concentration. The time for 50 per cent destruction of 500 cm^3 of 10 μM phenol solution was 7.2 min.

Matthews [45] also studied the kinetics of photooxidation of twenty two organic solutes to CO_2 over UV illuminated film of Degussa P25 titanium dioxide over a 100 fold concentration range for each solute. The dependence of the photooxidation rate on concentration obeyed a two coefficient Langmuir expression for each solute. In the case of phenol, under experimental conditions: 20W lamp irradiation source, 40°C solution temperature and 300ml min^{-1} circulation rate, the reaction rate constant and the adsorption

equilibrium constant were found as 0.024±0.004 mg/l, and 10.2±0.9 mg/l min respectively. A reaction mechanism was proposed involving holes, hydroxyl radicals and O_2. Peroxyhydroxycyclohexadienly and mucondialdehyde type compounds were given as important intermediates. Further degradation of these compounds results in the formation of CO_2 and H_2O.

Guardia *et. al.* [46] studied resorcinol degradation in a flow system. They developed a flow analysis spectrophotometric method for the determination of resorcinol in waters by means of its reaction with p-aminophenol to produce a complex compound that shows maximum absorption at 540nm. This method had some advantages such as low limits of detection, reproducibility, economy and speed, as well as some disadvantages. Disadvantages concerned the final waste that contains unreacted p-aminophenol and also the complex formed by the reaction between resorcinol and p-aminophenol. This mixture of compounds could be dangerous and hence detoxification became important. Therefore, they performed degradation with an additional detoxification step based on the in-line TiO_2 catalysed photodegradation. After the measurement step the waste stream was merged with a TiO_2 slurry and then passed through a UV photochemical reactor under irradiation wavelength of 254 nm. Under these conditions, the waste can be completely detoxified, providing a non-polluting method of analysis.

4. EXPERIMENTAL

4.1. The Gas Recycling Reactor

A gas recycling reactor has been used for the photodegradation experiments (Figure 4.1.1). It consists of a 36.2 cm long Pyrex tube with an inner diameter of 3.5 cm. To allow temperature regulation via water circulation, there is a sealed inner glass tube in the gas recycling reactor with a thickness of 2 cm. The suspension (200 ml) was contained in the annulus formed between the two tubes. The gas above the suspension was pumped using a Cole-Parmer peristaltic pump. A sintered glass disk, placed at the bottom of the reactor, provides circulation of air and prevents settlement of the suspension. All connections were made with Tygon tubing. The reactor was placed in an irradiation box (70 cm in length, 22 cm in width) containing six 20 W black light fluorescent lamps (General Electric F 20 T 12/BLB) that provide light of wavelength 320-440 nm (Figure 4.1.2). The lamps are positioned to surround the reaction vessel from three sides. Lamps could be lit individually as well as in conjunction with each other. The front side of the irradiation box was designed to operate as a door with the reactor attached. This maintains a uniform geometry throughout the experiments. A fan was placed at the top of the box and air was also continually circulated through the box in order to eliminate any heating effects of the lamps.
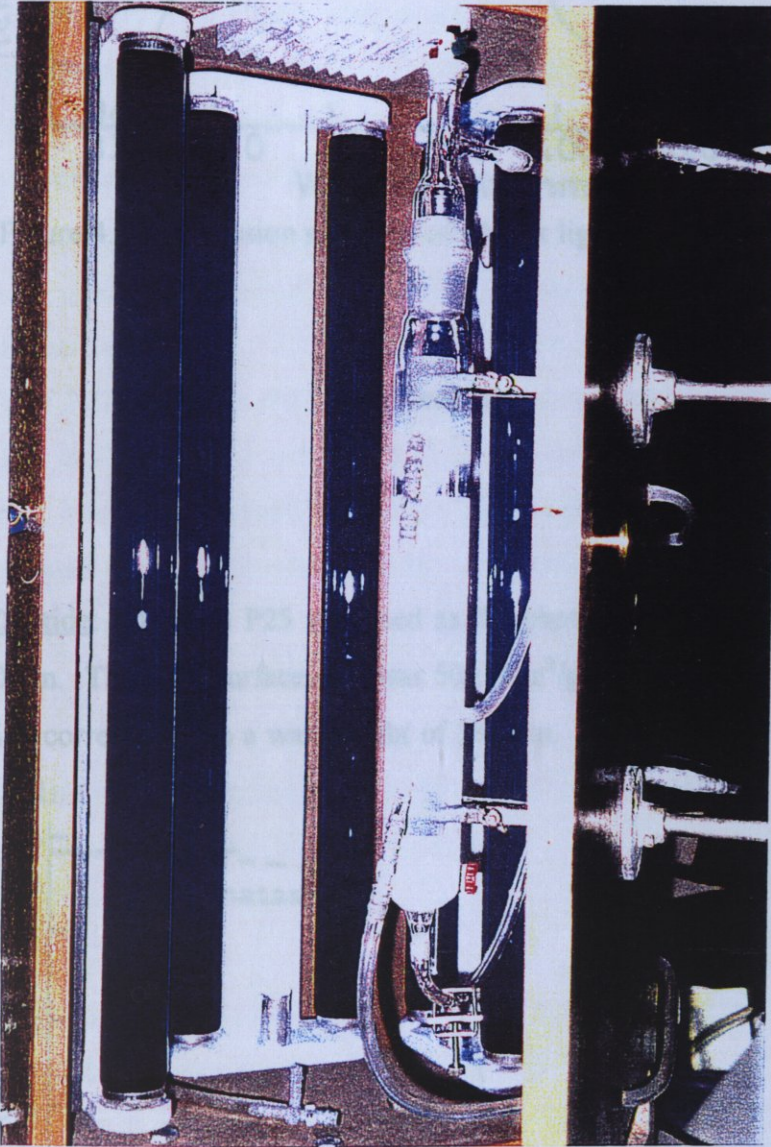
Figure 4.1.1. Gas Recycling Reactor.
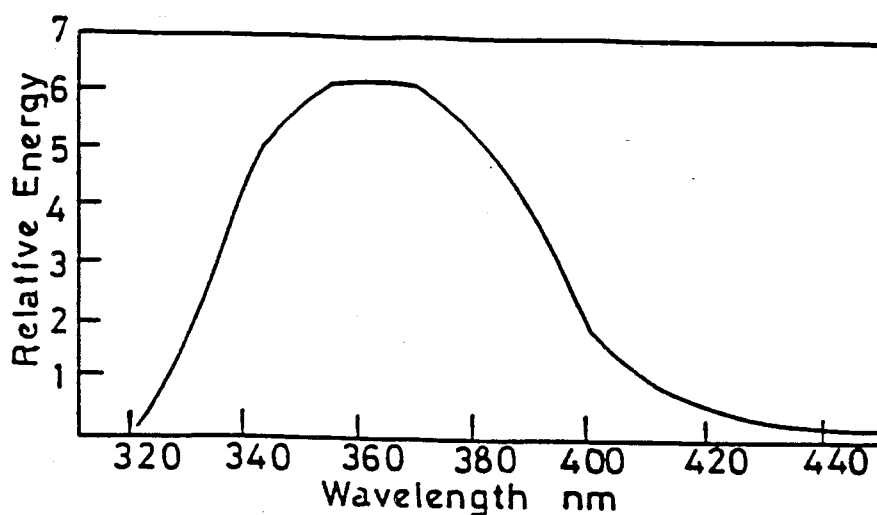
Figure 4.1.2. Emission spectrum of a black light fluorescent lamp.

4.2. Reagents

Titanium Dioxide: Degussa P25 was used as the photocatalyst. The average particle size was 30 nm. The BET surface area was 50 ± 15 m^2/g. TiO$_2$ has a bandgap energy of 3.2 eV which corresponds to a wavelenght of 380 nm. Its absorption spectrum is given in Figure 4.2.1.
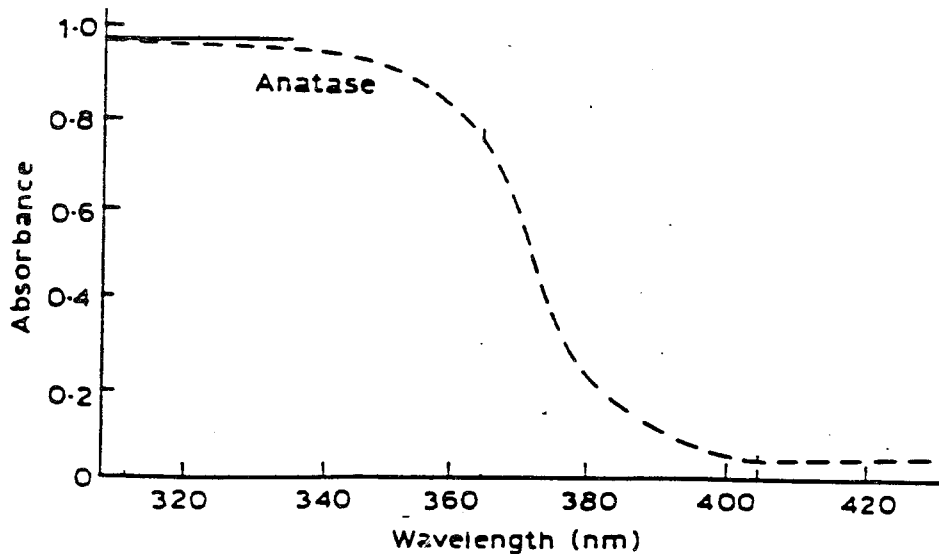
Figure 4.2.1. Absorption of TiO$_2$.

X-ray diffraction data has confirmed that the metal deposited and undeposited TiO_2 are in the anatase form (Appendix B).

Phenolic Compounds: Selected chemicals used in this study are listed in Table 4.2.1. 1,3-dihydroxybenzene (1,3-DHB) behaves similarly to monophenols and undergoes all of the typical reactions of phenol [47]. The high price of 1,3-DHB limits its use to two main applications: rubber products and wood adhesives. 1,3-DHB based resins are used in these applications because of their resistance to high temperatures and their durability under mechanical stress. In developed regions of the world, smaller amounts of 1,3-DHB are used as a chemical intermediate in the production of plastics additives, textile dyes, and explosives. 1,3-DHB is a skin, eye, and mucous membrane irritant. Exposure to 1,3-DHB causes skin burns, convulsions and death. Its lethal dose in rats is given as 370 mg/kg [47]. It was found to be less toxic than phenol, but with similar toxic effects. 3,5-DHT, 1,3-DHMB and 3,5-DHBA behave similarly to 1,3-DHB. Their toxicity is higher compared to the 1,3-DHB. Phenol like toxicity symptoms are induced by these compounds.
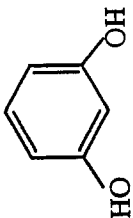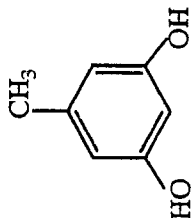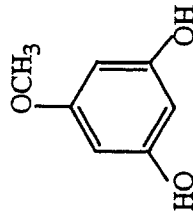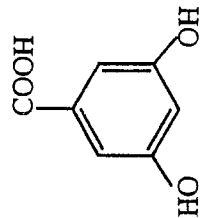
Hydrogen Peroxide and Methanol: Reagent grade hydrogen peroxide (30 per cent) and methanol (99.5 per cent) were obtained from Merck.

Sodium Hydroxide and Perchloric Acid: Reagent grade NaOH (Merck) and $HClO_4$ (70 per cent, Merck) were used for the pH adjustment of the solutions.

All chemicals used in the experiments were of laboratory reagent grade and they were used without further purification. Singly distilled water was deionized and used for the preparation of all solution.

Table 4.2.1. Selected chemicals for the photocatalytic degradation.

IUPAC Names	Commercial-Other Names	Abbreviations used in this study	Chemical Structure	Supplier	Per cent Purity
1,3-Dihydroxybenzene	Resorcinol 1,3-Benzenediol m-Dihydroxybenzene	1,3-DHB		Fluka	>99
3,5-Dihydroxytoluene	Orcinol monohydrate 5-Methylresorcinol	3,5-DHT		Fluka	98
1,3-Dihydroxy-5-methoxybenzene	3,5-Dihydroxyanisol 5-Methoxyresorcinol	1,3-DHMB		Fluka	97
3,5-Dihydroxybenzoic acid	-	3,5-DHBA		Aldrich-Sigma	97

4.3. Sample Preparation

Stock solutions of phenolic compounds were prepared as 100 μM at their natural pH's unless otherwise stated. 1g/L of TiO_2 and 144 ml/min of flow rate of air were used for all experiments unless otherwise stated [48]. Prior to the photodegradation experiments, the suspension (containing 200 ml of the substrate and 1g/L of TiO_2) was stirred for about 30 minutes in the dark to achieve an adsorption equilibrium for the substrate on the photocatalyst. Solutions were always wrapped with aluminum foil and kept in the dark in order to prevent any interference from ambient light before irradiation.

4.4. Analysis

4.4.1. Gas Chromatography (GC)

The amount of CO_2, which was produced as a final degradation product of substrates was determined by a Shimadzu (Gow Mac) gas chromatograph equipped with a thermal conductivity detector and a Porapak N column. He was used as a carrier gas at a flow rate of 60 ml/min. Calibrations were carried out using measured volumes of CO_2 added to the gas phase loop under identical conditions with the experiments. Sampling was made from the top of the Pyrex tube on which a mini inert valve is attached.

4.4.2. High Performance Liquid Chromatography (HPLC)

Following photodegradation, the concentration of remaining substrates was analyzed by high performance liquid chromatograph (HPLC, CECIL 1100 series), using a CE 1100 liquid chromatography pump with CE 1220 variable wavelength monitor and a UV-detector. The stationary phase was a Hypersil ODS column (particle size 10 μm). The mobile phase was a methanol:water (50:50) mixture for 1,3-DHB, 3,5-DHT, and 1,3-DHMB. For 3,5-DHBA, the mobile phase was potassium dihydrogen phosphate (KH_2PO_4):methanol (70:30). The pH of KH_2PO_4 is regulated to 3.00 by phosphoric acid addition before mixing with methanol. The measurements were performed at λ=274 nm for 1,3-DHB, 3,5-DHT, and 1,3-DHMB, and at λ=302 nm for 3,5-DHBA. All samples were filtered using Millipore films (0.45 μm) before the measurements.

4.4.3. Actinometric Study

Potassium ferrioxalate actinometer is used to determine the number photons per unit time coming from each of six 20 W black light fluorescent lamps. Details of the actinometric study, preparation of actinometric solutions, and the procedure for actinometric measurements are given in our previous study [49].

4.5. Metal Deposited TiO_2 Samples

Metal ions which have an ionic radius similar to that of Ti^{+4} (0.75 Å) were chosen for deposition on the TiO_2 surface (Figure 4.5.1). Metal salts used as precursors for deposited ions are listed in Table 4.5.1. They are used without further purification.

								Al^{3+} (0.68)
Ti^{4+} (0.75)	V^{4+} (0.70)	Cr^{3+} (0.76)	Mn^{2+} (0.79)	Fe^{3+} (0.79)	Co^{2+} (0.69)	Ni^{2+} (0.83)	Zn^{2+} (0.88)	
	Nb^{5+} (0.78)							
	Ta^{5+} (0.78)							

Figure 4.5.1. Periodic chart of deposited metal ions. All the oxidation states represent those of precursor metal ions. The numbers in parentheses are the ionic radii (Å). Ti^{4+} refers to undeposited TiO_2.

Table 4.5.1. List of metal salts.

Salt Form	Ion Form	Supplier	Per cent Purity
VSO_4	Vanadium ion (V^{4+})	Fluka	96
$Cr(NO_3)_3.9H_2O$	Chromium ion (Cr^{3+})	Fluka	97
$MnCl_2.4H_2O$	Manganese ion (Mn^{2+})	Merck	99
$Fe(NO_3)_3.9H_2O$	Ferric ion (Fe^{3+})	Merck	99
$CoCl_2.6H_2O$	Cobalt ion (Co^{2+})	Merck	99
$NiCl_2.6H_2O$	Nickel ion (Ni^{2+})	Merck	99
$ZnCl_2$	Zinc ion (Zn^{2+})	Fluka	98
$NbCl_5$	Niobium ion (Nb^{5+})	Fluka	99.9
$TaCl_5$	Tantalum ion (Ta^{5+})	Fluka	99.9
$AlCl_3$	Aluminium ion (Al^{3+})	Merck	97

4.6. Preparation of Deposited Samples

Deposited TiO_2 samples were prepared in the presence of added metal salts to give a deposition level of 1.0 per cent by weight, unless otherwise mentioned. The method used for the deposition process involved irradiation of the slurry for 75 minutes in an optical bench reactor described below. After centrifugation at 4000 rev/min for one hour and subsequent filtration, the product was collected and dried at 100°C until completely dry. Grinding provided a homogeneous mixture. Deposited samples displayed various colors depending on the kind of metal ions: V^{4+} and Fe^{3+} samples are yellowish, Cr^{3+}-deposited greenish, Co^{2+}-deposited bright blue, and Mn^{2+}-deposited bright pink.

4.7. The Optical Bench Reactor

The optical bench reactor was used for the preparation of metal deposited TiO_2 samples. A 250W medium pressure Hg lamp, a lens holder, a plane mirror and a sample holder are the major elements of the apparatus (Figure 4.7.1).

The excitation source was a 250 W medium pressure Hg lamp with an arc size 2x4 mm. This lamp contains a number of UV lines of which more than 40 percent are below 400 nm. The same actinometric method (4.4.3) was used to measure the number of photons per second from Hg lamp in optical bench reactor. The lamp emits 1.85×10^{16} photon/s.

The sample holder was a 150 ml beaker, and its contents were stirred by means of a magnetic stirrer. The plane mirror (7x5 cm) was placed at an angle of 45° just above the

beaker. First light falls on the mirror and is then reflected to strike the slurry in the beaker as shown in Figure 4.7.1. A pyrex cell containing water is used as a filter to block transmission of light >300 nm.
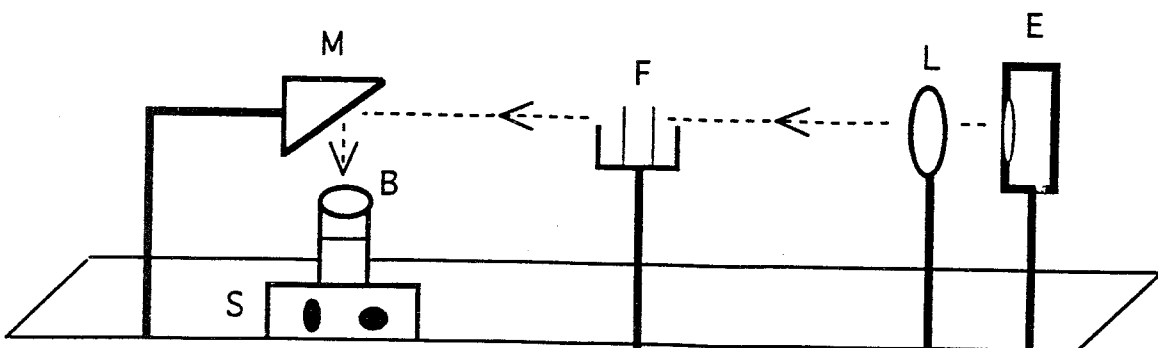
Figure 4.7.1. Schematic set-up of an optical bench reactor. M: Plane mirror placed at an angle of 45°, F: Filter compartment, L: Converge lens, E: Excitation source; medium pressure Hg lamp, B: Sample holder; 150 ml beaker, S: Magnetic stirrer.

Specific treatments of the catalyst are given in the following sections.

4.8. Preparation of Deposited TiO_2 Samples With and Without a Hole Scavenger

Without a hole scavenger: The necessary amount of the metal salt to give a 1 per cent concentration of deposited ion was dissolved in 100 ml water prior to the addition of TiO_2.

With a hole scavenger: Instead of 100 ml water, 20 ml methanol was diluted in 80 ml of water. This solution was used as the dispersion medium. Methanol was added in order to act as a hole scavenger. The optimum concentration of methanol 20 per cent by volume was found by trial and error [50].

4.9. Preparation of Fe^{3+} Deposited TiO_2 As a Function of Fe^{3+} Concentration

Fe^{3+} deposited TiO_2 samples were prepared with different concentrations of Fe^{3+} without a hole scavenger. The concentration of Fe^{3+} is regulated to obtain 0.5, 1, 2, 3, and 5 per cent deposition levels. Depending on the concentration, color of Fe^{3+}-deposited samples changes from bright yellow (0.5 per cent) to dark yellow (bright brown) (5 per cent).

4.9.1. Preparation of Heat-Treated Fe^{3+} Deposited TiO_2

In order to investigate the effect of particle agglomeration on the photoreactivity, different percentages of Fe^{3+} deposited TiO_2 samples are dried at 400°C, after the centrifuge and filtration steps. In the case of heat treated samples, color changes from yellowish to dark brown.

Analysis of metal deposited TiO_2 samples are given in the following sections.

4.10. Surface Area Measurement by the BET Method

Surface areas of undeposited and deposited TiO_2 samples prepared as described in section 4.8 were measured with a Micromeritics Flowsorb II 2300 instrument. The instrument determines the quantity of nitrogen gas that adsobs as a single layer of molecules on the samples. The area covered by each gas molecule is known within relatively narrow limits. The area of the sample is thus directly calculable from the number of adsorbed molecules. Details of the method, the apparatus, and the procedure are given in the reference [51]. Table 4.10.1 gives the results of surface area measurements of undeposited and deposited TiO_2.

TABLE 4.10.1. Surface area measurements at 150°C using BET method.

Sample	Surface Area (m^2/g)
TiO_2	45.4±1.4
V^{4+}/TiO_2	43.9±1.2
Cr^{3+}/TiO_2	47.6±2.1
Mn^{2+}/TiO_2	43.2±1.6
Fe^{3+}/TiO_2	41.6±0.7
Co^{2+}/TiO_2	44.5±0.9
Ni^{2+}/TiO_2	46.0±1.7
Zn^{2+}/TiO_2	45.2±0.4
Nb^{5+}/TiO_2	39.0±1.2
Ta^{5+}/TiO_2	41.6±1.2
Al^{3+}/TiO_2	39.2±1.1

4.11. Atomic Absorption Spectroscopy

A quantitative measurement of the Fe^{3+} concentration deposited on the surface of TiO_2 was performed on a Varian Spectraa 250 Plus atomic absorption spectrophotometer, equipped with a Varian Fe hollow cathode lamp. Since the optimum working range of the lamp is given as 2.5 to 10 μg/ml, the concentrations of standard solutions are regulated in this range. For each run, the instrument was calibrated with freshly prepared standard solutions. After irradiation in the optical bench reactor, samples were centrifuged for 2 hours. After the centrifugation step, a 1 ml aliquot is taken, and then diluted to 100 ml. Dilution of the samples prior to reading in atomic absorption spectrophotometer was necessary to ensure that the concentration was in the working range of the Fe lamp. In order measure the concentration of Fe^{+3} staying in the solution phase after a photodegradation run, different percentages of Fe^{+3} deposited TiO_2 were irradiated for 1 hour in the gas recycling reactor. After irradiation, the sample is treated in the same manner as the standards before reading in atomic absorption spectrophotometer.

5. 1,3-DIHYDROXY BENZENE (1,3-DHB)

5.1. Effect of 1,3-DHB Concentration

When photoinduced mineralization of 1,3-DHB ($C_6H_4(OH)_2$) occurs stoichiometrically, the total reaction is given by:

$$C_6H_4(OH)_2 + 13/2\ O_2 \rightarrow 6CO_2 + 3H_2O \qquad (5.1)$$
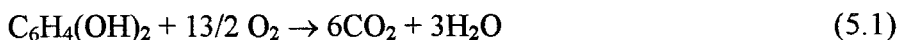
The reaction is followed by monitoring the decrease in 1,3-DHB concentration and the resulting the increase in the amount of CO_2 evolved. For initial 1,3-DHB concentrations ranging from 10 μM-1000 μM, 1,3-DHB degradation is followed at five minute intervals for a total of 30 min. Figure 5.1.1 (Table 5.1.1) depicts the decrease of 1,3-DHB concentration with respect to time. For all concentrations examined, there is a decrease in the total concentration with 30 min irradiation. The fastest initial decrease is observed for 10 μM. For concentrated solutions of 1000 μM samples, an initial decrease is observed, but the depletion begins to level off at about 75 μM following 15 min irradiation. This can be further seen in the inset of Figure 5.1.1 (Table 5.1.2) which plots the natural log of the ratio of the initial 1,3-DHB concentration versus the concentration at given irradiation times. The resulting graph shows a linear dependence for 10 μM-100 μM concentrations, indicating that the rate of 1,3-DHB destruction is described as a first order reaction in 1,3-DHB concentration. However, we see deviations from this for the highest concentration of 1000 μM 1,3-DHB with the resulting curve again reaching a constant plateau for 15 min irradiation time.
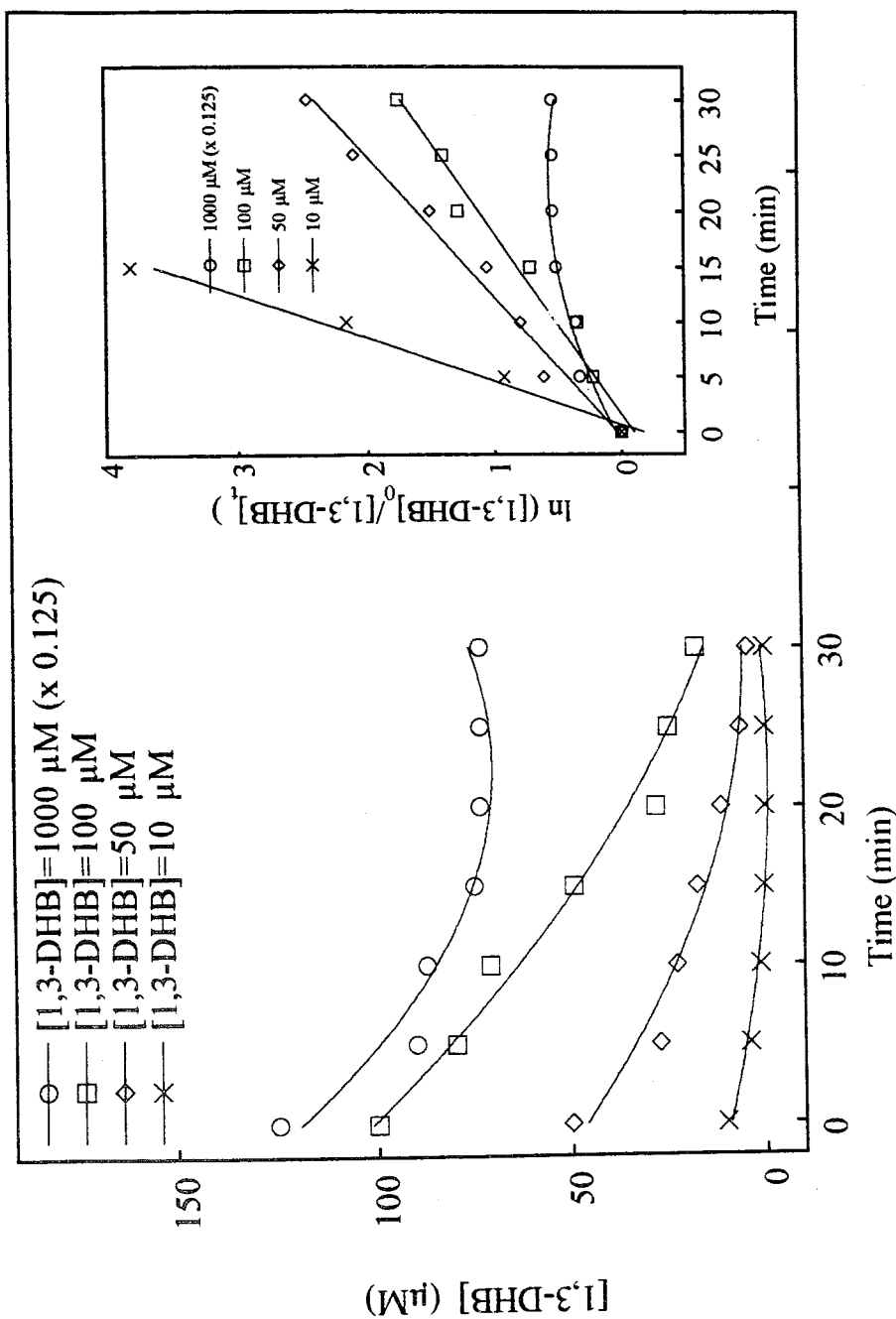
Figure 5.1.1. Effect of 1,3-DHB concentration on the degradation of 1,3-DHB.

Inset: Natural log of the ratio of the initial 1,3-DHB concentration at given irradiation times.

Conditions: $[TiO_2]$=1g/L, Flow Rate=144 ml/min, pH=5.4, T=298 K, I_0=10.8x10^{-6} einstein/min.

Table 5.1.1. Effect of 1,3-DHB concentration on the degradation of 1,3-DHB.

Each numerical value represents the concentration of 1,3-DHB remaining in the solution.

Time (min)	[1,3-DHB]$_0$				
	1000 μM	100 μM	50 μM	10 μM	
0	1000	100	50	10	
5	721	79.9	27.2	3.97	
10	700	71.1	22.7	1.15	
15	601	49.2	17.4	0.22	
20	587	27.9	11.2	0	
25	586	24.6	6.15	0	
30	586	17.4	4.28	0	

Table 5.1.2. $\ln([1,3\text{-DHB}]_0/[1,3\text{-DHB}]_t)$ versus time data as a function of initial 1,3-DHB concentration.

Time (min)	$[1,3\text{-DHB}]_0$			
	1000 µM	100 µM	50 µM	10 µM
0	0	0	0	0
5	0.33	0.22	0.61	0.92
10	0.36	0.34	0.79	2.16
15	0.51	0.71	1.06	3.82
20	0.53	1.28	1.49	-
25	0.53	1.40	2.09	-
30	0.53	1.75	2.46	-
y= (µM) x= (min)	y=0.165+0.01558x R=0.856	y=-0.102+0.06107x R=0.985	y=0.003+0.07899x R=0.990	y=-0.177+0.25378x R=0.992

If the dependence is truly first order, then varying the initial 1,3-DHB concentration should not affect the apparent first order rate constant. As is easily seen in the inset of Figure 5.1.1, although the curves are linear for 10 μM-100 μM solutions (and initially for 1000 μM), however they exhibit widely differing slopes. Table 5.1.3 shows that for the photocatalytic degradation of 1,3-DHB, as the initial concentration is increased, the apparent first order rate constant decreases.

TABLE 5.1.3. Kinetic data for 1,3-DHB degradation.

[1,3-DHB] (μM)	k' (1/min)	$R_{[1,3\text{-DHB}]}$ (μM/min)
1000*	0.015	15.58
100	0.061	4.023
50	0.078	3.949
10	0.253	2.358

*For 1000 μM, k' is detected for the initial 15 min irradiation time.

This demonstrates that the kinetics of 1,3-DHB destruction are not truly first order in 1,3-DHB concentration, and therefore should be described as pseudo-first order following the equation 5.2:

$$-\ln \frac{[1,3-\text{DHB}]_t}{[1,3-\text{DHB}]_0} = k't \qquad (5.2)$$

depends on $[1,3\text{-DHB}]_0$ indicating that the reaction is not a simple first order reaction. Augugliaro [26] and Okamoto [20] found the same concentration dependence for phenol.

Wei and Wan [29] investigated phenol degradation over a broad range of phenol concentration from 1 to 2000 μM. They expressed k' as follows:

$$k' = k_o P_{\cdot OH} P_{Sub} \tag{5.3}$$

where k_o is the reaction rate constant, $P_{\cdot OH}$ is the probability for generating $^\cdot$OH radicals from the TiO_2 surface, and P_{Sub} is the probability of the $^\cdot$OH radical reacting with the organic substrate. k_o is independent of the $[Sub]_o$, but $P_{\cdot OH}$ and P_{Sub} will be affected by $[Sub]_o$. To determine P_{Sub}, Wei and Wan applied the Eley-Rideal kinetic model. According to the Eley-Rideal kinetic model, reaction occurs between $^\cdot$OH radicals on the surface of TiO_2 and substrate molecules from the fluid. This type of mechanism is characterized by a low activation energy and structure insensitivity.

In the following discussion, we have applied the same model for 1,3-DHB decomposition, and P_{Sub} is replaced with $P_{1,3\text{-DHB}}$. From the Eley-Rideal kinetics, $P_{1,3\text{-DHB}}$ is related to the mass transfer rate between the 1,3-DHB concentration in the bulk solution and that bound to the surface of the TiO_2 particle. It is given by

$$P_{1,3\text{-DHB}} = \frac{[1,3-\text{DHB}]_s}{[1,3-\text{DHB}]_b} \tag{5.4}$$

where $[1,3\text{-DHB}]_s$ denotes the 1,3-DHB concentration at the surface of TiO_2 and $[1,3\text{-DHB}]_b$ denotes the 1,3-DHB concentration in the bulk solution.

For $P_{\cdot OH}$, the photocatalytic degradation of aromatic compounds through hydroxylation by hydroxyl radicals is considered. Adsorbed OH^- ions at the surface of TiO_2 are the active sites for the generation of $\cdot OH$ radicals. However, the competition between OH^- ions and 1,3-DHB ions for surface sites, reduces the rate of formation of $\cdot OH$ radicals [21]. The effect of surface coverage of 1,3-DHB and of its oxidative intermediates on $P_{\cdot OH}$ is given as:

$$P_{\cdot OH} = \frac{f_{OH}}{f_{1,3-DHB} + f_I} \tag{5.5}$$

where f_{OH}, $f_{1,3\text{-DHB}}$, f_I are the fractional site coverage by the OH^- ion, 1,3-DHB, and the intermediates of the 1,3-DHB decomposition reaction, respectively. The fractional site coverages can be written as:

$$f_{OH} = \frac{K_{OH}[OH]}{1 + K_{1,3-DHB}[1,3-DHB] + K_I[I] + K_{OH}[OH]} \tag{5.6}$$

$$f_{1,3-DHB} = \frac{K_{1,3-DHB}[1,3-DHB]}{1 + K_{1,3-DHB}[1,3-DHB] + K_I[I] + K_{OH}[OH]} \tag{5.7}$$

$$f_I = \frac{K_I[I]}{1 + K_{1,3-DHB}[1,3-DHB] + K_I[I] + K_{OH}[OH]} \tag{5.8}$$

where K_{OH}, $K_{1,3\text{-}DHB}$, K_I are the adsorption equilibrium constants of OH^-, 1,3-DHB, and the intermediates, respectively. Equations (5.6)-(5.8) are substituted into the equation (5.5) and $P_{\bullet OH}$ is found as:

$$P_{\bullet OH} = \frac{K_{OH}[OH]}{K_{1,3\text{-}DHB}[1,3-DHB] + K_I[I]} \qquad (5.9)$$

For calculating initial rates, we can make the simplifying assumption that the intermediate concentration is small relative to the concentration of 1,3-DHB,

$$K_{1,3\text{-}DHB}[1,3\text{-}DHB] \approx K_{1,3\text{-}DHB}[1,3\text{-}DHB]_0 \gg K_I[I] \qquad (5.10)$$

Then the denominator of equation (5.9) becomes as follows:

$$K_{1,3\text{-}DHB}[1,3\text{-}DHB] + K_I[I] = K_{1,3\text{-}DHB}[1,3\text{-}DHB]_0 \qquad (5.11)$$

and (5.9) can be written as:

$$P_{\bullet OH} = \frac{K_{OH}[OH]}{K_{1,3\text{-}DHB}[1,3-DHB]_0} \qquad (5.12)$$

Thus, from equation (5.12), it can be seen that as the initial concentration of 1,3-DHB increases the probability of the generation of $^{\cdot}$OH radicals decreases. This explains the observed deviation from linearity for the highest concentration of 1000 μM 1,3-DHB.

By substituting (5.4) and (5.12) into (5.3), k' can be written as

$$k' = k_0 \frac{K_{OH}[OH]}{K_{1,3-DHB}[1,3-DHB]_0} \frac{[1,3-DHB]_s}{[1,3-DHB]_b} \qquad (5.13)$$

From equation (5.13), it is shown that k' is dependent on the $[1,3\text{-DHB}]_0$ whereas k_0 is not.

The evolution CO_2 as a function of initial 1,3-DHB concentration is shown in Figure 5.1.2 and in Table 5.1.4. This study was carried out for times up to 90 min. All concentrations have a linear dependence for the initial 30 min of irradiation. The rate is seen to steadily increase in one hour for both 100 μM and 1000 μM 1,3-DHB concentrations, but the rate is then observed to level off, showing a saturation in the initial degradation rates. A similar behavior is observed for lower concentrations of 1,3-DHB, i.e. 50 μM and 10 μM but now the saturation in the initial degradation rates is observed earlier than that for higher concentrations. By monitoring the production of CO_2, and assuming the stoichiometric reaction (5.1) is followed, complete degradation is observed in 30 min for 10 μM 1,3-DHB and in 60 min for 50 μM 1,3-DHB, whereas at concentrations of 100 μM and 1000 μM the time required for complete degradation exceeds the 90 min irradiation time.
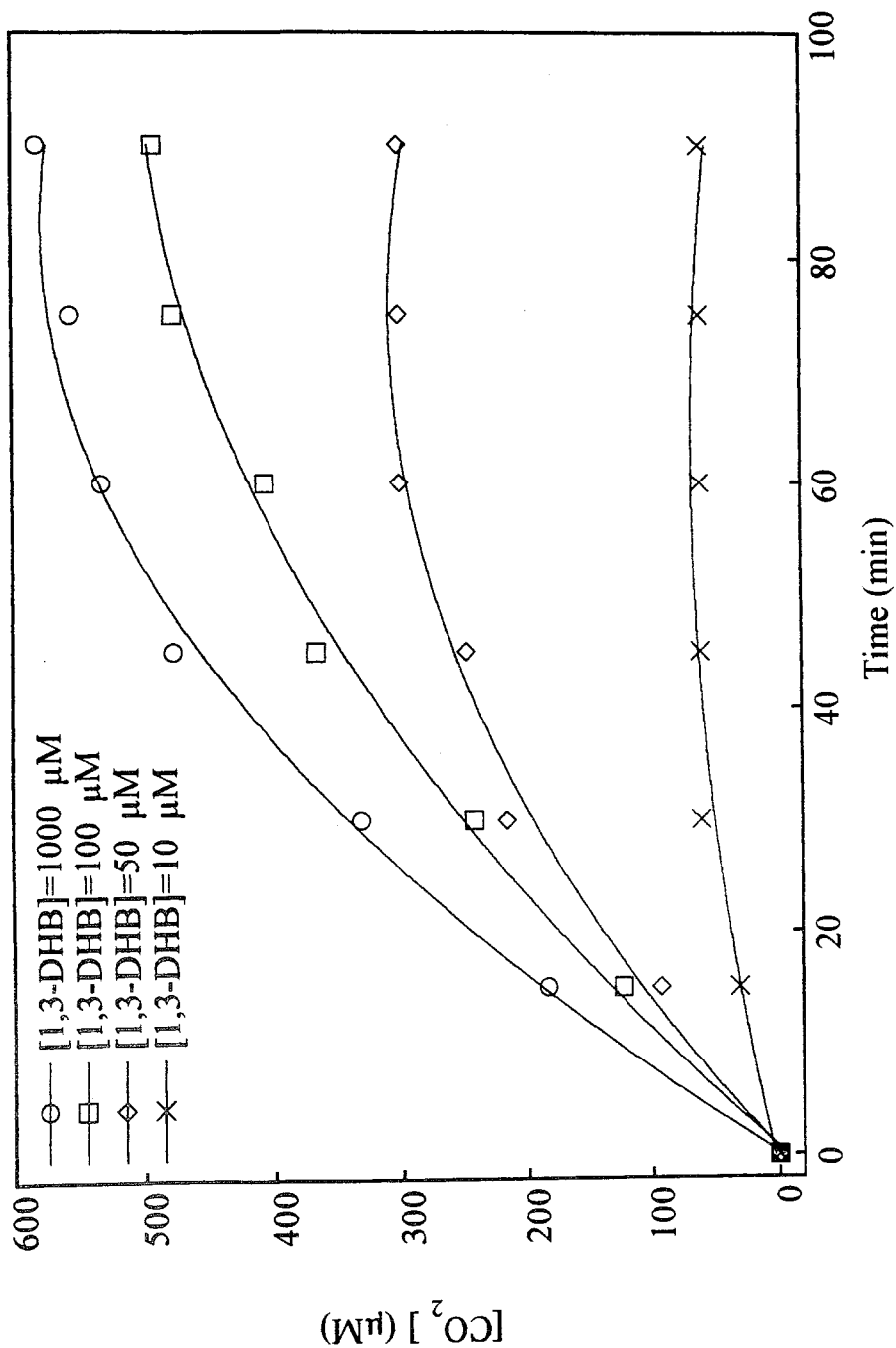
Figure 5.1.2. Effect of initial 1,3-DHB concentration on the concentration of CO_2 evolved as a function of irradition time. Conditions: $[TiO_2]=1g/L$, Flow Rate=144 ml/min, pH=5.4, T=298 K, $I_0=10.8 \times 10^{-6}$ einstein/min.

Table 5.1.4. Effect of initial 1,3-DHB concentration on the concentration of CO_2 evolved as a function of irradiation time. Equations represent the linear portion of the data, i.e. 60 min irradiation time.

Time (min)	$[1,3\text{-DHB}]_0$			
	1000 µM	100 µM	50 µM	10 µM
0	0	0	0	0
15	184	123	93.1	30.3
30	332	242	216	60
45	477	366	247	60
60	532	406	300	60
75	556	476	300	60
90	581	491	300	60
y= (µM) x= (min)	y=33.61+10.3x R=0.986	y=16.41+9.05x R=0.988	y=20.41+5.03x R=0.975	Y=12.12+0.99x R=0.883
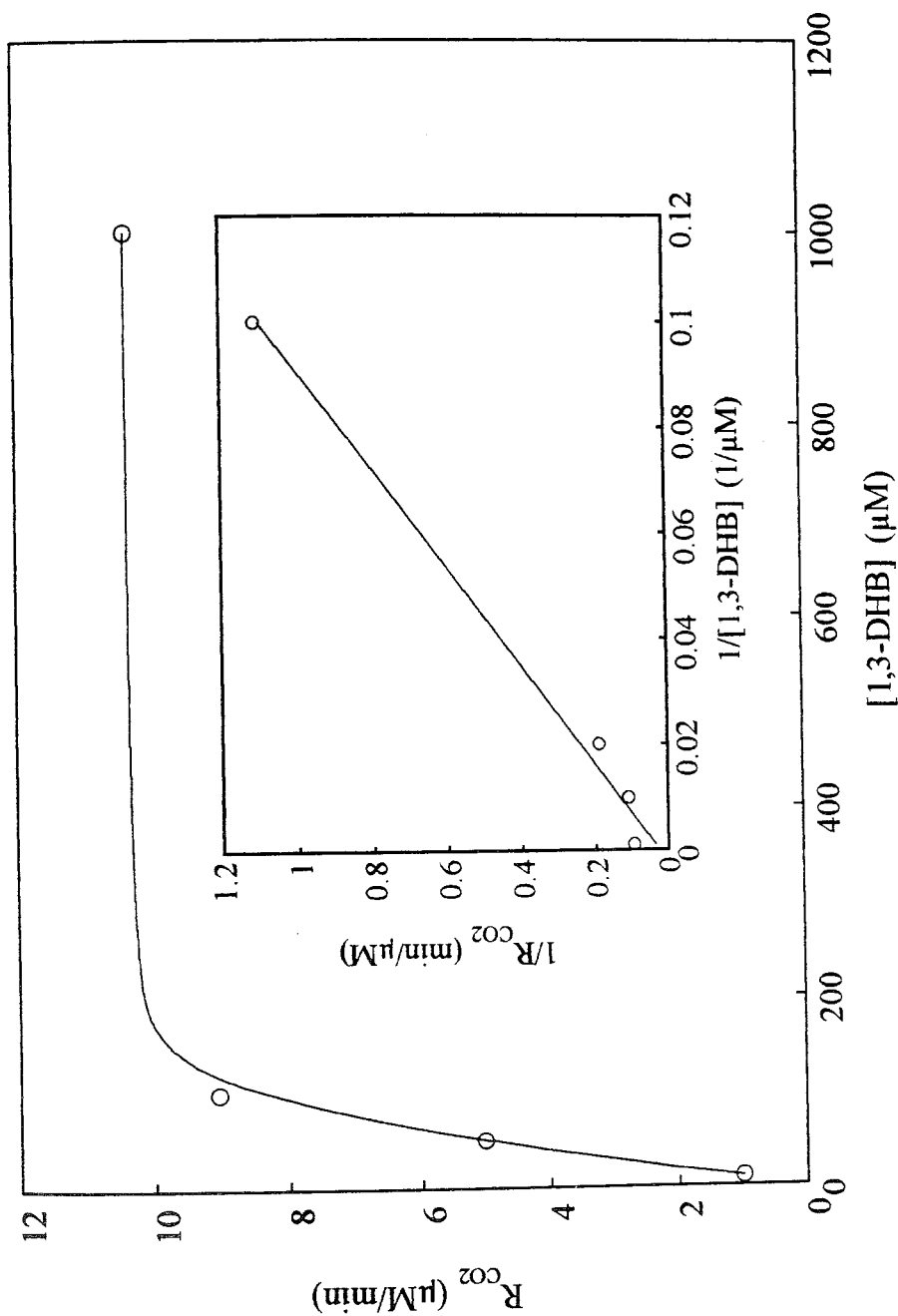
Figure 5.1.3. Rate of CO$_2$ production versus 1,3-DHB concentration.

Inset: 1/R$_{CO2}$ as a function of 1/[1,3-DHB]. Conditions: [TiO$_2$]=1g/L, Flow Rate=144 ml/min, pH=5.4, T=298 K, I$_0$=10.8x10^{-6} einstein/min.

the initial concentration of 1,3-DHB is increased. The inset of Figure 5.1.3 plots the inverse of the CO_2 rate ($1/R_{CO2}$) as a function of the inverse of 1,3-DHB concentration (1/[1,3-DHB]) and yields a straight line with R=0.995. This demonstrates the validity of a Langmuir-Hinshelwood kinetic model for this system. Numerical results are given in Table 5.1.5. The reaction rate constant, k, is found as 15.48 μM/min, and the adsorption constant of 1,3-DHB on TiO_2, K, is found as 6.97×10^{-3} 1/μM. For phenol, under similar experimental conditions; [TiO_2]=1 g/L, 20 W black light, K is found as 6.78×10^{-3} 1/μM [41].

Table 5.1.5. Effect of 1,3-DHB concentration on the formation rate of CO_2.

[1,3-DHB] (μM)	R_{CO2} (μM/min)	1/[1,3-DHB] (1/μM)	$1/R_{CO2}$ (min/μM)
1000	10.35	0.001	0.09
100	9.05	0.010	0.11
50	5.03	0.020	0.19
10	0.99	0.100	1.11

Based on the stoichiometry for the process (equation 5.1), the degradation per cent of 1,3-DHB for 30 min irradiation time and per cent formation of CO_2 both for 30 min and for 90 min irradiation have been calculated and are given in Table 5.1.6.

Table 5.1.6. Degradation percentage of 1,3-DHB and formation percentage of CO_2.

[3,5-DHT] (μM)	Per cent Degradation of 1,3-DHB	Per cent Formation of CO_2	
	in 30 min	in 30 min	in 90 min
1000	41.4	5.53	9.68
100	82.6	40.3	81.8
50	91.4	72.1	100
10	100	100	100

The results can be summarized as follows:

1. As the concentration of 1,3-DHB increases, the degradation percentages decrease due to the decreased probability of $^{\bullet}OH$ radical generation (equation 5.12).

2. For 30 min irradiation times, higher concentrations of 1,3-DHB yield a lower per cent CO_2 formation relative to 1,3-DHB degradation. This can be explained by the formation of some intermediates throughout the degradation process of 1,3-DHB which could not easily mineralized to CO_2. For the lowest concentration, i.e. 10 μM 1,3-DHB, the observed percentages coincide due to the formation of a smaller amount of intermediates. Under these conditions, they can be consumed faster because of less competing reactions and also decreased competition for surface sites on TiO_2.

3. For 90 min irradiation, the per cent CO_2 coincides with the per cent degradations of 100 μM, 50 μM, and 10 μM 1,3-DHB indicating that the reactive intermediates have now been mineralized. However, for the highest concentration, the CO_2 percentage is still lower compared to the 1,3-DHB degradation.

5.2. Effect of pH

The photocatalytic degradation of 1,3-DHB is strongly dependent on the pH value of the 1,3-DHB solutions. This dominant effect of pH is due to competitive factors including dissociation of 1,3-DHB, adsorption of OH$^-$ ions, and adsorption of 1,3-DHB ions.

To monitor the effect of pH on 1,3-DHB degradation, three sets of experiments have been performed. The first set of experiments monitors the pH changes of 1,3-DHB/TiO$_2$ suspensions before (pH$_1$) and after one hour irradiation (pH$_2$). The results for pH's 3.5, 5.4 (natural pH), 7.0, 9.0, 11.0 are given in Table 5.2.1.

Table 5.2.1. Resulting pH changes before (pH$_1$) and after irradiation (pH$_2$) for 1,3-DHB/TiO$_2$ suspensions.

pH	pH$_1$	pH$_2$	ΔpH=pH-pH$_2$
3.5	3.5	3.5	0
5.4	4.7	4.5	0.9
7.0	6.1	5.6	1.4
9.0	8.3	5.9	3.1
11.0	10.9	10.7	0.3

The point of zero charge (pzc) of TiO$_2$ in water, determined by measuring the changes of pH that occur when TiO$_2$ is added to water, is 4.7 [31]. Thus, the decrements in the pH values (pH$_1$) occuring after the addition of TiO$_2$ are due to the relatively acidic pzc value of TiO$_2$ for pH's greater than 4.7.

Except for pH 3.5, the pH of the suspensions was found to further decrease after irradiation.

$$+ H^+ \quad pK=9.81 \qquad (5.14)$$
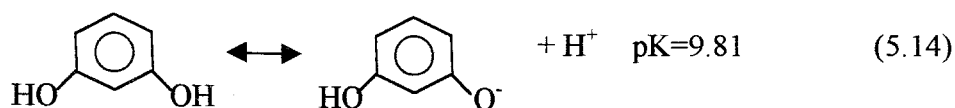
According to equation (5.14), decreasing the pH inhibits the dissociation process (i.e. equation shifs to the left) and decreases the 1,3-DHB adsorption on the TiO$_2$ surface. As a result, the probability of the reaction between $^\bullet$OH radicals (produced from OH$^-$ ions present on the TiO$_2$ surface) and the 1,3-DHB ion reaches a minimum value. Thus, no change in the pH value after one hour irradiation time will be obtained.

pH 5.4 is the natural pH of the 1,3-DHB solution, i.e. no acid or base is added to the solution to regulate the pH. The decrement observed, ΔpH, is due to the consumption of OH$^-$ ions by the reaction between $^\bullet$OH radicals and 1,3-DHB ions.

At higher pH values, i.e. pH 7.0-11.0, the dissociation of 1,3-DHB into the 1,3-DHB ion is favored (i.e. equation (5.14) shifts to the right). When pH increases, the number of hydroxyl groups on the TiO$_2$ surface also increases. The highest decrement, ΔpH, is obtained at pH 9.0 and the lowest is at pH 11.0 All these decrements are due to the reactions between $^\bullet$OH radicals and 1,3-DHB ions. However, although more OH$^-$ ions are introduced into the solution at pH 11, after irradiation, the pH$_2$ value, 10.7, does not differ much from pH 11. This means that OH$^-$ ions stay in the solution phase instead of being adsorbed on the TiO$_2$ surface. The competition between OH$^-$ ions and 1,3-DHB ions at this pH decreases the number of $^\bullet$OH radicals, resulting in the lowest decrement among the higher pH's.

A second set of experiments are performed to follow the degradation of 1,3-DHB at different pH values both in the absence and in the presence of TiO₂ under irradiation. Tables 5.2.2 and 5.2.3, and Figures 5.2.1, 5.2.2, 5.2.3 and 5.2.4 give the results of these experiments. In each set of experiments, the initial 1,3-DHB concentration is 100 μM. 1g/L TiO₂ is used for the experiments including the photocatalyst.

In the absence of TiO₂, all pH's have the same trend initially. At pH 3.5, a small amount of degradation is observed after 50 min irradiation. In the case of pH 5.4, there is no initial decay for times ≤20 min. At pH 9.0, degradation of 1,3-DHB is lower compared to that of pH 11 but higher compared to pH 3.5 and natural pH. The maximum degradation is obtained with pH 11.0, thus the presence of excess OH⁻ ions are functioning as the active species for the degradation. During the irradiation, the reaction solution at pH 11.0 is examined at ten minutes intervals with an UV spectrophotometer. It is observed that the absorption peak of 1,3-DHB broadens and the maximum shifts to the higher wavelengths. Thus the decrease in the 1,3-DHB concentration in the solution can be explained by the formation of new products during the irradiation period.

In the presence of TiO₂, the rate of degradation of 1,3-DHB is higher compared to the results in the absence of TiO₂. At pH 11.0, OH⁻ ions are sufficiently concentrated to compete with 1,3-DHB ions. 1,3-DHB ions which are formed at higher pH values tend to replace OH⁻ ions on the TiO₂ surface. As a result, the rate of degradation decreases compared to pH 9.0. This is in contrast to the results in the absence of TiO₂ under these conditions, where the highest degradation rate is obtained with pH 9.0 and the lowest is with pH 3.5. At pH 3.5, the solution pH is lower than the pzc of TiO₂. Thus, the surface of TiO₂ favors the adsorption of 1,3-DHB in its anionic form. However, according to dissociation process of 1,3-DHB equation (5.14), decreasing the pH of the medium increase the H⁺ ion concentration, therefore forcing the 1,3-DHB to remain in its undissociated form. As a result, the adsorption of 1,3-DHB on the surface at pH 3.5 is not favored. At pH 5.4, the

Table 5.2.2.   Effect of pH on the degradation of 1,3-DHB in the absence of TiO_2.

Each numerical value represents the remaining 1,3-DHB in the solution.

Time (min)	$[1,3\text{-DHB}]_0=100\ \mu M$				
	pH=3.5	pH=5.4	pH=9.0	pH=11.0	
0	100	100	100	100	
5	100	100	100	100	
10	100	100	94.9	95.9	
15	100	100	94.6	85.1	
20	100	100	93.8	82.5	
25	100	93.1	89.8	82.1	
30	100	92.7	88.4	63.3	
45	100	91.9	86.9	53.5	
60	92.4	87.7	81.2	44.6	

Table 5.2.3. Effect of pH on the degradation of 1,3-DHB in the presence of TiO_2.

Each numerical value represents the remaining 1,3-DHB in the solution.

Time (min)	$[1,3\text{-DHB}]_0=100\ \mu M$			
	pH=3.5	pH=5.4	pH=9.0	pH=11.0
0	100	100	100	100
5	92.6	79.9	61.8	91.8
10	84.7	71.1	52.3	63.7
15	83.4	49.2	28.8	53.9
20	80.1	27.9	27.5	38.6
25	75.7	24.6	21.1	27.5
30	32.1	17.4	16.1	17.1
45	25.3	2.71	1.19	1.53
60	21.9	1.35	0	0
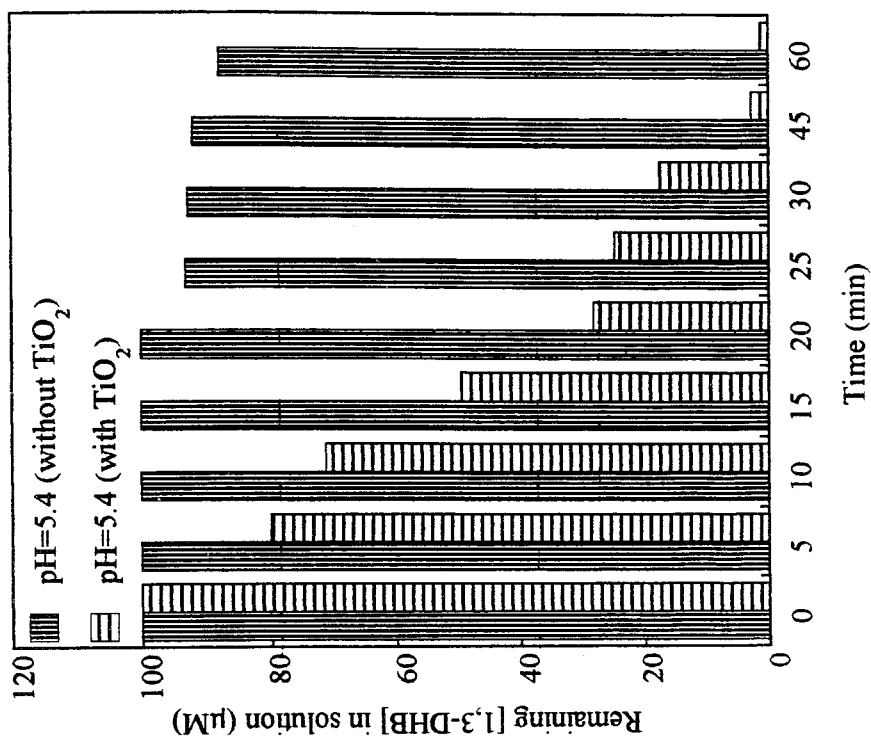
Figure 5.2.2. Remaining [1,3-DHB] in solution at pH=5.4 in the presence and in the absence of TiO$_2$.
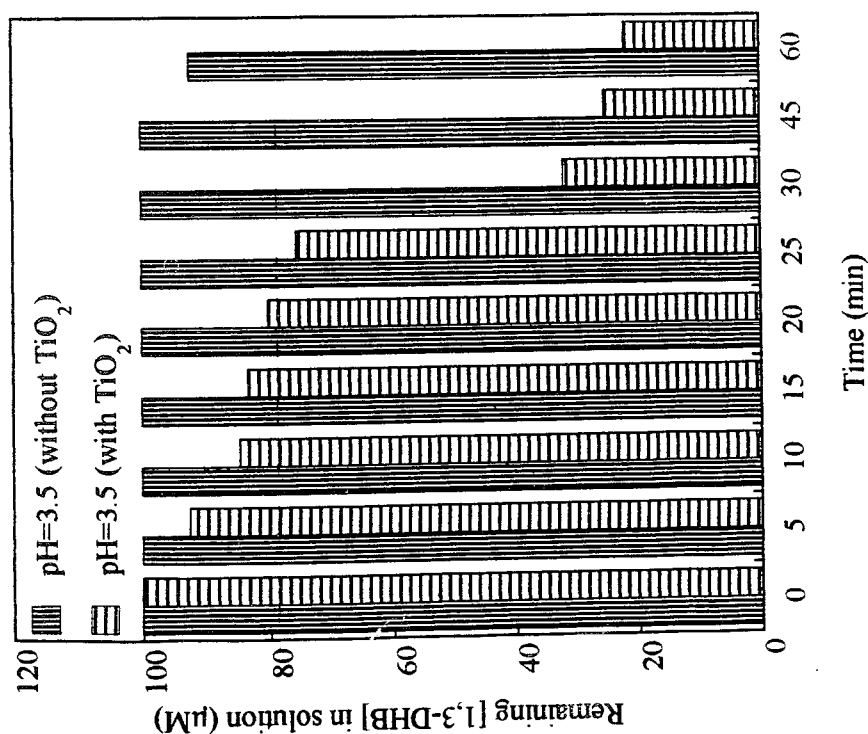
Figure 5.2.1. Remaining [1,3-DHB] in solution at pH=3.5 in the presence and in the absence of TiO$_2$.
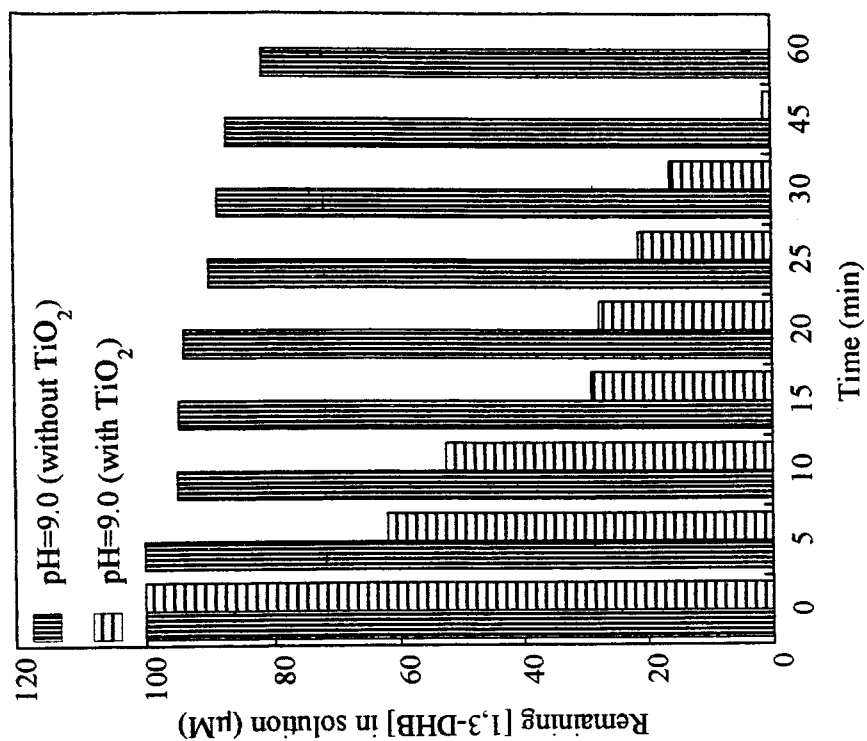
Figure 5.2.4. Remaining [1,3-DHB] in solution at pH=11.0 in the presence and in the absence of TiO_2.
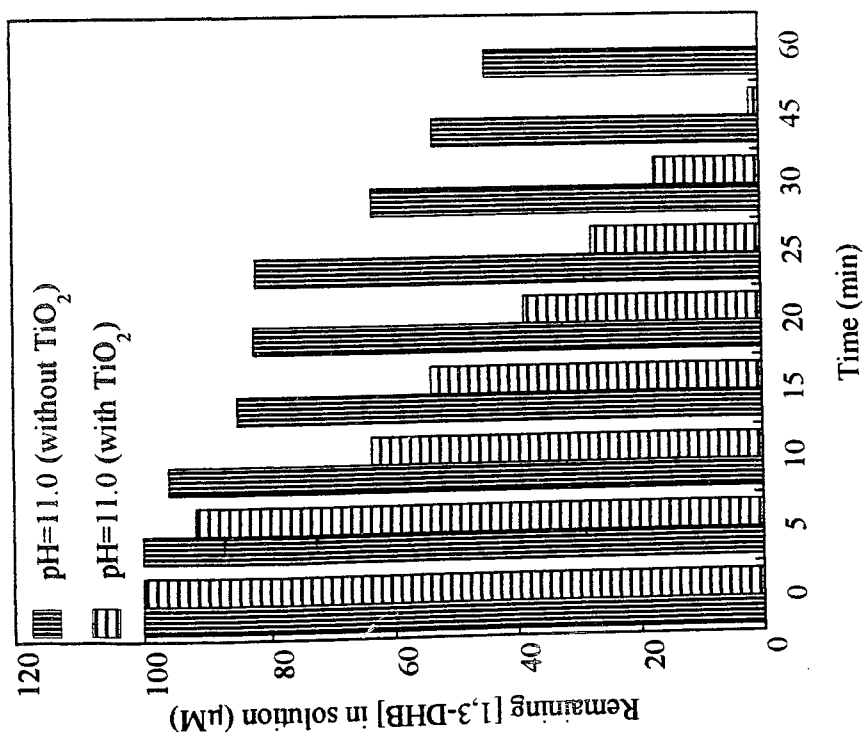
Figure 5.2.3. Remaining [1,3-DHB] in solution at pH=9.0 in the presence and in the absence of TiO_2.

surface of TiO_2 is still positive and favors negatively charged species. Thus, the decrease in the amount of 1,3-DHB in the solution phase can be due to the degradation not on the surface of TiO_2 but within a few monolayers around the TiO_2 particles. When results at pH 5.4 are compared those at pH 3.5, it is observed that the remaining amount of 1,3-DHB in the solution is lower, i.e. the degradation is higher. Since pH 5.4 is the natural pH of 1,3-DHB, no acid or base is added to regulate the pH of the medium. Thus, lack of the H^+ ion addition prevents the shift in the equilibrium (equation 5.14) to the left. In alkaline media, the surface of TiO_2 is negatively charged and favors positively charged species, but at pH 9.0 and 11.0, we observed higher degradation rates. At high pH, formation of $^{\bullet}OH$ radicals from adsorbed OH^- ions is favored [31] and the anionic form of 1,3-DHB is induced according to equation 5.14. These leads us to believe that 1,3-DHB photodegradation takes place in the fluid phase by oxidation with desorbed $^{\bullet}OH$ radicals.

The third set of experiments are performed to examine the effects of pH on 1,3-DHB decomposition. The formation of CO_2 is followed at different pH values; pH 3.5, pH 5.4, pH 7.0, and pH 9.0 (Figure 5.2.5 and Table 5.2.4). A linear increase in the formation of CO_2 is obtained in 40 min irradiation time and the highest rate is observed at pH 9.0 (Figure 5.2.5 inset). An analogous trend is obtained in the rate of degradation of 1,3-DHB and in the formation rate of CO_2 (Figure 5.2.6 and Table 5.2.5). The maximum degradation rate of 1,3-DHB and the maximum formation rate of CO_2 are both obtained at pH 9.0. However it should be noted for the formation of CO_2 at pH 11.0, the presence of CO_2 could not be analyzed. Under highly alkaline conditions, CO_2 remains in solution as CO_3^{2-} and therefore cannot be detected [52].
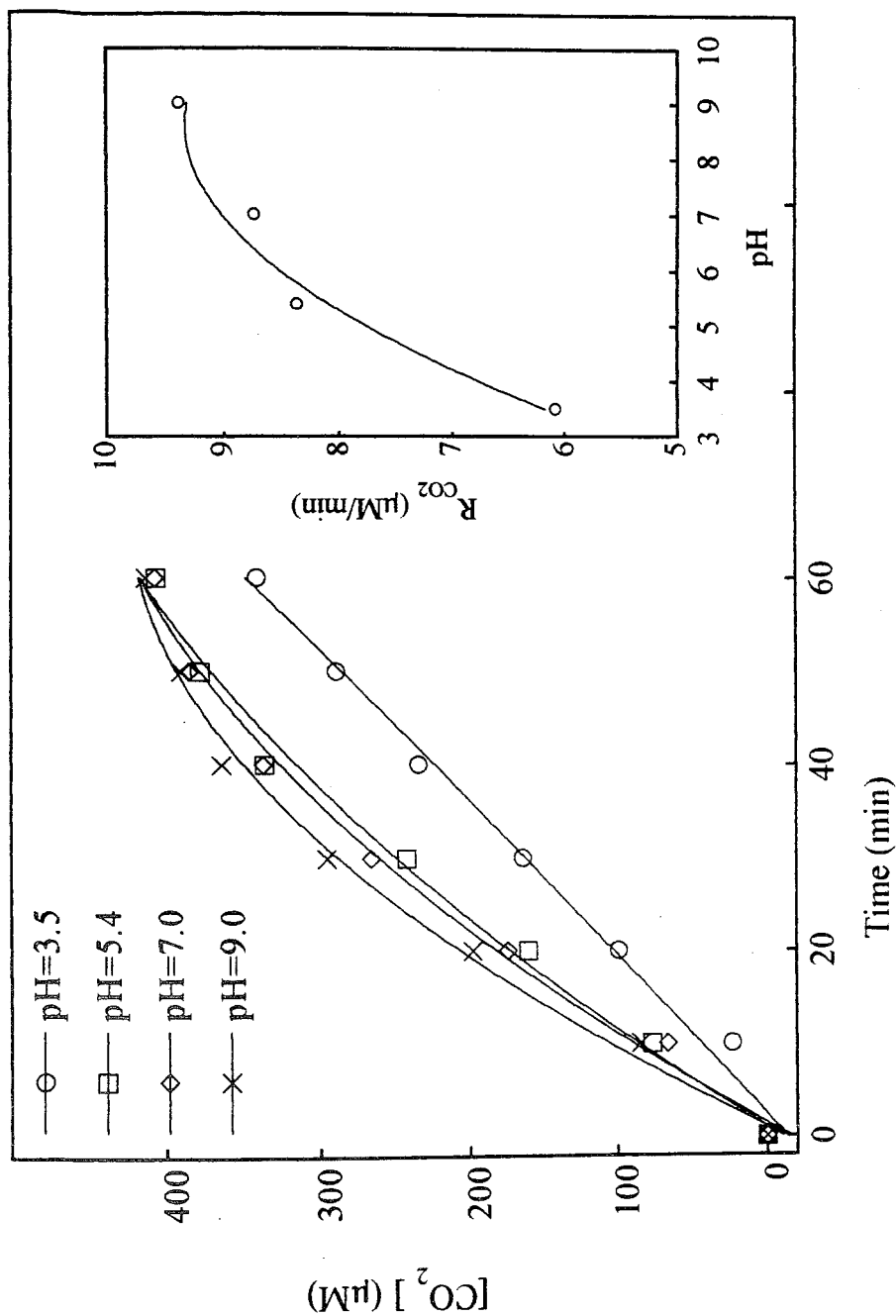
Figure 5.2.5. Effect of pH on the concentration of CO_2 produced.

Inset: R_{CO_2} as a function of pH.. Conditions: $[TiO_2]$=1g/L, Flow Rate=144 ml/min, $[1,3\text{-}DHB]_0$=100 μM, T=298 K, I_0=10.8x10^{-6} einstein/min.

Table 5.2.4. Effect of pH on the concentration of CO_2 produced.
Equations represent the linear portion of the data, i.e. 40 min irradiation time.

Time (min)	CO_2 (µM)			
	pH=3.5	pH=5.4	pH=7.0	pH=9.0
0	0	0	0	0
10	23.5	76.7	66.1	84.5
20	99.6	160	174	198
30	164	242	266	295
40	234	336	337	364
50	289	378	385	390
60	341	406	407	413
y= (µM) x= (min)	y=-17.5+6.09x R=0.989	y=-4.52+8.37x R=0.999	y=-6.16+8.74x R=0.997	y=0.61+9.39x R=0.997
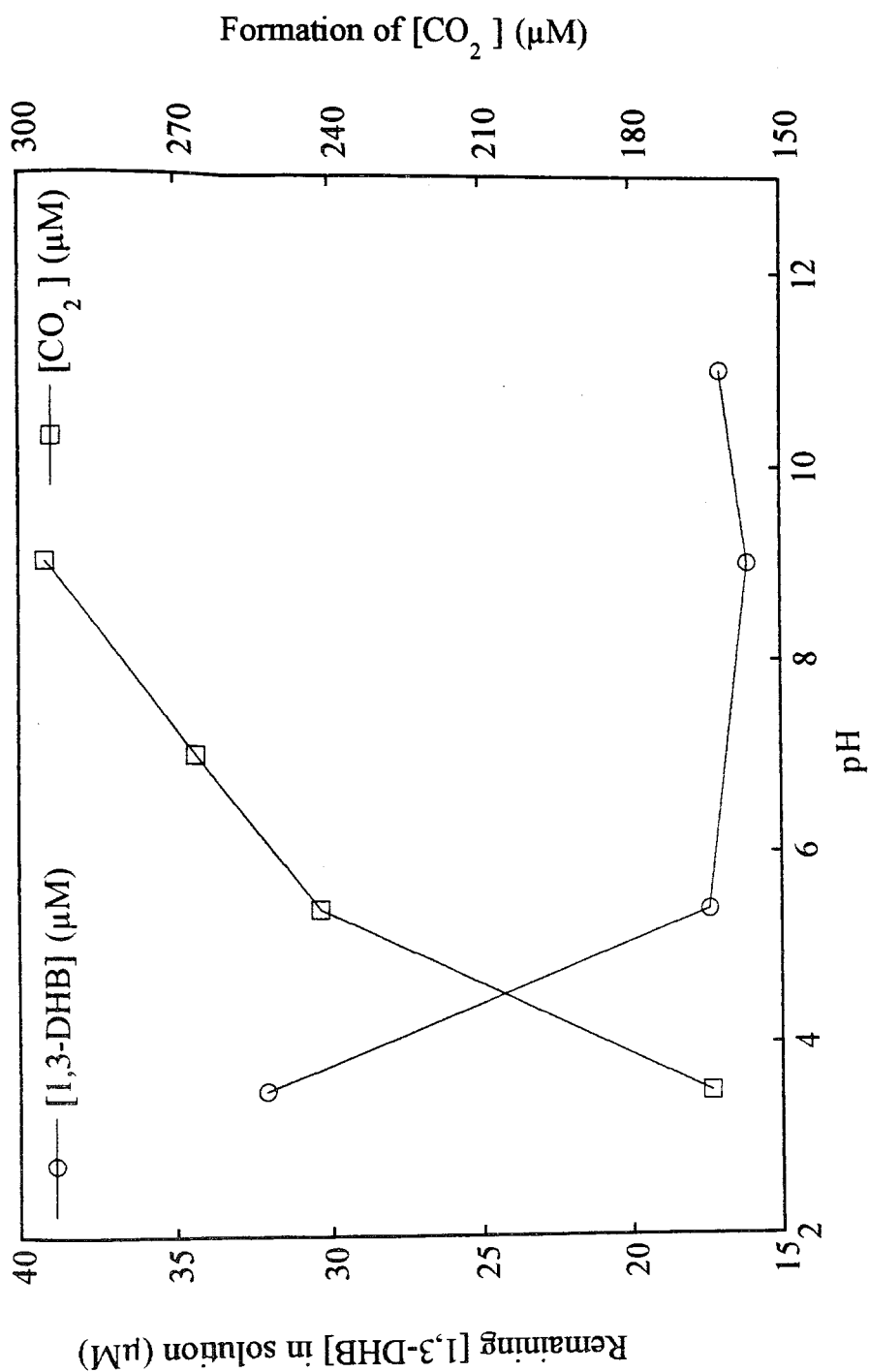
Figure 5.2.6. Concentration of CO_2 produced and remaining 1,3-DHB in solution as a function of pH after 30 min irradiation. Conditions: $[TiO_2]=1g/L$, Flow Rate=144 ml/min, $[1,3\text{-}DHB]_0=100\ \mu M$, T=298 K, $I_0=10.8\times10^{-6}$ einstein/min.

Table 5.2.5. Effect of pH on the formation of CO_2 and

on the concentration of 1,3-DHB remaining in solution after 30 min irradiation.

pH	[1,3-DHB] (μM)	CO_2 (μM)
3.5	32.1	164
5.4	17.4	242
7.0	-*	266
9.0	16.1	295
11.0	17.1	-*

*These points were not measured.

5.3. Effect of Irradiation Time

In Figure 5.3.1, the per cent decrease in the degradation of 1,3-DHB and the per cent increase in the formation of CO_2 are plotted together versus irradiation time, for 100 µM 1,3-DHB at its natural pH (5.4). At the end of one hour irradiation, 98.9 per cent destruction of 1,3-DHB is obtained (Table 5.3.1). The irradiation period increases in the formation of CO_2, suggesting that intermediate decomposition products compete with 1,3-DHB for the photogenerated radical oxidizing species.

Table 5.3.1. Effect of irradiation time.

1,3-DHB: Each numerical value represents the per cent of 1,3-DHB remaining in the solution. CO_2: Each numerical value represents the per cent of CO_2 formation.

Time (min)	Per cent 1,3-DHB	Per cent CO_2
0	100	0
5	79.9	0.61
10	71.1	12.8
15	49.2	20.5
20	27.9	26.6
25	24.6	38.8
30	17.4	40.3
45	2.71	61.1
60	1.35	67.7
75	-	79.3
90	-	81.8
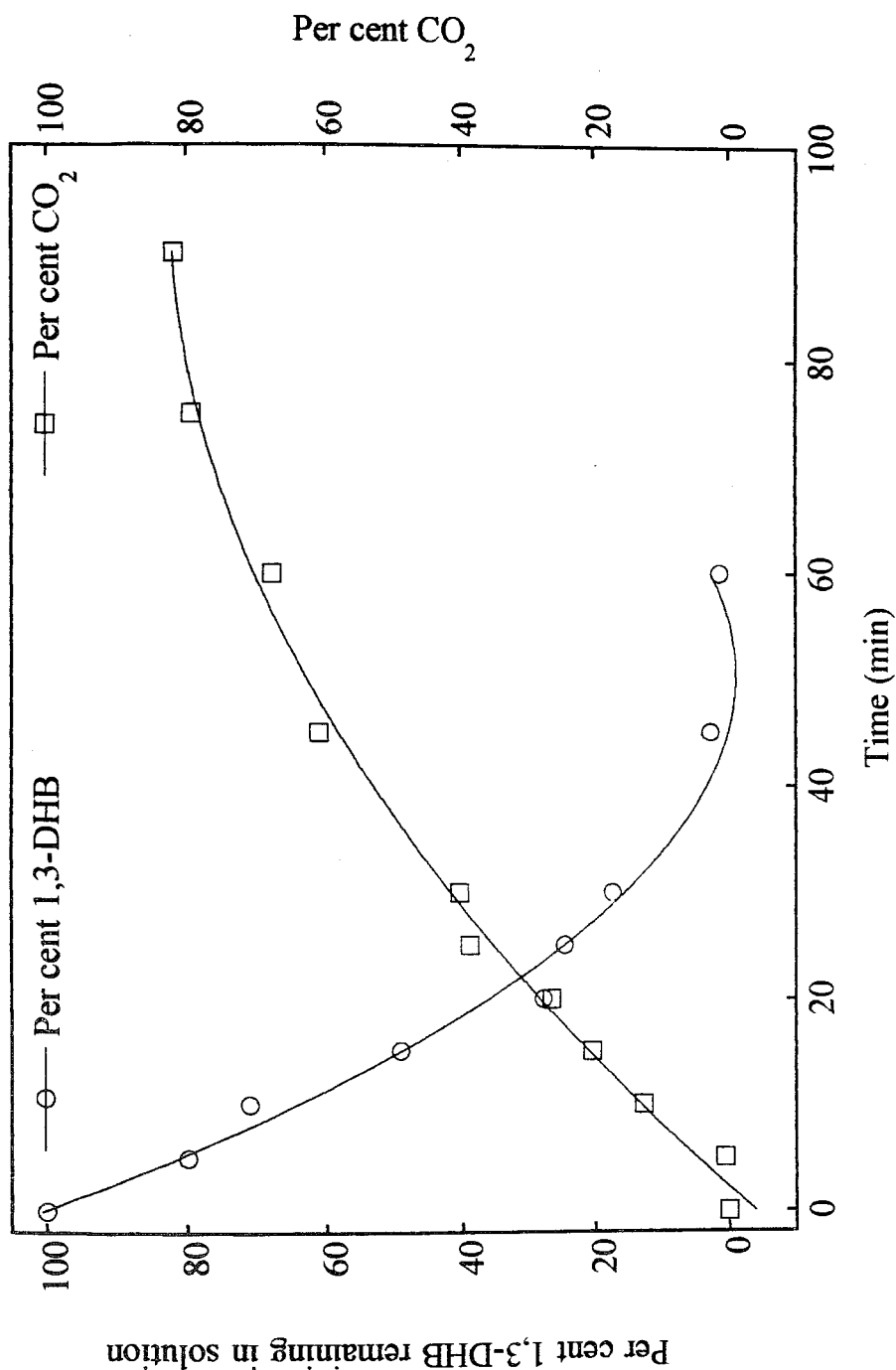
Figure 5.3.1. The per cent of 1,3-DHB remaining in solution and the per cent of CO_2 formation as a function of irradiation time. Conditions: $[TiO_2]=1g/L$, Flow Rate$=144$ ml/min, $[1,3-DHB]_0=100$ μM, pH$=5.4$, T$=298$ K, $I_0=10.8$x10^{-6} einstein/min.

5.4. Effect of Temperature

The effect of temperature on the rate of CO_2 formation is monitored in the range 298-333 K for irradiation times of 90 min (Figure 5.4.1, Table 5.4.1). In order to take into account the decrease in solubility of CO_2 with increasing temperature, calibrations are repeated under the same experimental conditions in the range 298-333 K (Appendix A). For all temperatures studied, the overall decomposition behaviour appears the same but with a decrease in decomposition times as temperature increases. This is indicative of an Arrhenius type behaviour and the rate of CO_2 production is found to be linear for irradiation times up to 30 min. The activation energy of 1,3-DHB degradation is deduced from the Arrhenius-type plot (Figure 5.4.1 inset) and is found to be 11.2 kJ/mol.

Comparing the activation energy of 1,3-DHB with that of phenol and substituted phenols, it is seen that the reported activation energies of phenolic compounds usually lie in the range 5-16 kJ/mol. Okamoto *et. al.* [20] found the activation energy for phenol degradation as 10 kJ/mol. For 4-chlorophenol disappearance, the activation energy was found as 5.5 kJ/mol [33]. This low value was interpreted as resulting from the temperature independent adsorption/desorption processes. For 4-chlorophenol, under different experimental conditions, a term $\alpha(T)$ is used to take into account the decrease in the solubility of CO_2 with increasing temperature, and a measure of the true rate of CO_2 photogeneration is given by the term $\alpha(T)R_{CO_2}$. Thus the activation energy for 4-chlorophenol degradation was calculated from the $\ln[\alpha(T)R_{CO_2}$ vs $1/T]$ plot, and found as 16 ± 2 kJ/mol [37]. The activation energy for photooxidation of salicylic acid was determined to be 11.0 ± 0.8 kJ/mol [44].
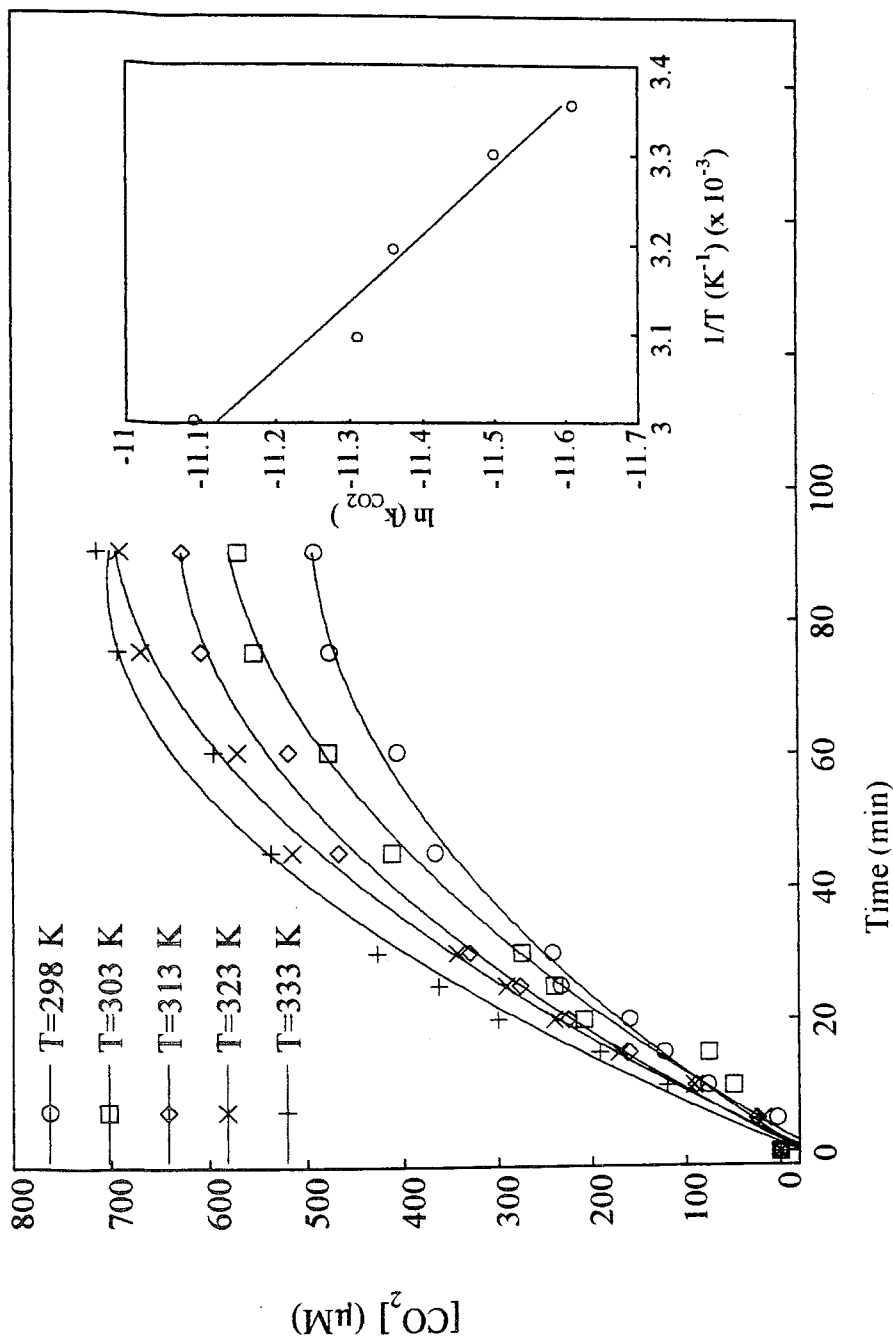
Figure 5.4.1. Effect of temperature on the concentration of CO_2 produced.

Inset: Arrhenius plot. Conditions: $[TiO_2]=1g/L$, Flow Rate=144 ml/min, $[3,5\text{-}DHT]_0=100$ µM, pH=5.4, $I_0=10.8\times10^{-6}$ einstein/min.

Table 5.4.1. Effect of temperature on the concentration of CO_2 evolved.

Equations represent the linear portion of the data, i.e. 30 min irradiation time.

Time (min)	CO_2 (µM) 298 K	303 K	313 K	323 K	333 K
0	0	0	0	0	0
5	3.62	0	24.4	18.2	23.8
10	68.1	49.1	89.1	91.3	120
15	123	75.4	160	171	192
20	160	208	225	240	300
25	233	240	276	291	363
30	242	274	330	343	427
45	366	411	467	514	536
60	406	477	518	570	594
75	476	553	607	668	692
90	491	569	626	689	713
y= (µM) x= (min)	y=-16.1+9.05x R=0.986	y=-27.3+10.1x R=0.960	y=-16.8+11.6x R=0.996	y=-19.7+12.3x R=0.994	y=-25.5+15.3x R=0.994

5.5. Effect of H_2O_2

Different concentrations of hydrogen peroxide were used to investigate its effect on the formation of CO_2 for the photocatalytic degradation of 1,3-DHB. Overall, addition of H_2O_2 is found to enhance the degradation of 1,3-DHB and lead to faster rates of CO_2 evolution. This effect is enhanced as H_2O_2 concentration is increased but seems to reach a limiting value around 5×10^{-3} M with little significant change being observed upon further increase of H_2O_2 concentration (Figure 5.5.1, Table 5.5.1).

The enhancement in the degradation rates observed upon H_2O_2 addition can be explained as follows: When H_2O_2 is added to the system, $^{\bullet}OH$ radicals are formed by the reaction of H_2O_2 with electrons (5.15). These radicals are then able to react with adsorbed 1,3-DHB (5.16) and produce CO_2 as a final product of the degradation process.

$$H_2O_2 + e^- \rightarrow {}^{\bullet}OH + OH^- \qquad (5.15)$$

$$C_6H_4(OH)_2 \text{ (ads)} + {}^{\bullet}OH \rightarrow \rightarrow CO_2 + H_2O \qquad (5.16)$$
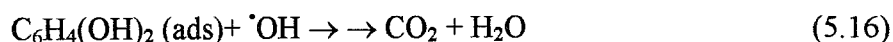
If excess H_2O_2 is used, $^{\bullet}OH$ radicals may either combine together to terminate the free radicals (5.17) or react with H_2O_2 to produce hydroperoxyl radicals, which are much less reactive compared to hydroxyl radicals (5.18). Thus, the amount of $^{\bullet}OH$ radicals for the oxidation process decreases. This results in a decrease in the amount of CO_2 evolved compared to the case with low concentrations of H_2O_2.
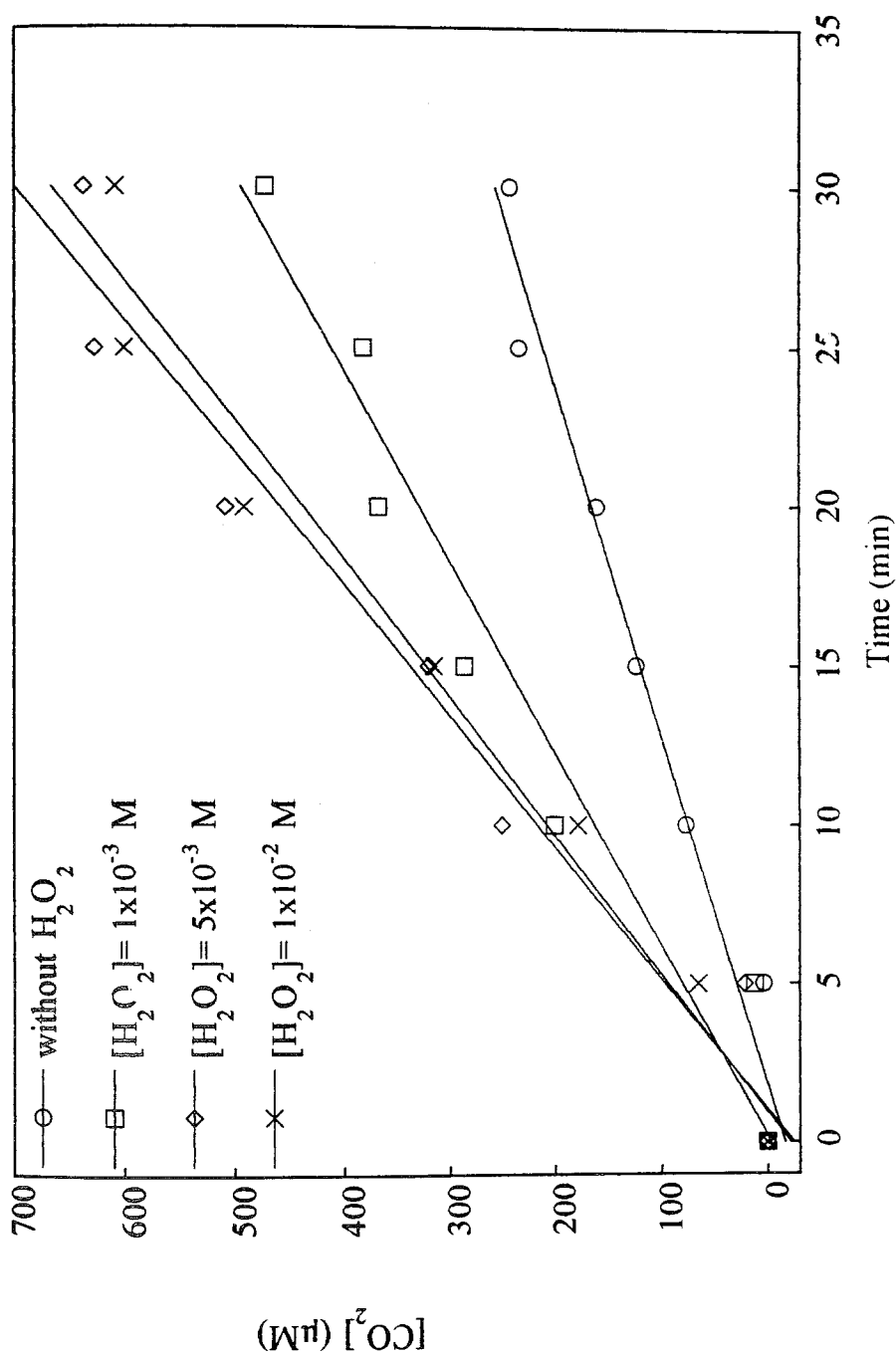
Figure 5.5.1. Effect of H_2O_2 concentration on the concentration of CO_2 produced.

Conditions: $[TiO_2]=1g/L$, Flow Rate=144 ml/min, $[3,5\text{-}DHT]_0=100\ \mu M$, $I_0=10.8\times10^{-6}$ einstein/min

pH=5.4, T=298 K.

Table 5.5.1. Effect of H_2O_2 concentration on the concentration of CO_2 evolved.

Time (min)	CO_2 (μM)			
	Without H_2O_2	1×10^{-3} M	H_2O_2 5×10^{-3} M	1×10^{-2} M
0	0	0	0	0
5	3.63	11.9	21.4	64.4
10	76.7	200	250	178
15	123	286	320	315
20	160	367	508	491
25	233	381	627	600
30	242	472	637	608
y= (μM)	y=-16.1+9.06x	y= -3.28+16.6x	y=-24.5+24.1x	y=-21.4+22.9x
x= (min)	R=0.986	R=0.974	R=0.981	R=0.986

$$\cdot OH + \cdot OH \rightarrow H_2O_2 \qquad\qquad (5.17)$$

$$H_2O_2 + \cdot OH \rightarrow H_2O + HO_2\cdot \qquad\qquad (5.18)$$

When the experimental results are compared with photocatalytic mineralization of phenol in the presence of H_2O_2 [35], it is observed that increasing the H_2O_2 concentration from 1×10^{-3} M to 1×10^{-2} M decreases the formation rate of CO_2 (Table 5.5.2).

Table 5.5.2. Comparison between the rate of phenol degradation and the rate of 1,3-DHB degradation in the presence of H_2O_2 [35].

$[H_2O_2]$ (M)	k_{phenol} (μM/min)	$k_{1,3\text{-}DHB}$ (μM/min)
0	5.05	9.06
1×10^{-3}	15.67	16.58
5×10^{-3}	21.15	24.14
1×10^{-2}	19.19	22.92

The kinetics of reactions in the presence of H_2O_2 are different from those in a system without H_2O_2. Auguliaro *et. al.* [26], investigated phenol degradation in the presence of hydrogen peroxide and oxygen. On the basis of their results, the hydrogen peroxide, oxygen and phenol species adsorb onto the titanium dioxide surface according to their chemical nature, to their relative concentrations and to the physicochemical properties of the sites. They explained the destiny of photogenerated pairs according to the energetic levels of adsorbed species and on the rates of the charge transfer processes. They hypothesized that the parallel reactions of O_2 and H_2O_2 with photogenerated pairs show a second order kinetics for phenol degradation.

For 1,3-DHB photodegradation the same parallel reactions are valid since degradation does not occur in the absence of oxygen from the reacting mixture. When the effect of concentration is discussed, it is assumed that the oxygen adsorption step does not play an important role in the degradation rate due to the presence of sufficient O_2. However, in the presence of H_2O_2, O_2 adsorbed on the TiO_2 surface competes with H_2O_2 in the process of electron trapping. The radicals formed by the reaction between an electron and the adsorbed O_2 interact with 1,3-DHB by the following reactions (5.19-5.23):

$$O_2\,(ads) + e^- \rightarrow O_2^{\cdot-} \tag{5.19}$$

$$O_2^{\cdot-} + H^+ \rightarrow HO_2^{\cdot} \tag{5.20}$$

$$OH^-\,(ads) + h^+ \rightarrow {}^{\cdot}OH \tag{5.21}$$

$$C_6H_4(OH)_2\,(ads) + {}^{\cdot}OH \rightarrow HO^{\cdot}C_6H_4(OH)_2\,(ads) \tag{5.22}$$

$$HO^{\cdot}C_6H_4(OH)_2\,(ads) + HO_2^{\cdot} \rightarrow CO_2 + H_2O \tag{5.23}$$
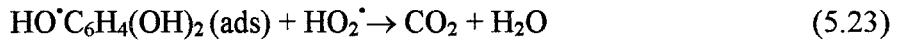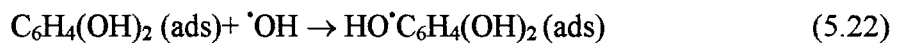
Both processes, i.e. the reactions between low concentrations of H_2O_2 and electrons, and the reactions between O_2 and electrons, generate radical species able to determine the oxidation of adsorbed 1,3-DHB. As a result, formation of CO_2 from 1,3-DHB degradation can occur through two parallel reaction pathways which is also assumed for phenol photodegradation [26]:

$$\frac{d[CO_2]}{dt} = (k_1 f_{H2O2} + k_2 f_{O2}) f_{1,3-DHB} \tag{5.24}$$

where k_1 is the rate constant of radical species produced by H_2O_2 photodecomposition, k_2 is the rate constant of radical species produced by O_2 photoreduction, f_{H2O2} is the fractional

coverage of H_2O_2 on TiO_2, f_{O2} is the fractional coverage of O_2 on TiO_2, and $f_{1,3\text{-DHB}}$ is the fractional coverage of 1,3-DHB on TiO_2. So, d[CO_2]/dt becomes;

$$\frac{d[CO_2]}{dt} = \frac{k_1 K_{H2O2}[H_2O_2] + k_2 K_{O2}[O_2]}{1 + K_{O2}[O_2] + K_{H2O2}[H_2O_2]} \quad \frac{K[C_6H_4(OH)_2]}{1 + K[C_6H_4(OH)_2]_0} \quad (5.25)$$

where K_{H2O2} is the adsorption constant of H_2O_2 on TiO_2, K_{O2} is the adsorption constant of O_2 on TiO_2, and K is the adsorption constant of 1,3-DHB on TiO_2.

The simultaneous presence of O_2 and H_2O_2 improves the 1,3-DHB degradation unless an excess concentration of H_2O_2 is used. Although both O_2 and H_2O_2 compete for adsorption onto the TiO_2 surface and for the charge transfer processes, they inhibit the electron-hole recombination reaction and they produce radical species essential for the degradation of 1,3-DHB. The two independent mechanisms for utilizing O_2 and H_2O_2 makes the 1,3-DHB degradation kinetics second-order.

5.6. Effect of Methanol

In photocatalytic reactions, the initiation of mineralization reactions starts with the attack of ˙OH radicals to the adsorbed molecules. In the presence of methanol, ˙OH radicals are known to react with methanol through abstraction of an hydrogen atom (5.26). Then, in the presence of oxygen, formaldehyde is formed as the stable product (5.27) [53].

$$\cdot OH + CH_3OH \rightarrow \cdot CH_2OH + H_2O \qquad (5.26)$$

$$\cdot CH_2OH + O_2 \rightarrow HCHO + HO_2\cdot \qquad (5.27)$$
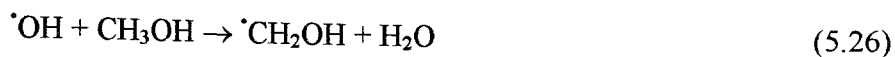
Therefore, the amount of $\cdot OH$ radicals which are available to react with adsorbed molecules decreases.

By the introduction of methanol into the reacting solution of 100 μM 1,3-DHB, we aim to follow the progress of degradation process with a decreased number of hydroxyl radicals. In one hour irradiation time, it is observed that rate of formation of CO_2 in the presence of methanol is 2.86 times smaller than that of CO_2 in the absence of methanol (Table 5.6.1, Figure 5.6.1). Therefore, the methanol decreases the yield of mineralization reaction.

Table 5.6.1. Formation of CO_2 in the presence and in the absence of methanol.

Time (min)	Without Methanol	With Methanol
0	0	0
10	3.63	0
20	76.7	10.1
30	123	27.1
40	160	40.6
50	233	66.1
60	242	93.3
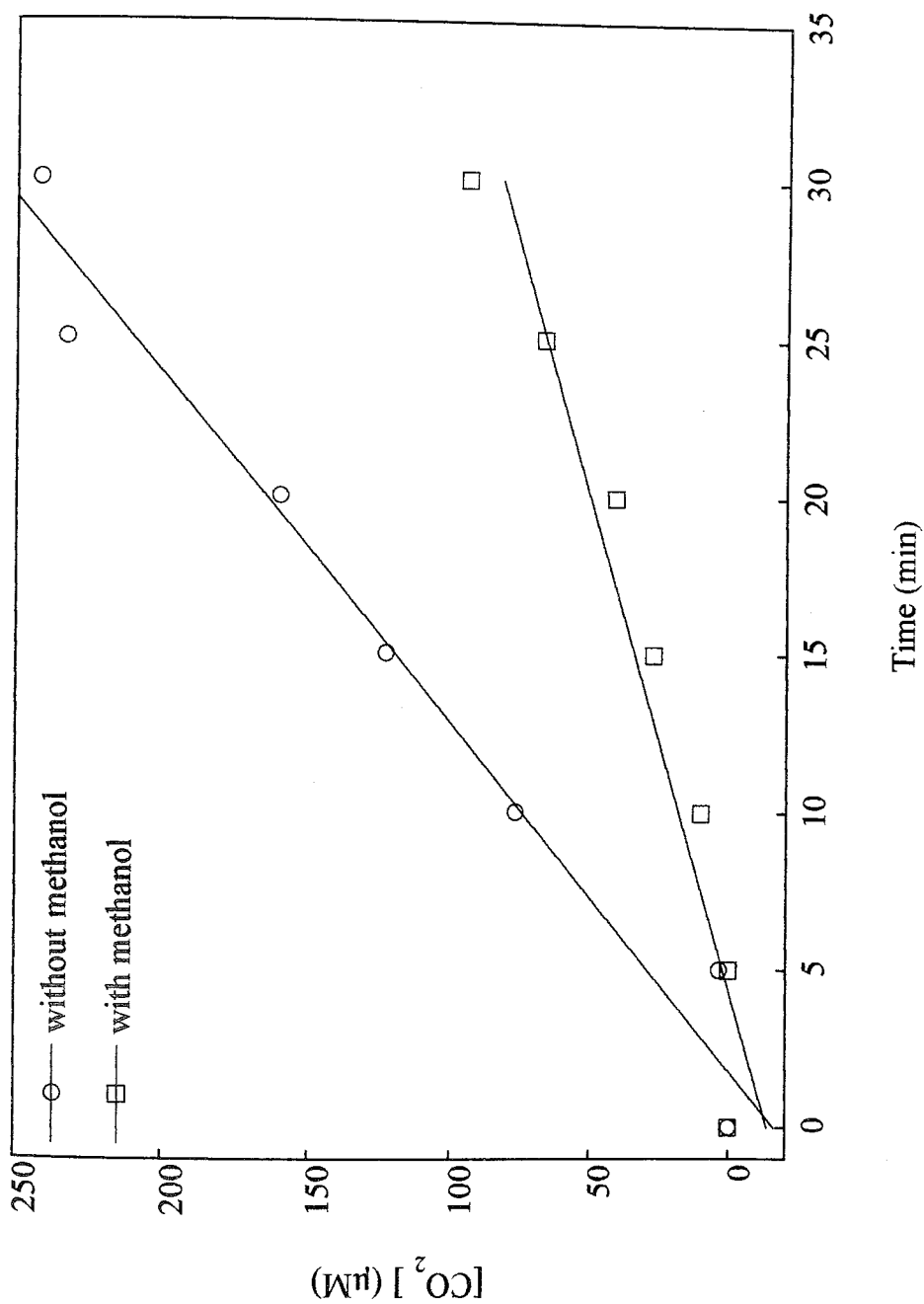
Figure 5.6.1. Effect of methanol addition on the concentration of CO_2 produced.

Conditions: $[TiO_2]=1g/L$, Flow Rate=144 ml/min, $[3,5\text{-}DHT]_0=100$ μM, $I_0=10.8\times10^{-6}$ einstein/min

pH=5.4, T=298 K.

5.7. Effect of Incident Photon Flux

The incident photon flux for each lamp is measured using potassium ferrioxalate actinometry which is based on the photochemical conversion of the ferrioxalate ion into Fe(II) as described by Calvert and Pitts [54]. It is found that each lamp emits 1.8×10^{-6} einstein/min in the wavelength region (300–400nm).

When the per cent concentration of 1,3-DHB remaining in solution and the per cent of CO_2 formation are plotted together for 30 min irradiation time for various incident photon fluxes, the maximum amount of CO_2 formation and the minimum amount of 1,3-DHB concentration in solution, i.e. maximum degradation of 1,3-DHB, are obtained with six lamps (10.8×10^{-6} einstein/min) (Table 5.7.1, Figure 5.7.1).

Table 5.7.1. Effect of incident photon flux (I_0) in 30 min irradiation time. [1,3-DHB]: Each numerical value represents the per cent of 1,3-DHB remaining in the solution. [CO_2]: Each numerical value represents the per cent of CO_2 formation.

Number of lamps	I_0 (einstein/min) ($\times 10^{-6}$)	[1,3-DHB] (μM)	[CO_2] (μM)
-	-	100	0
1	1.8	88.7	3.25
2	3.6	81.6	11.7
3	5.4	69.9	21.3
4	7.2	62.4	31.5
5	9.0	54.9	39.7
6	10.8	17.4	40.3
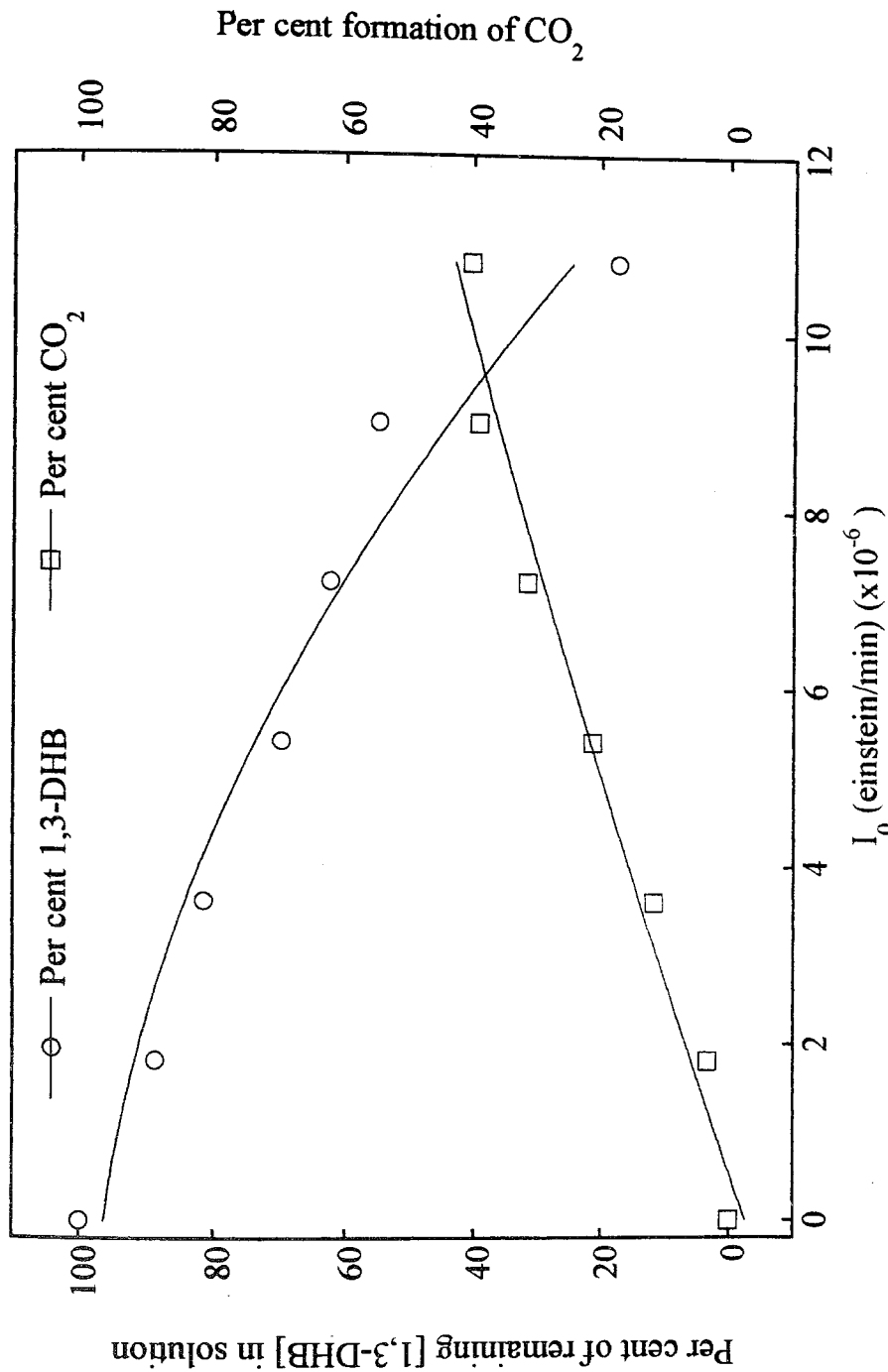
Figure 5.7.1. The per cent of 1,3-DHB remaining in solution and the per cent of CO$_2$ formation as a function of incident photon flux. Conditions: [TiO$_2$]=1g/L, Flow Rate=144 ml/min, [1,3-DHB]$_0$=100 μM, pH=5.4, T=298 K.

Figure 5.7.2 and Table 5.7.2 show the relation between formation of CO_2 and the incident photon flux, I_0. It indicates that increasing the number of lamps increases the amount of CO_2 formation from a 100 µM 1,3-DHB solution. This is because increasing the incident photon flux increases the production rate of electron-hole pairs. However, the opportunity for electron-hole recombination also increases. Thus, the relative number of the photoinduced carriers taking part in the redox reactions on the surface of TiO_2 decreases. This results in a decrease of formation rate of CO_2 when the flux is high (Figure 5.7.3, Table 5.7.3). When rate is plotted versus the square root of incident photon flux, a better linearity is obtained, which indicates the validity of the above discussion (Figure 5.7.3 inset).

5.8. Determination of Quantum Yield

TiO_2 particles are not capable of absorbing all the incident photon flux from a given source due to the light scattering off the particle surface. Sun and Bolton [53] used an integrated sphere to estimate the fraction of light absorbed in a TiO_2 suspension. The principle of the integrated sphere model is that, when incident light of flux I_0 passes through a sample, light both from that transmitted through the sample and that scattered from the particles, can be completely reflected by an inner highly reflecting surface. The light radiation level in the sphere can then be monitored by a detector.

In Figure 5.8.1, a reference solution without particles is put at position b between a reflection plate and the sphere.
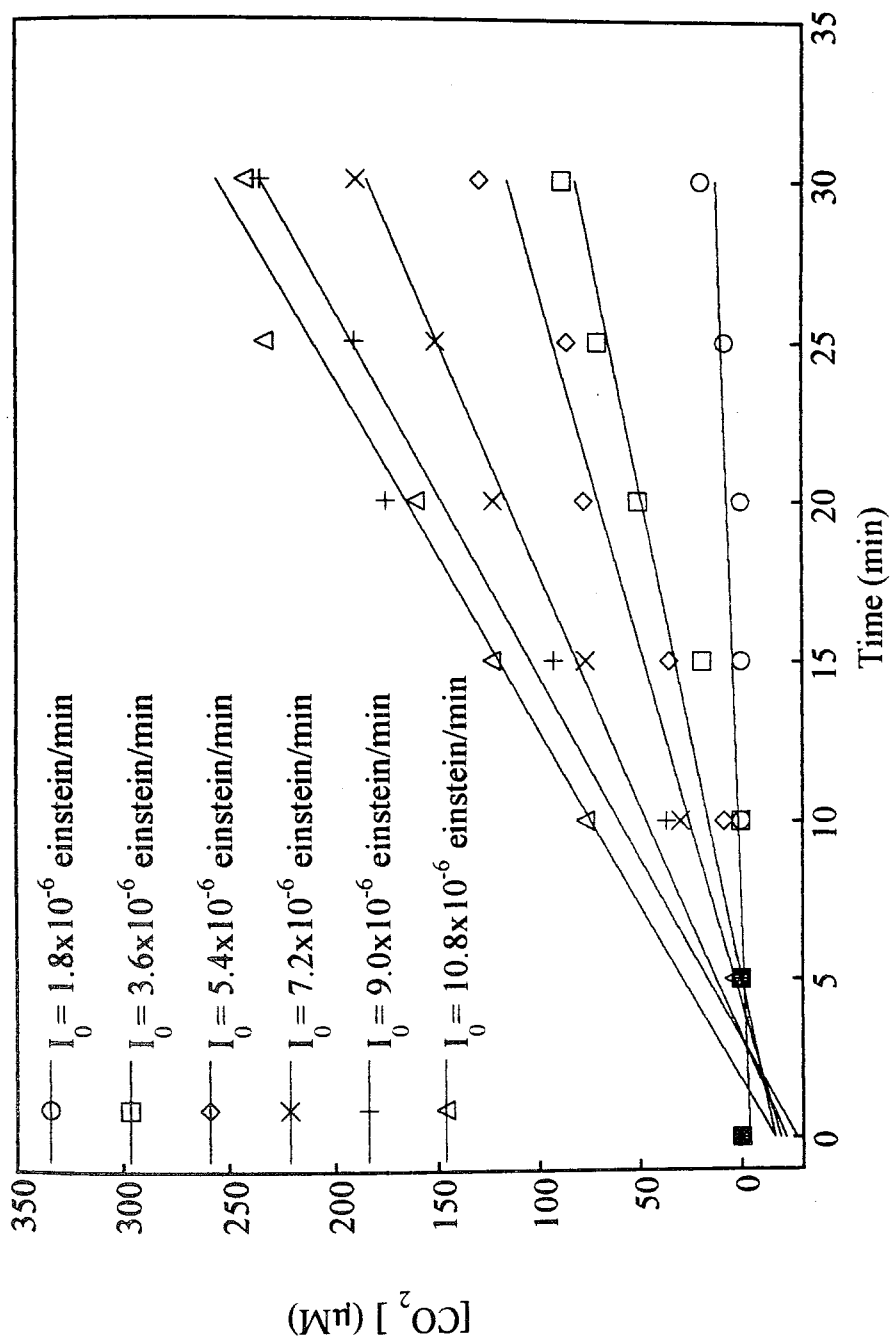
Figure 5.7.2. Effect of incident photon flux on the concentration of CO_2 produced.

Conditions: $[TiO_2]$=1g/L, Flow Rate=144 ml/min, $[1,3\text{-DHB}]_0$=100 μM, pH=5.4, T=298 K.

Table 5.7.2. Effect of incident photon flux on the concentration of CO_2 evolved.

Time (min)	I_0 (einstein/min)					
	1.8×10^{-6}	3.6×10^{-6}	5.4×10^{-6}	7.2×10^{-6}	9.0×10^{-6}	10.8×10^{-6}
0	0	0	0	0	0	0
5	0	0	0	0	1.51	3.62
10	0	0	8.36	29.7	36.7	76.7
15	0	18.8	35.1	76.5	92.3	123
20	0	50.1	77.1	122	175	160
25	7.62	61.6	85.1	150	190	233
30	19.5	70.1	128	189	235	242
y= (μM) x= (min)	y=-4.02+0.53x R=0.763	y=-16.1+2.06x R=0.950	y=-19.1+4.44x R=0.962	y=-21.8+6.85x R=0.985	y=-26.9+8.74x R=0.978	y=-16.1+9.06x R=0.986
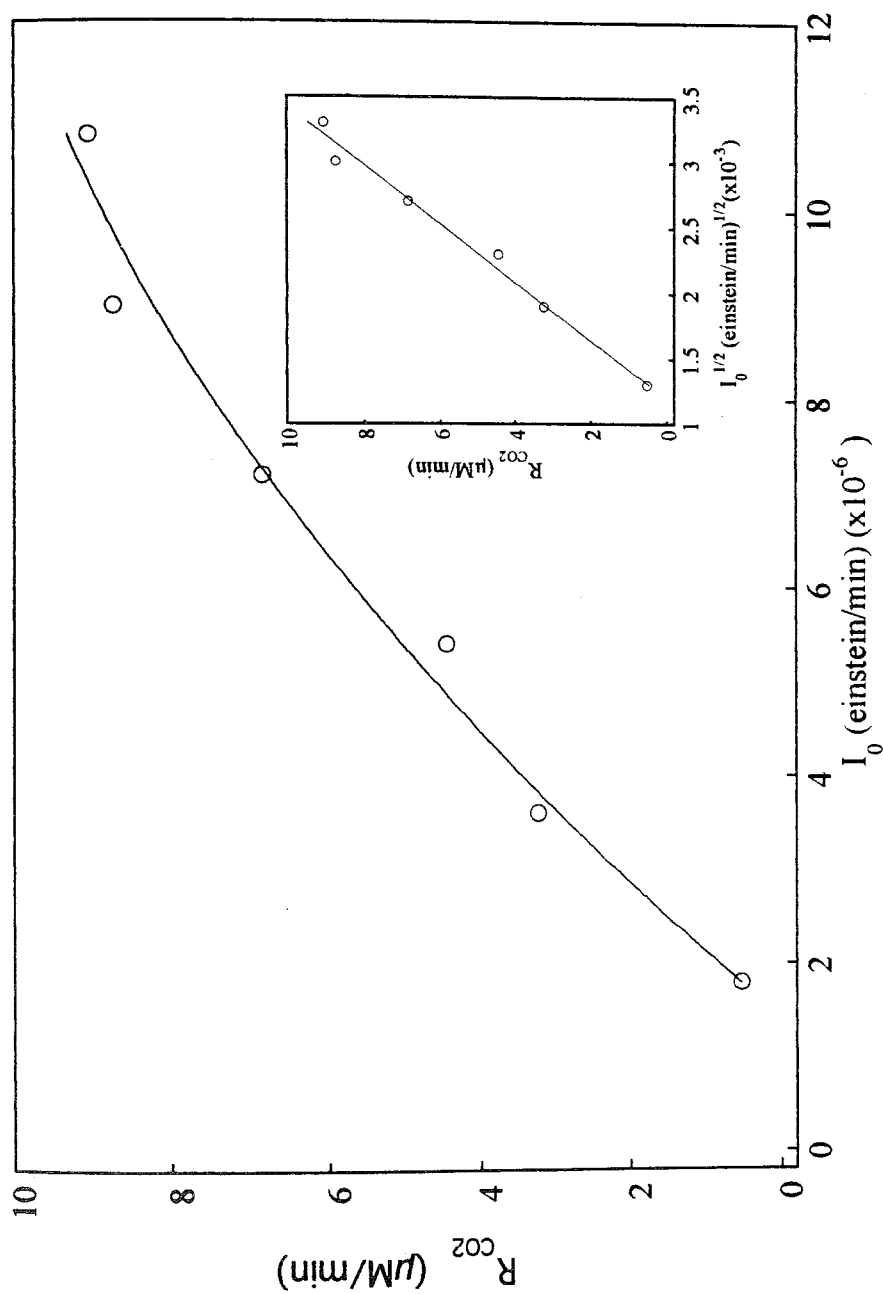
Figure 5.7.3. Rate of CO_2 production versus incident photon flux.

Inset: R_{CO2} as a function of $1/(I_0)^{1/2}$. Conditions: $[TiO_2]=1g/L$, Flow Rate=144 ml/min, $[1,3\text{-DHB}]_0=100 \mu M$, pH=5.4, T=298 K.

Table 5.7.3. Effect of incident photon flux on the rate of CO_2 formation.

I_0 (einstein/min) ($\times 10^{-6}$)	$(I_0)^{1/2}$ (einstein/min)$^{1/2}$ ($\times 10^{-3}$)	R_{CO2} (mol/min) ($\times 10^{-7}$)
1.8	1.3	1.06
3.6	1.9	4.11
5.4	2.3	9.18
7.2	2.7	13.7
9.0	3.0	17.4
10.8	3.3	18.1
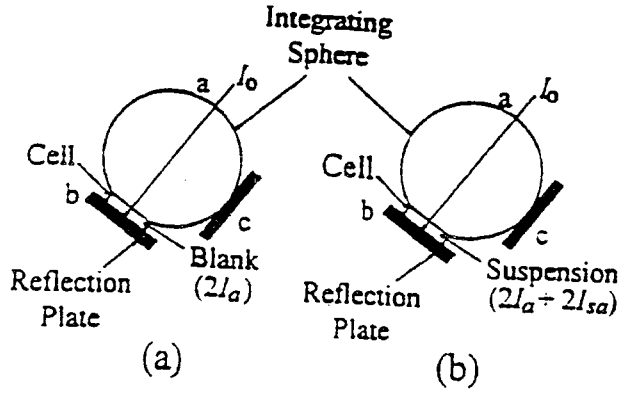
Figure 5.8.1. Integrating sphere assembly used for the absorbance measurement of a suspension: (a) reference measurement; (b) sample measurement [53].

The instrumental reading A_1 is;

$$A_1 = -\log \frac{I_0 - 2I_a}{I_0} \tag{5.28}$$

where I_0 is the incident photon flux, I_a is the photon flux absorbed by the homogeneous solution, and the coefficient 2 arises from the fact that the incident light passes through the solution twice, once when incident light passes through the solution and then it reflects from the reflection plate. When a sample containing a suspension is put at the same position as that of the homogeneous solution, the instrumental reading A_2 is;

$$A_2 = -\log \frac{I_0 - 2I_a - 2I_{sa}}{I_0} \tag{5.29}$$

where I_{sa} is the photon flux absorbed by particles in the suspension. From equations 5.28 and 5.29, the fraction of light absorbed by the particles, f, is;

$$f = \frac{I_{sa}}{I_0} = \frac{10^{-A1} - 10^{-A2}}{2} \tag{5.30}$$

Serpone [16] used the integrating sphere method to determine the fraction of light absorbed by Degussa P25 TiO_2. It is found that there is a significant deviation between the absorbance spectra of the 100 mg/L titania sample using the integrating sphere method and the spectrum of the titania sample obtained using normal spectroscopic methods. The fraction of light absorbed is found by the difference between the response of the instrument for a solution with no titania particles and the response of the instrument for the titania collodial. In the study, phenol was used as the standard process and the quantum yield, ϕ ($\phi = \zeta_r \phi_{Phenol}$) was determined from relative photonic efficiency, ζ_r, and the quantum yield for the photocatalyzed degradation of phenol (ϕ_{Phenol}).

In our study, we have selected 1,3-DHB as the standard probe and Degussa P25 as the standard photocatalyst. The effects of pH, concentration of reactant and temperature on ζ_r are examined for the photodegradation of three substituted 1,3-DHB's: 3,5-DHT, 1,3-DHMB and 3,5-DHBA. These results will be discussed in the related chapters.

Since 1,3-DHB is the standard probe, we need to know the apparent quantum yield for 1,3-DHB ($\phi_{1,3-DHB}$) to convert the relative photonic efficiencies into the corresponding quantum yields of photooxidation of 3,5-DHT, 1,3-DHMB and 3,5-DHBA ($\phi = \zeta_r \phi_{1,3-DHB}$). Since the appropriate instrumentation is not available in our laboratory, we want to find the

quantum yield for the photocatalyzed oxidative degradation of 1,3-DHB with the help of Serpone's results [16].

Serpone changed the TiO_2 loading from 0.1 to 4 g/L and estimated the fraction of light absorbed assuming Beer's Law to be followed at higher TiO_2 loadings. For 1 g/L TiO_2 loading and 3.058×10^{-6} einstein/min incident photon flux, the fraction of the absorption value was found as 0.1385. The following assumptions are used in our study:

1. We have monitored the formation of CO_2 varying the incident photon flux in the presence of 1 g/L TiO_2 (Figure 5.7.2). The second studied flux, with a value of 3.6×10^{-6} einstein/min, is close to the value 3.058×10^{-6} einstein/min with 1 g/L TiO_2 loading and a value of 0.1385 fraction of absorption in Serpone's paper. In order to find the fraction of light absorption with 3.6×10^{-6} einstein/min incident intensity, we multiply the value 0.1385, with a factor of 1.18 (assuming linearity between the incident photon flux and the fraction of light absorption), which comes from the ratio between 3.6×10^{-6} einstein/min and 3.058×10^{-6} einstein/min. As a result, the fraction of absorption for 3.6×10^{-6} einstein/min is found as 0.163 (Table 5.8.1).

Table 5.8.1. Fraction of light absorption "f" and quantum yield "ϕ" as a function of incident photon flux in the presence of 1g/L TiO_2.

TiO_2 Loading (g/L)	I_0 (einstein/min) ($\times 10^{-6}$)	f	ϕ
1.00	3.058*	0.1385*	0.14*
1.00	3.600	0.163**	0.21**

*: Values are from Serpone's paper for degradation of phenol [16].

**: Calculated fraction of absorption and quantum yield for degradation of 1,3-DHB.

2. Since absorption varies linearly with the incident photon flux, according to Beer's Law, we assume the same linearity between the fraction of light absorption and the incident photon flux. Thus, for the studied incident intensities, the corresponding fractions of absorptions and the quantum yields for the formation of CO_2 and for the degradation of 1,3-DHB in 30 min irradiation time are calculated (Table 5.8.2).

Table 5.8.2. Quantum yields as a function of incident photon flux.

[TiO$_2$]= 1.00 g/L					
I_0 (einstein/min) (x10^{-6})	f	R_{CO2} (mol/min) (x10^{-7})	$R_{1,3-DHB}$ (mol/min) (x10^{-7})	ϕ_{CO2}	$\phi_{1,3-DHB}$
1.8	0.082	1.06	0.75	0.72	0.51
3.6	0.163	4.11	1.23	0.70	0.21
5.4	0.245	9.18	2.01	0.69	0.15
7.2	0.326	13.7	2.51	0.58	0.11
9.0	0.408	17.4	3.01	0.47	0.08
10.8	0.489	18.1	3.11	0.34	0.06

R_{CO2}: Rate of formation of CO_2. $R_{1,3-DHB}$: Rate of degradation of 1,3-DHB.

The initial rates of formation of CO_2 and degradation of 1,3-DHB show deviations from linearity as the incident intensity increases (Figure 5.8.2 and inset). This is an expected result since increasing the photon flux increases the opportunity for electron-hole recombination. An analogous trend is observed when quantum yields are evaluated with respect to incident photon flux (Figure 5.8.3 and inset).
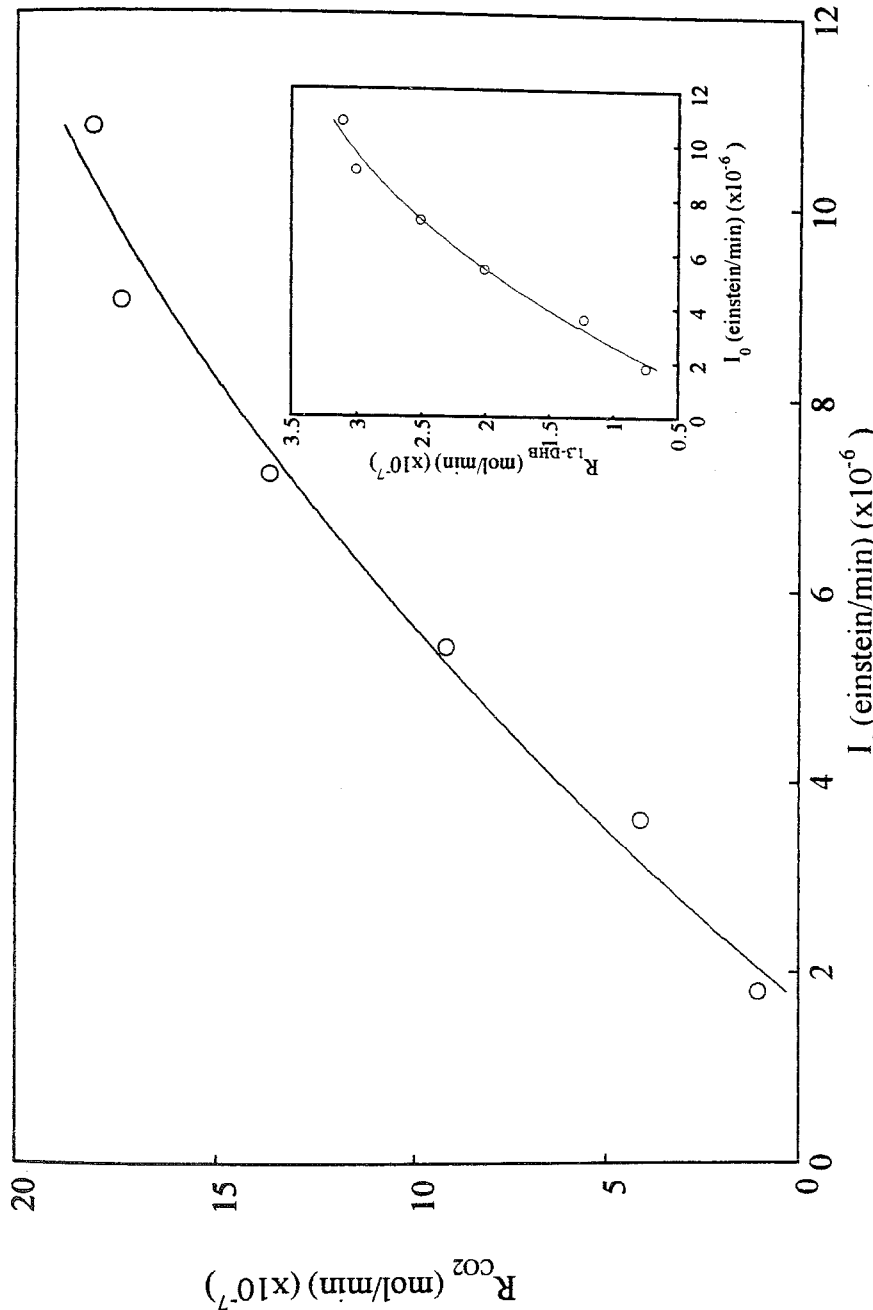
Figure 5.8.2. Rate of CO_2 production versus incident photon flux.

Inset: $R_{1,3-DHB}$ as a function of I_0. Conditions: $[TiO_2]$=1g/L, Flow Rate=144 ml/min, $[1,3-DHB]_0$=100 μM, pH=5.4, T=298 K.
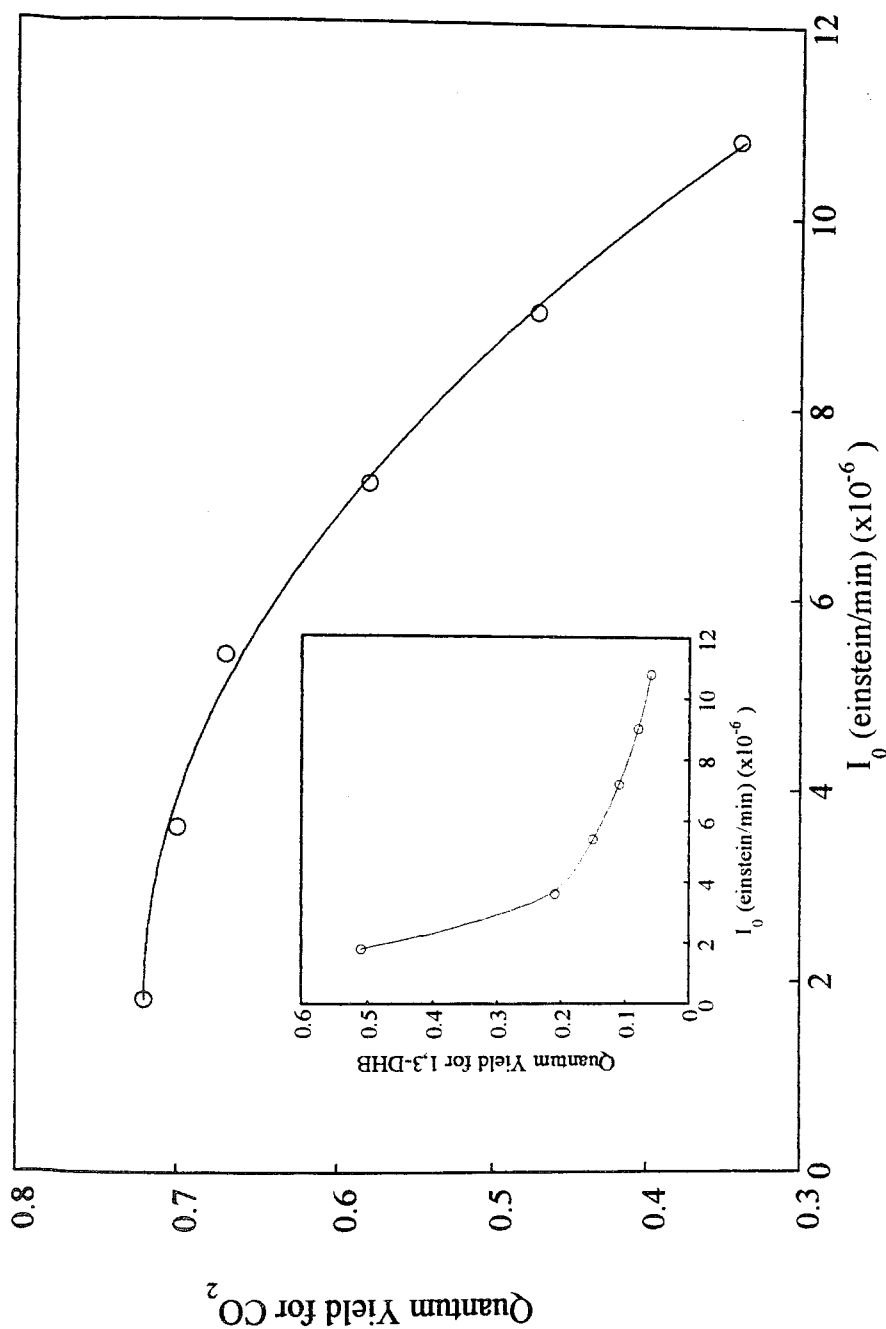
Figure 5.8.3. Quantum yield for CO_2 production as a function of incident photon flux.

Inset: Quantum yield for 1,3-DHB degradation as a function of I_0. Conditions: $[TiO_2]=1g/L$, Flow Rate=144 ml/min, $[1,3-DHB]_0=100$ μM, pH=5.4, T=298 K.

3. The amount of TiO_2 loading is also investigated for the production of CO_2 by using a constant incident photon flux, 10.8×10^{-6} einstein/min. Serpone estimated the fraction of light absorbed at concentrations greater than 0.10 g/L TiO_2 loadings by using Beer's Law. We made the same estimation for the concentrations greater and lower than 1.00 g/L TiO_2, i.e. a linear increase is assumed for concentrations greater than 1.00 g/L, and a linear decrease is assumed for concentrations lower than 1.00 g/L. Quantum yields are calculated according to the estimated fractions of absorption (Table 5.8.3).

Table 5.8.3. Quantum yields as a function of TiO_2 loadings.

$I_0=10.8 \times 10^{-6}$ (einstein/min)					
TiO_2 loading (g/L)	f	R_{CO2} (mol/min) $(\times 10^{-7})$	$R_{1,3-DHB}$ (mol/min) $(\times 10^{-7})$	ϕ_{CO2}	$\phi_{1,3-DHB}$
0.10	0.049	7.93	1.32	1.51	0.25
0.30	0.147	9.81	1.63	0.62	0.10
0.50	0.245	12.8	2.13	0.48	0.08
1.00	0.489	18.1	3.02	0.34	0.06
2.00	0.978	15.3	2.55	0.14	0.02
4.00	1.956	7.93	1.32	0.04	0.006

$R_{1,3-DHB}$: Calculated from the stoichiometric mineralization reaction (equation 5.1).

Figure 5.8.4 shows that the initial rate of CO_2 production and the initial rate of 1,3-DHB degradation increase linearly from 0.10 to 1.00 g/L loading and then exhibits a negative deviation at 4 g/L. Since, as the titania loading increases, the suspension becomes more opaque to light, only photons absorbed by titania particles onto which a 1,3-DHB molecule is pre-adsorbed may be effective in carrying out the redox chemistry. Dependence of quantum yields on the loading of TiO_2 are given in Figure 5.8.5. The decreasing trends in quantum yields as a function of TiO_2 loading are expected. However, the quantum yield for
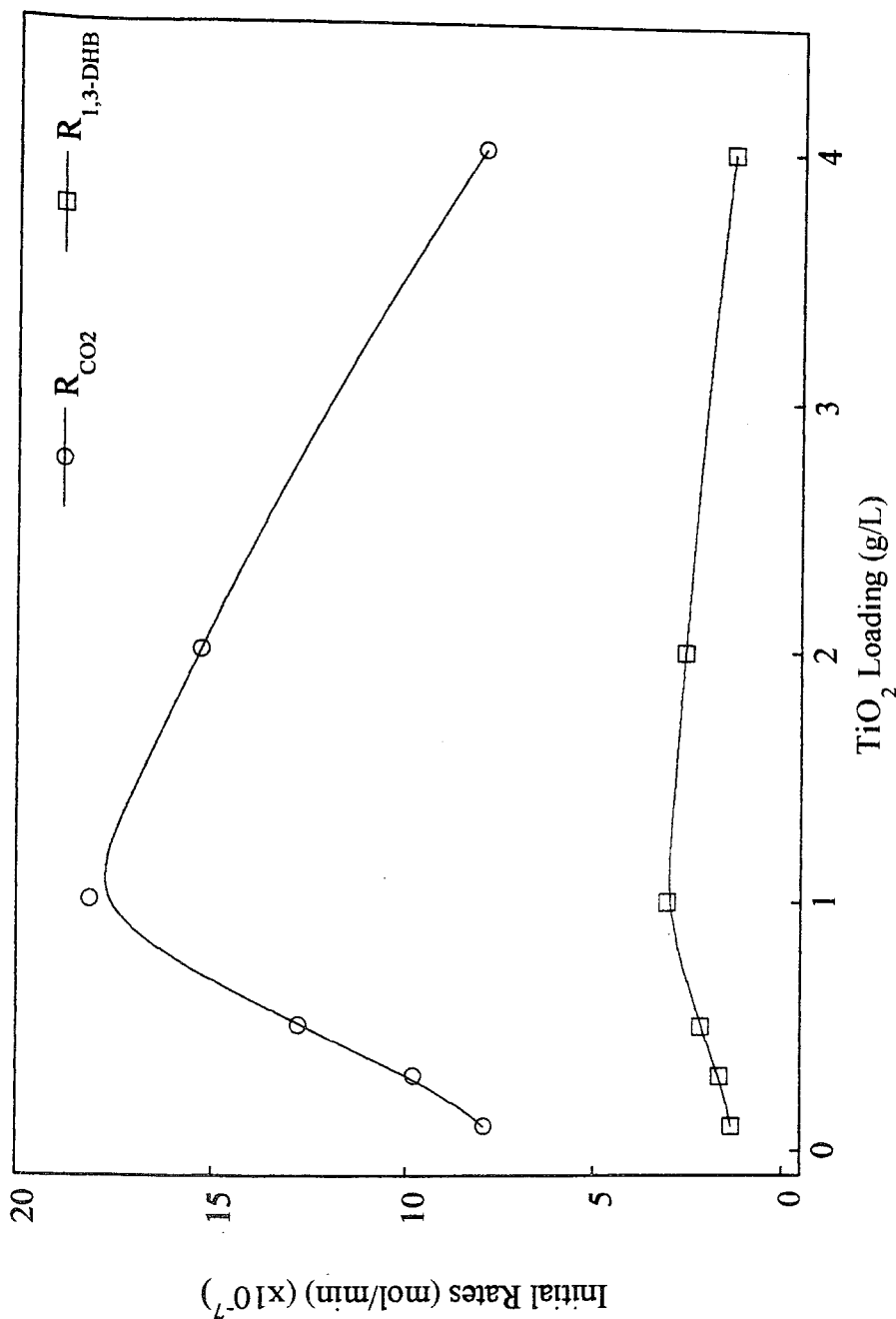
Figure 5.8.4. Initial rate of CO_2 production and initial rate of 1,3-DHB degradation as a function of TiO_2 loading. Conditions: Flow Rate=144 ml/min, $[1,3\text{-DHB}]_0$=100 µM, pH=5.4, T=298 K, I_0=10.8x10^{-6} einstein/min.
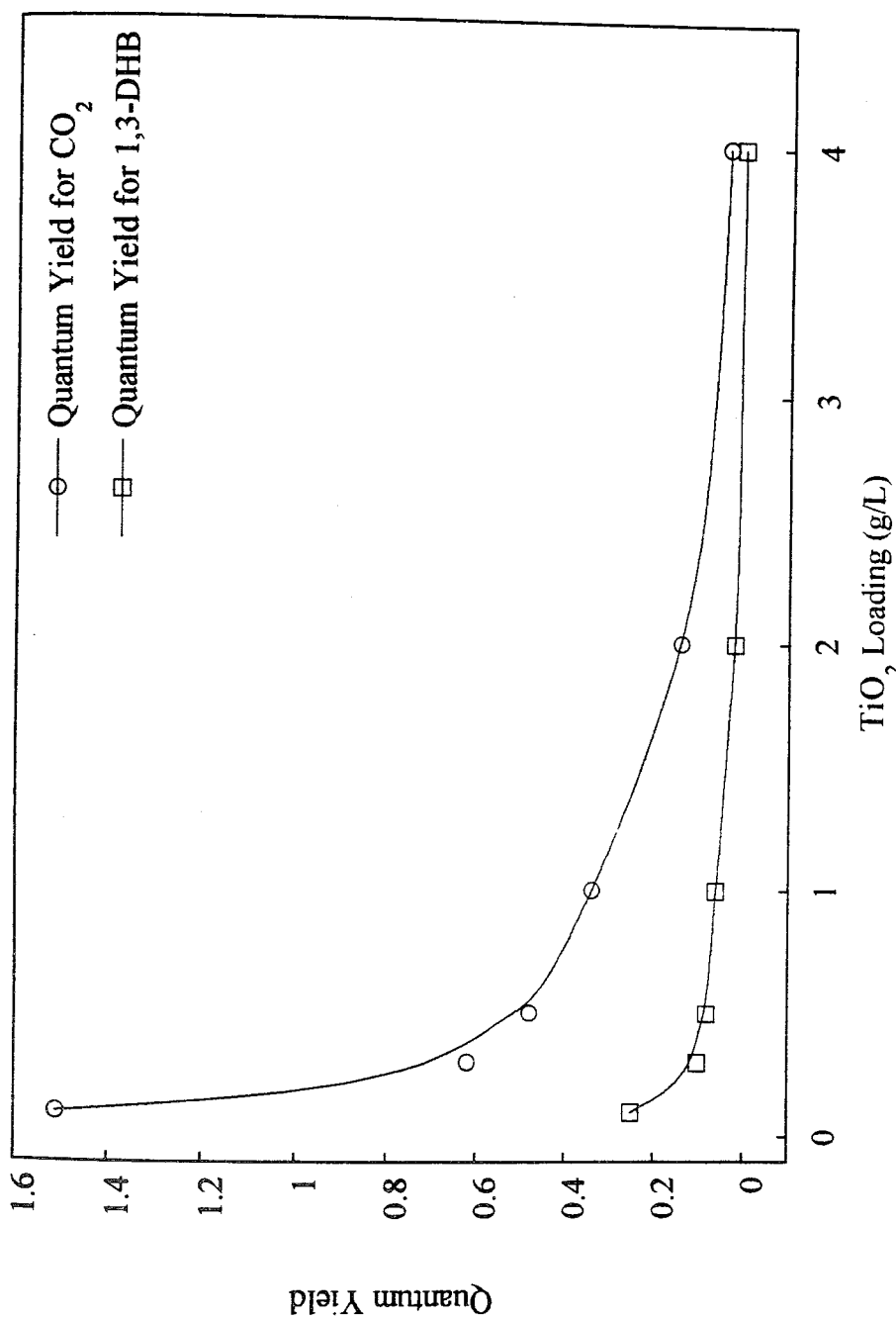
Figure 5.8.5. Quantum yield for CO_2 production and quantum yield for 1,3-DHB degradation as a function of TiO_2 loading. Conditions: Flow Rate=144 ml/min, $[1,3\text{-DHB}]_0$=100 μM, pH=5.4, T=298 K, I_0=10.8x10^{-6} einstein/min.

CO_2 formation in 0.10 g/L TiO_2 loading exceeds the maximum theoretical value of, 1.00. This suggests there is some error introduced in our use of Serpone's results to estimate quantum yields under different experimental conditions. A possible cause for this are the differences between the fractions of light absorption for phenol degradation and the fractions of light absorption for the formation of CO_2 in 1,3-DHB degradation. When these two fractions are plotted together (Figure 5.8.6), the ratio between the slopes is found as 4.40. If we correct the quantum yield of 1.51 according to slope ratio 4.40, we can obtain the quantum yield for 0.10 g/L TiO_2 loading as 0.34. Since we are looking for relative photonic efficiencies, and all data exhibit the expected increase according to Beer's law, this should not affect relative values.

Since throughout our study a TiO_2 concentration of 1 g/L and the incident photon flux of 10.8×10^{-6} einstein/min are used, the relative photonic efficiencies of the compounds 3,5-DHT, 1,3-DHMB and 3,5-DHBA will be discussed in chapters six, seven, and eight, respectively. They will be converted into the corresponding quantum yields using $\phi = \zeta_r \phi_{1,3\text{-DHB}}$ where $\phi_{1,3\text{-DHB}} = 0.06$, or $\phi = \zeta_r \phi_{CO_2}$ where $\phi_{CO_2} = 0.34$.
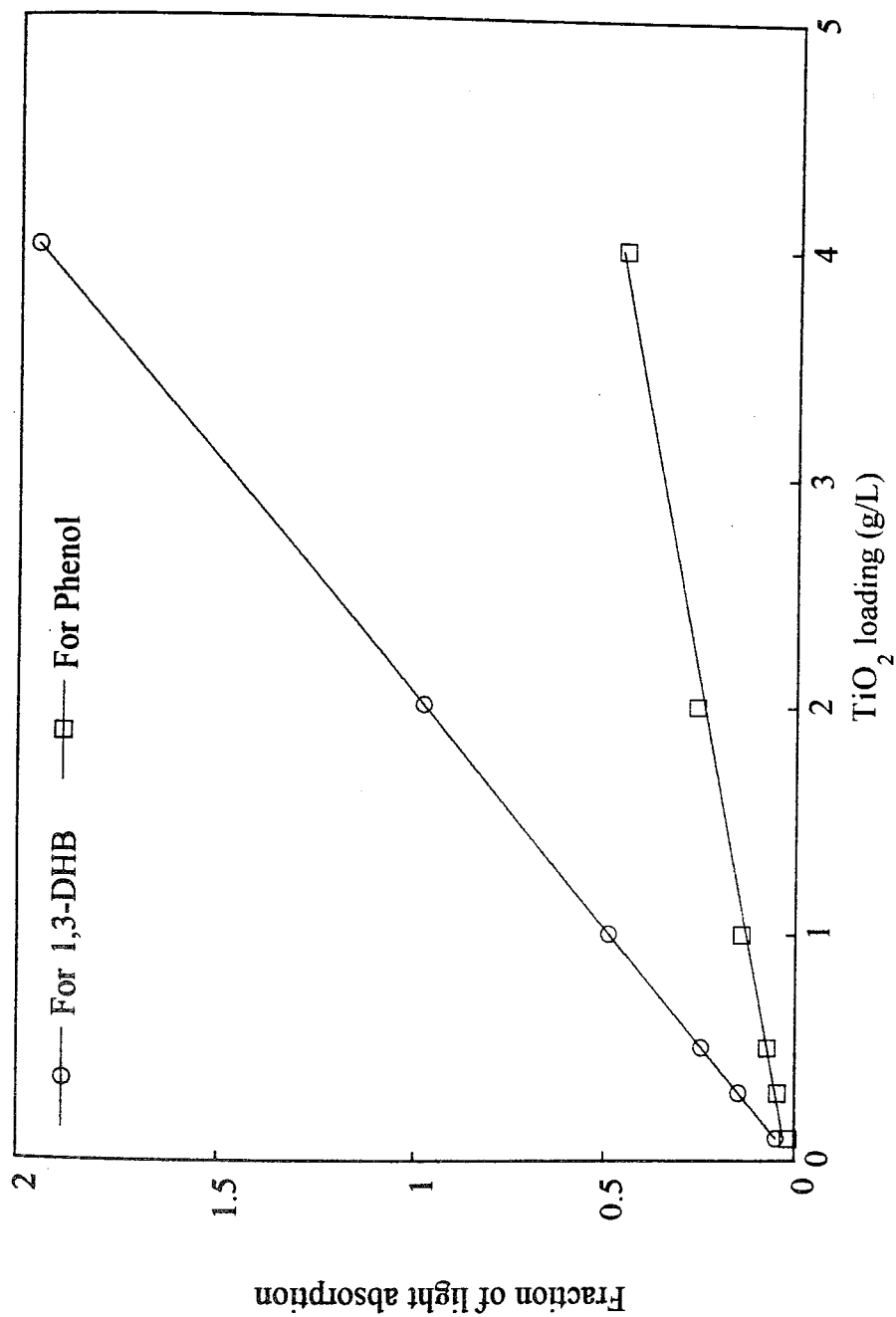
Figure 5.8.6. Comparison between fraction of light absorption for phenol degradation and the fraction of light absorption for the formation of CO_2 in 1,3-DHB degradation.

5.8. Postulated Mechanism: Route for Oxidation

A kinetic analysis is performed for the photocatalytic decomposition of phenol [Trillas,92], to ascertain which of the phenol decomposition routes are most important, i.e. direct phenol oxidation with photogenerated holes or reaction with ˙OH radicals. Following a similar mechanistic study, we can evaluate the route of oxidation of 1,3-DHB.

The following initial charge transfer steps together with their respective rate equations are considered for phenol (5.31-5.35). For the same purpose, we used the same charge transfer reactions and rate equations for 1,3-DHB ($C_6H_4(OH)_2$).

$$TiO_2 + h\nu \rightarrow h^+ + e^- \qquad I \qquad (5.31)$$

$$h^+ + e^- \rightarrow heat \qquad k_1\,[h^+] \qquad (5.32)$$

$$O_2 + e^- \rightarrow O_2^{\cdot-} \qquad k_2\,[O_2][e^-] \qquad (5.33)$$

$$OH^- + h^+ \rightarrow {}^{\cdot}OH \qquad k_3\,[OH^-][h^+] \qquad (5.34)$$

$$C_6H_4(OH)_2 + h^+ \rightarrow\rightarrow CO_2 + H_2O \qquad k_4[C_6H_4(OH)_2][h^+] \qquad (5.35)]$$
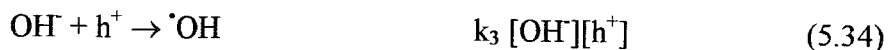
I is the rate of the light absorption by TiO_2 particles, k_1, k_2, k_3 and k_4 are the rate constants of the corresponding processes and $[e^-]$ is included in k_1. If a steady-state condition is assumed, i.e, the rate of photon arrival is equal to the rate of electron and hole consumption, then:

$$I = (k_1 + k_3\,[OH^-] + k_4\,[C_6H_4(OH)_2])\,[h^+] = k_2\,[O_2][e^-] \qquad (5.36)$$

The initial rate may be written as $R_i = k_4 [C_6H_4(OH)_2] [h^+]$, by assuming 1,3-DHB oxidation is the rate determining step. Then,

$$R_i = \frac{k_4[C_6H_4(OH)_2]I}{k_1 + k_3[OH] + k_4[C_6H_4(OH)_2]} \quad (5.37)$$

Assuming that rate of electron-hole recombination is very low compared to the rate of 1,3-DHB oxidation and $^{\cdot}OH$ radicals formation, then:

$$R_i = \frac{k_4[C_6H_4(OH)_2]I}{k_3[OH] + k_4[C_6H_4(OH)_2]} \quad (5.38)$$

and rearranging:

$$\frac{1}{R_i} = \frac{k_3[OH]}{k_4[I]} \frac{1}{[C_6H_4(OH)_2]} + \frac{1}{I} \quad (5.39)$$

According to this equation, when the reciprocal of the initial rate of CO_2 formation ($1/R_{CO2}$) versus $1/[C_6H_4(OH)_2]$ is plotted, the resulting graph should give a straight line. From our data, we obtain a straight line (Figure 5.1.3 inset), from which the slope; $k_3[OH]/k_4I$, is found as 9.2668. The rate of incident photon flux with the fraction of absorption 0.489, is calculated as 2.64×10^{-5} einstein dm^{-3} min^{-1} from the I_0 value (10.8×10^{-6} einstein/min) used throughout this study for a 200 ml reaction solution. Considering the natural pH (pH=5.4)

of 1,3-DHB, a ratio of $k_3/k_4 = 9.8\times10^4$ is deduced. This result implies that the formation of $^{\cdot}$OH radicals is more favored than that of the photogenerated holes for the oxidation of 1,3-DHB. The same trend is also obtained for phenol with a ratio of $k_3/k_4 = 3.8\times10^4$ [31].

6. 3,5-DIHYDROXYTOLUENE (3,5-DHT)

6.1. Effect of 3,5-DHT Concentration

The effect of 3,5-DHT ($C_7H_6(OH)_2$) concentration on the degradation process is examined in the range of 10 μM to 1000 μM (Figure 6.1.1, Table 6.1.1). The stoichiometric reaction for the complete mineralization of 3,5-DHT is given by:

$$C_7H_6(OH)_2 + 8O_2 \rightarrow 7CO_2 + 4H_2O \tag{6.1}$$
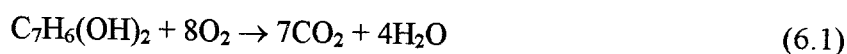
Two sets of experiments are performed to follow the stoichiometric reaction (6.1). The first set investigates the photocatalytic decomposition of 3,5-DHT at 5 min intervals for 30 min of irradiation, then at 10 min intervals untill 60 min irradiation, and at 30 min intervals following 60 min irradiation time for each concentration. A rapid decrease (around 50 per cent) in 3,5-DHT concentration is observed for 10 μM, 50 μM and 100 μM solutions after 5 min irradiation . However, for the highest concentration, 1000 μM, a lower initial decrease is obtained after 5 min irradiation. For the initial concentrations of 10 μM, 50 μM and 100 μM 3,5-DHT, 100 per cent degradation is achieved in 15 min, 40 min, 90 min irradiation times respectively. But, only 61 per cent degradation is obtained with 1000 μM solution after 180 min irradiation. Figure 6.1.1 inset (Table 6.1.2) shows the natural log of the ratio of the initial 3,5-DHT concentration to the concentration at given irradiation times. Linearity is observed for 10 μM to 1000 μM. Table 6.1.3 shows the apparent first order rate constants which decrease as the initial 3,5-DHT concentrations increase. Thus, the kinetics of 3,5-DHT decomposition are not truly first order in 3,5-DHT concentration, and can be described as pseudo-first order. Since an analogous trend is also obtained with 1,3-DHB, we may assume that all kinetic discussions made with 1,3-DHB are also valid for 3,5-DHT. Therefore, according to
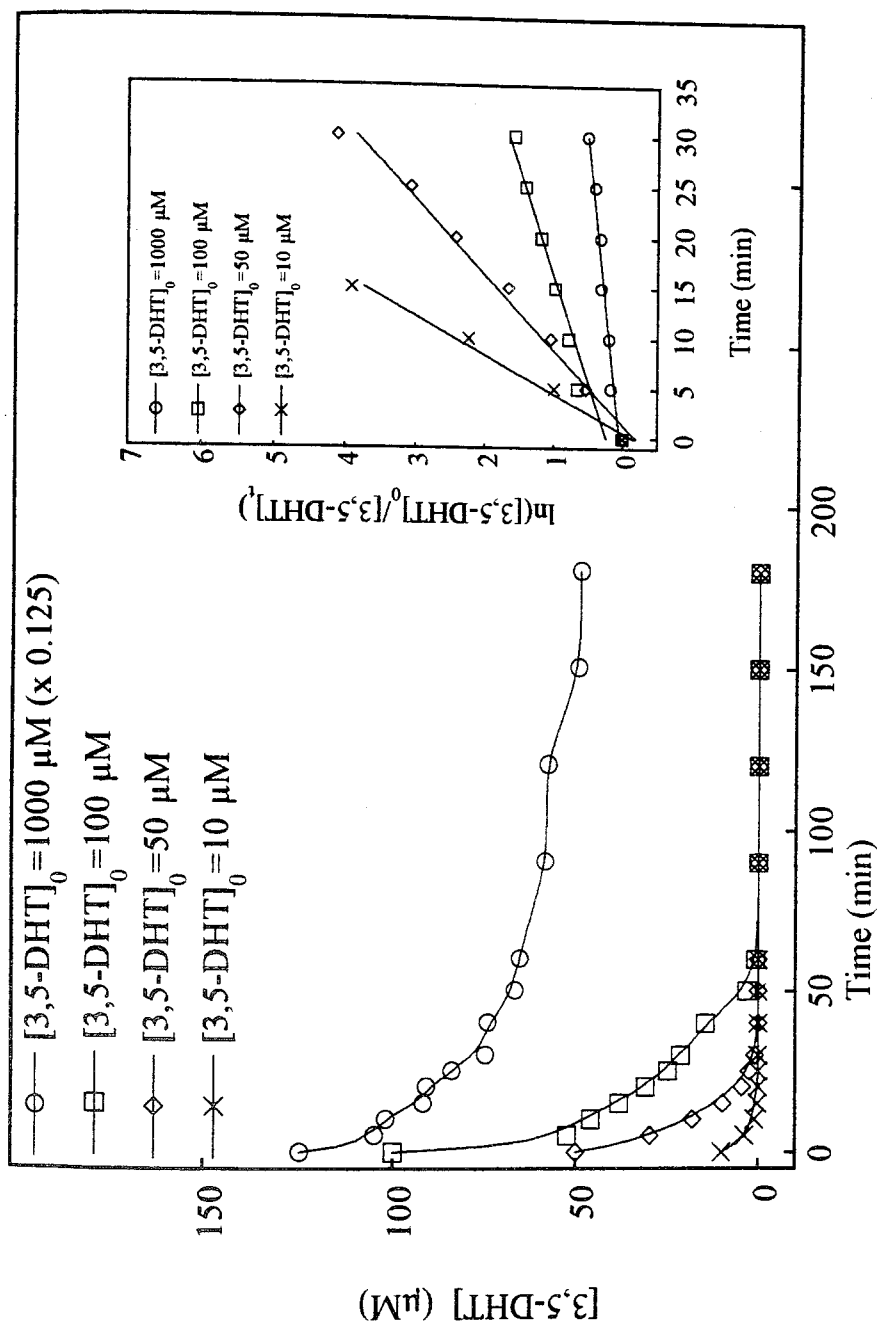
Figure 6.1.1. Effect of 3,5-DHT concentration on the degradation of 3,5-DHT.

Inset: Natural log of the ratio of the initial 3,5-DHT concentration at given irradiation times.

Conditions: $[TiO_2]=1g/L$, Flow Rate=144 ml/min, pH=5.2, T=298 K, $I_0=10.8 \times 10^{-6}$ einstein/min.

Table 6.1.1. Effect of 3,5-DHT concentration on the degradation of 3,5-DHT. Each numerical value represents the concentration of 3,5-DHT remaining in the solution.

Time (min)	$[3,5\text{-DHT}]_0$			
	1000 μM	100 μM	50 μM	10 μM
0	1000	100	50	10
5	840	52.3	29.5	3.69
10	815	45.7	17.8	1.07
15	735	37.9	9.57	0.21
20	728	30.8	4.49	0
25	672	24.6	2.36	0
30	599	21.1	0.82	0
40	594	14.3	0	0
50	535	3.12	0	0
60	524	0.62	0	0
90	468	0	0	0
120	462	0	0	0
150s	396	0	0	0
180	390	0	0	0

Table 6.1.2. $\ln([3,5\text{-DHT}]_0/[3,5\text{-DHT}]_t)$ versus time data as a function of initial 3,5-DHT concentration.

Time (min)	[3,5-DHT]$_0$			
	1000 μM	100 μM	50 μM	10 μM
0	0	0	0	0
5	0.17	0.65	0.53	0.99
10	0.20	0.78	1.03	2.23
15	0.31	0.97	1.65	3.91
20	0.32	1.18	2.41	-
25	0.40	1.40	3.06	-
30	0.51	1.56	4.11	-
y= (μM) x= (min)	y=0.165+0.01558x R=0.856	y=-0.102+0.061107x R=0.985	y=0.003+0.07899x R=0.990	y=-0.177+0.25378x R=0.992

equation 5.12, as the initial concentration of 3,5-DHT increases, the probability of $^{\cdot}OH$ radical generation decreases which then explains the decrease in the apparent first order rate constant.

TABLE 6.1.3. Kinetic data for 3,5-DHT degradation.

[3,5-DHT]$_0$ (μM)	k (1/min)	Rate (μM/min)
1000	0.015	15.58
100	0.061	6.107
50	0.078	3.949
10	0.253	2.537

The second set of experiments monitor the evolution of CO_2 in the concentration range of 10 μM to 1000 μM (Figure 6.1.2, Table 6.1.4). A linear increase in the formation of CO_2 is obtained for 180 min irradiation time for the highest concentration, 1000 μM. The percentage of CO_2 at the end of this period is only 23 per cent of the theoretical maximum based on the stoichiometric reaction 6.1. However, for 100 μM, after one hour, formation of CO_2 reaches a plateau. At the end of one hour irradiation, the percentage of CO_2 was 41. When the irradiation period is extended from 90 min to 180 min, the percentage of CO_2 for 100 μM 3,5-DHT concentration increases. For 50 μM, 100 per cent CO_2 is obtained in one hour irradiation, whereas complete degradation of 3,5-DHT is achieved in 40 min irradiation. For the lowest concentration, 10 μM, 100 per cent degradation and 100 per cent formation of CO_2 are obatined in 15 min and in 40 min irradiation times respectively (Table 6.1.5).
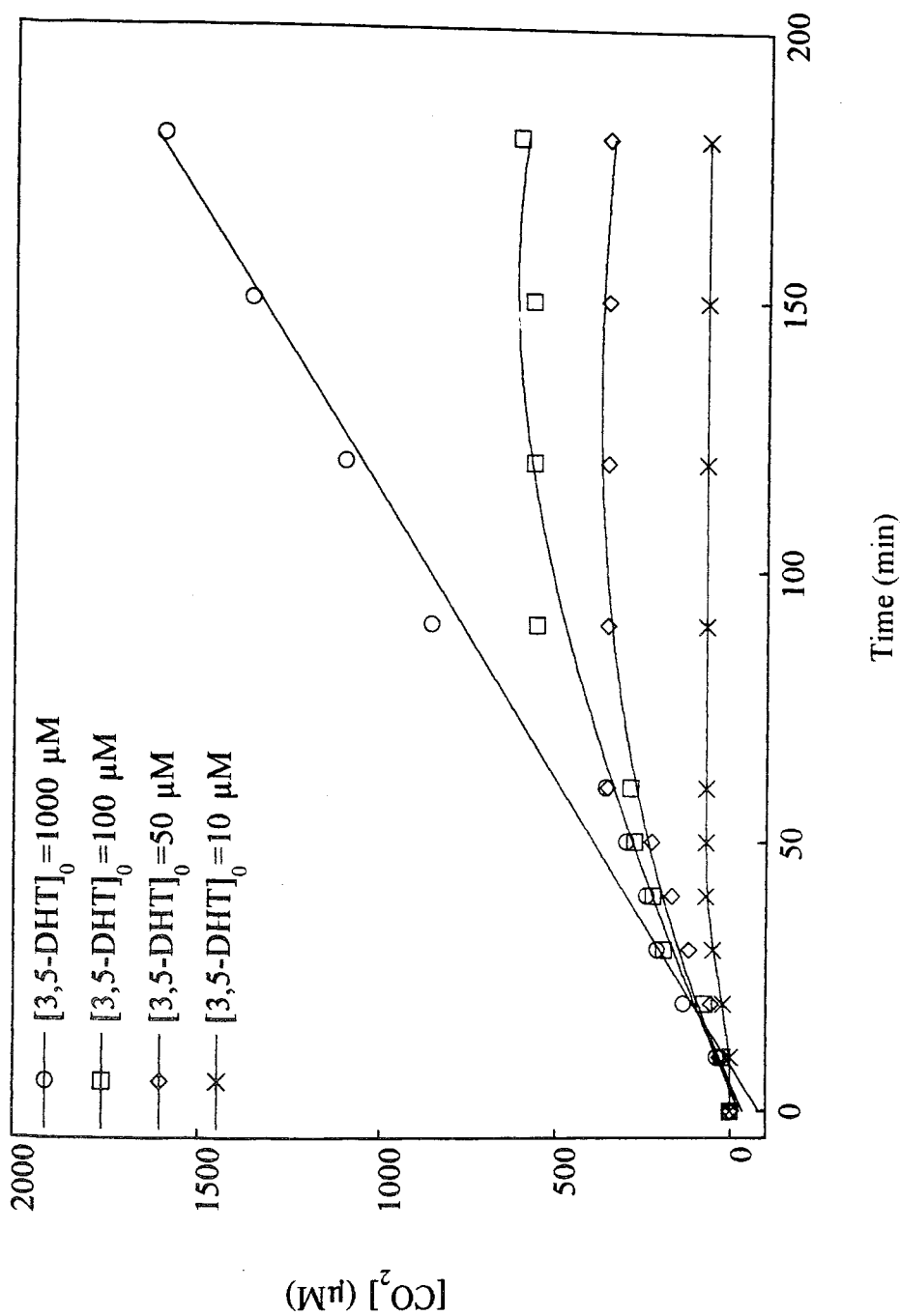
Figure 6.1.2. Effect of initial 3,5-DHT concentration on the concentration of CO_2 evolved as a function of irradition time. Conditions: $[TiO_2]=1g/L$, Flow Rate=144 ml/min, pH=5.2, T=298 K, $I_0=10.8 \times 10^{-6}$ einstein/min.

Table 6.1.4. Effect of initial 3,5-DHT concentration on the concentration of CO_2 evolved as a function of irradiation time. Equations represent the linear portion of the data, i.e. 40 min irradiation time.

Time (min)	[3,5-DHT]$_0$			
	1000 μM	100 μM	50 μM	10 μM
0	0	0	0	0
10	39.4	22.4	30.3	0
20	135	73.7	55.1	20.7
30	210	190	117	49.2
40	240	220	166	70
50	298	273	224	70
60	358	284	350	70
90	856	553	350	70
120	1100	562	350	70
150	1360	565	350	70
180	1600	603	350	70
y= (μM) x= (min)	y=-5.24+6.51x R=0.986	y=-20.3+6.09x R=0.970	y=-10.1+4.19x R=0.985	y=-9.86+1.89x R=0.966

Table 6.1.5. Degradation percentage of 3,5-DHT and formation percentage of CO_2.

[3,5-DHT] (μM)	Per cent Degradation of 3,5-DHT		Per cent Formation of CO_2	
	in 60 min	in 180 min	in 60 min	in 180 min
1000	48	5.1	61	23
100	99	41	100	86
50	100	100	100	100
10	100	100	100	100

At the end of the second set of experiments, a Langmuir-Hinshelwood model was employed to obtain the reaction rate constant and the adsorption constant for the photocatalytic degradation reaction of 3,5-DHT. The model is used to evaluate the rate of CO_2 formation as a function of the initial 3,5-DHT concentration (Table 6.1.6). Figure 6.1.3 plots the rate of CO_2 versus the 3,5-DHT concentration. The inset in Figure 6.1.3, plots the inverse of CO_2 rate ($1/R_{CO2}$) as a function of inverse of 3,5-DHT ($1/[3,5-DHT]$) concentration. A straight line is obtained from Figure 6.1.3 inset, from which the reaction rate constant, k is found as 6.87 μM/min, and adsorption constant, K is found as 37.8×10^{-3} 1/ μM.

Table 6.1.6. Effect of 3,5-DHT concentration on the formation rate of CO_2.

[3,5-DHT] (μM)	R_{CO2} (μM/min)	$1/[3,5-DHT]$ (1/μM)	$1/R_{CO2}$ (min/μM)
1000	6.51	0.001	0.15
100	6.08	0.01	0.17
50	4.19	0.02	0.24
10	1.89	0.1	0.53
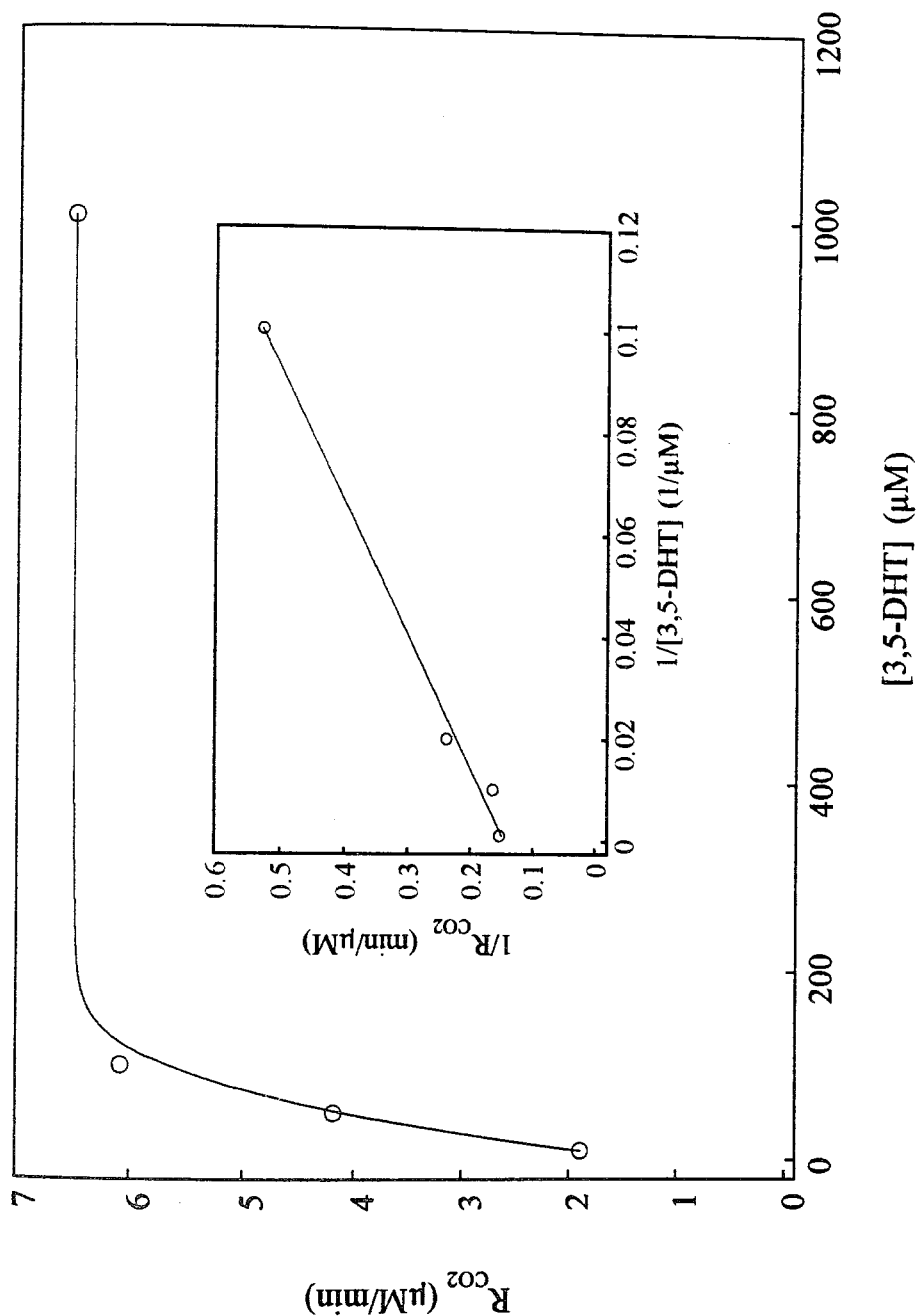
Figure 6.1.3. Rate of CO$_2$ production versus 3,5-DHT concentration.

Inset: 1/R$_{CO_2}$ as a function of 1/[3,5-DHT]. Conditions: [TiO$_2$]=1g/L, Flow Rate=144 ml/min, pH=5.2, T=298 K, I$_0$=10.8x10^{-6} einstein/min.

6.2. Effect of pH

The effect of pH on the degradation of 3,5-DHT and on the formation of CO_2 is investigated in three sets of experiments.

The first set of experiments monitor pH changes in the 3,5-DHT/TiO_2 systems in the dark (before irradiation) (pH_1) and after one hour irradiation (pH_2) (Table 6.2.1).

Table 6.2.1. Resulting pH changes before (pH_1) and after irradiation (pH_2) for 3,5-DHT/TiO_2 suspensions.

pH	pH_1	pH_2	$\Delta pH = pH - pH_2$
3.5	3.5	3.5	0
5.2	4.3	4.2	1.0
7.0	6.3	5.2	1.8
9.0	8.7	6.1	2.9
11.0	10.8	10.3	0.7

For pH 3.5, no decrease in the pH value is observed due to inhibition of dissociation (equation 6.2 shifts to the left) and thus adsorption of 3,5-DHT on the TiO_2 surface. For the higher pH's, consumption of OH^- ions results in a decrease in the pH values; pH_2. However, the competition between OH^- ions and 3,5-DHT ions at pH 11 decreases the available binding sites for OH^- ions on the TiO_2 surface. Thus, the OH^- ions stay in the solution phase and their presence does not change the solution pH.

$$+ H^+ \qquad\qquad (6.2)$$
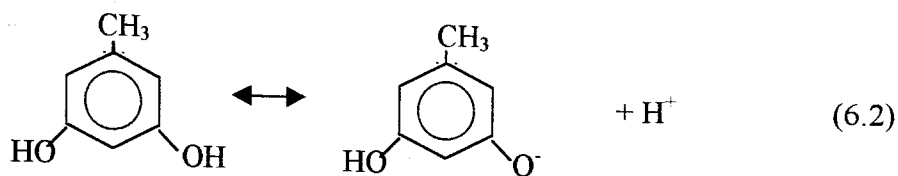
The second set of experiments follow the degradation of 3,5-DHT under irradiation, in the presence and in the absence of TiO_2. The amounts of remaining 3,5-DHT in the solution are given in Figures 6.2.1, 6.2.2, 6.2.3, and 6.2.4, and Tables 6.2.2 and 6.2.3. In the absence of TiO_2, degradation is possible but inefficient compared to the degradation in the presence of TiO_2. The highest degradation, 100 per cent, in the absence of TiO_2, is obtained at pH 11. However, in the presence of TiO_2, the degradation rate is maximum at pH 9.0. This is due to the competition between OH⁻ ions and 3,5-DHT ions at pH 11.

The last set of experiments examine the effect of pH for the formation of CO_2 (Figure 6.2.5, Table 6.2.4). pH 11 could not be analyzed due to the formation of the CO_3^{2-} species. The highest rate of formation of CO_2 is obtained with pH 9.0 (Figure 6.2.5 inset), which is in good agreement with the result for the degradation rate of 3,5-DHT in the presence of TiO_2 after 30 min irradiation time (Figure 6.2.6, Table 6.2.5).

Figure 6.2.2. Remaining [3,5-DHT] in solution at pH=5.2 in the presence and in the absence of TiO$_2$.
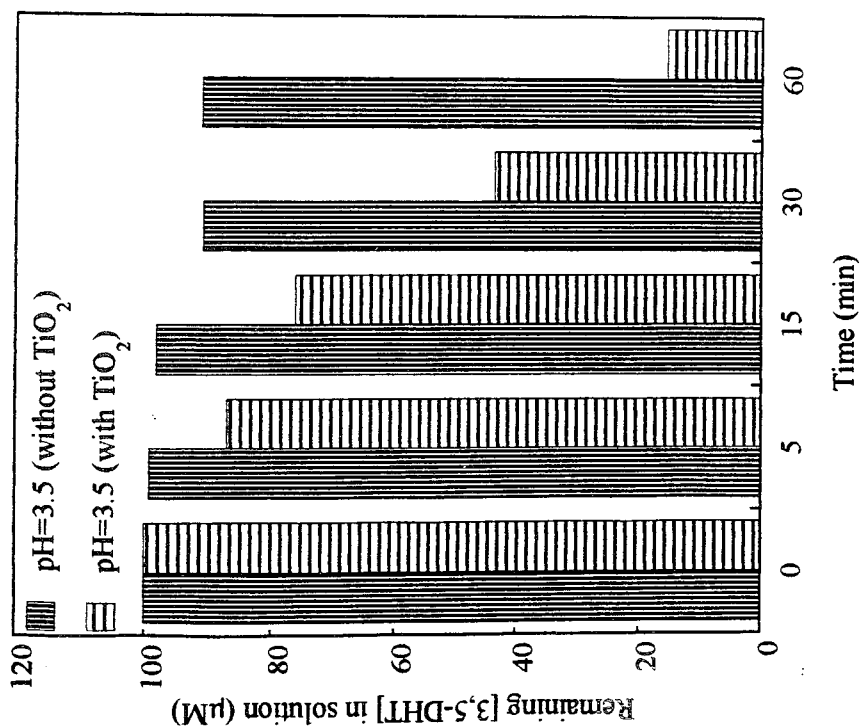
Figure 6.2.1. Remaining [3,5-DHT] in solution at pH=3.5 in the presence and in the absence of TiO$_2$.

Figure 6.2.4. Remaining [3,5-DHT] in solution at pH=11.0 in the presence and in the absence of TiO_2.
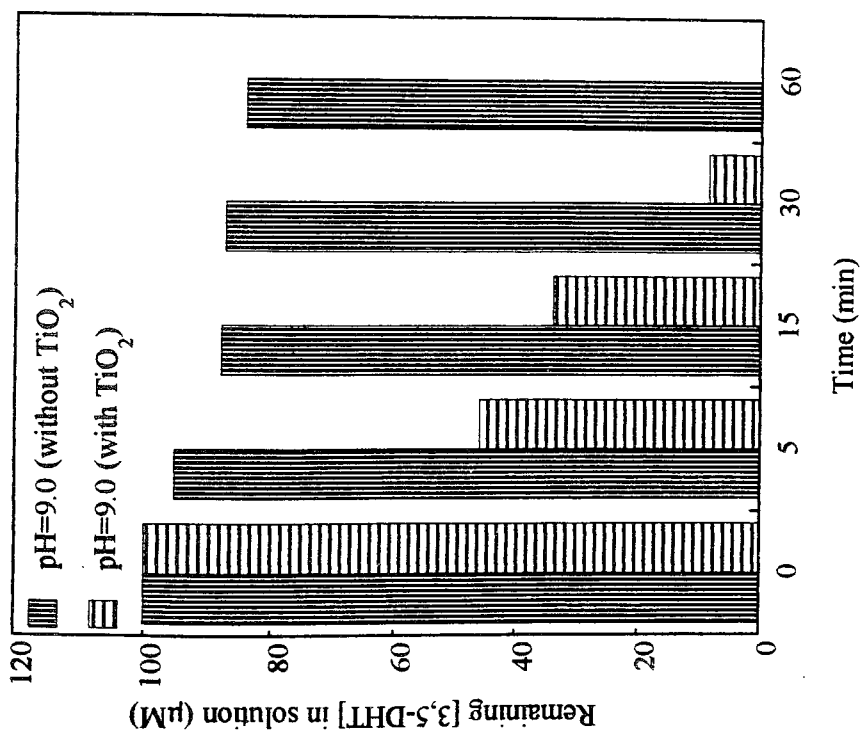
Figure 6.2.3. Remaining [3,5-DHT] in solution at pH=9.0 in the presence and in the absence of TiO_2.

Table 6.2.2. Effect of pH on the degradation of 3,5-DHT in the absence of TiO_2.

Each numerical value represents the remaining 3,5-DHT concentration in the solution.

Time (min)	$[3,5\text{-DHT}]_0=100\ \mu M$			
	pH=3.5	pH=5.2	pH=9.0	pH=11.0
0	100	100	100	100
5	99.1	98.3	95.2	100
15	98.1	97.8	87.9	94.2
30	91.1	95.5	87.4	60.6
60	90.9	90.2	84.1	0

Table 6.2.3. Effect of pH on the degradation of 3,5-DHT in the presence of TiO_2.

Each numerical value represents the remaining 3,5-DHT concentration in the solution.

Time (min)	[3,5-DHT]$_0$=100 µM				
	pH=3.5	pH=5.2	pH=9.0	pH=11.0
0	100	100	100	100
5	87.1	52.3	45.9	97.3
15	76.2	37.9	33.8	62.4
30	43.6	21.1	8.37	22.7
60	15.3	0.62	0	0
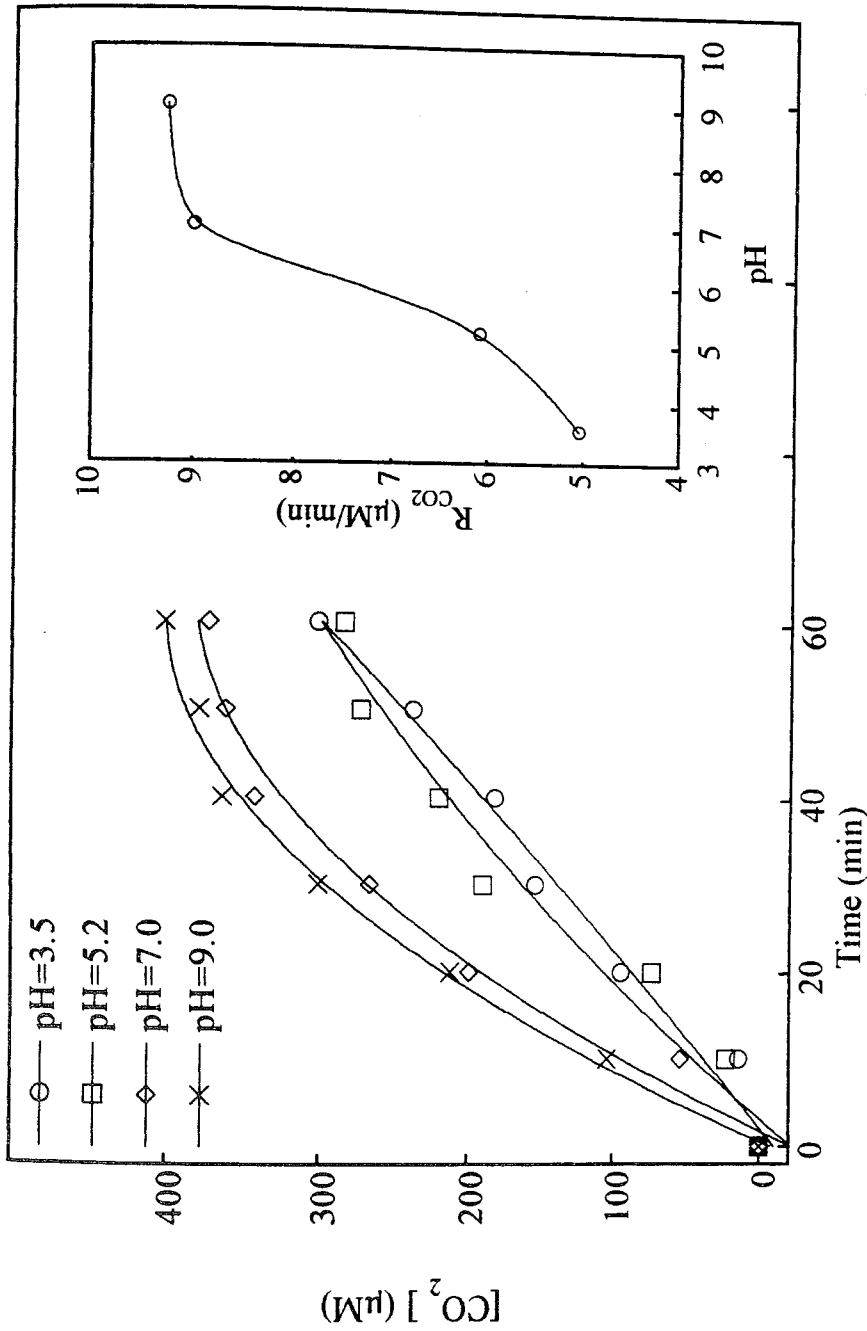
Figure 6.2.5. Effect of pH on the concentration of CO_2 produced.

Inset: R_{CO2} as a function of pH.. Conditions: $[TiO_2]$=1g/L, Flow Rate=144 ml/min, $[3,5\text{-}DHT]_0$=100 μM, T=298 K, I_0=10.8x10^{-6} einstein/min.

Table 6.2.4. Effect of pH on the concentration of CO_2 produced.

Equations represent the linear portion of the data, i.e. 40 min irradiation time.

Time (min)	CO_2 (μM)			
	pH=3.5	pH=5.2	pH=7.0	pH=9.0
0	0	0	0	0
10	14.2	22.4	53.8	104
20	95.1	73.7	199	212
30	154	190	267	301
40	182	220	343	364
50	238	273	362	379
60	302	284	373	401
y= (μM) x= (min)	Y=-11.7+5.04x R=0.980	y=-8.79+5.36x R=0.977	y=-7.28+8.99x R=0.989	y=11.2+9.25x R=0.995
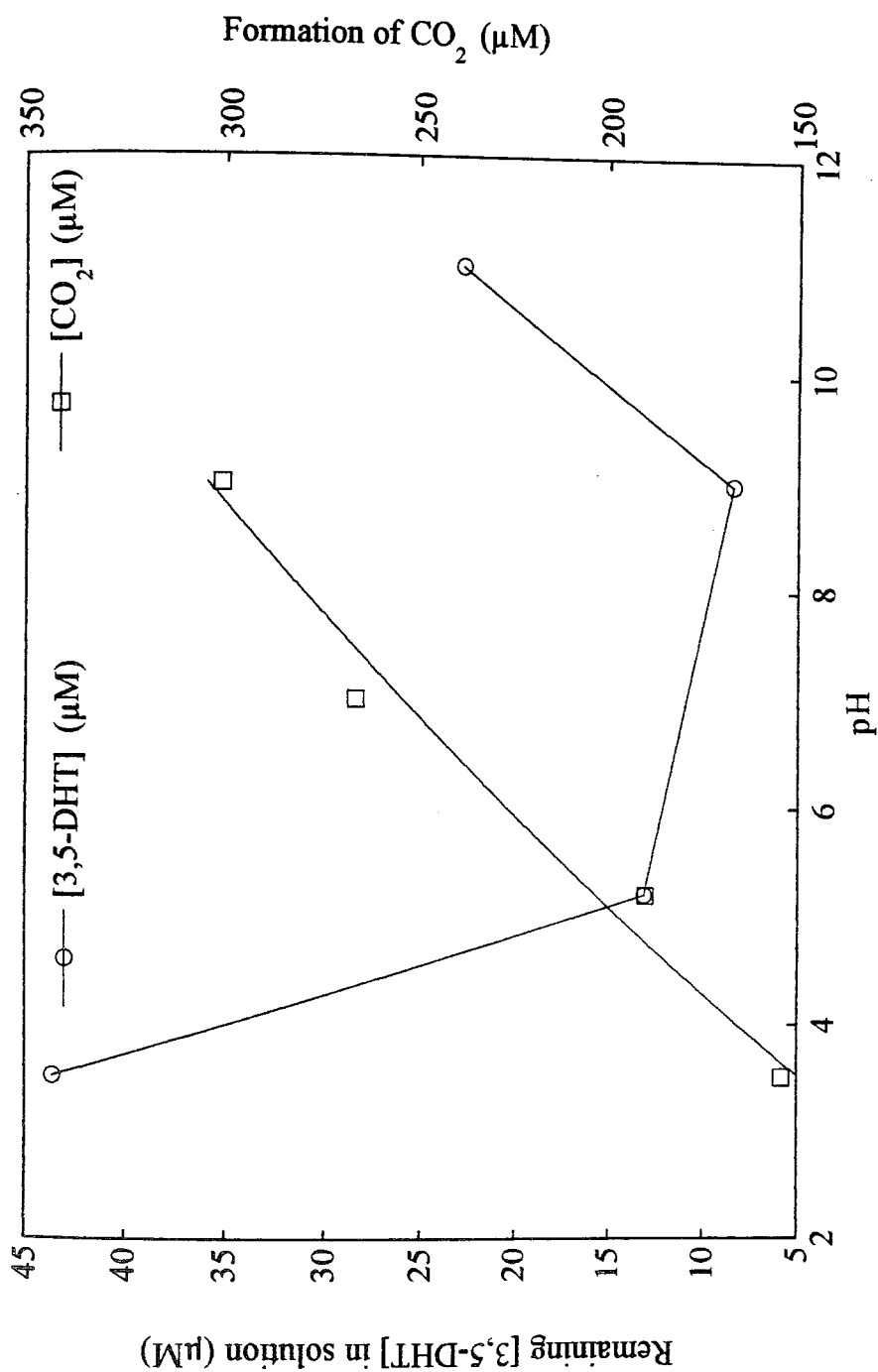
Figure 6.2.6. Concentration of CO_2 produced and remaining 3,5-DHT in solution as a function of pH after 30 min irradiation. Conditions: $[TiO_2]=1g/L$, Flow Rate=144 ml/min, $[3,5-DHT]_0=100 \mu M$, T=298 K, $I_0=10.8 \times 10^{-6}$ einstein/min.

Table 6.2.5. Effect of pH on the formation of CO_2 and on the concentration of 3,5-DHT remaining in solution after 30 min irradiation.

pH	[3,5-DHT] (μM)	CO_2 (μM)
3.5	43.6	154
5.2	13.1	190
7.0	-*	267
9.0	8.37	301
11.0	22.7	-*

*These points were not measured.

6.3. Effect of Irradiation Time

Figure 6.3.1 (Table 6.3.1) shows the per cent of 3,5-DHT remaining in the solution and the per cent of CO_2 formation for 100 μM 3,5-DHT. At the end of one hour irradiation, 99.4 per cent degradation of 3,5-DHT and 40.6 per cent formation of CO_2 are obtained. Higher CO_2 percentages are observable by extending the irradiation time.

6.4. Effect of Temperature

The temperature dependence of the initial CO_2 formation rate from the 3,5-DHT decomposition is investigated in the range 298-333 K for 60 min irradiation time (Figure 6.4.1, Table 6.4.1). In order to account the decrease in the solubility of CO_2 with increasing temperature, calibrations are repeated in the studied temperature range (Appendix A). The rate of CO_2 production is found to be linear for 40 min irradiation time. Figure 6.4.1 inset illustrates the Arrhenius plot of CO_2 formation. The apparent activation energy is calculated from the slope of Figure 6.4.1 inset a 17.4 kJ/mol.
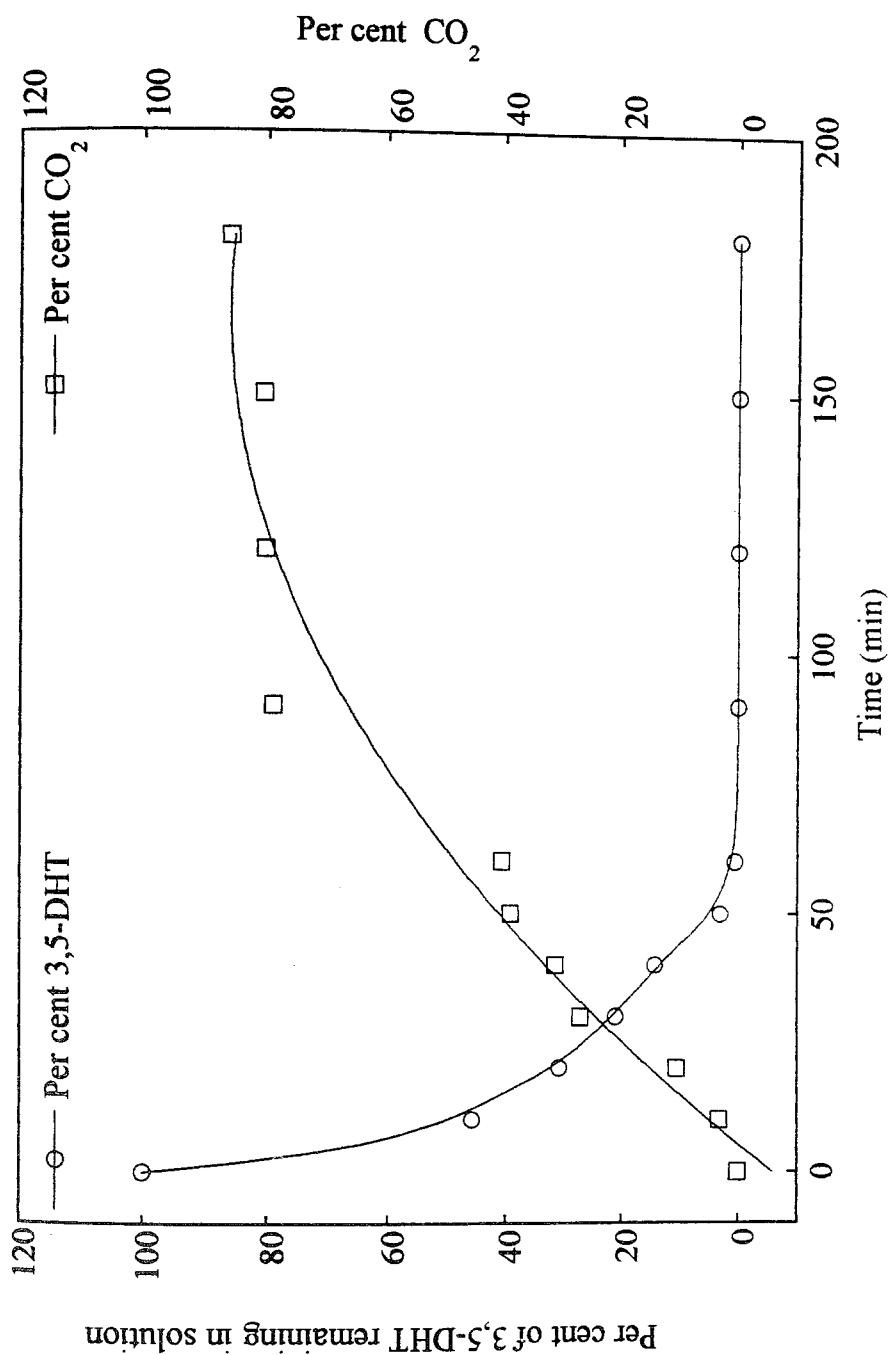
Figure 6.3.1. The per cent of 3,5-DHT remaining in solution and the per cent of CO_2 formation as a function of irradiation time. Conditions: $[TiO_2]=1g/L$, Flow Rate=144 ml/min, $[3,5-DHT]_0=100$ μM, pH=5.2, T=298 K, $I_0=10.8 \times 10^{-6}$ einstein/min.

Table 6.3.1. Effect of irradiation time.

3,5-DHT: Each numerical value represents the per cent of 3,5-DHT remaining in the solution.

CO_2: Each numerical value represents the per cent of CO_2 formation.

Time (min)	Per cent 3,5-DHT	Per cent CO_2
0	100	0
10	45.7	3.21
20	30.8	10.5
30	21.1	27.1
40	14.3	31.4
50	3.12	39.1
60	0.62	40.6
90	0	79.1
120	0	80.3
150	0	80.7
180	0	86.1
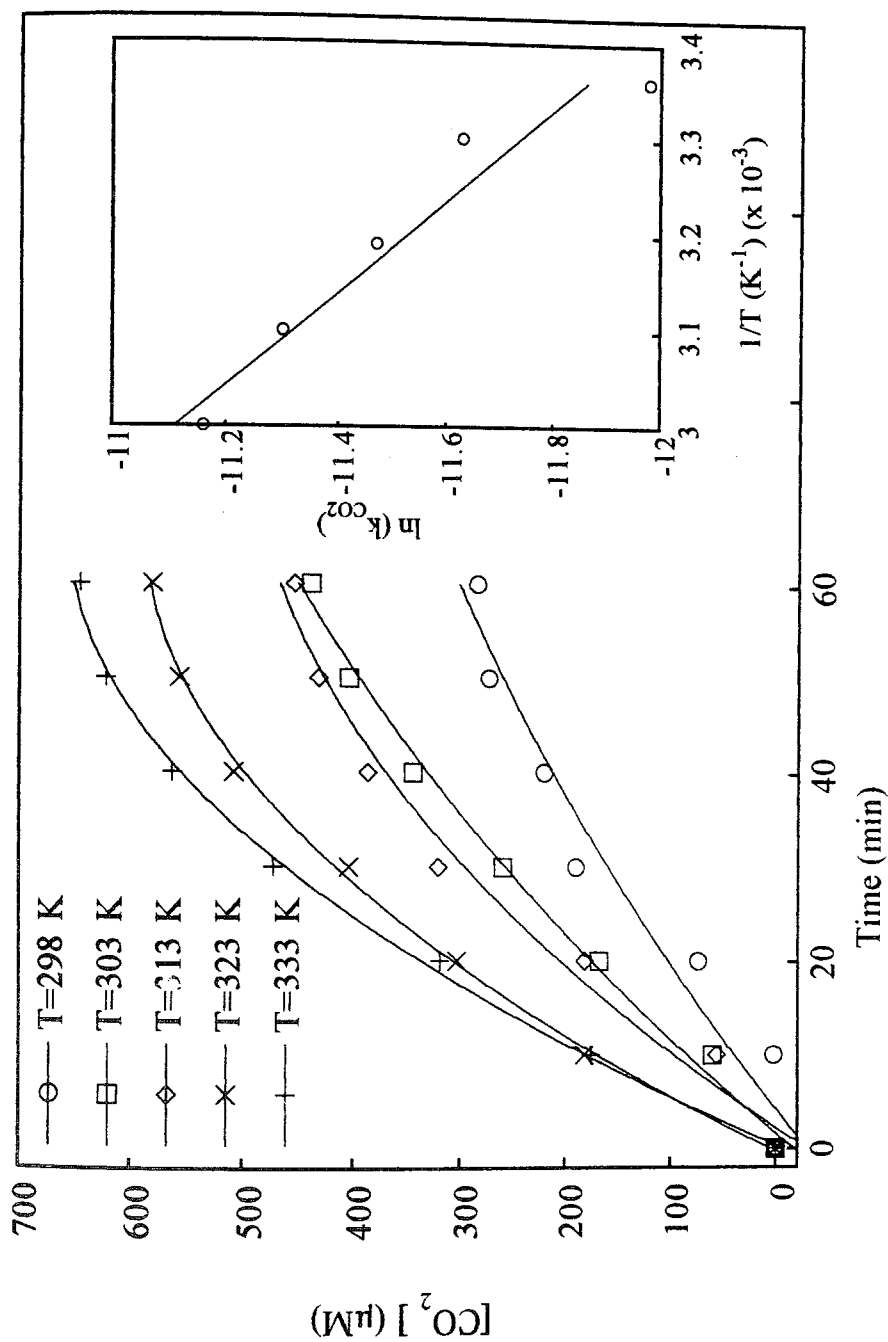
Figure 6.4.1. Effect of temperature on the concentration of CO_2 produced.

Inset: Arrhenius plot. Conditions: $[TiO_2]=1g/L$, Flow Rate=144 ml/min, $[3,5\text{-}DHT]_0=100\ \mu M$, pH=5.2, $I_0=10.8\times10^{-6}$ einstein/min.

Table 6.4.1. Effect of temperature on the concentration of CO_2 evolved.

Equations represent the linear portion of the data, i.e. 40 min irradiation time.

Time (min)	CO_2 (μM)					
	298 K	303 K	313 K	323 K	333 K	
0	0	0	0	0	0	
10	22.4	59.5	55.6	98.8	104	
20	73.7	168	182	208	221	
30	190	260	321	321	420	
40	220	345	387	461	519	
50	273	404	432	537	562	
60	284	439	454	579	608	
y= (μM) x= (min)	y=-8.79+5.36x	y=-11.6+8.91x	y=-10.8+10.2x	y=-11.1+11.4x	y=-18.1+13.5x	
	R=0.977	R=0.997	R=0.994	R=0.998	R=0.993	

6.5. Postulated Mechanism: Route of Oxidation

In order to ascertain the route of oxidation for 3,5-DHT, i.e. oxidation with photogenerated holes or reaction with $^{\bullet}$OH radicals, the same initial charge transfer reactions and rate equations of 1,3-DHB are assumed to be valid also for 3,5-DHT. Therefore, the initial rate equation will be as follows for 3,5-DHT:

$$\frac{1}{R_i} = \frac{k_3[OH^-]}{k_4[I]} \frac{1}{[C_7H_6(OH)_2]} + \frac{1}{I} \qquad (6.3)$$

where k_3 is the rate constant of the oxidation process with $^{\bullet}$OH radicals and k_4 is rate constant of the oxidation process with photogenerated holes, and R_i is the initial rate of CO_2 formation.

According to equation (6.3), when the reciprocal of the initial rate of CO_2 formation (1/R_{CO2}) versus 1/[$C_7H_6(OH)_2$] is plotted (Figure 6.1.3 inset), a straight line is obtained whose slope is equal to the value of $k_3[OH]/k_4I$. The rate of incident photon flux with the fraction of absorption 0.489, is calculated as 2.64×10^{-5} einstein dm^{-3} s^{-1}. From the slope, 3.8441 and considering the natural pH (pH=5.2) of 3,5-DHT, a ratio of $k_3/k_4 = 6.42 \times 10^4$ is deduced. Thus formation of $^{\bullet}$OH radicals is more favored than the photogenerated holes for the oxidation of 3,5-DHT.

6.6. Relative Photonic Efficiencies

Taking 1,3-DHB as the probe molecule, the relative photonic efficiencies of 3,5-DHT are calculated according to equation 6.4.

$$\zeta = \frac{\text{rate of formation of } CO_2 \text{ for } 3,5-DHT}{\text{rate of formation of } CO_2 \text{ for } 1,3-DHB} \qquad (6.4)$$

The effects of 3,5-DHT concentration, pH and temperature on relative photonic efficiencies are examined (Figure 6.6.1). It is observed that there is no general trend for the relative photonic efficiencies with the variations in concentration of 3,5-DHT, pH and temperature. A more detailed information will be given in the discussion chapter.
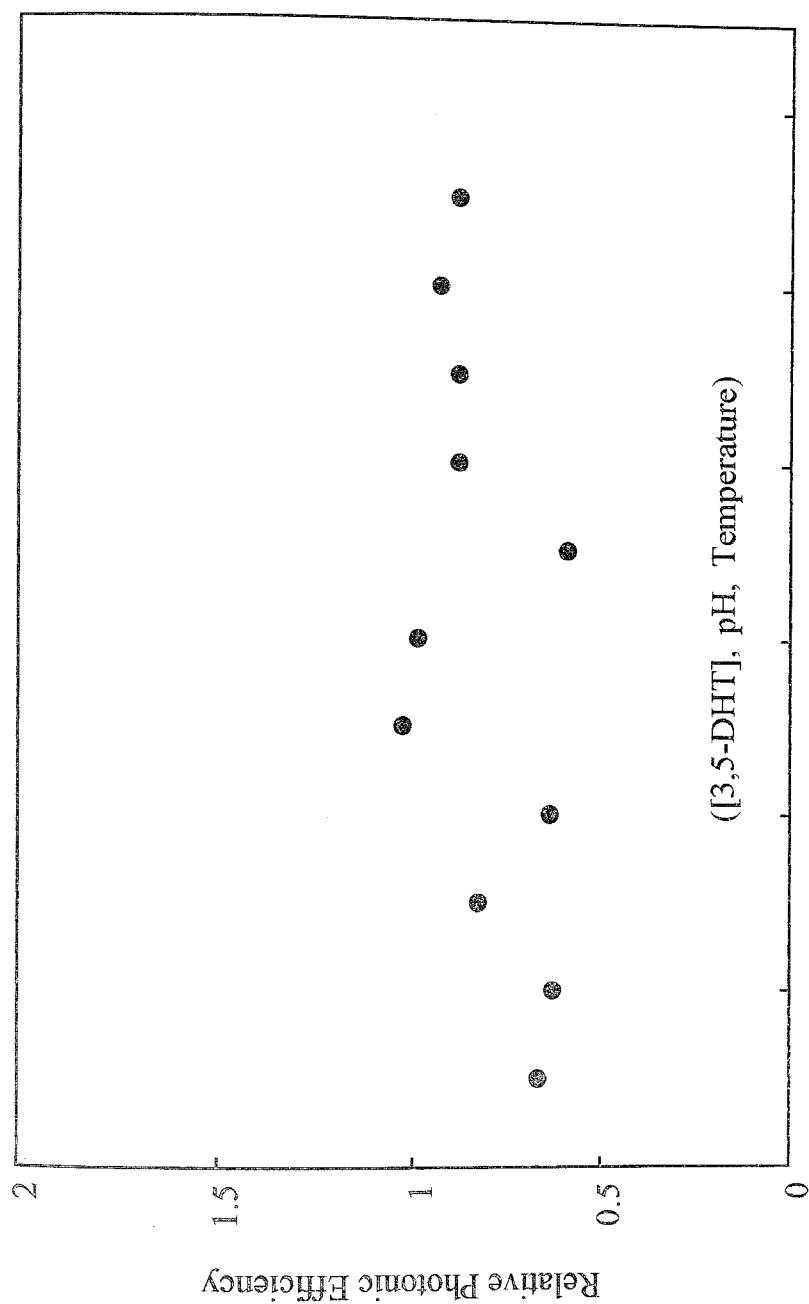
Figure 6.6.1. Relative photonic efficiencies as a function of 3,5-DHT concentration, pH and temperature for 3,5-DHT.

7. 1,3-DIHYDROXY-5-METHOXYBENZENE (1,3-DHMB)

7.1. Effect of 1,3-DHMB Concentration

Photocatalytic degradation of 1,3-DHMB is examined according to the mineralization reaction 7.1 and under two sets of experimental conditions:

$$C_7H_6O(OH)_2 + 15/2\ O_2 \rightarrow 7CO_2 + 4H_2O \qquad (7.1)$$
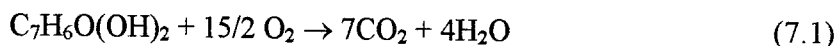
The first set of experiments monitor the decrease in the initial concentration of 1,3-DHMB, in a concentration range of 500 μM to 2000 μM (Figure 7.1.1, Table 7.1.1). Concentrations of 1,3-DHMB less than or equal to 100 μM are not included in the investigation range since the corresponding peak of 100 μM 1,3-DHMB in the HPLC was too small and difficult to follow. Therefore, the lowest concentration; 500 μM is used throughout the experiments unless otherwise mentioned. In the temporal evolution of CO_2, 100 μM 1,3-DHMB is analyzed and can be compared to the corresponding data taken for other reagents.

The linearity in Figure 7.1.1 inset (Table 7.1.2) indicates the kinetics of 1,3-DHMB degradation are zeroth order. Numerical results of apparent zero order rate constants and rates are given in Table 7.1.3. As the initial concentration of 1,3-DHMB increases, the reaction rate becomes constant due to reaching the limit of available surface sites for the species to be adsorbed on the TiO_2 surface.
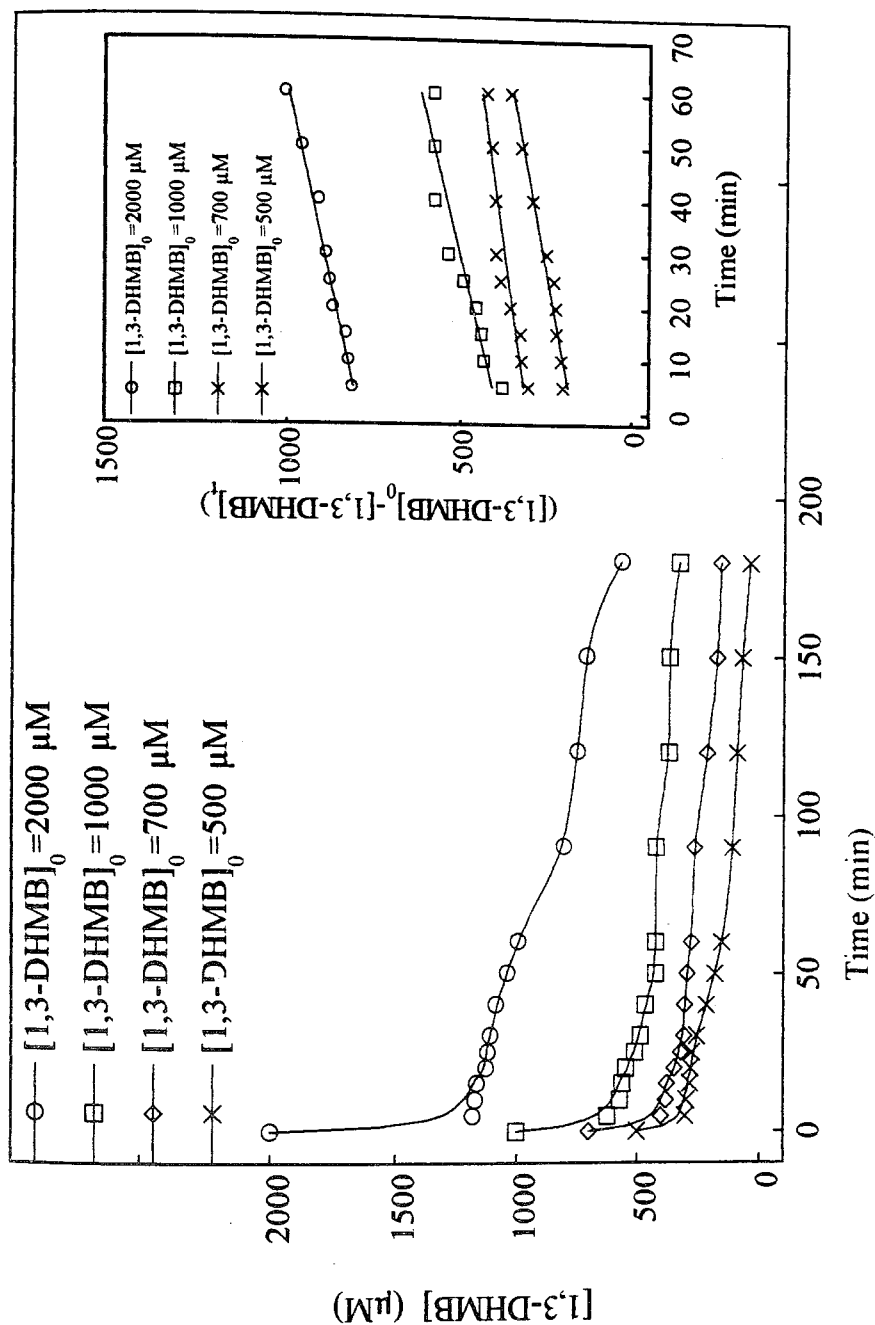
Figure 7.1.1. Effect of 1,3-DHMB concentration on the degradation of 1,3-DHMB.

Inset: ([1,3-DHMB]$_0$-[1,3-DHMB]$_t$) versus irradiation time. Conditions: [TiO$_2$]=1g/L, Flow Rate=144 ml/min, pH=5.4, T=298 K, I$_0$=10.8x10^{-6} einstein/min.

Table 7.1.1. Effect of 1,3-DHMB concentration on the degradation of 1,3-DHMB.
Each numerical value represents the concentration of 1,3-DHMB remaining in the solution.

Time (min)	$[1,3\text{-DHMB}]_0$				
	2000 µM	1000 µM	700 µM	500 µM	
0	2000	1000	700	500	
5	1183	622.8	399.1	299.7	
10	1173	569.4	380.3	295.9	
15	1165	560.7	376.1	280.6	
20	1127	545.5	346.8	278.6	
25	1119	508.6	317.6	273.1	
30	1108	484.7	304.3	253.2	
40	1087	464.7	302.7	211.8	
50	1039	423.1	291.8	179.5	
60	994.3	422.3	276.6	149.5	
90	806.5	421.6	263.1	107.1	
120	747.3	369.5	210.1	88.84	
150	709.3	366.5	170.5	67.32	
180	563.7	326.4	156.6	35.88	

Table 7.1.2. ([1,3-DHMB]$_0$-[1,3-DHMB]$_t$) versus time data as a function of initial 1,3-DHMB concentration.

Time (min)	[1,3-DHMB]$_0$			
	2000 µM	1000 µM	700 µM	500 µM
5	817	377	301	200
10	827	431	320	204
15	835	439	324	219
20	873	455	353	221
25	881	491	382	227
30	892	535	396	247
40	913	577	397	288
50	961	578	408	321
60	1006	578	423	351
y= (µM) x= (min)	y=794+3.36x R=0.990	y=388+3.81x R=0.943	y=304+2.22x R=0.938	y=172+2.88x R=0.984

Table 7.1.3. Kinetic data for 1,3-DHMB degradation.

[1,3-DHMB]$_0$ (μM)	k (1/min)	Rate (1/min)
2000	3.36	3.36
1000	3.80	3.80
700	2.22	2.22
500	2.89	2.89

Decreasing the concentration of 1,3-DHMB, the reaction is going towards pseudo-first order kinetics as observed in 1,3-DHB and 3,5-DHT. Since it is not possible to measure this compound at lower concentrations, we cannot observe purely pseudo-first order kinetics.

The second set of experiments (Figure 7.1.2, Table 7.1.4) monitors the evolution of CO_2 in the 100 μM-2000 μM concentration range. When the rate of CO_2 production versus 1,3-DHMB concentration is plotted (Figure 7.1.3, Table 7.1.5), a sharp increase is observed for initial concentrations ranging from 100μM to 1000 μM, but for 2000 μM 1,3-DHMB solution, a plateau is observed in the rate of CO_2 evolution. When the inverse of the rate of CO_2 production versus the inverse of 1,3-DHMB concentration is plotted, 100 μM is not included since it levels off in the resulting plot. From the linearity in the inset of Figure 7.1.3, the reaction rate constant, k is found as 13.07 μM/min and the adsorption constant, K is found as 4.22×10^{-3} 1/μM.
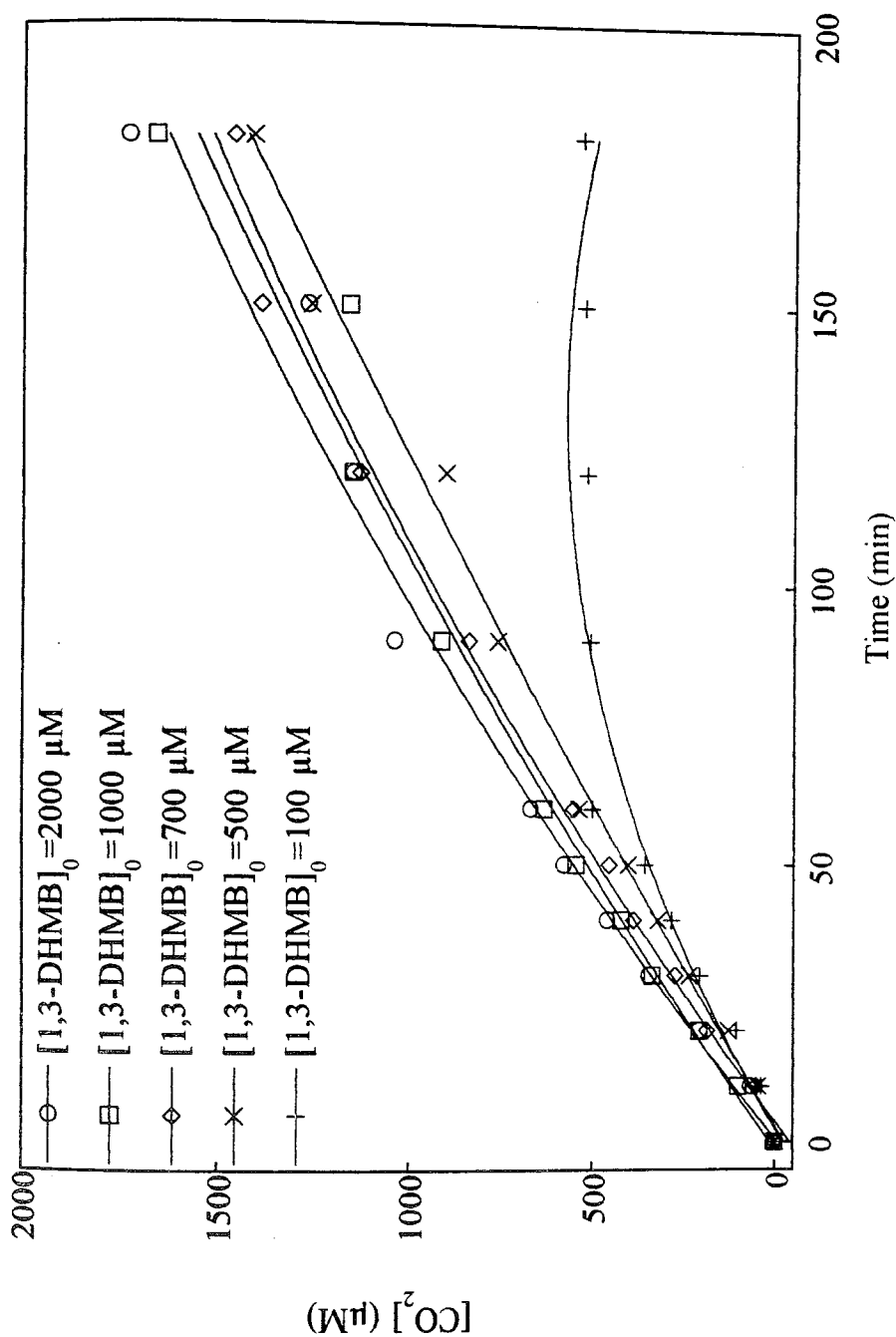
Figure 7.1.2. Effect of initial 1,3-DHMB concentration on the concentration of CO_2 evolved as a function of irradition time. Conditions: $[TiO_2]=1g/L$, Flow Rate=144 ml/min, pH=5.4, T=298 K, $I_0=10.8\times10^{-6}$ einstein/min.

Table 7.1.4. Effect of 1,3-DHMB concentration on the concentration of CO_2 evolved as a function of irradiation time. Equations represent the linear portion of the data, i.e. 60 min irradiation time.

Time (min)	[1,3-DHMB]$_0$				
	2000 µM	1000 µM	700 µM	500 µM	100 µM
0	0	0	0	0	0
10	65.3	99.8	49.2	44.3	36.3
20	206	206	185	125	104
30	344	334	272	233	204
40	460	419	386	318	281
50	578	543	454	400	354
60	669	630	551	536	500
90	1040	913	836	758	505
120	1150	1150	1130	900	512
150	1270	1160	1390	1260	519
180	1730	1660	1460	1410	526
y= (µM) x= (min)	y=-20.4+11.7x R=0.997	y=-1.46+10.7x R=0.999	y=-14.4+9.51x R=0.996	y=-24.9+8.69x R=0.996	y=-36.4+8.26x R=0.989
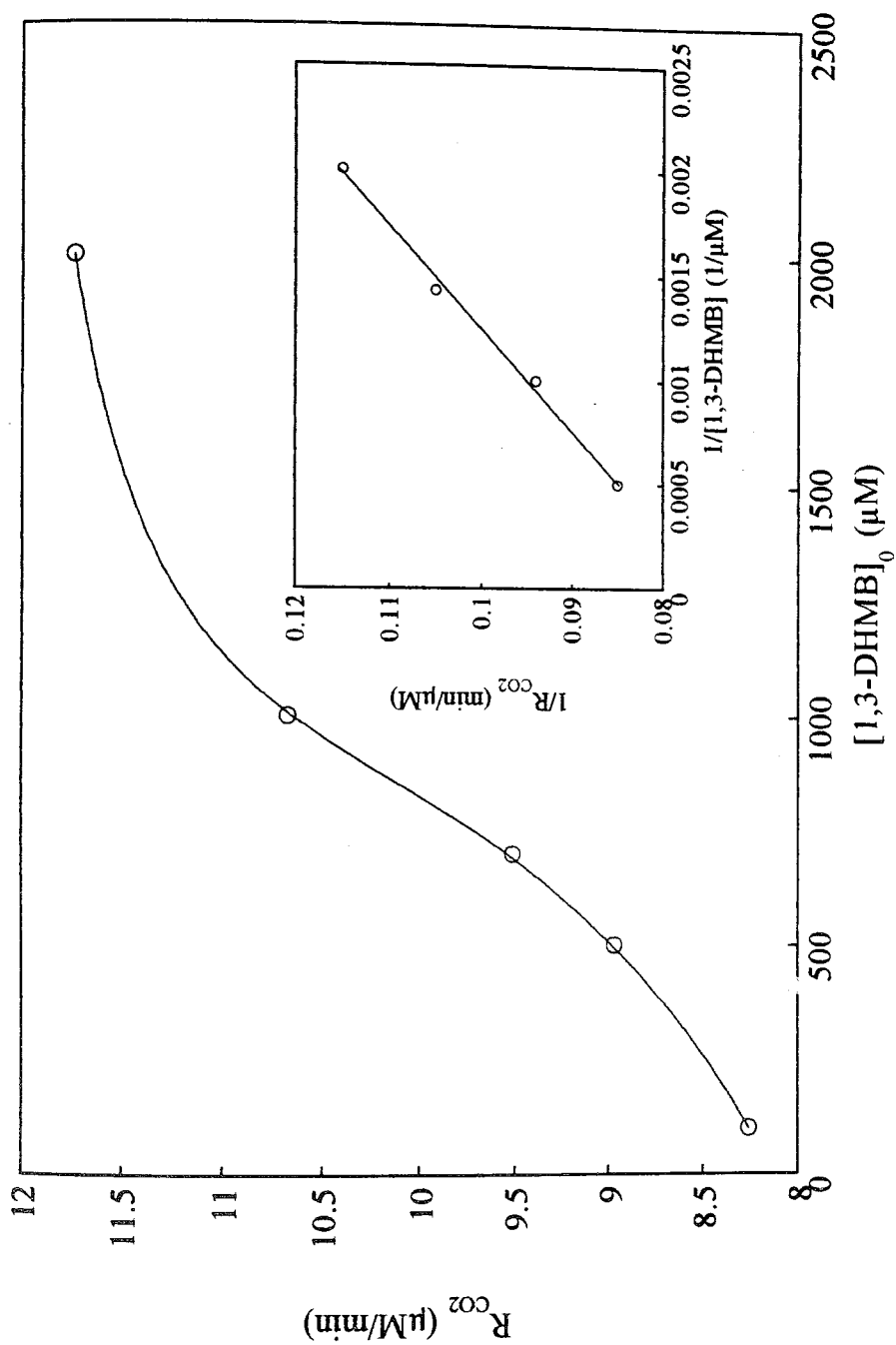
Figure 7.1.3. Rate of CO_2 production versus 1,3-DHMB concentration.

Inset: $1/R_{CO2}$ as a function of $1/[1,3\text{-DHMB}]$. Conditions: $[TiO_2]=1g/L$, pH=5.4,

Flow Rate=144 ml/min, T=298 K, $I_0=10.8\times10^{-6}$ einstein/min.

Table 7.1.5. Effect of 1,3-DHMB concentration on the rate of formation of CO_2.

[1,3-DHMB]$_0$ (μM)	R_{CO2} (μM/min)	1/[1,3-DHMB]$_0$ (1/μM)	1/R_{CO2} (min/μM)
2000	11.74	0.0005	0.085
1000	10.68	0.0010	0.094
700	9.513	0.0014	0.105
500	8.687	0.0020	0.115
100	8.258	0.0100*	0.121*

*: 100 μM is not included in the 1/R_{CO2} versus 1/[1,3-DHMB]$_0$ plot.

In Table 7.1.6, the numerical results for the per cent degradation of 1,3-DHMB and the per cent formation of CO_2 are summarized.

Table 7.1.6. Degradation percentage of 1,3-DHMB and formation percentage of CO_2.

[1,3-DHMB] (μM)	Per cent Degradation of 1,3-DHMB		Per cent Formation of CO_2	
	in 60 min	in 180 min	in 60 min	in 180 min
2000	50	72	4.8	12
1000	58	68	9.0	28
700	61	78	11	30
500	70	93	15	40

As expected, both increase the irradiation period from 60 min to 180 min, and decreasing the initial 1,3-DHMB concentration has been found to increase the percent degradation. The lowest percentages are obtained with the highest concentration, 2000 μM. This is a result of the high concentration of intermediates remaining in the reacting media even after 180 min of irradiation. By decreasing the initial concentration of 1,3-DHMB, the percentages increase due to the presence of lower concentrations of intermediates which may subsequently degrade in the time scale of the experiment. By increasing the irradiation time, the percentages again increase demonstrating the mineralization of intermediates which occurs if the experiment is allowed to continue. However, complete degradation cannot be achieved for any concentration studied without exceeding 180 min irradiation.

7.2. Effect of pH

As for the other compounds studied, a series of experiments have been performed to look at the effect of pH on the degradation of 1,3-DHMB and evolution of CO_2. The first set of experiments control the pH of 1,3-DHMB/TiO_2 suspensions before and after irradiation (Table 7.2.1).

Table 7.2.1. Resulting pH changes before (pH_1) and after irradiation (pH_2) for 1,3-DHMB/TiO_2 suspensions.

pH	pH_1	pH_2	$\Delta pH = pH - pH_2$
3.5	3.5	3.5	0
5.2	4.5	4.2	1.2
7.0	6.3	4.3	2.7
9.0	8.9	5.3	3.7
11.0	10.8	10.7	0.3

With the addition of TiO_2, the pH of suspensions, pH_1, changes due to the pzc value of TiO_2 (4.7). Since pH 3.5 is lower than pzc of TiO_2, no change is observed in the corresponding pH of 3.5. After irradiation, a noticeable decrement is observed due to the consumption of OH^- ions during photocatalytic degradation except for pH 3.5. Since dissociation of 1,3-DHMB (equation 7.2) is inhibited in acidic media (i.e. dissociation shifts to the left) the amount of it absorbed on the TiO_2 surface decreases, resulting in no change in the pH_2 value.

$$\text{(structure: OCH}_3\text{ ring with HO and OH)} \leftrightarrow \text{(structure: OCH}_3\text{ ring with HO and O}^-\text{)} + H^+ \qquad (7.2)$$
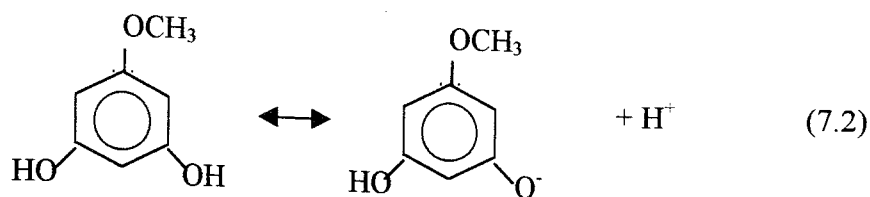
Tables 7.2.2 and 7.2.3 give the results of the second set of experiments in which the degradation of 1,3-DHMB is followed under irradiation both in the absence and presence of TiO_2. In the absence of TiO_2, the decomposition times were found to fluctuate as pH increase, but for pH's; 3.5, 5.4 and 11.0, no decrease in the concentration of 1,3-DHMB remaining in the solution was found for irradiation times of less than 25 min. Upon addition of TiO_2 the corresponding amount of 1,3-DHMB remaining in the solution was found to decrease, indicating the favorable role of the photocatalyst in the degradation. The competition between OH^- ions and 1,3-DHMB ions for the surface sites on the photocatalyst decreases the rate of degradation at pH 11.0. Figures 7.2.1, 7.2.2, 7.2.3 and 7.2.4 compare the 1,3-DHMB concentrations remaining in the solution in the absence and in the presence of TiO_2 at different pH's. The lowest amount remains in the solution corresponds to pH 9.0 in the presence and in the absence of TiO_2.

The last set of experiments monitors the formation of CO_2 at different pH values. A linear increase in the production of CO_2 is observed for 60 min irradiation time (Figure 7.2.5, Table 7.2.4). Figure 7.2.5 inset shows the rate of CO_2 evolution as a function of pH. The highest rate is obtained at pH 9.0. The effect of pH on the formation of CO_2 and the degradation of 1,3-DHMB is shown together in Figure 7.2.6 after 30 min irradiation time. The lowest concentration of 1,3-DGMB and the highest concentration of CO_2 are both obtained at pH 9.0 (Table 7.2.5), indicating this is the optimum pH for photocatalysis under experimental conditions used.

Table 7.2.2. Effect of pH on the degradation of 1,3-DHMB in the absence of TiO_2.
Each numerical value represents the remaining 1,3-DHMB concentration in the solution.

Time (min)	[1,3-DHMB]$_0$=500 µM			
	pH=3.5	pH=5.4	pH=9.0	pH=11.0
0	500	500	500	500
5	500	500	500	500
10	500	500	500	500
15	500	500	416	500
20	500	500	404	500
25	500	500	401	500
30	500	491	341	500
40	500	390	339	458
50	500	367	285	408
60	497	351	126	386

Table 7.2.3. Effect of pH on the degradation of 1,3-DHMB in the presence of TiO_2.
Each numerical value represents the remaining 1,3-DHMB concentration in the solution.

Time (min)	[1,3-DHMB]$_0$=500 μM			
	pH=3.5	pH=5.4	pH=9.0	pH=11.0
0	500	500	500	500
5	350	300	164	354
10	283	296	161	289
15	281	281	72.3	215
20	279	278	52.2	174
25	276	273	37.6	152
30	265	253	27.9	32.8
40	252	212	-	-
50	236	180	-	-
60	239	150	-	-

Figure 7.2.2. Remaining [1,3-DHMB] in solution at pH=5.4 in the presence and in the absence of TiO$_2$.
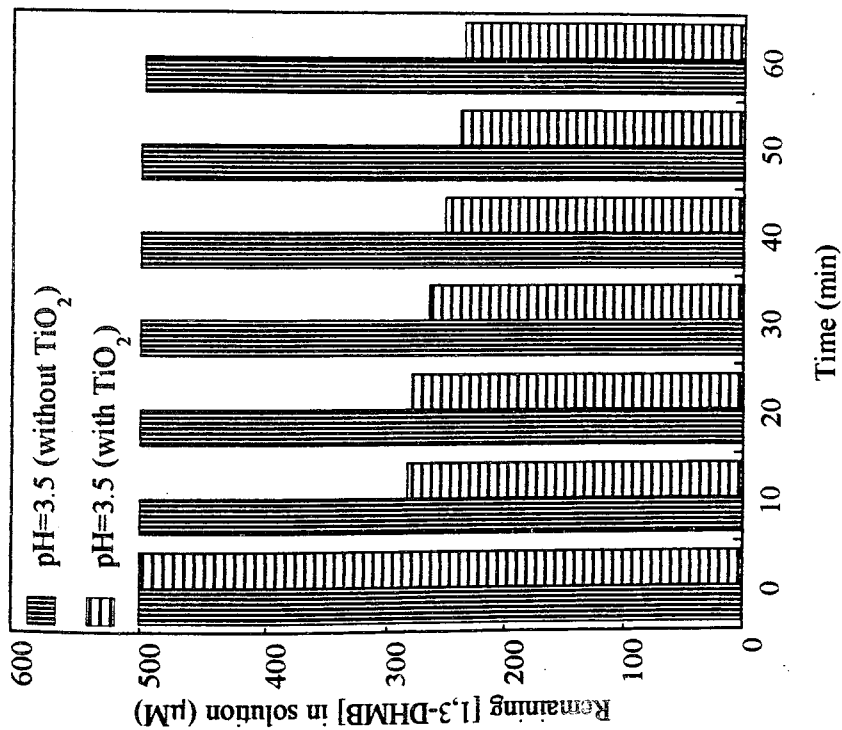
Figure 7.2.1. Remaining [1,3-DHMB] in solution at pH=3.5 in the presence and in the absence of TiO$_2$.

Figure 7.2.4. Remaining [1,3-DHMB] in solution at pH=11.0
in the presence and in the absence of TiO$_2$.
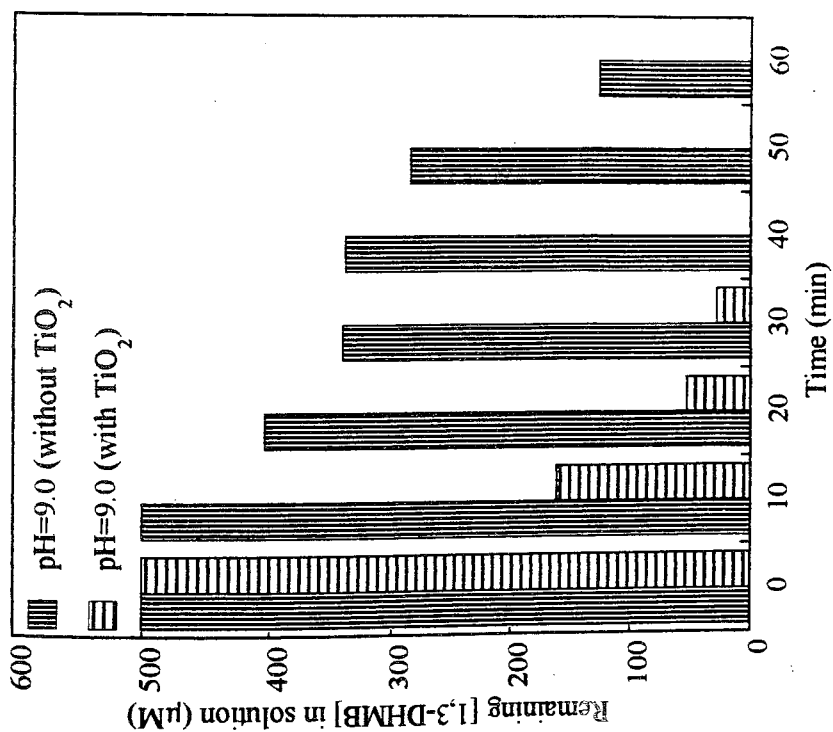
Figure 7.2.3. Remaining [1,3-DHMB] in solution at pH=9.0
in the presence and in the absence of TiO$_2$.
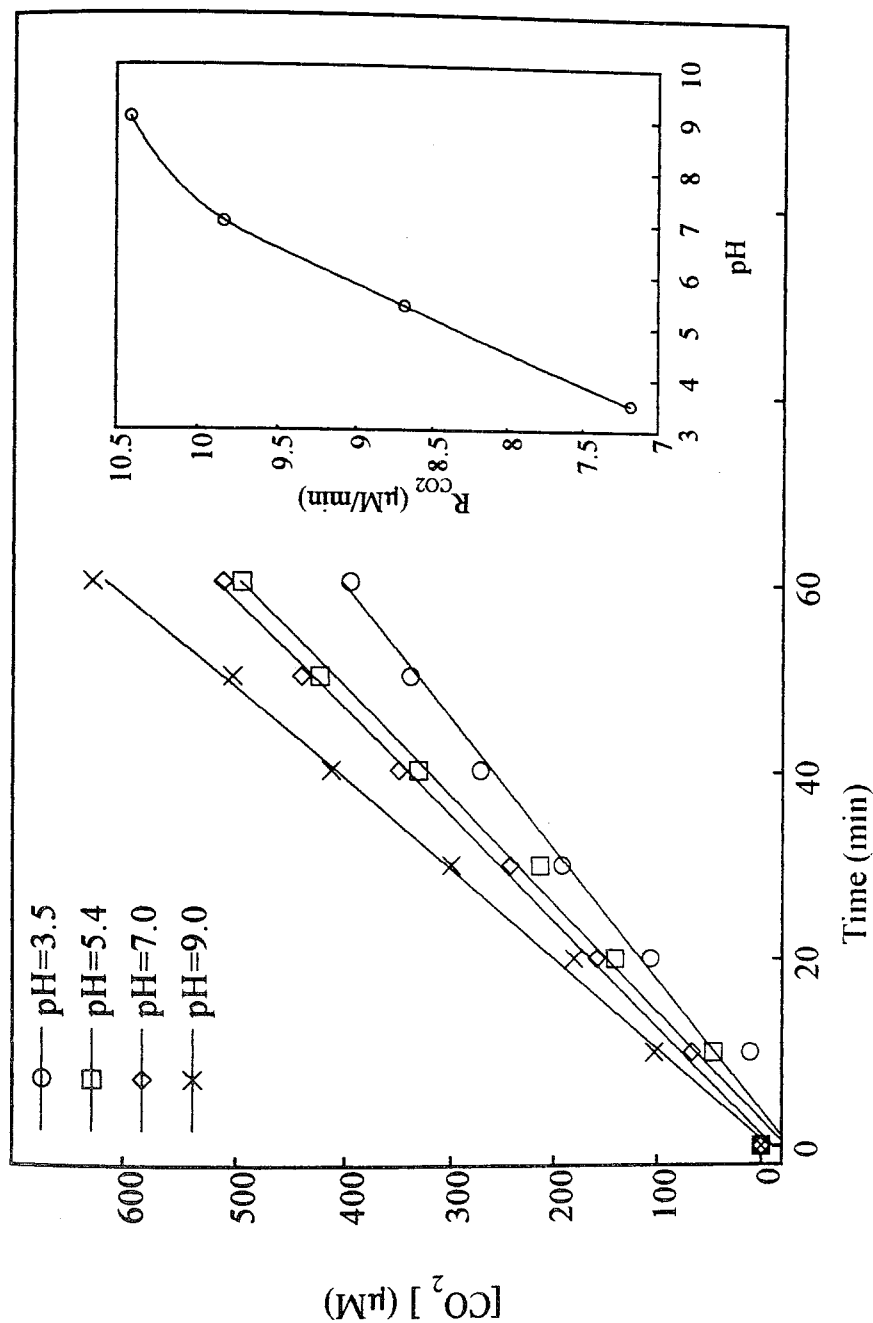
Figure 7.2.5. Effect of pH on the concentration of CO_2 produced.

Inset: R_{CO2} as a function of pH.. Conditions: $[TiO_2]=1g/L$, Flow Rate=144 ml/min, $[1,3\text{-}DHMB]_0=500 \mu M$, T=298 K, $I_0=10.8 \times 10^{-6}$ einstein/min.

Table 7.2.4. Effect of pH on the concentration of CO_2 produced. Equations are for 60 min irradiation time.

Time (min)	CO_2 (µM)			
	pH=3.5	pH=5.4	pH=7.0	pH=9.0
0	0	0	0	0
10	10.4	45.3	66.5	103
20	107	141	159	181
30	193	214	243	300
40	272	331	350	413
50	339	424	441	503
60	396	495	512	628
y= (µM) x= (min)	y=-27.2+7.18x R=0.992	y=-24.9+8.69x R=0.996	y=-12.2+8.84x R=0.999	y=-8.43+10.4x R=0.999
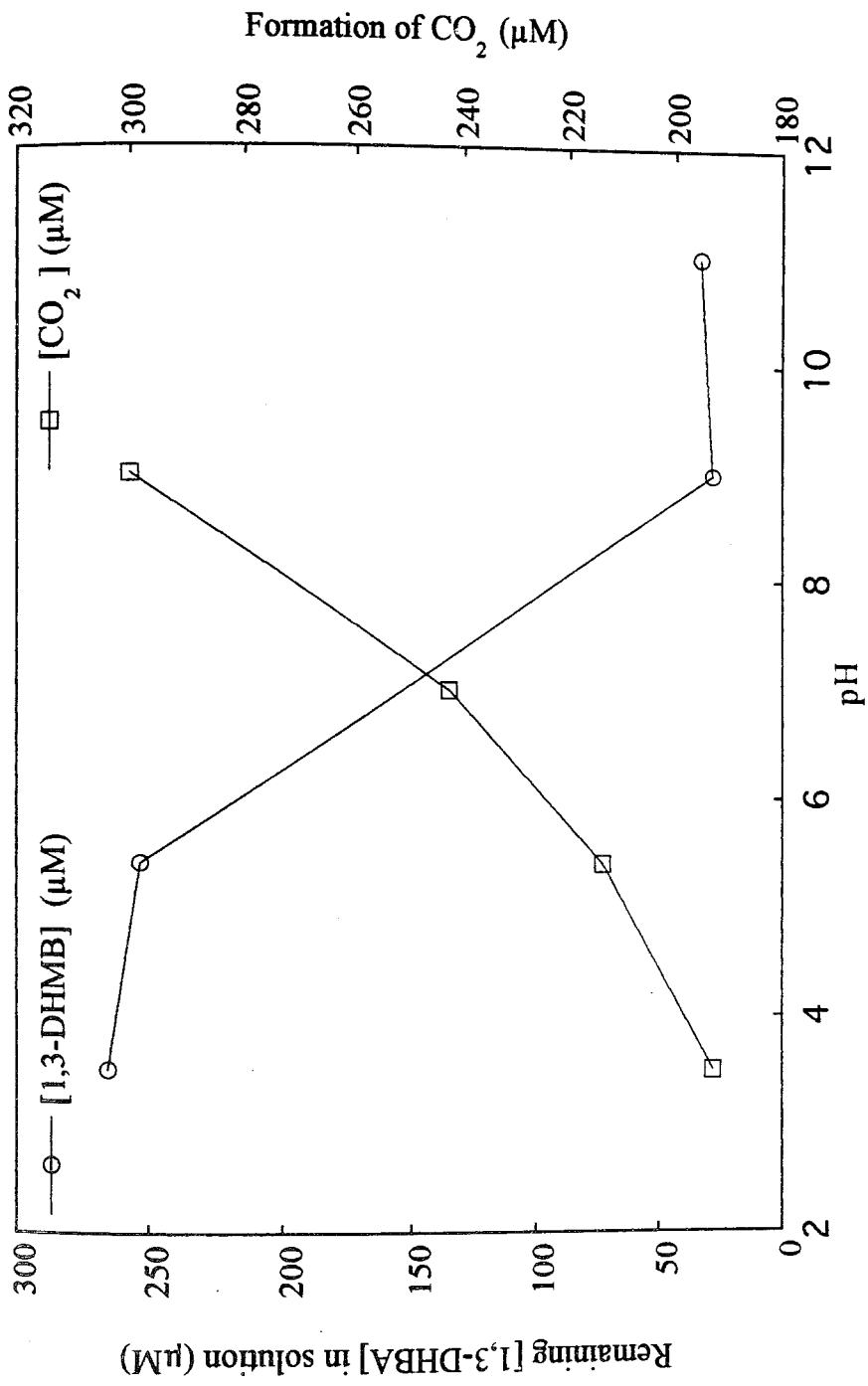
Figure 7.2.6. Concentration of CO_2 produced and remaining 1,3-DHMB in solution as a function of pH after 30 min irradiation. Conditions: $[TiO_2]=1g/L$, Flow Rate=144 ml/min, $[1,3\text{-DHMB}]_0=500$ μM, T=298 K, $I_0=10.8 \times 10^{-6}$ einstein/min.

Table 7.2.5. Effect of pH on the formation of CO_2
and degradation of [1,3-DHMB] after 30 min irradiation.

pH	[1,3-DHMB] (μM)	CO_2 (μM)
3.5	265	193
5.4	253	214
7.0	-*	243
9.0	27.9	300
11.0	32.8	-*

*These points were not measured.

7.3. Effect of Irradiation Time

The effect of irradiation time is investigated for 500 μM 1,3-DHMB. Figure 7.3.1 and Table 7.3.1 give the results of the per cent of remaining 1,3-DHMB in solution and the per cent formation of CO_2. Extending the irradiation time to 180 min, decreases the per cent of remaining 1,3-DHMB, i.e. increases the degradation rate and also increases the per cent of CO_2 production.

Table 7.3.1. Effect of irradiation time.

Per cent 1,3-DHMB: Each numerical value represents the per cent of remaining 1,3-DHMB in the solution. Per cent CO_2: Each numerical value represents the per cent formation of CO_2.

Time (min)	Per cent 1,3-DHMB	Per cent CO_2
0	100	0
10	59.2	1.29
20	55.7	4.03
30	50.6	6.11
40	42.4	9.46
50	39.9	12.1
60	29.9	14.1
90	21.4	21.7
120	17.8	25.7
150	13.5	36.1
180	7.18	40.3
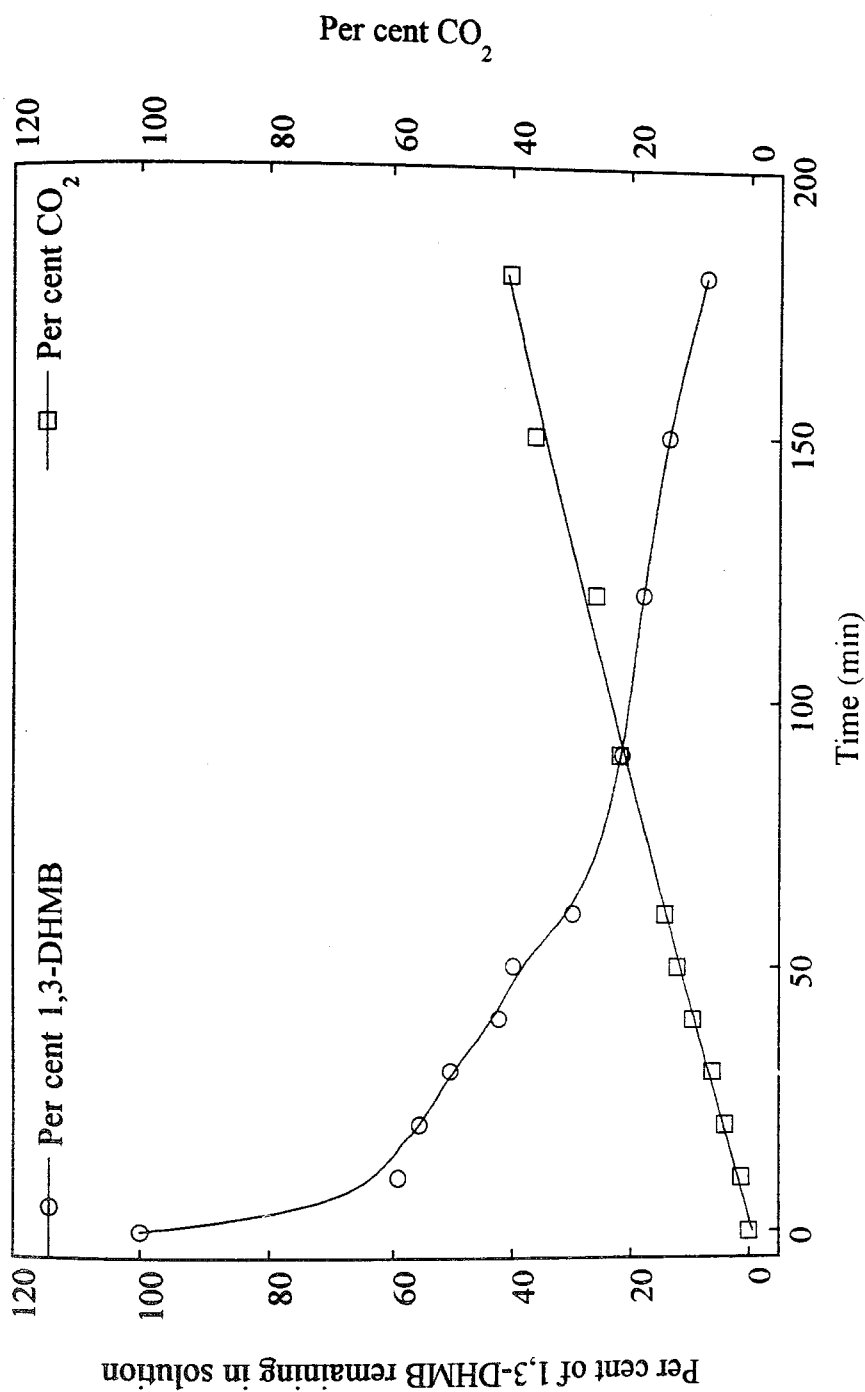
Figure 7.3.1. The per cent of 1,3-DHMB remaining in solution and the per cent of CO_2 formation as a function of irradiation time. Conditions: $[TiO_2]$=1g/L, Flow Rate=144 ml/min, $[1,3\text{-DHMB}]_0$=500 μM, pH=5.4, T=298 K, I_0=10.8x10^{-6} einstein/min.

7.4. Effect of Temperature

The formation of CO_2 is also investigated in the temperature range 298-333 K for 60 min irradiation time (Figure 7.4.1, Table 7.4.1). Calibrations are repeated in the studied temperature range (Appendix A). From the Arrhenius type plot (Figure 7.4.1 inset), the apparent activation energy is calculated as 17.1 kJ/mol.

7.5. Postulated Mechanism: Route of Oxidation

In order to ascertain the route of oxidation for 1,3-DHMB, i.e. oxidation with photogenerated holes or reaction with ˙OH radicals, the same initial charge transfer reactions and rate equations of 1,3-DHB and 3,5-DHT are assumed to be valid also for 1,3-DHMB. Therefore, the initial rate equation will be as follows for 1,3-DHMB:

$$\frac{1}{R_i} = \frac{k_3[OH]}{k_4[I]} \frac{1}{[C_7H_6O(OH)_2]} + \frac{1}{I} \tag{7.3}$$

where k_3 is rate constant of the oxidation process with ˙OH radicals and k_4 is rate constant of the oxidation process with photogenerated holes, and R_i is the initial rate of CO_2 formation.

According to equation (7.3), when the reciprocal of the initial rate of CO_2 formation $(1/R_{CO2})$ versus $1/[C_7H_6O(OH)_2]$ is plotted (Figure 7.1.3 inset), a straight line is obtained with correlation coefficient of 0.988. The rate of incident photon flux, I_0, is calculated
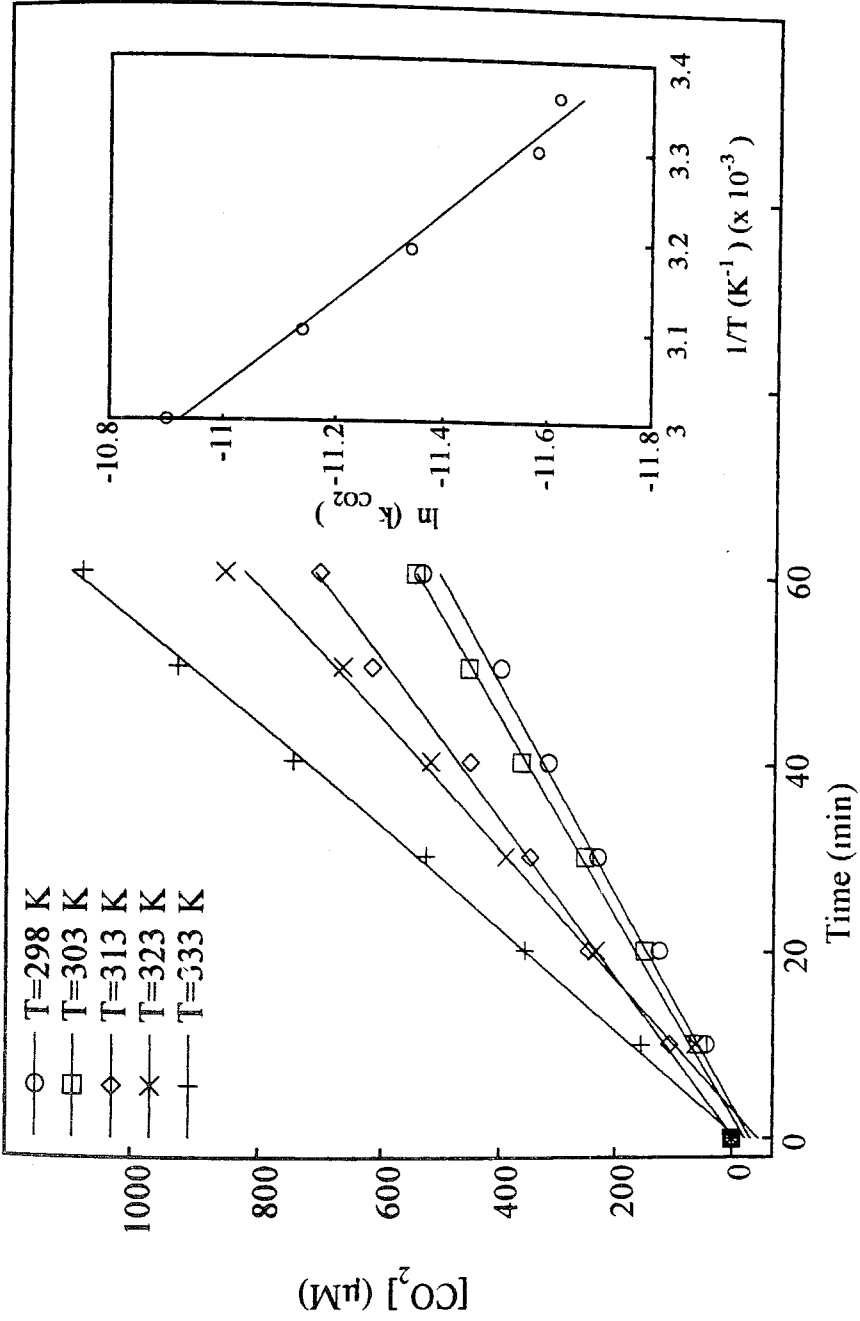
Figure 7.4.1. Effect of temperature on the concentration of CO_2 produced.

Inset: Arrhenius plot. Conditions: $[TiO_2]$=1g/L, Flow Rate=144 ml/min, pH=5.4

$[1,3\text{-DHMB}]_0$=500 μM, , I_0=10.8x10^{-6} einstein/min.

Table 7.4.1. Effect of temperature on the concentration of CO_2 evolved.

Time (min)	CO_2 (µM)				
	298 K	303 K	313 K	323 K	333 K
0	0	0	0	0	0
10	45.3	56.6	107	62.3	156
20	141	151	247	234	357
30	214	255	349	391	527
40	331	364	452	519	746
50	424	455	618	667	930
60	495	547	705	856	1080
y= (µM) x= (min)	y=-24.9+8.69x R=0.996	y=-22.8+9.47x R=0.998	y=-4.07+11.9x R=0.998	y=-45.4+14.5x R=0.996	y=-12.4+18.5x R=0.999

as 2.64×10^{-5} einstein dm^{-3} s^{-1}. From the slope of $1/R_{CO2}$ versus $1/[C_7H_6O(OH)_2]$, a $k_3[OH]/k_4I$ value of 0.0765 is obtained. Considering the natural pH (pH=5.4) of 1,3-DHMB, a ratio of $k_3/k_4 = 1.91 \times 10^5$ is deduced. Thus the formation of $^{\cdot}OH$ radicals is more favored than the photogenerated holes for the oxidation of 1,3-DHMB.

7.6. Relative Photonic Efficiencies

The relative photonic efficiencies for 1,3-DHMB are calculated according to equation 7.4.

$$\zeta = \frac{\text{rate of formation } CO_2 \text{ for } 1,3-\text{DHMB}}{\text{rate of formation } CO_2 \text{ for } 1,3-\text{DHB}} \tag{7.4}$$

As in the case of 3,5-DHT, 1,3-DHB is used as the probe molecule. It is found that the relative photonic efficiencies as a function of 1,3-DHMB concentration, pH and temperature are close to each other and do not show a general trend (Figure 7.6.1). A detailed information is given in the discussion chapter.
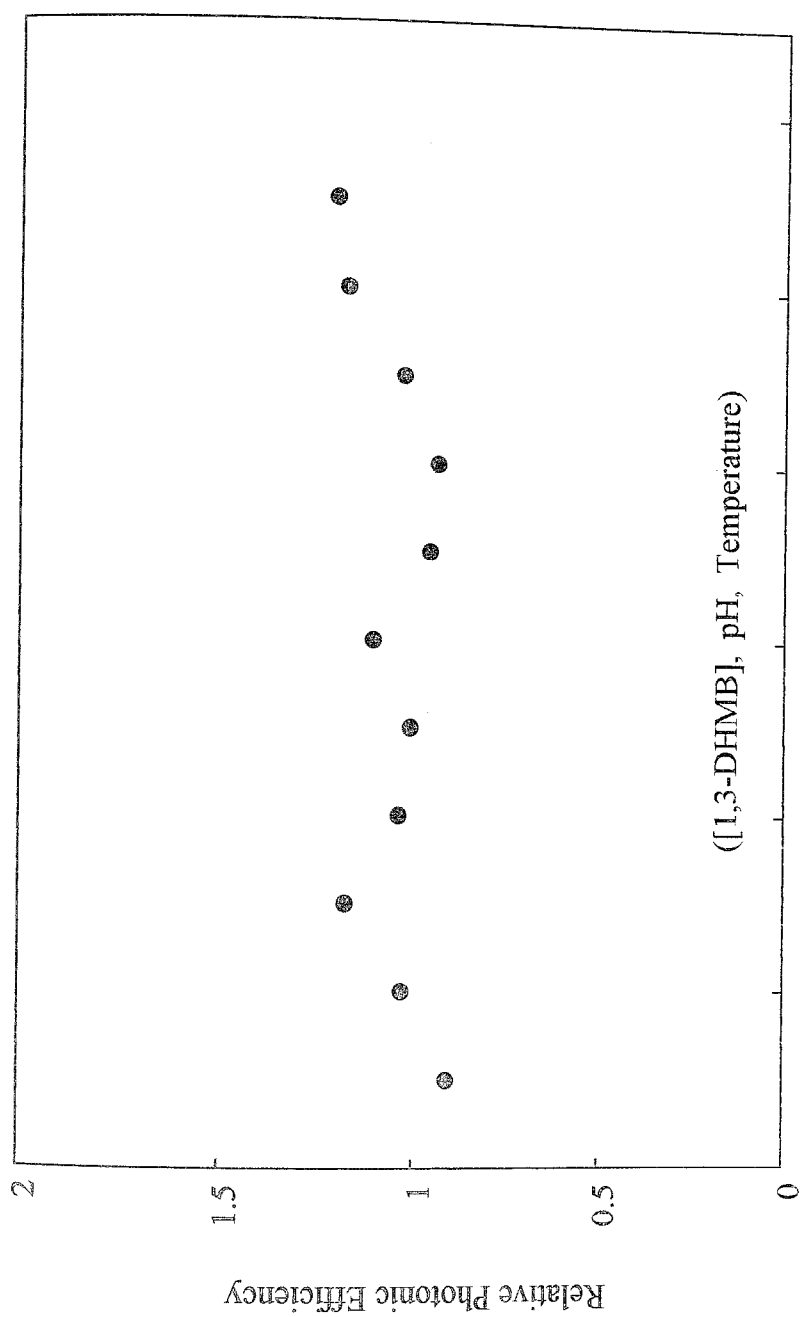
Figure 7.6.1. Relative photonic efficiencies as a function of 1,3-DHMB concentration, pH and temperature for 1,3-DHMB.

8. 3,5-DIHYDROXYBENZOIC ACID (3,5-DHBA)

8.1. Effect of 3,5-DHBA Concentration

The effect of 3,5-DHBA concentration on the photocatalytic degradation of 3,5-DHBA is examined in the range of 75 μM to 1000 μM (Figure 8.1.1, Table 8.1.1). The stoichiometric reaction for complete degradation is given by:

$$C_7H_4O_2(OH)_2 + 13/2O_2 \rightarrow 7CO_2 + 3H_2O \qquad (8.1)$$
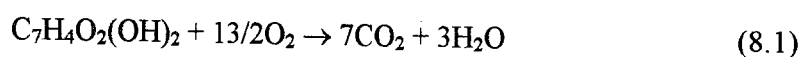
In the first set of experiments the degradation of 3,5-DHBA is monitored. With 10 μM concentration, the corresponding peak of 3,5-DHBA cannot be detected that is why this concentration is not included in the investigation range. A rapid decrease (more than 50 per cent) in the 3,5-DHBA concentration is observed for 75 μM, 100 μM and 200 μM solutions after 5 min irradiation. A lower initial decrease is obtained with the highest concentration, 1000 μM. 100 μM is used throughout the experiments, unless otherwise mentioned.

The linearity in Figure 8.1.1 inset (Table 8.1.2) indicates the kinetics of 3,5-DHBA degradation are zeroth order. Numerical results are given in Table 8.1.3.
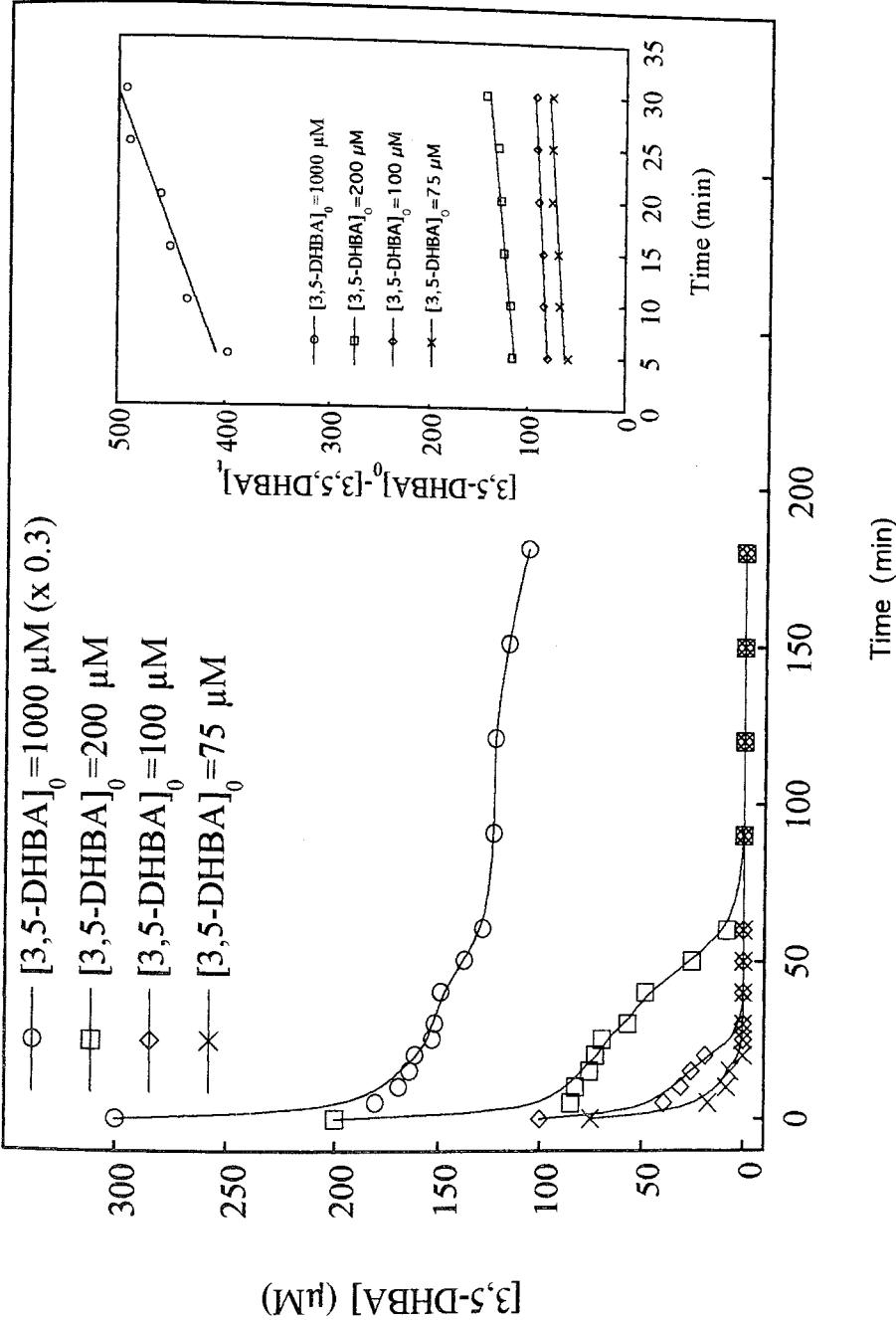
Figure 8.1.1. Effect of 3,5-DHBA concentration on the degradation of 3,5-DHBA.

Inset: ([3,5-DHBA]$_0$-[3,5-DHBA]$_t$) versus irradiation time. Conditions: [TiO$_2$]=1g/L, pH=4.4, Flow Rate=144 ml/min, T=298 K, I$_0$=10.8x10^{-6} einstein/min.

Table 8.1.1. Effect of 3,5-DHBA concentration on the degradation of 3,5-DHBA. Each numerical value represents the concentration of 3,5-DHBA remaining in the solution.

Time (min)	$[3,5\text{-DHBA}]_0$			
	1000 μM	200 μM	100 μM	75 μM
0	1000	200	100	75
5	602.8	84.85	21.21	17.35
10	564.5	82.51	16.54	8.08
15	548.1	75.66	15.97	6.46
20	539.1	72.75	10.57	0
25	510.7	69.58	9.21	0
30	507.1	56.94	8.24	0
40	497.9	48.27	0	0
50	459.3	25.15	0	0
60	429.7	8.11	0	0
90	411.6	0	0	0
120	408.9	0	0	0
150	386.6	0	0	0
180	355.1	0	0	0

Table 8.1.2. ([3,5-DHBA]$_0$-[3,5-DHBA]$_t$) versus time data.

Time (min)	[3,5-DHBA]$_0$			
	1000 μM	200 μM	100 μM	75 μM
5	397.1	115.2	78.79	57.65
10	435.5	117.5	83.46	66.92
15	452.1	124.3	84.03	68.54
20	460.9	127.3	89.43	75
25	489.3	130.4	90.79	75
30	492.8	143.1	91.76	75
y= (μM) x= (min)	y=389.7+3.71x R=0.971	y=108.2+1.44x R=0.964	y=77.15+1.52x R=0.969	y=57.94+1.07x R=0.909

Table 8.1.3. Kinetic data for 3,5-DHBA degradation.

[3,5-DHT]$_0$ (µM)	k (1/min)	Rate (1/min)
1000	3.71	3.71
200	1.44	1.44
100	1.52	1.52
75	1.67	1.07

In second set of experiments, evolution of CO_2 is monitored in the 75 µM-1000 µM concentration range (Figure 8.1.2, Table 8.1.4). In the plot of rate of CO_2 production versus 3,5-DHBA concentration, a plateau is observed with the increase in concentration (Figure 8.1.3, Table 8.1.5). To obtain the reaction rate constant, k and adsorption constant, K, the inverse of the rate of CO_2 evolution is plotted against the inverse of 3,5-DHBA concentration. From the Figure 8.1.3 inset, k is found as 15.68 µM/min and K is found as 27.1×10^{-3} 1/µM.

When the degradation percentage of 3,5-DHBA and the formation percentage of CO_2 are examined, it is observed that these percentages increase when the irradiation period is prolonged and concentration of 3,5-DHBA is decreased. As obtained with the other compounds, the per cent production of CO_2 is lower than the per cent degradation which is due to the formation of intermediates which can resist mineralization and also compete with 3,5-DHBA for the hydroxyl radicals (Table 8.1.6).
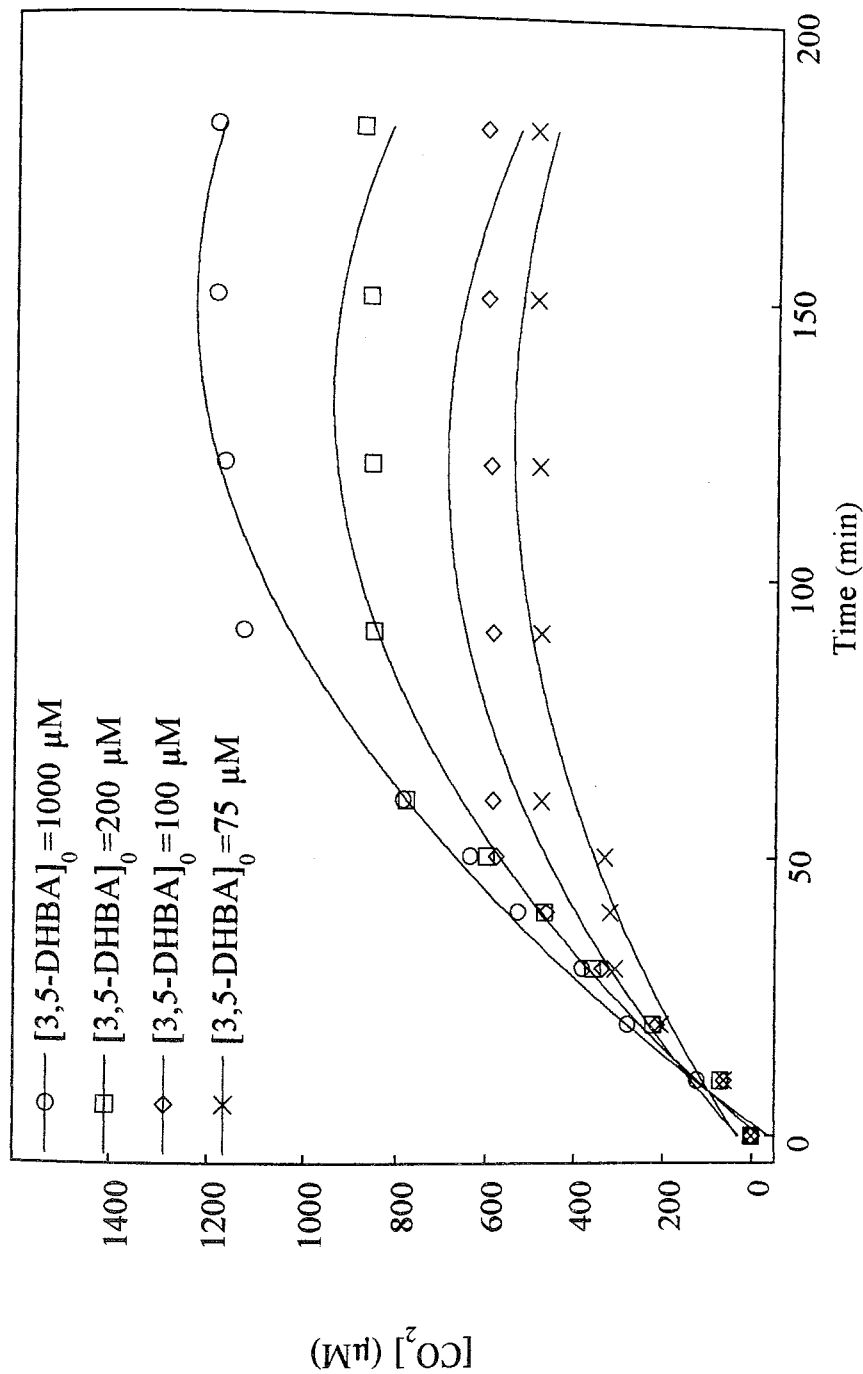
Figure 8.1.2. Effect of initial 3,5-DHBA concentration on the concentration of CO_2 evolved as a function of irradition time. Conditions: $[TiO_2]=1g/L$, Flow Rate=144 ml/min, pH=4.4, T=298 K, $I_0=10.8 \times 10^{-6}$ einstein/min.

Table 8.1.4. Effect of initial 3,5-DHBA concentration on the concentration of CO_2 evolved as a function of irradiation time. Equations represent the linear portion of the data, i.e. 60 min irradiation time.

Time (min)	[3,5-DHBA]$_0$			
	1000 μM	200 μM	100 μM	75 μM
0	0	0	0	0
10	122	70.6	62.5	61.3
20	279	211	211	203
30	383	358	336	307
40	529	467	464	320
50	638	600	578	332
60	787	779	585	476
90	1130	852	586	477
120	1170	858	593	483
150	1190	862	602	490
180	1190	879	606	493
y= (μM) x= (min)	y=-1.21+13.3x R=0.999	y=-20.9+12.2x R=0.995	y=-25.6+12.1x R=0.994	y=1.12+8.86x R=0.974
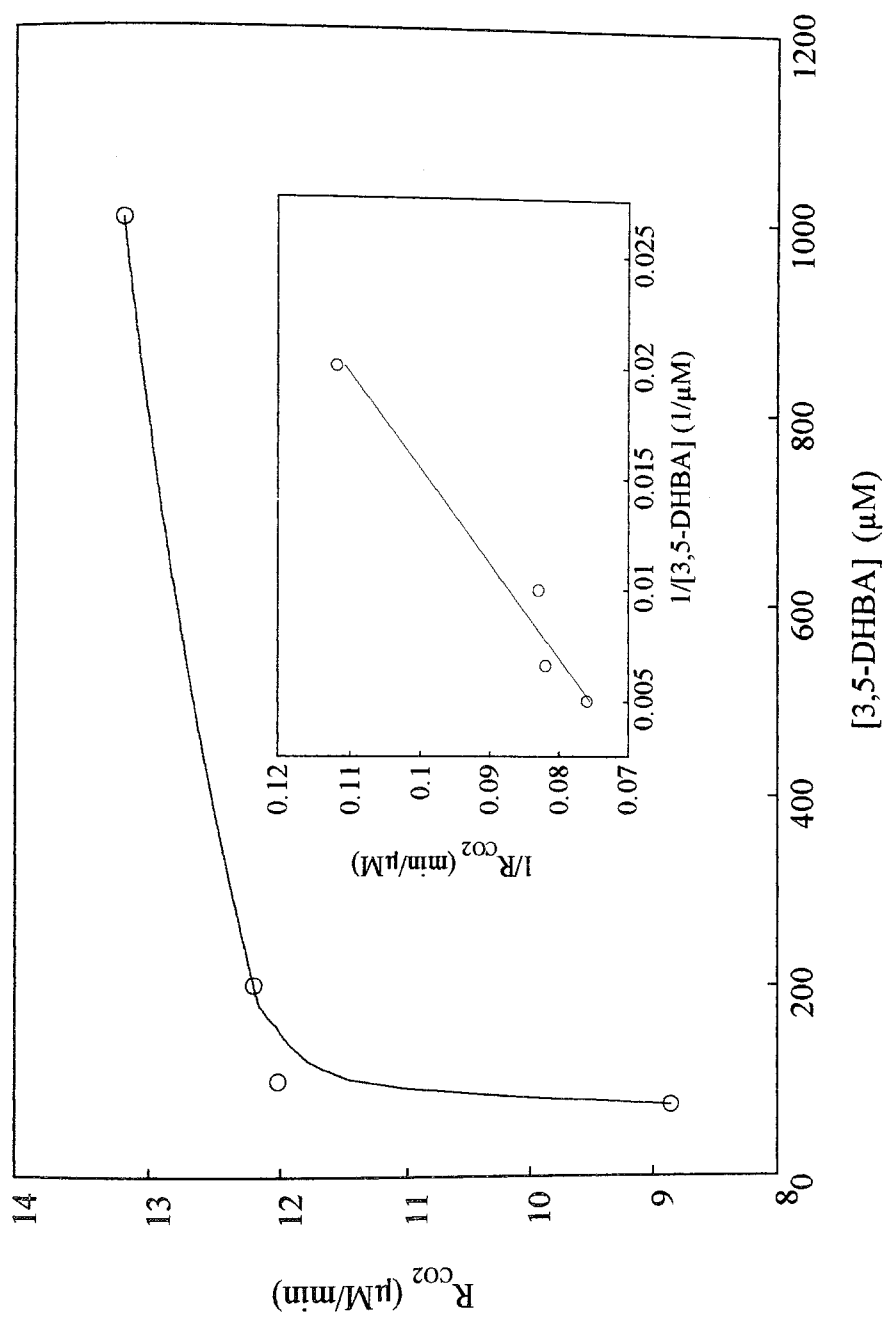
Figure 8.1.3. Rate of CO_2 production versus 3,5-DHBA concentration.

Inset: $1/R_{CO2}$ as a function of $1/[3,5-DHBA]$. Conditions: $[TiO_2]=1g/L$, pH=4.4, Flow Rate=144 ml/min, T=298 K, $I_0=10.8 \times 10^{-6}$ einstein/min.

173

Table 8.1.5. Effect of 3,5-DHBA concentration on the formation rate of CO_2.

[3,5-DHBA] (μM)	R_{CO2} ($\mu M/min$)	1/[3,5-DHBA] ($1/\mu M$)	$1/R_{CO2}$ ($min/\mu M$)
1000	13.3	0.001	0.075
200	12.2	0.005	0.082
100	12.1	0.010	0.083
75	8.86	0.013	0.112

Table 8.1.6. Degradation percentage of 3,5-DHBA and formation percentage of CO_2.

[3,5-DHT] (μM)	Per cent Degradation of 3,5-DHBA		Per cent Formation of CO_2	
	in 60 min	in 180 min	in 60 min	in 180 min
1000	57	64	11	17
200	96	100	56	63
100	100	100	84	87
75	100	100	91	94

8.2. Effect of pH

The pH changes of the 3,5-DHBA/TiO_2 suspensions are again controlled in the first set of experiments (Table 8.2.1).

Table 8.2.1. Resulting pH changes before (pH_1) and after irradiation (pH_2) for 3,5-DHBA/TiO_2 suspensions.

pH	pH_1	pH_2	$\Delta pH = pH - pH_2$
3.5	3.5	3.4	0.1
4.4	4.4	4.1	0.3
7.0	6.2	5.9	1.1
9.0	8.2	6.5	2.5
11.0	10.9	10.5	0.5

For acidic pH's, pH 3.5 and pH 4.4, the pH_1 values do not differ when compared with the initial pH's. However, for neutral and alkaline pH's, decrements are observed in the

pH$_1$ values because of the acidic pzc value of TiO$_2$. After irradiation, the decrease in all pH values are due to the consumption of OH$^-$ ions.

The second set of experiments investigates the effect of pH on the photodegradation of 3,5-DHBA (Tables 8.2.2 and 8.2.3). In the absence of TiO$_2$, the remaining amount of 3,5-DHBA in the solution phase decreases with respect to irradiation time. When the decrements in the acidic media, pH 3.5 and pH 4.4, are compared with that of pH 9.0, it is observed that the remaining amount in the solution is lower at pH 3.5 and pH 4.4. This can be explained by the dissociation process of 3,5-DHBA.

$$+ H^+ \qquad pK=4.04 \qquad (8.2)$$
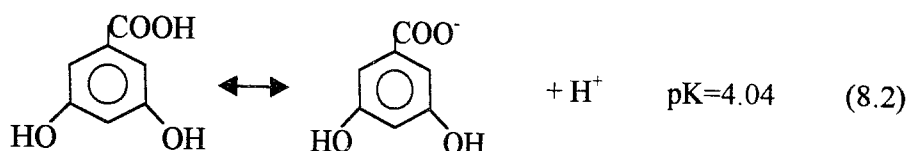
Since pH 3.5 and 4.4 are close to the pK of 3,5-DHBA, it can be assumed that degradation starts with the dissociation of 3,5-DHBA. However, at pH 11, the amount of 3,5-DHBA in the solution is lower compared to acidic pH's and pH 9.0. Thus, the excess OH$^-$ ions act as active species in the degradation process without TiO$_2$.

The initial rate of photodegradation in the presence of TiO$_2$ depends on both the rate in the bulk solution and that on the TiO$_2$ surface. At acidic pH values, the surface of TiO$_2$ is positively charged and favors adsorption of negatively charged species. Since pH 4.4 is close to the pK value of 4.04 (equation 8.2), the electrostatic interactions between the positive TiO$_2$ surface and the 3,5-DHBA anion lead to the adsorption of the latter onto the metal oxide. Adsorption is highest at pH 4.4 and the corresponding amounts of 3,5-DHBA remaining in the solution are lower, demonstrating the largest rate of degradation at pH 4.4. At pH 3.5, adsorption is still possible but to a lesser extend than

Table 8.2.2. Effect of pH on the degradation of 3,5-DHBA in the absence of TiO_2.

Each numerical value represents the remaining 3,5-DHBA concentration in the solution.

Time (min)	$[3,5\text{-DHBA}]_0 = 100\ \mu M$				
	pH=3.5	pH=4.4	pH=9.0	pH=11.0	
0	100	100	100	100	
5	92.63	91.96	94.71	90.06	
10	87.03	82.92	92.87	81.76	
15	85.89	82.92	90.72	74.49	
20	85.08	82.11	90.41	53.72	
25	81.46	80.49	90.14	43.23	
30	79.68	79.44	87.84	27.82	
40	78.89	76.83	83.55	15.55	
50	77.29	74.41	81.98	8.28	
60	72.51	72.86	76.71	0	

Table 8.2.3. Effect of pH on the degradation of 3,5-DHBA in the presence of TiO_2. Each numerical value represents the remaining 3,5-DHBA concentration in the solution.

Time (min)	$[3,5\text{-DHBA}]_0 = 100\ \mu M$			
	pH=3.5	pH=4.4	pH=9.0	pH=11.0
0	100	100	100	100
5	38.97	21.21	49.67	54.45
10	30.61	16.54	41.97	42.52
15	25.73	15.97	27.86	36.11
20	18.45	10.57	17.43	19.19
25	12.21	9.21	12.68	11.62
30	10.90	8.24	11.42	10.46

at pH 4.4. Increasing the solution pH diminished adsorption, which increases the amount remaining in the solution phase at pH 9.0 and 11.0. However, it is observed that degradation is still possible even in the alkaline media. This is due to the photodegradation process taking place in the bulk solution with desorbed $^{\bullet}OH$ radicals. At pH 11.0, excess OH^- ions compete with 3,5-DHBA ions for surface sites on the photocatalyst and decrease the generation of $^{\bullet}OH$ radicals. Thus, the highest degradation in the bulk phase is observed at pH 9.0. Figures 8.2.1, 8.2.2, 8.2.3, and 8.2.4 illustrate the remaining concentration of 3,5-DHBA in the solution phase with respect to irradiation time at different pH values.

The effect of pH is also examined for the formation of CO_2 (Figure 8.2.5, Table 8.2.4). The highest rates (Figure 8.2.5 inset) are observed in acidic media. The lowest rate is obtained at pH 7.0, but increasing the solution pH to pH 9.0 increased the evolution of CO_2 because of its degradation in the solution phase. These results correspond to those discussed for the second set of experiments (Figure 8.2.6, Table 8.2.5).

Figure 8.2.2. Remaining [3,5-DHBA] in solution at pH=4.4 in the presence and in the absence of TiO$_2$.
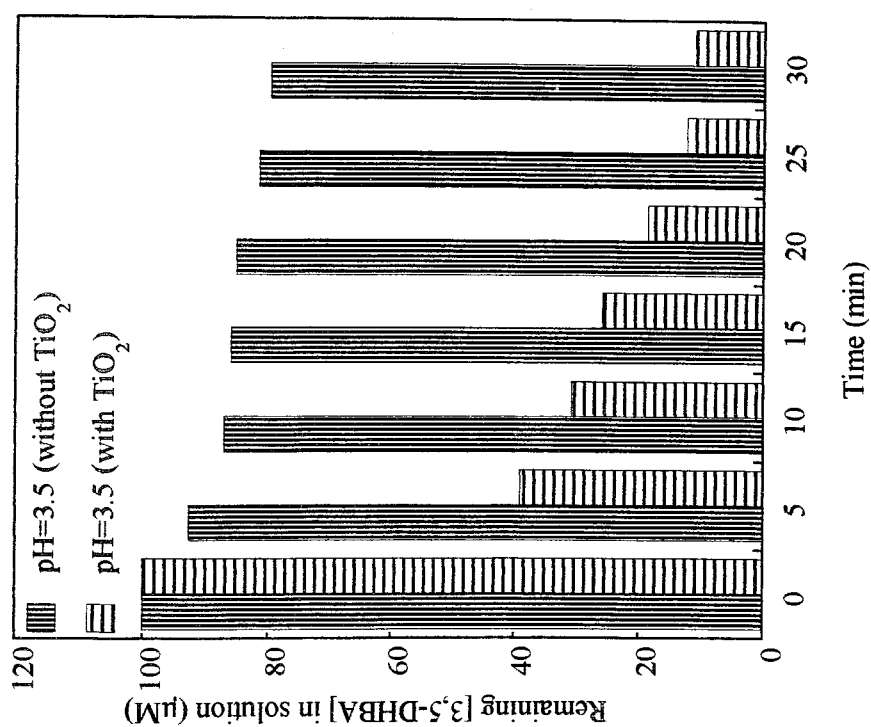
Figure 8.2.1. Remaining [3,5-DHBA] in solution at pH=3.5 in the presence and in the absence of TiO$_2$.
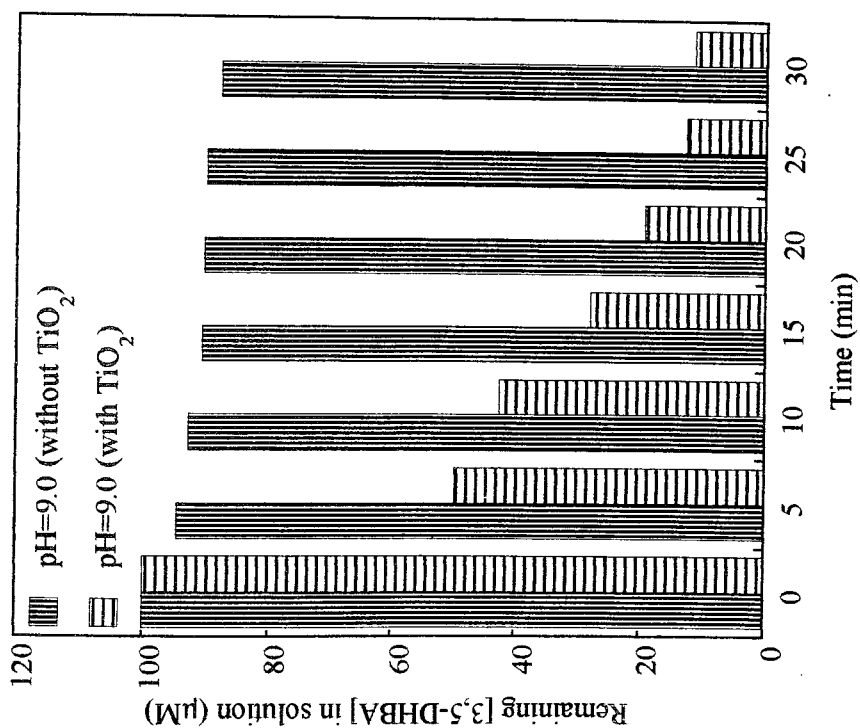
Figure 8.2.3. Remaining [3,5-DHBA] in solution at pH=9.0 in the presence and in the absence of TiO_2.
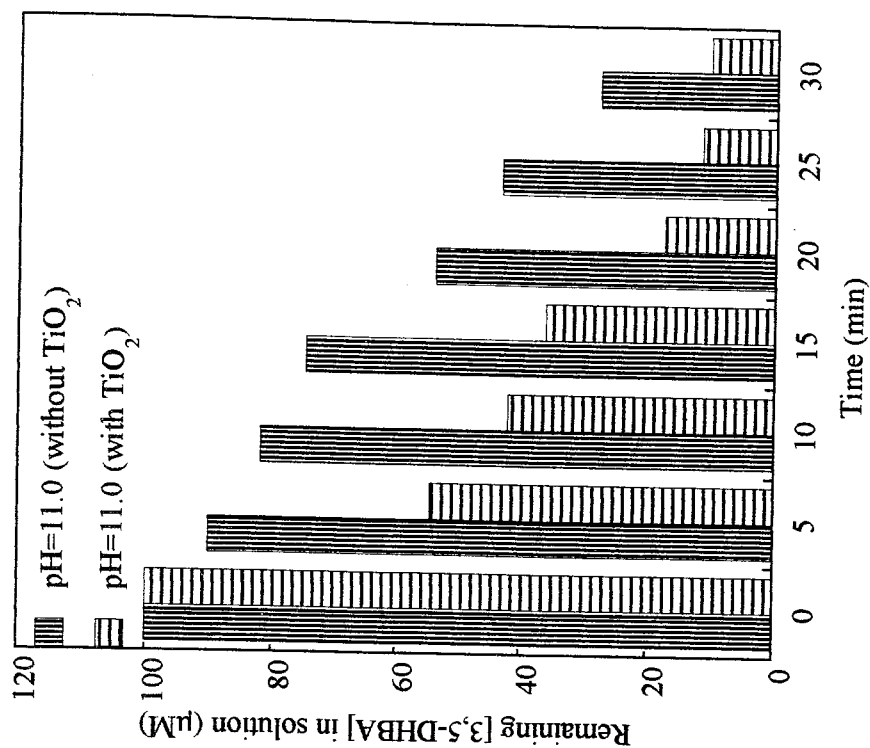
Figure 8.2.4. Remaining [3,5-DHBA] in solution at pH=11.0 in the presence and in the absence of TiO_2.
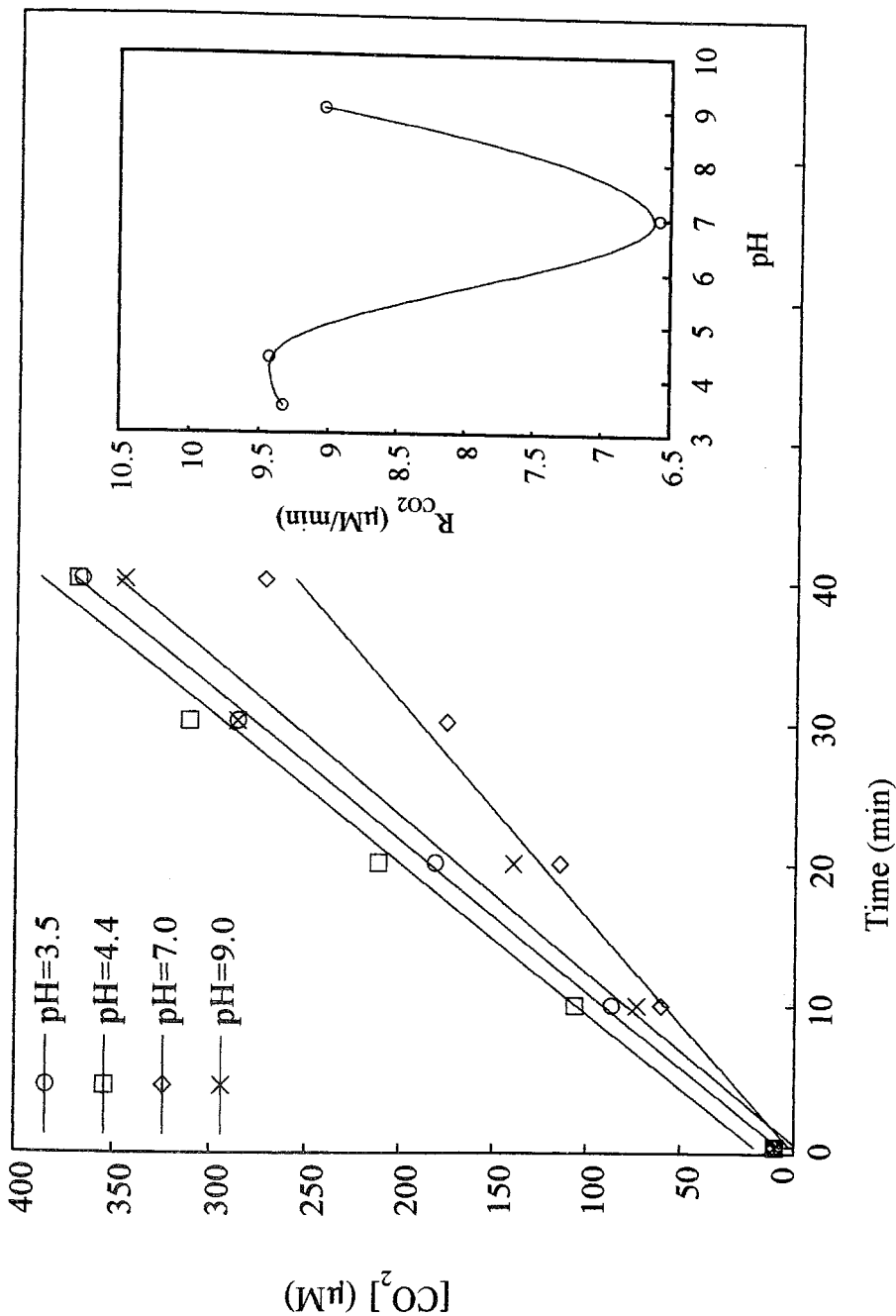
Figure 8.2.5. Effect of pH on the concentration of CO_2 produced.

Inset: R_{CO_2} as a function of pH.. Conditions: $[TiO_2]$=1g/L, Flow Rate=144 ml/min,

$[3,5\text{-}DHBA]_0$=100 μM, T=298 K, I_0=10.8x10^{-6} einstein/min.

Table 8.2.4. Effect of pH on the concentration of CO_2 produced.

Equations represent the linear portion of the data, i.e. 40 min irradiation time.

Time (min)	CO_2 (μM)			
	pH=3.5	pH=4.4	pH=7.0	pH=9.0
0	0	0	0	0
10	86.6	106	60.3	73.2
20	181	211	114	139
30	286	311	175	286
40	367	369	272	345
50	393	396	358	359
60	405	419	367	379
y= (μM) x= (min)	y=-2.56+9.33 x R=0.999	y=10.8+9.43 x R=0.995	y=-7.48+6.59 x R=0.993	y=-11.9+9.03 x R=0.989
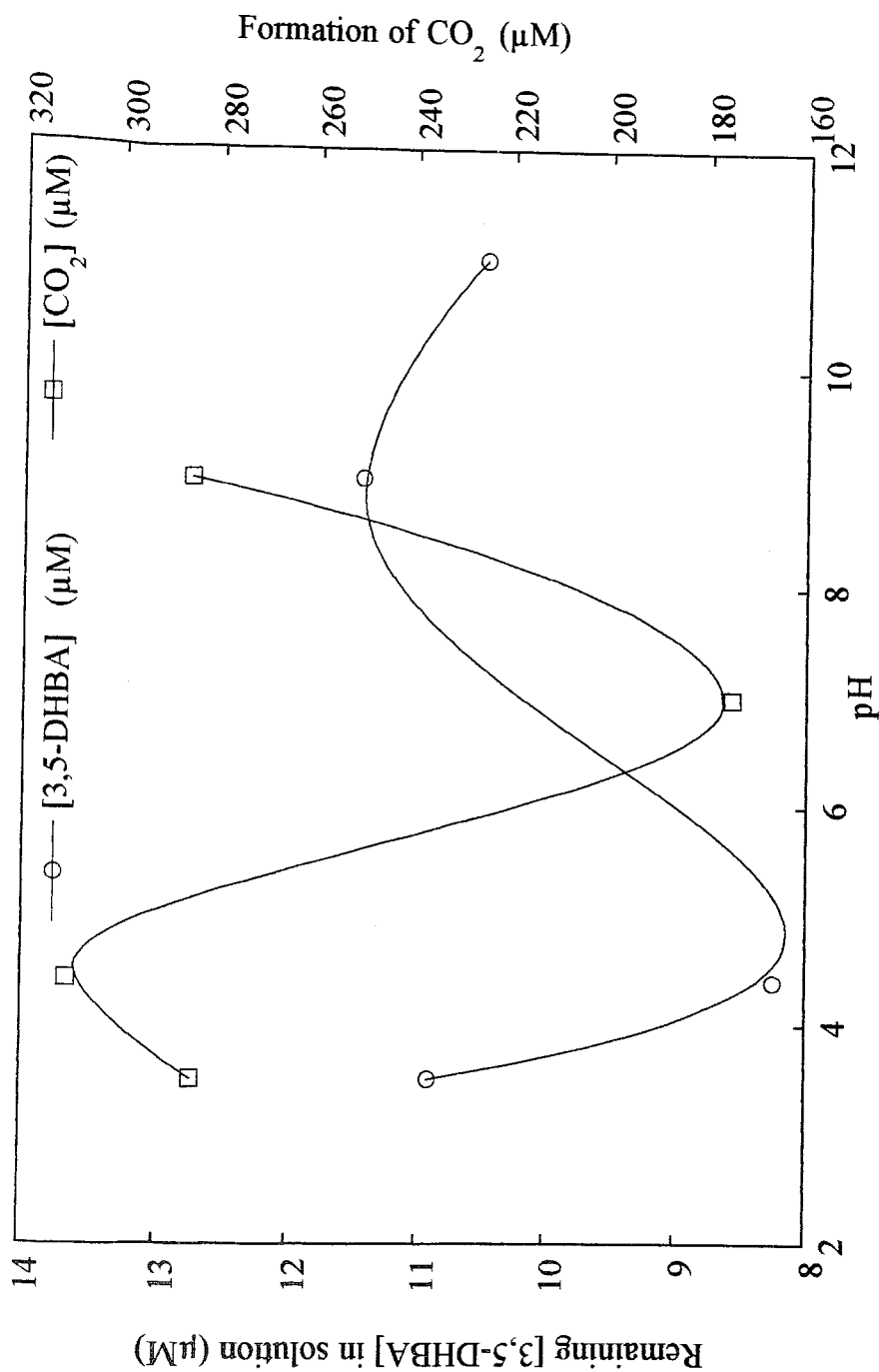
Figure 8.2.6. Concentration of CO_2 produced and remaining 3,5-DHBA in solution as a function of pH after 30 min irradiation. Conditions: $[TiO_2]=1g/L$, Flow Rate=144 ml/min, $[3,5\text{-}DHBA]_0=100\ \mu M$, $T=298\ K$, $I_0=10.8 \times 10^{-6}$ einstein/min.

Table 8.2.5. Effect of pH on the formation of CO_2
and concentration of 3,5-DHBA remaining after 30 min irradiation.

pH	[3,5-DHBA] (µM)	[CO_2] (µM)
3.5	10.90	286
4.4	8.24	311
7.0	-*	175
9.0	11.42	286
11.0	10.46	-*

*: These points were not measured.

8.3. Effect of Irradiation Time

The irradiation time effect is given in Table 8.3.1 and Figure 8.3.1. At the end of 30 min irradiation, the per cent of 3,5-DHBA remaining in solution and the per cent of CO_2 production are obtained as 92 per cent and 48 per cent, respectively. Differences in these percentages are due to the presence of intermediates in the reaction media. Extending the irradiation time to 180 min, increases the per cent of CO_2 production to 86.6 per cent.

Table 8.3.1. Effect of irradiation time.

Per cent 3,5-DHBA: Each numerical value represents the per cent of remaining 3,5-DHBA in the solution. Per cent CO_2: Each numerical value represents the per cent formation of CO_2.

Time (min)	Per cent 3,5-DHBA	Per cent CO_2
0	100	0
5	21.2	50.1
10	16.5	62.5
15	15.9	159
20	10.6	211
25	9.21	300
30	8.24	336
40	0	464
50	0	578
60	0	585
90	0	586
120	0	593
150	0	602
180	0	606
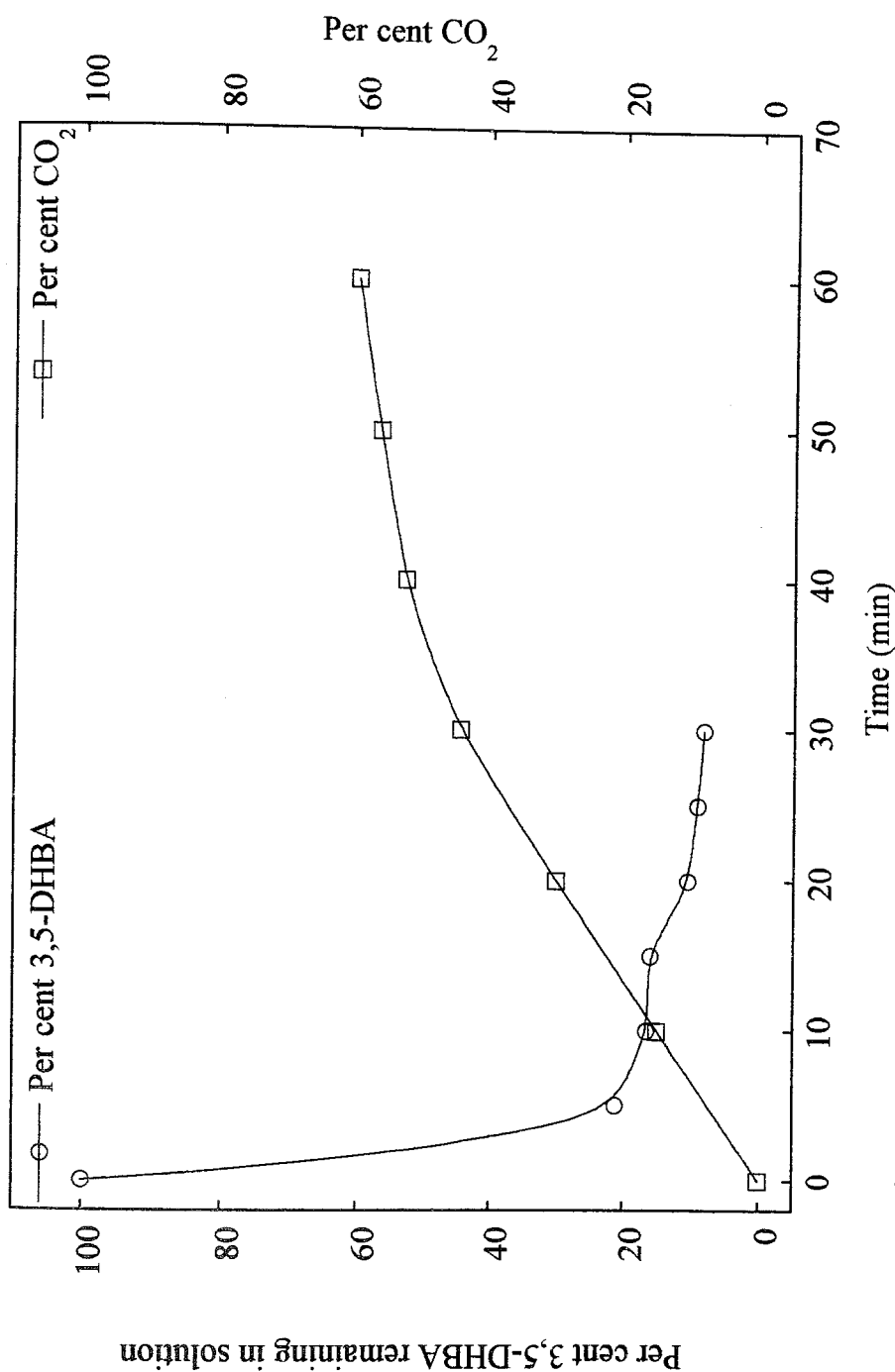
Figure 8.3.1. The per cent of 3,5-DHBA remaining in solution and the per cent of CO_2 formation as a function of irradiation time. Conditions: $[TiO_2]=1g/L$, Flow Rate=144 ml/min, $[3,5\text{-}DHBA]_0=100$ µM, pH=4.4, T=298 K, $I_0=10.8 \times 10^{-6}$ eistein/min.

8.4. Effect of Temperature

The effect of temperature on the rate of CO_2 evolution is followed in the range 298-333K for 60 min irradiation time (Figure 8.4.1, Table 8.4.1). Calibrations are repeated in the studied temperature range (Appendix A). From the Arrhenius type plot (Figure 8.4.1 inset), the apparent activation energy is calculated as 10.3 kJ/mol.

8.5. Postulated Mechanism: Route of Oxidation

The same initial charge transfer reactions and rate equations of 1,3-DHB, 3,5-DHT and 1,3-DHMB are assumed to be valid also for the route of oxidation of 3,5-DHBA. Therefore, the initial rate equation will be as follows for 3,5-DHBA:

$$\frac{1}{R_i} = \frac{k_3[OH]}{k_4[I]} \frac{1}{[C_7H_4O_2(OH)_2]} + \frac{1}{I} \tag{8.3}$$

where k_3 is the rate constant of the oxidation process with $^{\bullet}OH$ radicals and k_4 is the rate constant of the oxidation process with photogenerated holes, and R_i is the initial rate of CO_2 formation.

According to equation (8.3), the reciprocal of the initial rate of CO_2 formation ($1/R_{CO2}$) versus $1/[C_7H_4O_2(OH)_2]$ is plotted (Figure 8.1.3 inset), and from the slope a $k_3[OH]/k_4I$ value of 2.354 is obtained. Rate of light absorption, I, is calculated as
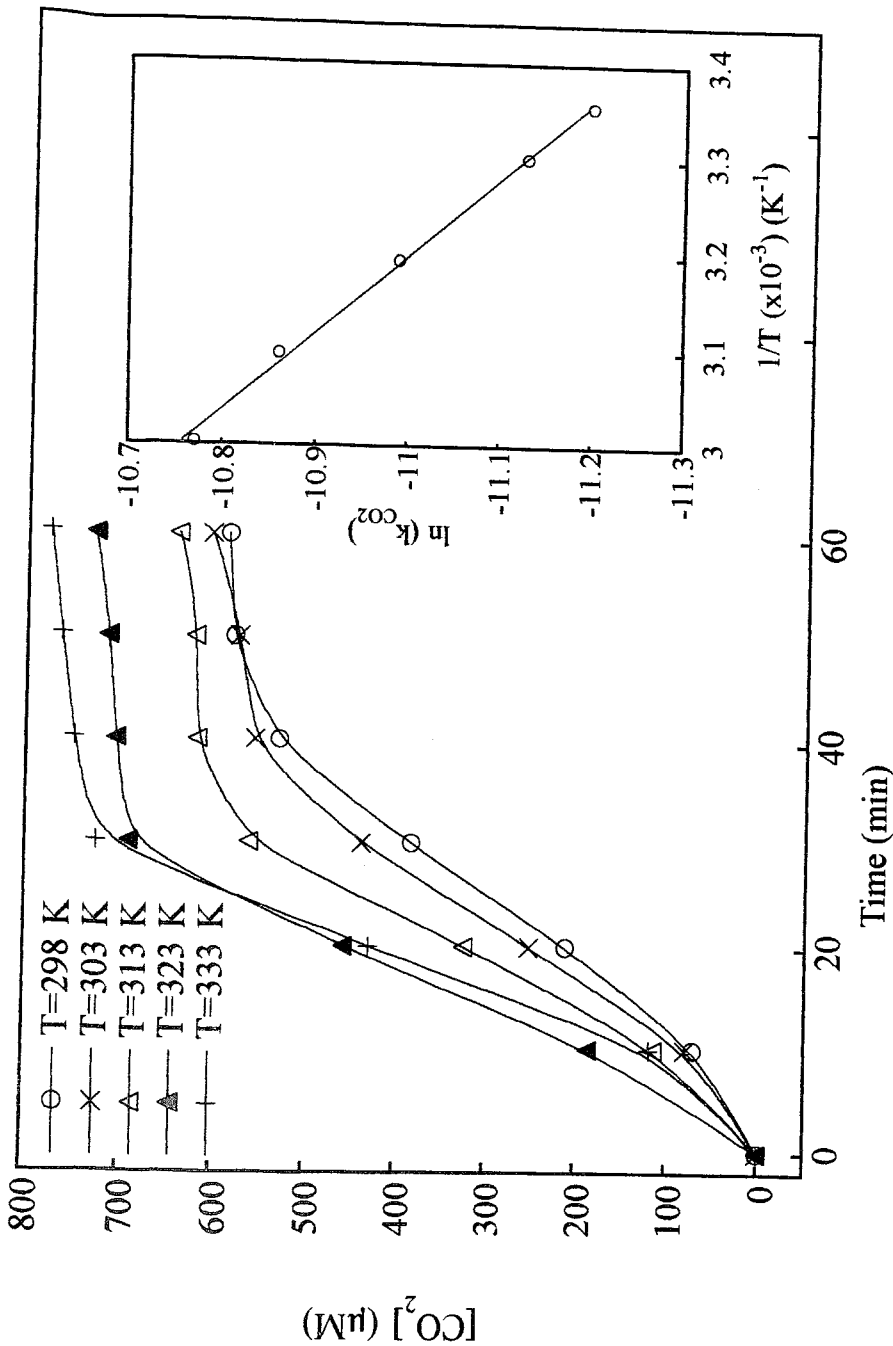
Figure 8.4.1. Effect of temperature on the concentration of CO_2 produced.

Inset: Arrhenius plot. Conditions: $[TiO_2]=1g/L$, Flow Rate=144 ml/min, pH=4.4

$[3,5\text{-}DHBA]_0=100 \ \mu M$, $I_0=10.8 \times 10^{-6}$ einstein/min.

Table 8.4.1. Effect of temperature on the concentration of CO_2 evolved.
Equations represent the linear portion of the data, i.e. 40 min irradiation time.

Time (min)	CO_2 (µM)				
	298 K	303 K	313 K	323 K	333 K
0	0	0	0	0	0
10	70.6	78.7	113	185	118
20	211	251	323	457	429
30	383	438	561	690	725
40	529	555	617	704	749
50	578	573	620	713	763
60	585	603	639	728	776
y= (µM) x= (min)	$y=-35.4+13.7x$ $R=0.991$	$y=-29.32+14.7x$ $R=0.993$	$y=-13.6+16.8x$ $R=0.985$	$y=-24.6+19.1x$ $R=0.974$	$y=-16.8+21.1x$ $R=0.973$

2.64×10^{-5} einstein dm^{-3} s^{-1}. Considering the natural pH (pH=4.4) of 3,5-DHBA, a ratio of $k_3/k_4 = 2.47 \times 10^5$ is deduced. Thus formation of $^{\cdot}$OH radicals is more favored than the photogenerated holes for the oxidation of 3,5-DHBA.

8.6. Relative Photonic Efficiencies

As the other compounds, 3,5-DHT and 1,3-DHMB, 1,3-DHB is used as the probe molecule to calculate the relative photonic efficiencies of 3,5-DHBA (equation 8.4).

$$\zeta = \frac{\text{rate of formation of } CO_2 \text{ for } 3,5 - DHBA}{\text{rate of formation of } CO_2 \text{ for } 1,3 - DHB} \qquad (8.4)$$

Variations in 3,5-DHBA concentration, pH and temperature do not affect the relative photonic efficiencies considerably (Figure 8.6.1). However, when efficiencies are compared, it is observed that the results of 3,5-DHBA are relatively higher than those obtained with 3,5-DHT and 1,3-DHMB. A detailed information is given in the discussion chapter.
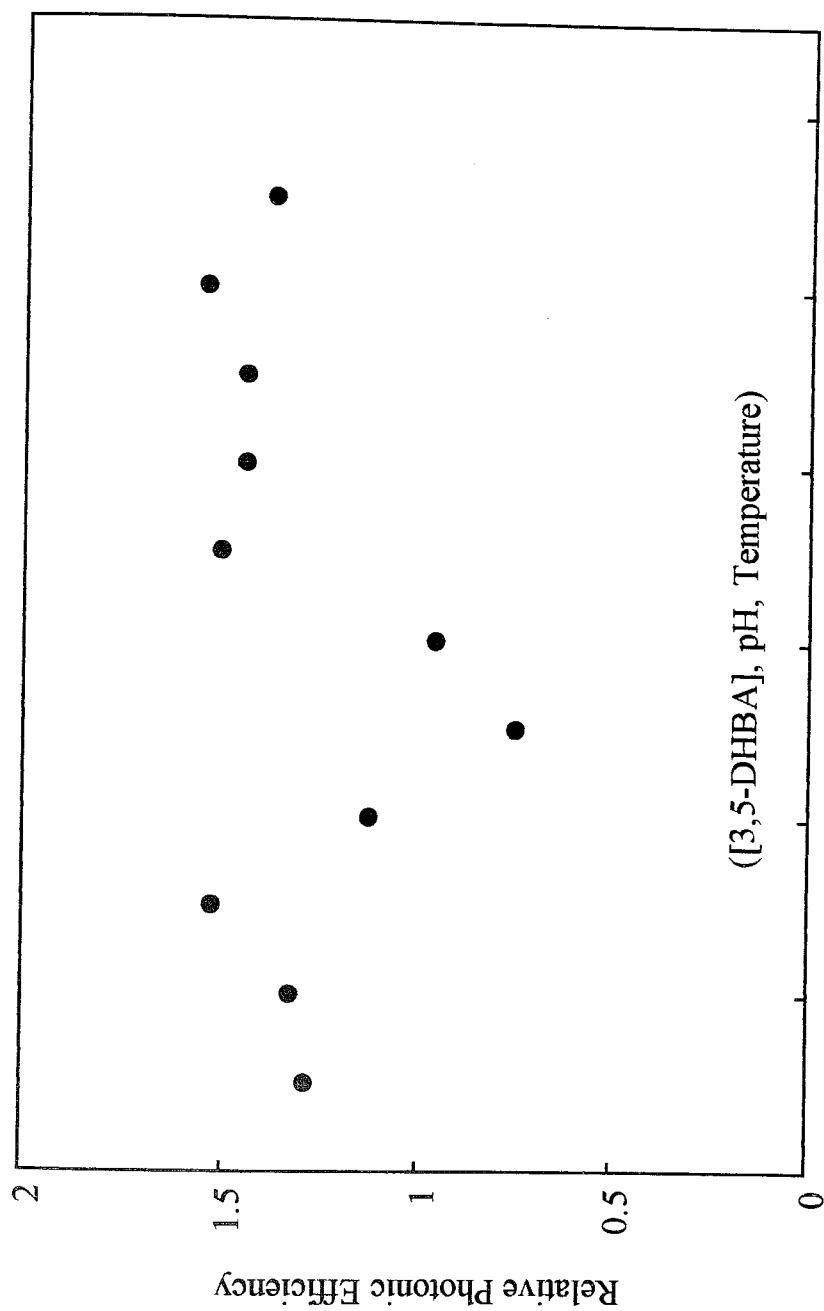
Figure 8.6.1. Relative photonic efficiencies as a function of 3,5-DHBA concentration, pH and temperature for 3,5-DHBA.

9. METAL DEPOSITION

In order to enhance the interfacial charge transfer reactions occuring for bulk phase TiO_2, the properties of the particles have been modified by selective surface treatments, one of which is the deposition of metals on the surface of TiO_2. TiO_2, due to its bandgap energy of ~3.2 eV, absorbs in the near UV and thus can utilize only a small fraction of the solar spectrum. By deposition of metals, absorption of light can be extended into the visible region. In addition to this, the presence of the metal ion significantly influences photoreactivity, charge carrier recombination rates, and interfacial electron-transfer rates [55, 56]. The photoreactivity of metal deposited TiO_2 appears to be a complex function of the deposited metal concentration, the energy level of metals within the TiO_2 lattice, their d-electronic configuration, the distribution of metals, and the light intensity. Transition metals are preferencially chosen for deposition on the metal oxide because of their d-electronic configurations and they have an ionic radius similar to that of Ti^{4+} making it possible for them to occupy surface sites. The nature of metal ion adsorption is not known exactly, however the general assumption is that metal ions may be in the reduced or hydrolyzed form on the surface of TiO_2.

This chapter will start by giving a review of transition metal electronic configurations and the resulting energy levels, then continue with a discussion of the nature of the adsorption of transition metals. A brief review of the photocatalytic properties of deposited TiO_2 will precede discussion of our experimental results.

9.1. Transition Metals

Transition elements are often defined as those which have partly filled d shells [57]. The transition elements are all metals, and generally have the properties of having high tensile strength and rigidity and they are conductors of heat and electricity. They form many colored and paramagnetic compounds because of the presence of partially filled d shells. There is nothing fundamentally different about the bonding in transition metals as compared with that of the main group elements. Transition elements are subdivided into the three main groups: (a) the main transition elements or d-block elements, (b) the lanthanide elements, (c) the actinide elements [58]. Our discussion will be concerned with the d-block elements.

The main transition group includes those elements that have partially filled d shells and no filled f orbitals. Thus, the element scandium, with the outer electron configuration $4s^2 3d^1$, is the lightest member. The succeeding elements in this row, Ti, V, Cr, Mn, Fe, Co, Ni and Cu, all have partly filled 3d shells. This group of elements are called the first transition elements. At zinc, the configuration is $3d^{10} 4s^2$. The second transition series starts with yttrium with a ground state outer electron configuration $5s^2 3d^2$. The following eight elements, Zr, Nb, Mo, Tc, Ru, Rh, Pd, and Ag, all have partially filled 4d shells. The third transition series begins with hafnium, having ground state outer electron configuration $6s^2 5d^2$ and the others Ta, W, Re, Os, Ir, Pt, and Au, all of which have partially filled 5d shells.

Crystal Field Theory is an approach to transition metal compounds which explains the UV and visible spectra (electronic) and magnetic properties in terms of a central ion surrounded by electron rich ligands. These ligands split the d orbitals into a pattern determined by the geometry of the coordination, the distance of approach of the ligands

and the tendency toward covalent bonding. Crytal field theory works best for the 3d-series.

The Crystal Field Approach: The five d orbitals are not equivalent in the presence of ligands. The dz^2 and dx^2-y^2 orbitals have lobes with the electron density directed towards the vertices of a regular octahedron. The dxy, dyz, dzx orbitals have lobes which project between the density formed by the octahedral field. The dxy, dyz, dzx orbitals are degenerate and labeled as t_{2g}, and the dz^2 and dx^2-y^2 orbitals are also degenerate, and are labeled as e_g. The e_g orbitals are of higher energy than the t_{2g} orbitals. The energy difference between e_g and t_{2g} orbitals is given as Δ_o. The e_g levels lie 3/5 Δ_o above the energy of the unsplit d orbitals and the t_{2g} levels lie 2/5 Δ_o below this value (Figure 9.1.1).
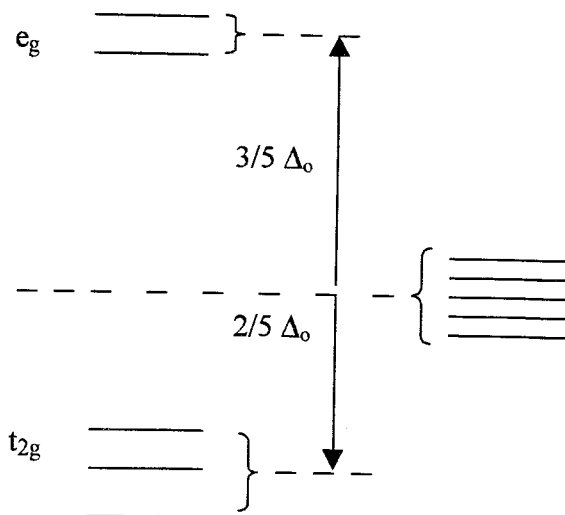
Figure 9.1.1. Energy level diagram showing the splitting of a set of d orbitals [57].

One, two or three electrons in the d orbitals enter the more stable t_{2g} orbitals with their spins parallel. Furthermore, for ions with eight, nine, and ten d electrons, there is only one possible way in which the orbitals may be occupied to give the lowest energy

configuration (Figure 9.1.2). For each of the remaining configurations, d^4, d^5, d^6, and d^7, two possibilities exist. The one representing the ground state depends on the values of Δ_o and P, an average pairing energy. The configurations with the highest number of unpaired electrons are called high spin configurations and those with the minimum number of unpaired spins are called the low spin configurations. The energies are simply sums of $-2/5$ Δ_o for each t_{2g} electron, $+3/5$ Δ_o for each e_g electron, and P for every pair of electrons occupying the same orbital. For a particular ion of the d^4, d^5, d^6, and d^7 type, the stronger the crystal field , the more likely it is that the electrons will crowd as much as possible into the more stable t_{2g} orbitals. Whereas in the weaker crystal fields, where $P>\Delta_o$, the electrons will remain spread out over the entire set of d orbitals. For ions of the type, d^1, d^2, d^3, d^8, and d^{10} the number of unpaired electrons is fixed at the same number irrespective of how strong the crystal field may become. The d^5 systems are exceptionally stable in their high spin states, whereas the d^6 systems are exceptionally stable in their low spin states (Figure 9.3).
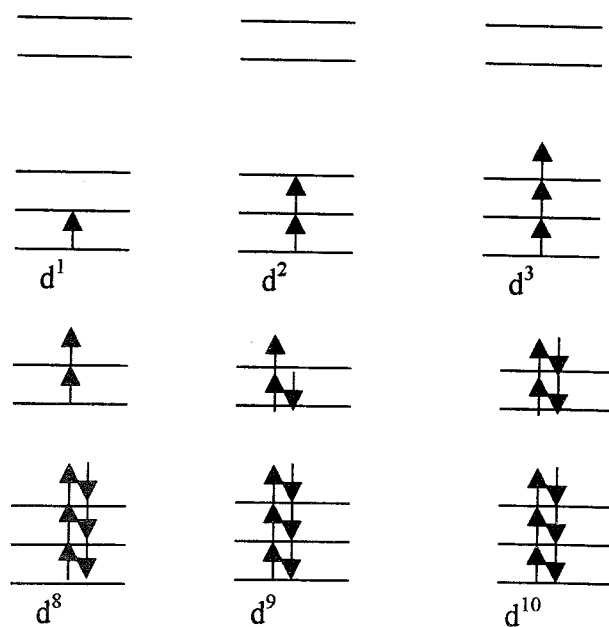
Figure 9.1.2. Ground state electron configurations for d^1, d^2, d^3, d^8, d^9, and d^{10} [57].

High spin states   Low spin states   High spin states   Low spin states

d^4

$t_{2g}^3 e_g^1$ t_{2g}^4

E= -3/5 Δ_o E= -3/5 Δ_o+P

d^5

$t_{2g}^3 e_g^2$ t_{2g}^5

E= 0   E= -2 Δ_o+2P

d^6

$t_{2g}^4 e_g^2$ t_{2g}^6

E= -2/5 Δ_o+P   E= -12/5 Δ_o+3P

d^7

$t_{2g}^5 e_g^2$ $t_{2g}^6 e_g^1$

E= = -4/5 Δ_o+2P   E= -9/5 Δ_o+3P
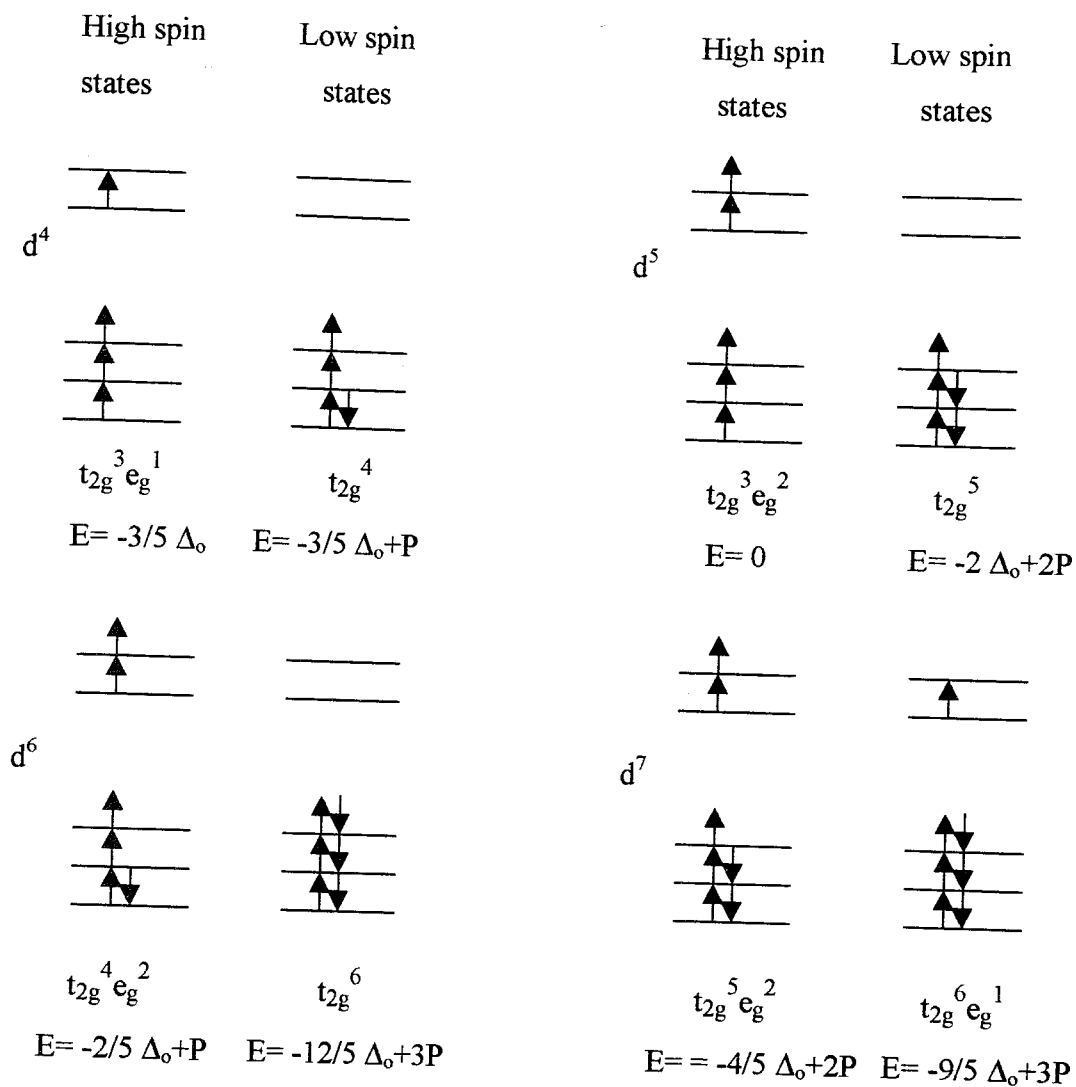
Figure 9.1.3. Two possibilities (high spin and low spin) for the ground state electron configurations d^4, d^5, d^6, and d^7 ions [57].

9.2. Adsorption Nature of Metals

With metal ions, the adsorbed species may have the same structure as that in the fluid phase or it may be in the reduced or hydrolyzed form. A limiting factor is the redox potential of the species (Table 9.2.1). For Mn^{2+}, Co^{2+}, Ni^{2+}, Cr^{3+}, V^{4+}, Zn^{2+}, and Al^{3+}, although some reduction takes place with photoexcited electrons, the back reaction

with photoexcited holes is spontaneous, and the TiO_2 particle acts as a short circuited electrode and rapid oxidation reduction of the species occurs on the surface. These ions may also be in the hydrolyzed form and strongly adsorbed on the hydroxylated TiO_2 surface [50].

The decrease in pH after addition of TiO_2 can be explained in terms of the adsorption of hydroxyl ions by TiO_2 (Table 9.2.2).

Table 9.2.1. Standard electrode potentials at 25°C [59].

Half Reaction	V^0 (Volts)
$Ti^{4+} + e^- \rightarrow Ti^{3+}$	0.00
$Ti^{3+} + e^- \rightarrow Ti^{2+}$	-0.37
$Ti^{2+} + 2e^- \rightarrow Ti$	-1.63
$V^{3+} + e^- \rightarrow V^{2+}$	-0.27
$V^{2+} + 2e^- \rightarrow V$	-1.19
$Cr^{3+} + e^- \rightarrow Cr^{2+}$	-0.41
$Cr^{2+} + 2e^- \rightarrow Cr$	-0.91
$Cr^{3+} + 3e^- \rightarrow Cr$	-0.74
$Mn^{3+} + e^- \rightarrow Mn^{2+}$	+1.51
$Mn^{2+} + 2e^- \rightarrow Mn$	-1.18
$Fe^{3+} + e^- \rightarrow Fe^{2+}$	+0.77
$Fe^{2+} + 2e^- \rightarrow Fe$	-0.44
$Fe^{3+} + 3e^- \rightarrow Fe$	-0.04
$Co^{3+} + e^- \rightarrow Co^{2+}$	+1.81
$Co^{2+} + 2e^- \rightarrow Co$	-0.28
$Ni^{2+} + 2e^- \rightarrow Ni$	-0.23
$Zn^{2+} + 2e^- \rightarrow Zn$	-0.76
$Al^{3+} + 3e^- \rightarrow Al$	-1.66

Table 9.2.2. Changes in the pH after addition of TiO_2.

Ion Form	pH before addition	pH after addition
V^{4+}	3.26	3.18
Cr^{3+}	3.43	3.35
Mn^{2+}	6.75	6.35
Fe^{3+}	2.47	2.26
Co^{2+}	5.51	5.03
Ni^{2+}	5.56	4.94
Zn^{2+}	5.70	5.54
Nb^{5+}	2.05	1.80
Ta^{5+}	2.49	2.42
Al^{3+}	4.28	4.06

9.3. Review

Even though the effect of metal ion deposition on the reactivity of TiO_2 has been a topic of investigation, direct comparisons and unifying conclusions are difficult to make since widely varying experimental conditions for sample preparation and for the determination of photoreactivity have been employed.

Litter and Navío [60] made a review on photochemical properties of iron doped TiO_2 semiconductors. They reported photocatalytic reactions (reductions and oxidations) using Fe-containing TiO_2 on different organic and inorganic substrates. Their opinion about the oxidation reactions is that the energy of the valence band is sufficient to oxidize phenol and most of the organic substrates. In other words, the electric field in the depletion layer is sufficient to hasten the electron-hole pair separation. Oxygen

molecules behave as traps for electrons, favoring the charge separation and enhancing the lifetime of holes. The presence of iron induces a displacement of the Fermi level but does not change the effectiveness of the electron-hole pair separation in comparison with pure anatase. They also reported that the presence of dopants in a liquid-solid regime can alter the morphology of the surface of the precursor, changing the number of active sites, the type of surface groups and the acid-base properties. Surface recombination can be enhanced by these factors negatively, affecting photoreactivity.

Palmisano and coworkers [61] investigated the photodegradation of phenol in liquid-solid regime by using a series of chromium ion containing titania specimens. For the same photoreaction, iron containing titania specimens were also studied for comparison. The samples containing chromium ions had molar concentrations of 0.2, 0.5, 1.0, 2.0, and 5.0 per cent, those containing iron ions had molar concentrations of 0.5 and 1.0 per cent. They conclude that the presence of dopants is not essential for organic decompositions. The anatase-electrolyte interface provides necessary conditions for the occurrence of the reaction. The presence of Cr and Fe dopants induces a displacement of the Fermi level, but this displacement appears not to affect the photoreactivity of titania, or in some cases, detrimentally affected it.

In 1994, Choi $et.$ $al.$ [55] investigated metal ion doping in quantum (Q) sized (2-4 nm) TiO_2 colloids in terms of both conduction band electron reduction of an electron acceptor (CCl_4 dechlorination) and the valence band oxidation of an electron donor ($CHCl_3$ degradation). They found that Fe^{3+}, Mo^{5+}, Ru^{3+}, Os^{3+}, Re^{5+}, V^{4+}, and Rh^{3+} significantly increase the photorecativity for both oxidation and reduction, while Co^{3+} and Al^{3+} doping decreases the photoreactivity. When degradation quantum yields are examined as a function of dopant level, it is observed that all dopants show an optimum concentration above which the observed quantum yields for $CHCl_3$ degradation decreases. The highest quantum yields are generally seen for 0.5 per cent metal ion concentration. They also studied the photoreactivity of heat treated samples and found that samples lose their photoreactivity as the temperature is increased.

Martin *et. al.* [62] studied a single dopant, vanadium, to investigate the dopant action on the photoreactivity of TiO_2. They observed that doping 1 per cent of the TiO_2 crystals with vanadium reduces the photooxidation of 4-chlorophenol compared to undoped aggregates. Charge carrier recombination by electron trapping and hole trapping are both possible due to the presence of surficial VO_2^+ and interstitial V^{4+} species at ambient conditions (25°C).

In our study, we present a systematic study of metal ion deposition on TiO_2 for 10 metal ions listed in the experimental section. The photoreactivities of metal deposited TiO_2 colloids are quantified in terms of the oxidation of 1,3-DHB, 3,5-DHT, 1,3-DHMB and 3,5-DHBA both in the presence and in the absence of a hole scavenger.

9.4. Photocatalytic Oxidation with Metal Deposited TiO_2
(Without Hole Scavenger)

The measured photoreactivities of 10 deposited TiO_2 colloids are summarized in Figure 9.4.1 in terms of the observed quantum yields for 1,3-DHB, 3,5-DHT, 1,3-DHMB and 3,5-DHBA.

Several metal ions, Fe^{3+}, Ni^{2+}, Zn^{2+}, were found to increase the photoreactivity significantly compared to undeposited TiO_2 however, some have little effect on the photooxidation reaction, Nb^{5+}, Ta^{5+}, Co^{2+}, Mn^{2+}, Al^{3+}, Cr^{3+}, V^{4+}.

							Al^{3+}
							0.22
							0.11
							0.12
							0.14

$*Ti^{4+}$	V^{4+}	Cr^{3+}	Mn^{2+}	Fe^{3+}	Co^{2+}	Ni^{2+}	Zn^{2+}
0.34^a	0.04	0.03	0.39	0.50	0.33	0.43	0.46
0.23^b	0.00	0.00	0.21	0.46	0.31	0.25	0.34
0.31^c	0.04	0.11	0.34	0.45	0.39	0.41	0.39
0.34^d	0.01	0.15	0.29	0.36	0.33	0.34	0.33

Nb^{5+}
0.35
0.31
0.36
0.30

Ta^{5+}
0.35
0.33
0.35
0.32

FIGURE 9.4.1. Periodic chart of the photocatalytic effects of various metal ions deposited on TiO_2. $*Ti^{4+}$ refers to the undeposited TiO_2. Each row represents the quantum yields for a) 1,3-DHB, b) 3,5-DHT, c) 1,3-DHMB, and d) 3,5-DHBA, respectively.

Metal ion depositions influence the photoreactivity of TiO_2 by acting as electron or hole traps (equations (9.1)-(9.2)).

$$M^{n+} + e^- \rightarrow M^{(n-1)+} \qquad \text{electron trap} \qquad (9.1)$$

$$M^{n+} + h^+ \rightarrow M^{(n+1)+} \qquad \text{hole trap} \qquad (9.2)$$
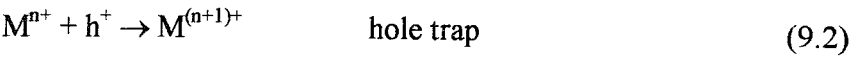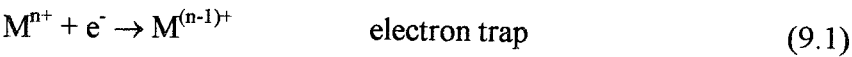
where the energy level for $M^{n+}/ M^{(n-1)+}$ lies below the conduction band and energy level for $M^{n+}/ M^{(n+1)+}$ lies above the valence band edge.

We try to establish an energy level diagram for TiO_2 (anatase 3.2 eV) including metal ions accoding to their standard electode potentials [63, 64].
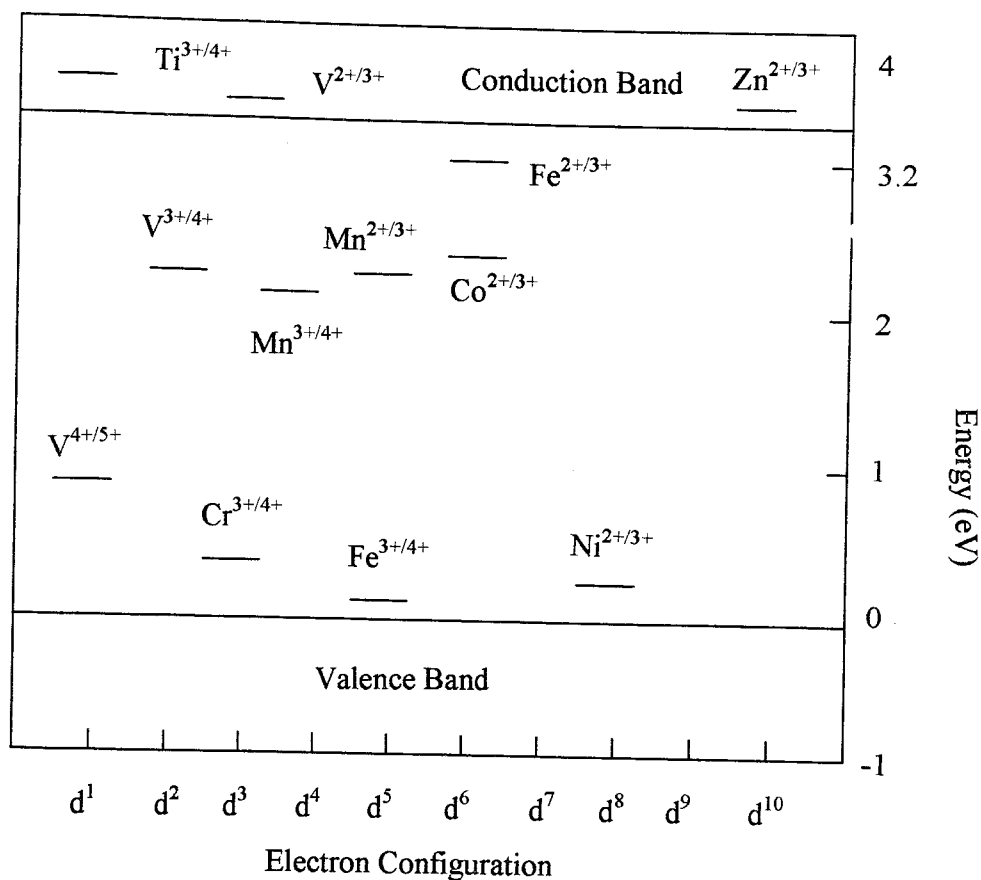
Figure 9.4.2. Energy levels of metal ions in TiO_2 (anatase).

According to energy level diagram in Figure 9.4.2, V^{4+}, Mn^{2+}, Co^{2+} and Fe^{3+} can act as both hole and electron traps, while Cr^{3+} and Ni^{2+} can serve only as hole traps. Even though Cr^{3+} and Fe^{3+} have similar energy levels in the TiO_2 lattice (0.3 eV and 0.1 eV above E_{vb}) , similar ionic radii and identical oxidation states, their efficiencies as deposited metals on the TiO_2 surface with respect to photoreactivity are different. Thus some general trends based on considerations of electronic configuration can be noted, but apparently energy levels alone cannot account for the observed experimental results.

A general photochemical charge trapping, recombination, detrapping and migration mechanism in the presence of deposited metal ions can be proposed as follows:

Charge pair generation: $TiO_2 + hv \rightarrow e_{cb}^- + h_{vb}^+$ (9.3)

Charge trapping: $Ti^{4+} + e_{cb}^- \rightarrow Ti^{3+}$ (9.4)

$M^{n+} + e_{cb}^- \rightarrow M^{(n-1)+}$ (9.5)

$M^{n+} + h_{vb}^+ \rightarrow M^{(n+1)+}$ (9.6)

$OH^- + h_{vb}^+ \rightarrow {}^{\bullet}OH$ (9.7)

Charge release and migration: $M^{(n-1)+} + Ti^{4+} \rightarrow M^{n+} + Ti^{3+}$ (9.8)

$M^{(n+1)+} + OH^- \rightarrow M^{n+} + {}^{\bullet}OH$ (9.9)

Recombination: $e_{cb}^- + h_{vb}^+ \rightarrow TiO_2$ (9.10)

$Ti^{3+} + {}^{\bullet}OH \rightarrow Ti^{4+} + OH^-$ (9.11)

$M^{(n-1)+} + h_{vb}^+ \rightarrow M^{n+}$ (9.12)

$M^{(n-1)+} + {}^{\bullet}OH \rightarrow M^{n+}$ (9.13)

$M^{(n+1)+} + e_{cb}^- \rightarrow M^{n+}$ (9.14)

$M^{(n+1)+} + Ti^{3+} \rightarrow M^{n+}$ (9.15)

Interfacial charge transfer: e_{cb}^- (or Ti^{3+}, $M^{(n-1)+}$) $+ Ox \rightarrow Ox^-$ (9.16)

h_{vb}^+ (or ${}^{\bullet}OH$, $M^{(n+1)+}$) $+ Red \rightarrow Red^+$ (9.17)
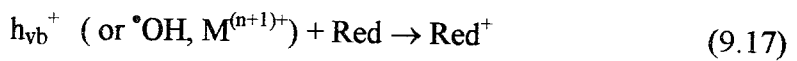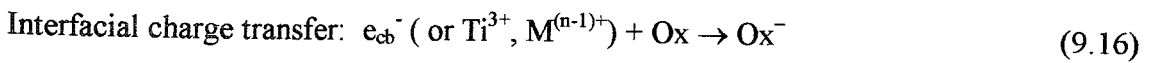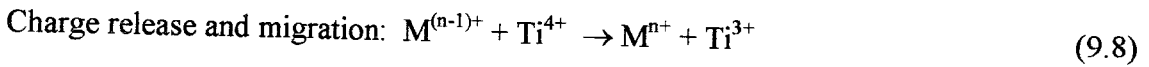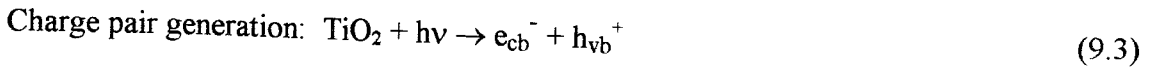
where M^{n+} is a deposited metal ion, Ox is an electron acceptor (oxidant) and Red is an electron donor (reductant). Deposited metals should act as both electron traps and hole traps to be photoactive. Trapping either an electron or a hole alone is ineffective because the immobilized charged species quickly recombines with its mobile counterpart. In addition to this, the possibility of charge detrapping and migration to the surface of previously trapped charges are important properties to be an effective deposited metal.

The difference in photoreactivities between Fe^{3+} and Cr^{3+} can be explained based on the above mechanism and the energy level diagram (Figure 9.4.2). The hole trapping by both Fe^{3+} and Cr^{3+} (equation 9.6) is favorable while electron trapping is probable only for Fe^{3+} (equation 9.5). The lower reduction potential (-0.41 V) of the electron trapping makes the energy of Cr^{3+} above the conduction band edge. Thus, the photoexcited electron in the presence of Cr^{3+} quickly recombines with a trapped hole (equation 9.14). The trapped holes in Fe^{4+} and Cr^{4+} either migrate to the surface (equation 9.9), or recombine (equations 9.14 and 9.15). The trapped hole in Fe^{4+} has a longer lifetime due to the immobilized electron in Fe^{2+}. According to crystal field theory, Fe^{2+} is relatively unstable due to the loss of exchange energy on going from d^5 to d^6 and tends to return to Fe^{3+} (d^5). However, the Fe^{2+}/Fe^{3+} energy level lies close to Ti^{3+}/Ti^{4+} level. Therefore, the trapped electron in Fe^{2+} can be easily transferred to Ti^{4+} (equation 9.8), which then leads to interfacial electron transfer (equation 9.16).

In general, deposited metals with a closed-shell electronic configuration, Nb^{5+}, Ta^{5+}, Al^{3+} were found to have little effect on the observed photoreactivity. The stability of a closed electronic shell makes hole or electron trapping unfavorable. Although Zn^{2+} has a closed shell (d^{10}), it showed a significant photoreactivity. This may be due to the increased surface area with Zn^{2+} loading which increases the number of available surface sites for substrate binding.

Co^{2+} and Mn^{2+} cannot trap an electron, since their two-electron reductions lie above the conduction band edges. When Co^{2+} traps a hole, it forms Co^{3+} which has a low reactivity. This is due to its stable low spin partly closed electron configuration (t_{2g}^{6}). Thus, interfacial charge transfer reactions cannot take place in the presence of Co^{3+}. When Mn^{2+} traps a hole, it forms Mn^{3+} which can trap electrons and holes. But there is a small energy difference between Mn^{2+} and Mn^{3+} which makes electron detrapping from Mn^{2+} diffucult.

Vanadium deposition of the crystals is found to reduce the photooxidation of rates of 4-chlorophenol relative to undeposited TiO_2 [63]. Authors prepared the vanadium deposited samples at different temperatures. For samples prepared at 25°C, vanadium is present primarily as VO_2^{+} (~90 per cent) and secondarily as interstitial V^{4+} (~10 per cent). For samples prepared at 200°C and 400°C, the deposition of vanadium as surficial islands of V_2O_5 occurs and a small fraction (~1 per cent) is also present as V^{4+}. Since we have prepared our samples at 100°C, we can assume that vanadium is present on TiO_2 as VO_2^{+}, V_4^{+}, and to a smaller extend as V_2O_5. Thus the reduction in the photooxidation rates of 1,3-DHB, 3,5-DHT, 1,3-DHMB and 3,5-DHBA can be explained by the following equations:

$$V(x) + e^{-} \rightarrow V(x\text{-}1) \tag{9.18}$$

$$V(x\text{-}1) + h^{+} \rightarrow TiO_2 \tag{9.19}$$

$$\text{or} \quad V(x\text{-}1) + {}^{\cdot}OH \rightarrow TiO_2 \tag{9.20}$$

$$V(x) + h^{+} \rightarrow V(x\text{+}1) \tag{9.21}$$

$$V(x\text{+}1) + e^{-} \rightarrow TiO_2 \tag{9.22}$$

where $V(x)$ represents V^{4+}.

Charge carrier recombination with electron trapping occurs for VO_2^+ through equations (9.18)-(9.20). In the case of V_2O_5, the presence of V^{4+} impurities in surficial V_2O_5 islands, promotes charge carrier recombination by hole trapping via equations (9.21)-(9.22).

9.5. Photocatalytic Oxidation with Metal Deposited TiO$_2$
(With Hole Scavenger)

When methanol is added during the preparation of metal deposited on TiO$_2$ samples, it is observed that the rates of formation of CO_2 are decreasing for 1,3-DHB, 3,5-DHT, 1,3-DHMB, and 3,5-DHBA (Figures 9.5.1, 9.5.2, 9.5.3, and 9.5.4). We know that methanol acts as a hole schavenger (Chapter 5). Thus its presence reduces the meeting probability of metals with the photoexcited holes (equation 9.6) and decreases the amount of metal deposition on the catalyst surface in their hole initiated-oxidized form. As a matter of fact, at the end of the preparation step, metals are attached to the surface of TiO$_2$ mostly in their metallic forms (M^0). When photodegradation starts, metals (M^0) tend to react with newly generated holes, while newly generated electrons react with an electron acceptor (Ox). Thus the interfacial charge transfer reaction (equation 9.17) of holes with an electron donor (Red) decreases significantly.

For both methods, without methanol and with methanol, the highest rates of CO_2 evolution are obtained with Fe^{3+}. Therefore a more detailed investigation of Fe^{3+} has been performed and is discussed in the following sections

Figure 9.5.1. Rate of CO₂ production as a function of deposited metals for 1,3-DHB.

208

Figure 9.5.2. Rate of CO_2 production as a function of deposited metals for 3,5-DHT.
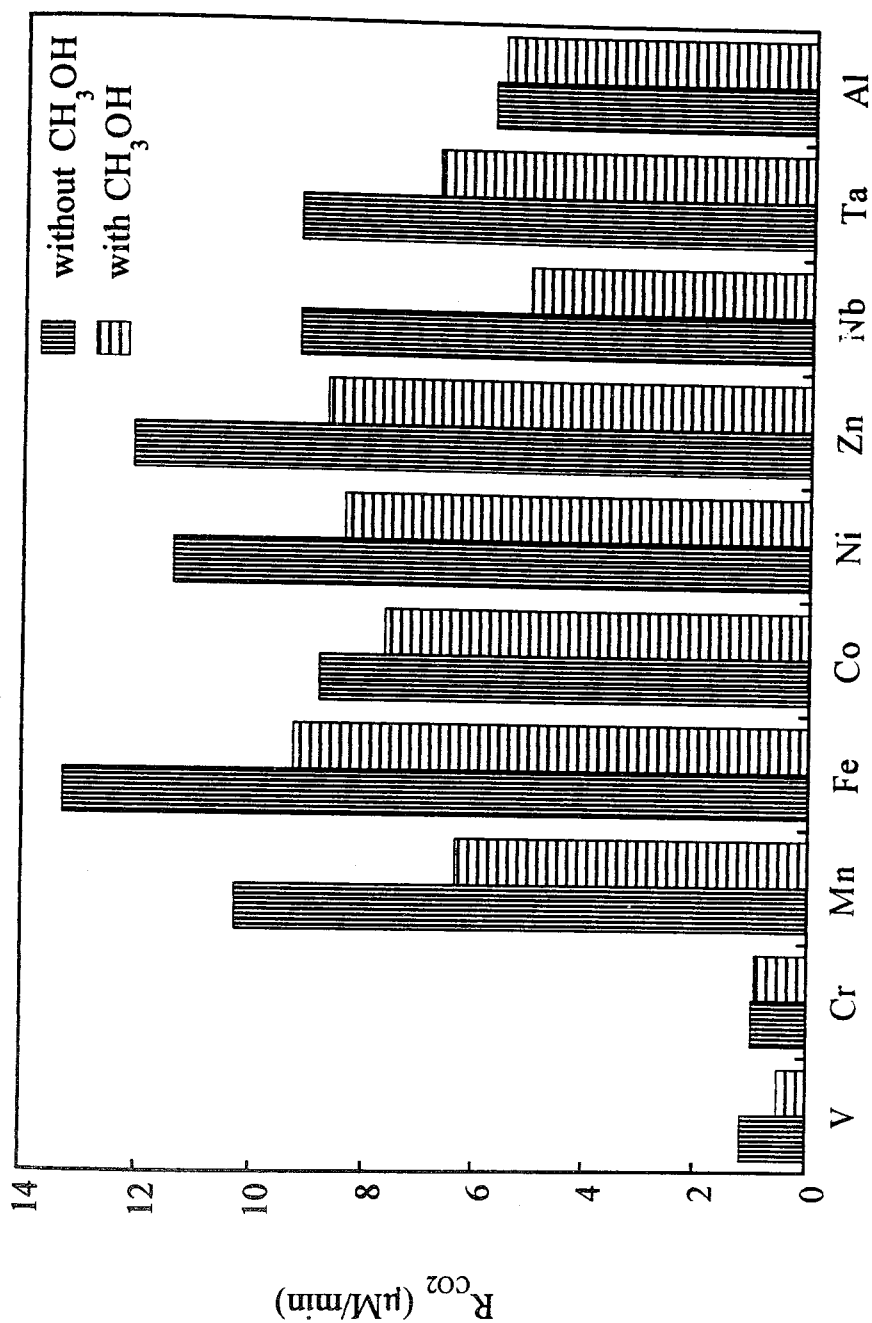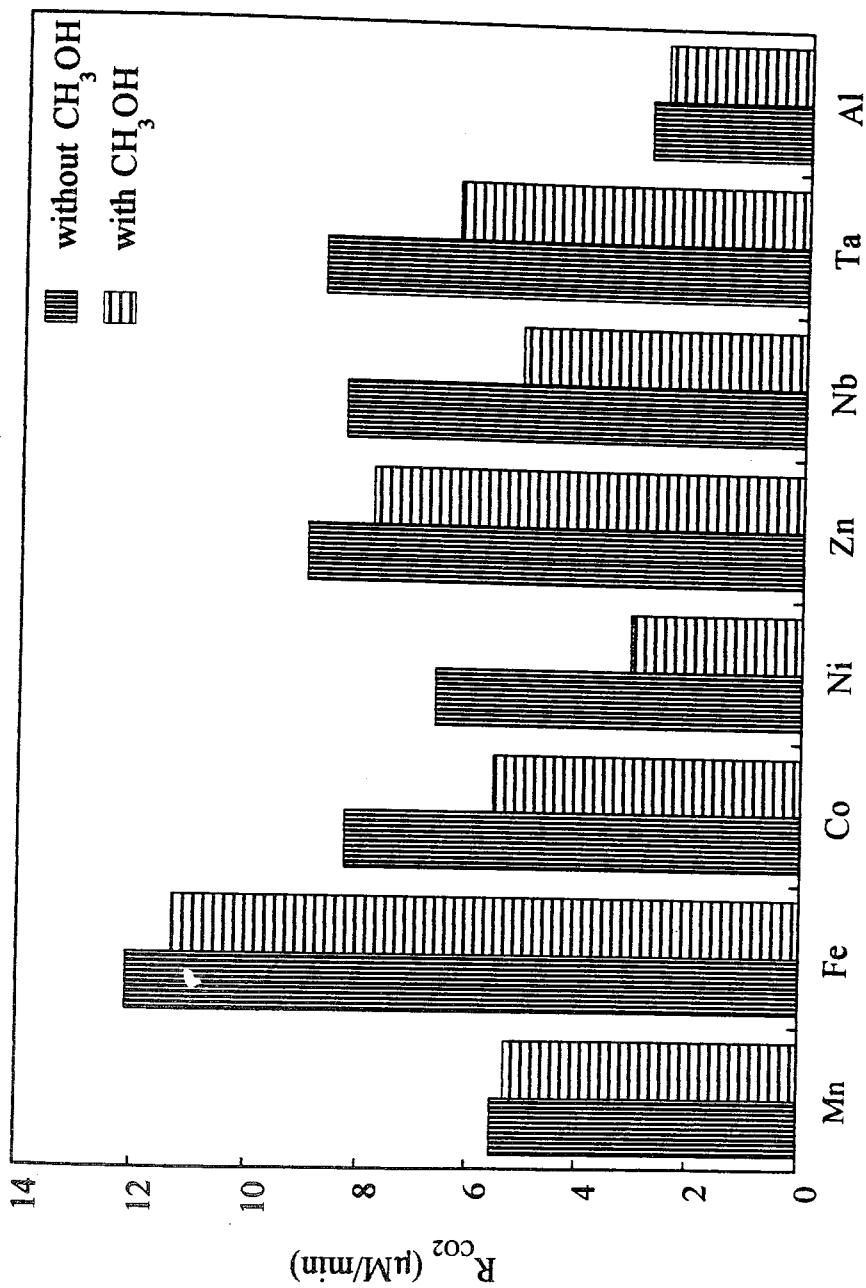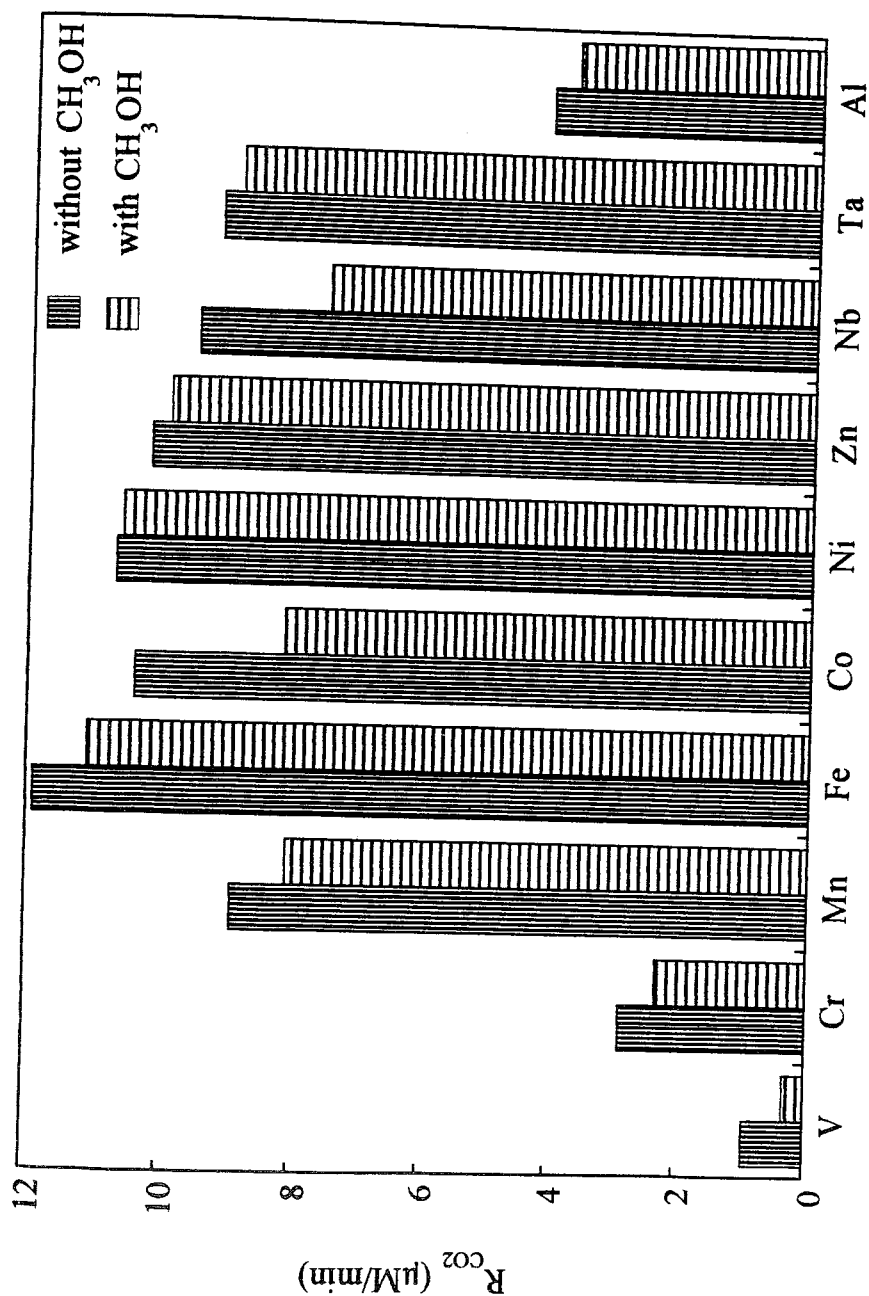
Figure 9.5.3. Rate of CO_2 production as a function of deposited metals for 1,3-DHMB.
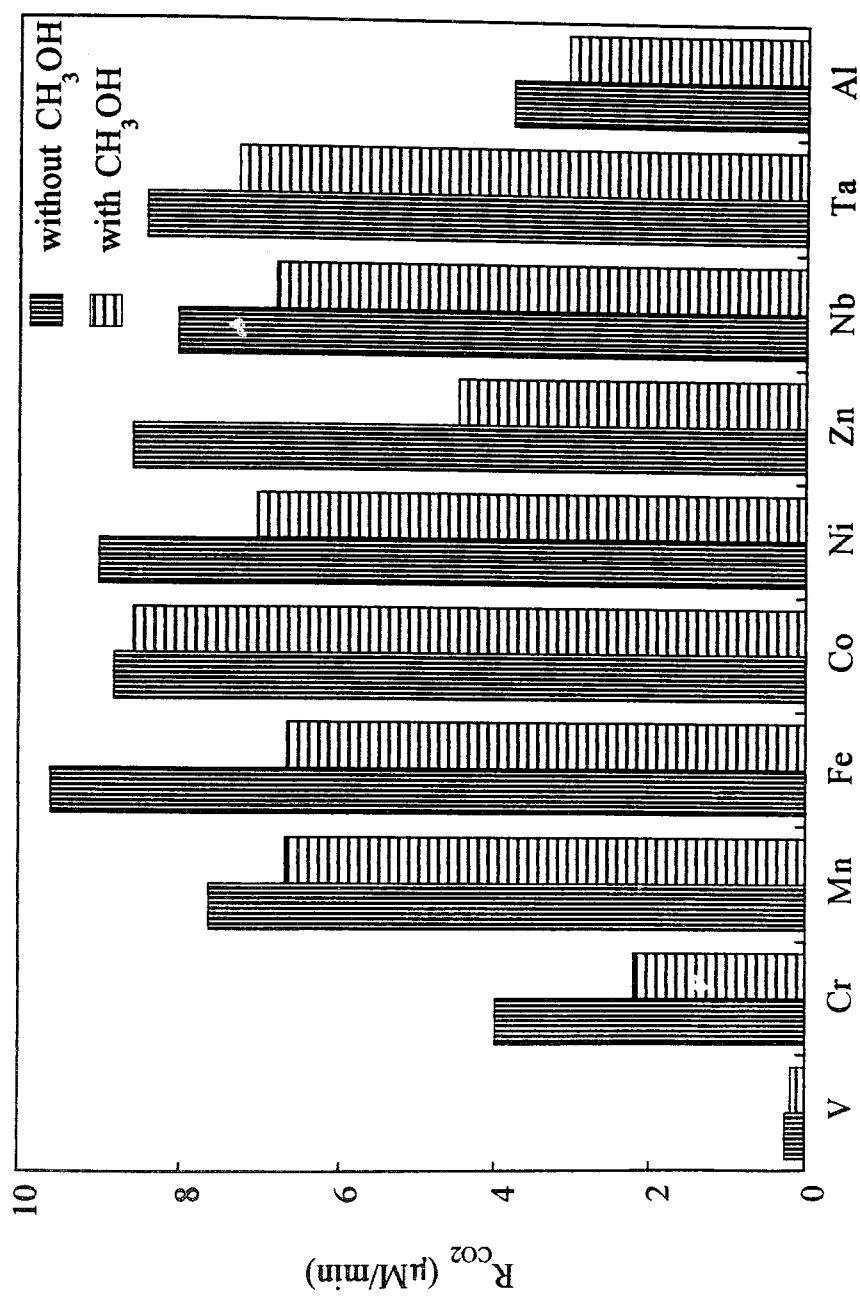
Figure 9.5.4. Rate of CO₂ production as a function of deposited metals for 3,5-DHBA.

9.6. Photoreactivity of Fe^{3+} Deposited TiO_2

Since photoreactivity of metal deposited TiO_2 is a function of the metal concentration, we followed the rate of CO_2 production at different Fe^{3+} concentrations (Table 9.6.1).

Table 9.6.1. Rate of formation of CO_2 as a function of Fe^{3+} concentration,

Fe^{3+} concentration	R_{CO2} (µM/min)			
	1,3-DHB	3,5-DHT	1,3-DHMB	3,5-DHBA
0.5 per cent	11.07	10.89	11.65	9.43
1.0 per cent	13.27	11.09	11.97	11.28
2.0 per cent	10.94	10.77	11.29	7.91
3.0 per cent	10.65	10.63	11.27	6.69
5.0 per cent	10.05	10.22	11.22	5.56

[1,3-DHB]$_0$=100 µM, [3,5-DHT]$_0$=100 µM, [1,3-DHMB]$_0$=100 µM, and [3,5-DHBA]$_0$=100 µM.

In all cases, the maximum rate of CO_2 production is obtained at 1.0 per cent above which the observed rates decrease. A quantitative measurement of the Fe^{3+} concentrations deposited on the surface of TiO_2 is followed by use of atomic absorption spectrophotometry and the numerical results are given in Table 9.6.2.

Table 9.6.2. Atomic absorption results.

$[Fe^{3+}]_0$ (ppm)	$[Fe^{3+}]_R$ (ppm)	$[Fe^{3+}]_{ADS}$ (ppm)	Percentage
2.5	0.66	1.84	73.6
4.0	1.02	2.98	74.5
6.0	1.59	4.41	73.5
8.0	5.33	2.67	33.4
10.0	9.83	0.17	1.70

$[Fe^{3+}]_0$= Initial concentration of Fe^{3+} before irradiation in the optical bench reactor.

$[Fe^{3+}]_R$= Concentration of Fe^{3+} remaining in the solution after 75 min irradiation.

$[Fe^{3+}]_{ADS}$= Concentration of Fe^{3+} adsorbed on TiO_2 surface after 75 min irradiation.

Percentage= Adsorption percentage of $[Fe^{3+}]_{ADS}$ with respect to $[Fe^{3+}]_0$.

The initial concentrations of Fe^{3+} before irradiation are ajdusted according to the optimum working range of atomic absorption spectrophotometer for iron samples. 2.5, 4.0, 6.0, 8.0, and 10.0 ppm corresponds to 0.5, 1.0, 2.0, 3.0, and 5.0 per cent Fe^{3+} concentrations, respectively. The amount of adsorbed Fe^{3+}, $[Fe^{3+}]_{ADS}$, decreases as the initial concentration of Fe^{3+}, $[Fe^{3+}]_0$, increases. The highest adsorption is obtained at 4 ppm which corresponds to 1.0 per cent deposition of Fe^{3+}. Thus, results obtained from the atomic absorption spectrophotometry coincide with the rate of formation of CO_2 for substrate degradations.

Bard [13] and Palmisano et. al. [61] reported that the thickness of the space charge layer is affected by the deposited metal content in accord to the following equation:

$$W = \left(\frac{2EE_0 V_s}{eN_d} \right)^{1/2} \approx \frac{1}{a} \tag{9.23}$$

in which W is the thickness of the space charge layer, E and E_0 are static dielectric constants of the semiconductor and of vacuum, V_s is the surface potential, N_d is the number of deposited donor atoms, and e is the electron charge. Equation 9.23 clearly indicates that W decreases as the deposition of metal content increases. It is also reported that N_d should be adjusted with respect to the absorption coefficient a (cm^{-1}) of the semiconductor so that most of the light is absorbed within the space charge region. A higher metal deposition will result in loss of quantum efficiency because of electron hole recombination in the bulk phase. According to our results, increasing the concentration of Fe^{3+}, decreases the penetration of light into the space charge region, by creating a cluster around the TiO_2 powder. As a result of light absorption outside the space charge region, the rate of electron hole recombination increases, and thus the amount of metal deposition on the catalyst surface decreases. All these effects serve to reduce the rate of CO_2 formation for the photocatalytic degradation of 1,3-DHB, 3,5-DHT, 1,3-DHMB and 3,5-DHBA.

We also measured the amount of Fe^{3+} concentration in the solution after photocatalytic degradation of 1,3-DHB in the gas recycling reactor (Table 9.6.3).

Table 9.6.3. Amount of Fe^{3+} concentration, $[Fe^{3+}]s$, in the solution.

$[Fe^{3+}]_{ADS}$ (ppm) before irradiation	$[Fe^{3+}]_s$ (ppm) after irradiation
1.84	0.003
2.98	0.006
4.41	0.004
2.67	0.003
0.17	0.002

Table 9.6.3 gives the amount of Fe^{3+} in the solution after one hour irradiation. The amounts of $[Fe^{3+}]s$ after irradiation are in the 10^{-8} M range, thus once the metal is deposited on the surface of the catalyst, it cannot deattach from the surface region.

9.7. Photoreactivity of Heat-Treated Fe^{3+} Samples

The effect of particle agglomeration on the photoreactivity is investigated for different percentages of Fe^{3+} containing samples which are heated to 400°C during the drying step. Table 9.7.1 summarizes the photoreactivities of heat treated different percentages of Fe^{3+} samples.

Table 9.7.1. Effect of heat treated Fe^{3+} samples on the photoreactivity.

Fe^{3+} concentration	R_{CO2} (µM/min) 400°C			
	1,3-DHB	3,5-DHT	1,3-DHMB	3,5-DHBA
0.5 per cent	3.76	3.65	4.19	3.55
1.0 per cent	2.41	2.09	2.43	1.97
3.0 per cent	1.20	1.03	1.56	0.84
5.0 per cent	0.54	0.55	0.57	0.60

All Fe^{3+} samples reduced their photoreactivity at 400°C. Since iron deposition increases the rate of CO_2 formation compared to the undeposited samples, we can assume that deposited iron is located in the surface region where charge transfer to the interface is easily achieved. However, upon heating particle agglomeration occurs and the deposited iron ions are no longer located at the surface. As a result, the chance of transferring trapped carriers to the interface decreases. Thus, all the iron deposition percentages

serve as recombination centers rather than as trap sites and thereby reducing the rate of CO_2 formation.

10. DISCUSSION

The photocatalytic degradation of 1,3-DHB, 3,5-DHT, 1,3-DHMB and 3,5-DHBA are followed in the presence of TiO_2. These compounds form a class of substituted phenols. It is the aim of this study to examine how efficiently a class of related organics may be degraded. Relative to 1,3-DHB, the substituents are electron donors for 3,5-DHT and 1,3-DHMB and an electron withdrawing group in the case of 3,5-DHBA. All substituents are in meta position. The effects of initial concentrations of organic reactants, the pH of the medium, temperature, incident photon flux, and irradiation time are examined kinetically. The effect of metal deposition on the TiO_2 is also investigated for the various compounds. In this chapter, we make a comparisons between the related experiments which were discussed in detail in chapters 5 through 9.

By doing the concentration experiments we can obtain the reaction order. It is found that the reaction is pseduo-first order for 1,3-DHB and 3,5-DHT at lower concentrations. As the concentration is increased to 1000 μM, these reactions tend to become zeroth order. For the other compounds investigated, 1,3-DHMB and 3,5-DHBA, we were unable to do perform the experiments at sufficiently low concentrations due to low signal intensity. So only zeroth order kinetics were obtained with these compounds. Due to the similarities in the over data trends, it is anticipated that these reaction would also exhibit pseudo-first order kinetics at low concentrations.

The substitution of an acid group was found to have no significant effect on the reaction rate at the natural pH (Table 10.1). A decrease in rate was observed when the ring is substituted with electron donating groups, CH_3 and OCH_3. There is no general trend in the case of adsorption constants. Both in the presence of an electron donating (3,5-DHT) and an electron withdrawing group (3,5-DHBA), an increase is observed in adsorption constants. Thus an electronic effect alone cannot be the reason for this increase.

Table 10.1. Reaction rate constants, k, and adsorption constants, K, for the reactant molecules at their natural pH's.

Reactants	k (μM/min)	K (1/μM) ($\times 10^{-3}$)
1,3-DHB	15.48	6.97
3,5-DHT	6.87	37.8
1,3-DHMB	13.07	4.22
3,5-DHBA	15.68	27.1

The effect of pH on the degradation rates and the formation of CO_2 are studied by varying the pH values from 3.5 to 11.0. The highest rates were obtained at pH 9.0 for 1,3-DHB, 3,5-DHT and 1,3-DHMB. These results are in accordance with the pK value of 1,3-DHB, 9.81. The experimental pK values were not available for 3,5-DHT and 1,3-DHMB but the correlation in the reactivity trends suggests that CH_3 and OCH_3 substitution has no significant effect on the acid ionization constant. Increasing the pH to 11.0 enhances the competition between OH^- ions and substrate ions, and thus decreases the rate. In the case of 3,5-DHBA, it is observed that the rate is highest at pH 4.4.

Degradation of reactant molecules and evolution of CO_2 were also investigated with increasing irradiation periods. When 30 min results are compared (Table 10.2), without a substituent (1,3-DHB) and with an electron withdrawing substituent (3,5-DHBA), the per cent degradation and the per cent CO_2 production show approximately the same trend. However, when electron donor groups are substituted, the percentages start to decrease. The relatively lowest percentages in the case of 1,3-DHMB can be due to the higher initial concentration of the reactant. One general observation is that percentage for CO_2 production is always lower than the percentange of degradations. This may be due to the presence of intermediates which appear during the photolysis and can compete with reactant molecules for the hydroxyl radicals.

Table 10.2. Degradation percentages of reactants and formation percentages of CO_2.

Reactants*	Per cent degradation	Per cent formation of CO_2
1,3-DHB	82.6	40.3
3,5-DHT	78.9	27.1
1,3-DHMB	49.4	6.11
3,5-DHBA	91.8	48.1

*[1,3-DHB]$_0$=100 μM, [3,5-DHT]$_0$=100 μM, [1,3-DHMB]$_0$=500 μM, [3,5-DHBA]$_0$=100 μM.

The effect of temperature on the rate of CO_2 formation for all reactant molecules is monitored in the range 298-333 K. The overall degradation behaviour appears the same but with a decrease in degradation times as temperature increases. This is indicative of an Arrhenius type behaviour and the activation energy of the degradation of each reactant is deduced from the corresponding Arrhenious type plots. Numerical results are given in Table 10.3. The lowest activation energy is found for 1,3-DHBA but all values are in the range generally observed for phenolic compounds (5-16 kJ/mol) [5].

Table 10.3. Activation energy data for the reactant molecules.

Reactants	Activation energy (kJ/mol)
1,3-DHB	11.2
3,5-DHT	17.4
1,3-DHMB	17.1
3,5-DHBA	10.3

For the route of oxidation, two possible mechanisms are suggested, direct oxidation with photogenerated holes or with hydroxyl radicals. When the ratio of the rate constants of these two processes are compared, it is observed that the formation of hydroxyl radicals are more favored than that of photogenerated holes for the oxidation of all reactants.

Table 10.4. Ratio between the reaction rate constants of formation of $^{\bullet}OH$ radicals, k_3 and the photogenerated holes, k_4 for the oxidation of reactants.

Reactants	$k_3/k_4\ (\times 10^4)$
1,3-DHB	9.80
3,5-DHT	6.42
1,3-DHMB	19.1
3,5-DHBA	24.7

Since the photoreactivity of TiO_2 can be enhanced in the presence of deposited metals, all the photocatalytic degradation processes are followed in the presence of 10 metal deposited TiO_2 colloids. Metals are selected according to their similar ionic radii to Ti^{4+}. Samples are prepared by two methods: without methanol and with methanol. It is found that Fe^{3+}, Ni^{2+} and Zn^{2+} increase the photoreactivity, whereas Nb^{5+}, Ta^{5+}, Co^{2+}, Mn^{2+}, Al^{3+}, Cr^{3+} and V^{4+} have little effect on the photooxidation. Since deposited metals influence the photoreactivity of TiO_2 by acting as electron or hole traps, their energy levels with respect to conduction band and valence band edges of TiO_2 are important. However, although Fe^{3+} and Cr^{3+} have similar energy levels in the TiO_2 lattice, they exhibit completely different efficiencies. This is due to the differences in the reactions of charge trapping, charge release and migration, recombination as well as interfacial charge transfer to an electron acceptor or an electron donor. In addition to these, electronic configurations of metals affect their reactivities. For transition metals, a closed-shell or a partly closed electronic configuration makes electron or hole trapping unfavorable. With the samples prepared in the presence of methanol, metals show the same trend but with a lower rate of CO_2 production. The presence of methanol increases the deposition of metallic form (M^0) of metals on the surface of the catalyst during the preparation steps of the samples. This reduces the reactions of holes with the electron donors in the photodegradation process.

For both methods, with and without methanol, Fe^{3+} shows the highest efficiency. Among the different concentrations of Fe^{3+} deposited samples, 1.0 per cent loaded samples produced the highest CO_2 concentration for all of the reactants. This agrees with the atomic absorption results in which the highest adsorption onto the TiO_2 surface is obtained with 1.0 per cent deposition. Increasing the percentage of Fe^{3+} loading, decreases the amount of adsorption on the catalyst surface. Inhibition of light penetration causes such an effect and makes the electron hole recombination process fast. Heating during the preparation step of iron loaded samples reduces the photoactivity. The location of iron deposition on the surface changes because of agglomeration upon heating. Thus, deposited iron serves as recombination centers rather than being a trap site.

To determine the quantum yields of all reactant molecules 1,3-DHB is selected as the standard probe. Thus, a detailed analysis about the incident photon flux and rate of formation of CO_2 for the photocatalytic oxidation of 1,3-DHB is done. It is observed that increasing the number of lamps increases the evolution of CO_2 due to higher production rate of electron-hole pairs. In the mean time, the opportunity of electron-hole recombination also increases. This results in a lower degradation rate.

Since TiO_2 particles are not capable of absorbing all the incident photon flux due to light scattering off the particle surface, an integrated sphere model is used to determine the fraction of light absorbed. Increasing the incident photon flux increases the fraction of light absorption. However, the rate of CO_2 formation and degradation of 1,3-DHB decreases. This is due to the increased opportunity of electron-hole recombination. An analogous trend is observed during the calculation of quantum yields with respect to incident photon flux. When the effect of TiO_2 loading is examined for the fraction of light absorption, there is a linear increase up to 1 g/L loading of TiO_2, and then a negative deviation is observed for concentrations higher than 1 g/L of TiO_2. This is because as loading increases the suspension becomes more opaque for the penetration of the light. As a result, rates and quantum yields decrease as a function of TiO_2 loading.

Since throughout this study a TiO_2 concentration of 1 g/L and the incident photon flux of 10.8×10^{-6} einstein/min are used, the rate of CO_2 formation, 1.81 $\mu M/min$ and the quantum yield, 0.34 for 1,3-DHB will be used for the determination of relative photonic efficiencies and quantum yields of other reactant molecules. The relative photonic efficiencies based on the rate of formation of CO_2 for 3,5-DHT, 1,3-DHMB and 3,5-DHBA are reported in Table 10.5 and Figure 10.1.

It is not possible to see a general trend for the relative photonic efficiencies as a function of the parameters changed. Some of the efficiencies are greater than unity indicating that the initial photocatalyzed oxidative degradation of selected substrates are more efficient than 1,3-DHB. However, some of the efficiencies are less than unity.

According to substrate concentration, substrates containing electron donor groups show lower relative efficiencies compared to that containing an electron withdrawing group. However, with the increase in concentration, while relative photonic efficiencies of 1,3-DHMB and 3,5-DHBA increase, the efficiency of 3,5-DHT decreases. With respect to pH, for acidic media, relative efficiency is higher for 3,5-DHBA. This may be due to the lower pK value of 3,5-DHBA which results in higher degradation rates or percentages at low pH's. By contrast, in alkaline media, 1,3-DHMB has the highest efficiency which corresponds to expected pK value of 9.81. In the neutral medium, 3,5-DHT and 1,3-DHMB have almost the same relative photonic efficiency whereas 3,5-DHBA has the lowest. When the temperature is examined as a parameter, it is observed that increasing the temperature does not make a considerable change for the efficiencies. However, when electron donor substituents of 3,5-DHT and 1,3-DHMB are compared with the electron withdrawing substituent of 3,5-DHBA, higher efficiencies are obtained with the latter.

Table 10.5. Relative photonic efficiencies for 3,5-DHT, 1,3-DHMB and 3,5-DHBA under various conditions relative to 1,3-DHB.

Parameter changed	Relative photonic efficiency ζ_r		
	3,5-DHT	1,3-DHMB	3,5-DHBA
*Reactant Conc. (μM)			
100	0.67	0.91	1.29
1000	0.63	1.03	1.33
**pH			
3.5	0.83	1.18	1.53
Natural	0.64	1.04	1.13
7.0	1.03	1.01	0.75
9.0	0.99	1.11	0.96
***Temperature (K)			
298	0.59	0.96	1.51
303	0.88	0.94	1.45
313	0.88	1.03	1.45
323	0.93	1.18	1.55
333	0.88	1.21	1.38

*: Conditions: $[TiO_2]$=1 g/L, pH=Natural, I_0=10.8x10^{-6} einstein/min, T=298 K

**: Conditions: $[TiO_2]$=1 g/L, [Reactant]= 100 μM, I_0=10.8x10^{-6} einstein/min, T=298 K

***: Conditions: $[TiO_2]$=1 g/L, [Reactant]= 100 μM, pH=Natural, I_0=10.8x10^{-6} einstein/min,

We would expect that electron donor groups, CH_3 and OCH_3, in 3,5-DHT and 1,3-DHMB respectively, increase the electron density over the aromatic ring and facilitate the attack by electrophilic ·OH radicals. Thus, the electron withdrawing group, COOH in the presence of 3,5-DHBA is expected to decrease the electron density over the ring by attracting electrons towards itself. However, as a result of all the above parameters it is not possible obtain a general trend according to electronic effects of substituents. Since these substituents are substituted in the meta position of the
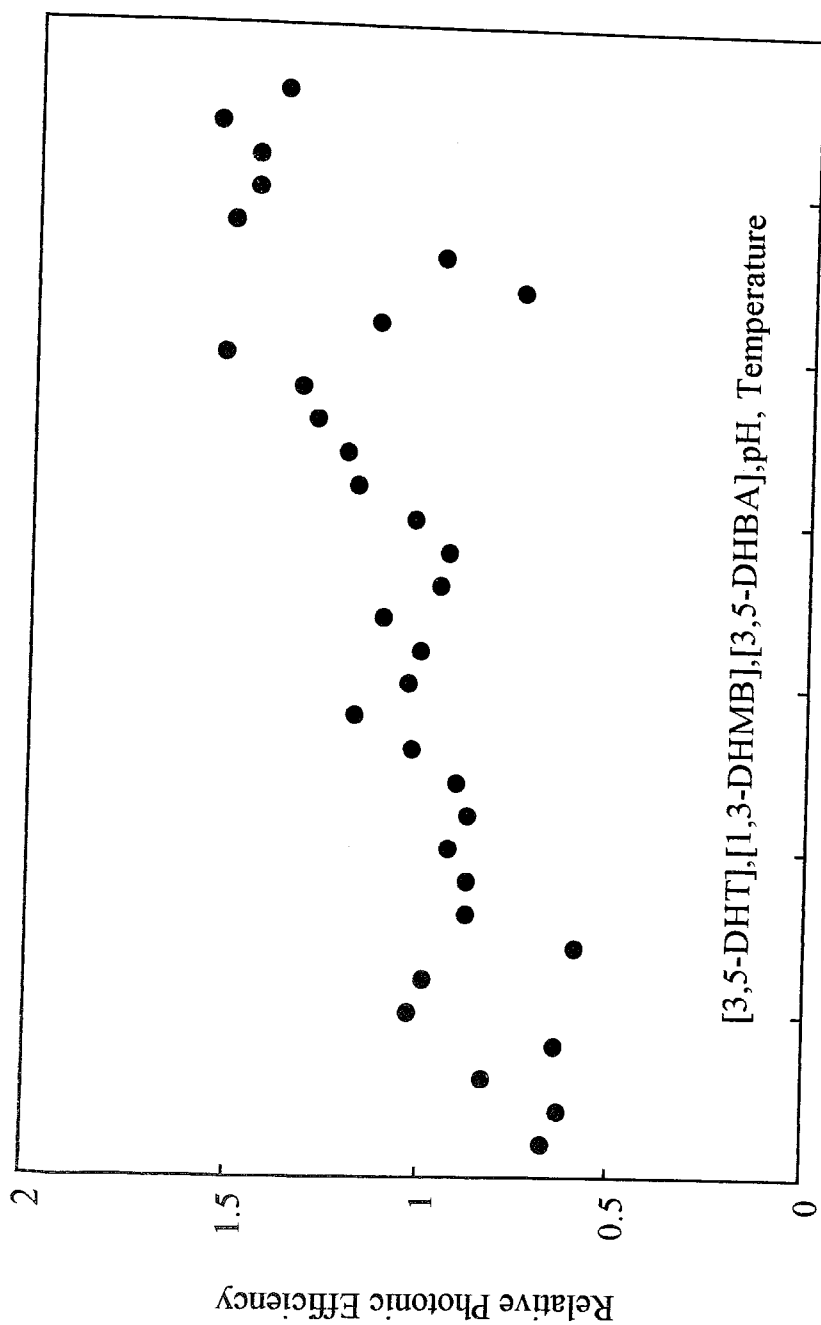
Figure 10.1. Relative photonic efficiencies as a function of reactant concentration, pH and temperature for 1,3-DHB, 3,5-DHT, 1,3-DHMB, and 3,5-DHBA.

1,3-DHB ring, they probably do not contribute significantly to the electron density of the ring. Therefore, the concept of relative photonic efficiencies does not have a specific applicability for meta-substituted resorcinols.

Quantum yields of reactants are found from $\phi = \zeta_r \, \phi_{1,3\text{-DHB}}$ at their natural pH's as 0.22, 0.35, and 0.38 for 3,5-DHT, 1,3-DHMB and 3,5-DHBA, respectively.

It is also well known that electron or hole scavengers can affect the rate of photocatalytic degradation. Based on this, the rate of formation of CO_2 for 1,3-DHB is investigated in the presence of methanol as a hole scavenger and in the presence of H_2O_2 as an electron scavenger. In the presence of methanol, the formation of CO_2 decreases since $^\bullet OH$ radicals are known to react with methanol and thus the amount of $^\bullet OH$ radicals which are able to react with adsorbed 1,3-DHB molecules decreases. The enhancement in the rate of formation of CO_2 upon addition of H_2O_2 is due to formation of $^\bullet OH$ radicals between the reaction of H_2O_2 with photogenerated electrons. However, it is also possible that $^\bullet OH$ radicals can combine together or react with H_2O_2 in the presence of excess H_2O_2. Thus, there is a limit for the H_2O_2 concentration beyond which the amount of $^\bullet OH$ radicals for the oxidation process decreases. Based on 1,3-DHB data with H_2O_2 and methanol we anticipate similar trends in the data for substituted resorcinols. Thus experiments are not performed for 3,5-DHT, 1,3-DHMB and 3,5-DHBA under these conditions.

11. CONCLUSION

In this study, the photocatalytic degradation of 1,3-DHB, 3,5-DHT, 1,3-DHMB and 3,5-DHBA are investigated. The results can be classified as follows:

Effect of reactant concentration: When the rate of reactant concentrations are considered, it is found that 1,3-DHB and 3,5-DHT obey pseudo-first order kinetics, whereas 1,3-DHMB and 3,5-DHBA obey zero order kinetics. For the rate of CO_2 formation, the obtained Langmuir type plot confirmed that reactions take place on the surface of the TiO_2.

Effect of pH: 1,3-DHB, 3,5-DHT, 1,3-DHMB are most efficient in CO_2 formation at pH 9.0. However, 3,5-DHBA represented highest efficiency at its natural pH 4.4. It is observed that in the presence of TiO_2., degradation rates of these reactant molecules are higher compared to those in the absence of TiO_2.

Effect of Irradiation Time: As a function of irradiation time, 98.9 per cent degradation of 1,3-DHB is obtained in 60 min irradiation time. For 3,5-DHT, 99.4 per cent degradation is achieved in 60 min irradiation. In the case of 1,3-DHMB, since the initial concentration is higher, 500 µM, the per cent degradation is 92.8 in 180 min irradiation. For 3,5-DHBA, 91.8 per cent degradation is observed in 30 min irradiation time. CO_2 percentages for all reactants need longer irradiation periods.

Effect of Temperature: Increasing the temperature increases the rate of CO_2 formation. The activation energy is calculated for 1,3-DHB, 3,5-DHT, 1,3-DHMB and 3,5-DHBA as 11.2 kJ/mol, 17.4 kJ/mol, 17.1 kJ/mol and 10.3 kJ/mol respectively.

Effect of H₂O₂ and Methanol: Addition of H_2O_2 as an electron trap enhances the CO_2 formation rate for 1,3-DHB, but there is a limit for the concentration of H_2O_2 above which ˙OH radicals are consumed in other reactions rather than taking part in oxidative routes. Methanol being an hole scavenger decreases the degradation rate by reacting photogenerated holes as well as ˙OH radicals.

Effect of Incident Photon Flux: Considering 1,3-DHB as the probe molecule, the effect of incident photon flux on the rate of CO_2 formation is examined. Higher fluxes increase the rate up to a limiting value beyond which electron-hole recombination takes place. Relative photonic efficiencies of 3,5-DHT, 1,3-DHMB and 3,5-DHB are based on the formation rate of CO_2 in 1,3-DHB. The effect of reactant concentration, pH of the medium and temperature of the system are investigated for the relative efficiencies. No direct relation is found between the electronic efficiencies of the substituents and the relative photonic efficiency. Quantum yields are obtained at the natural pH's of reactant molecules.

Effect of Metal Deposition: Metal deposition on the surface of the TiO_2 affects the photocatalytic degradation of reactant molecules. However, there are differences in the photoactivities of selected metals. These can be explained by the energy levels of metals with respect to the conduction band and valence band edges of TiO_2, differences in the reactions of charge trapping, charge release and migration, recombination and interfacial charge transfer. In addition to these, electronic configurations of transition metals are important. Preparation methods of deposited samples have considerable effects on the degradation rate of reactants. Samples prepared in the absence of methanol show higher efficiencies compared to those prepared in the presence of methanol. Photoreactivity also decreases with heat treated samples because of particle agglomeration.
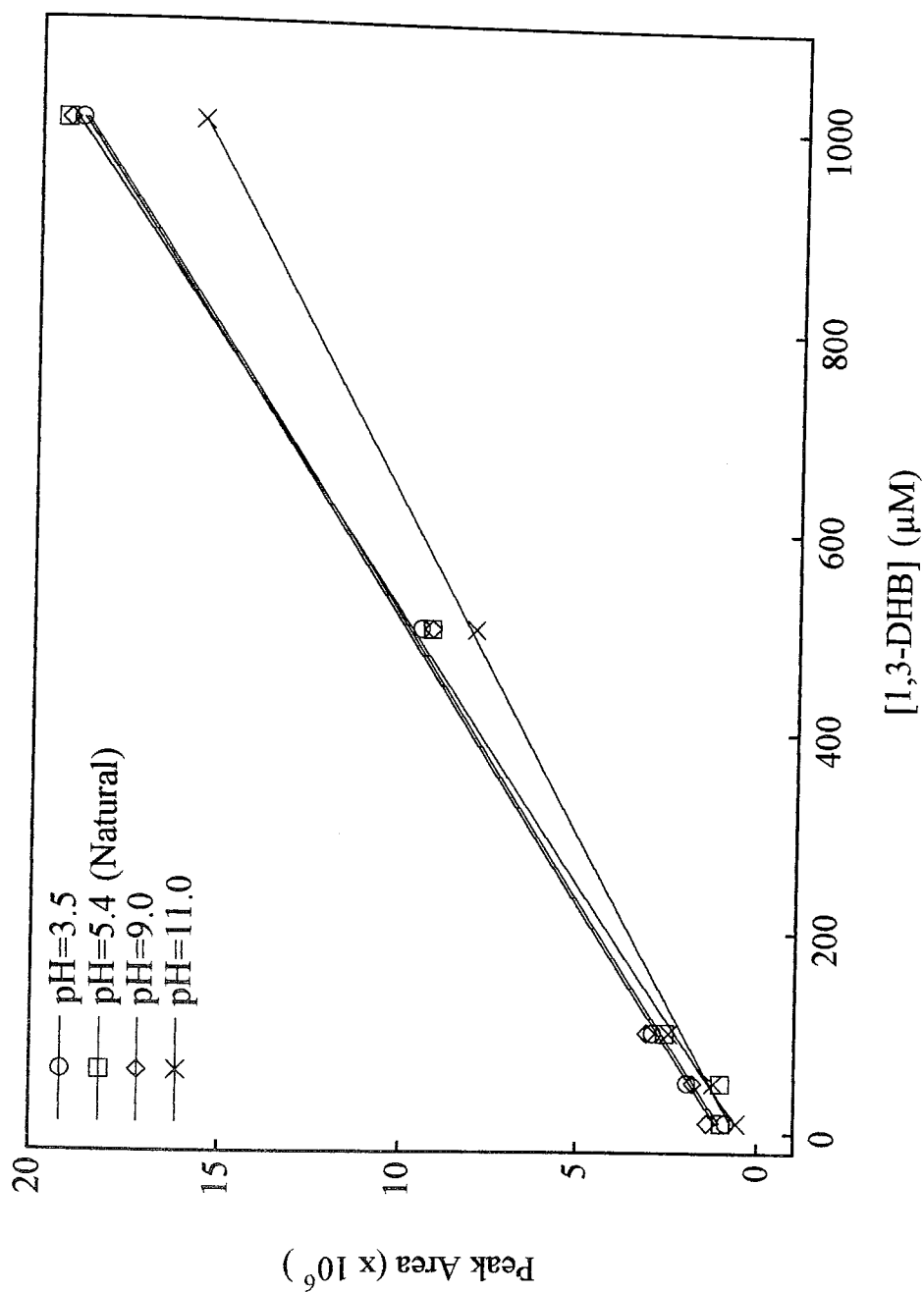
APPENDIX A

Figure A.1. pH calibration of 1,3-DHB in HPLC.

Table A.1. pH calibration of 1,3-DHB in HPLC.

[1,3-DHB] (μM)	pH=3.5	pH=5.4	pH=9.0	pH=11.0
1000	18.95	19.36	19.26	15.69
500	9.517	9.189	9.185	7.945
100	2.889	2.544	3.052	2.446
50	1.944	1.014	1.771	1.203
10	0.866	0.983	1.365	0.571
y = Peak Area (x10^6) x = [1,3-DHB] (μM)	y=0.88+0.017x R=0.999	y=0.42+0.019x R=0.998	y=0.97+0.018x R=0.998	y=0.57+0.015x R=0.999
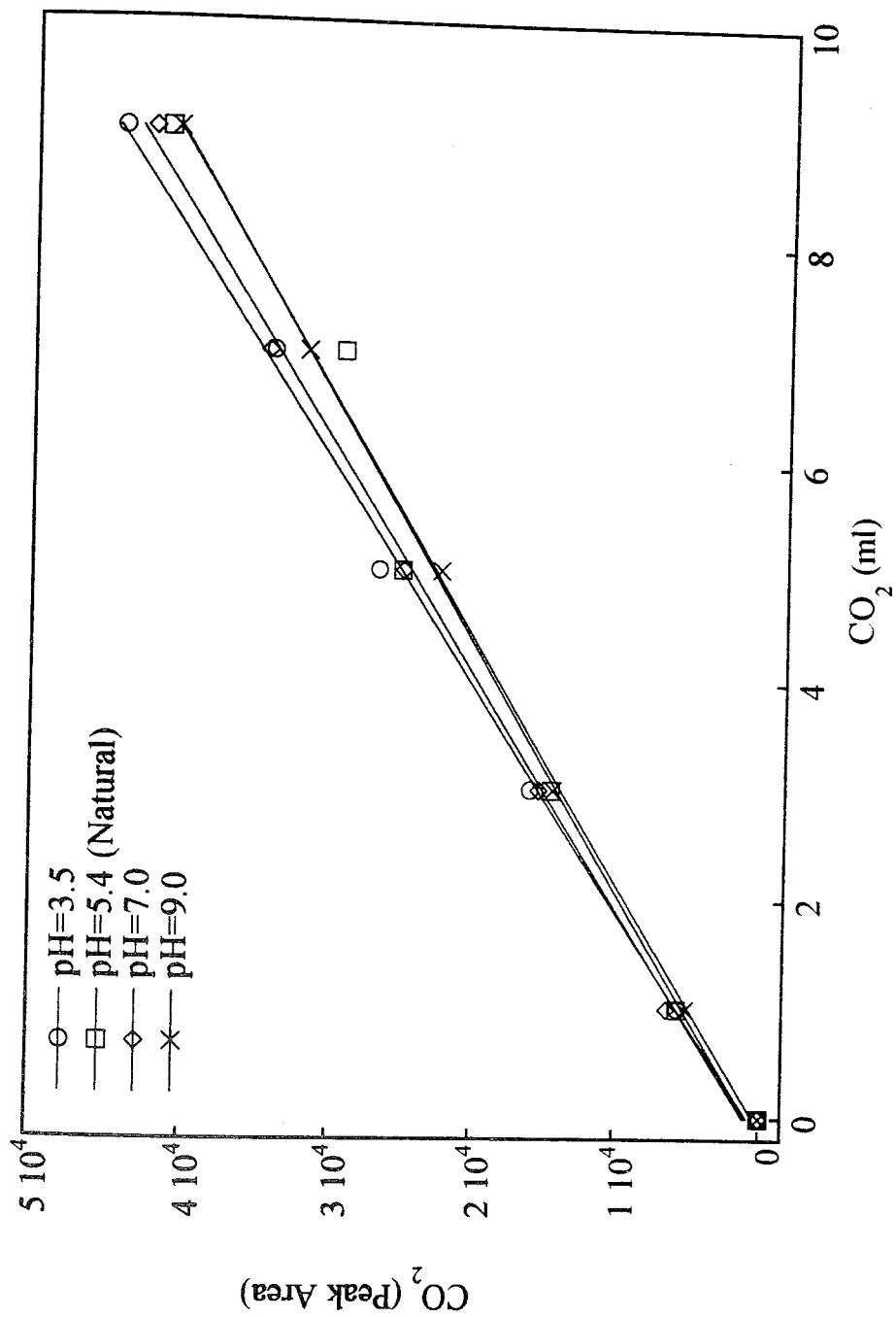
Figure A.2. pH calibration of 1,3-DHB in GC.

Table A.2. pH calibration of 1,3-DHB in GC.

| CO$_2$ (ml)	pH=3.5	pH=5.4	pH=7.0	pH=9.0
1	5622	5629	6344	5067
3	16019	14499	15387	14398
5	26733	25098	25007	22347
7	34105	29216	34424	31735
9	44329	41254	42287	40663
y = Peak Area x = CO$_2$ ml	y=814.5+4876.8x R=0.999	y=902.7+4411.2x R=0.994	y=1073.5+4680.3x R=0.998	y=389.1+4475.1x R=0.999
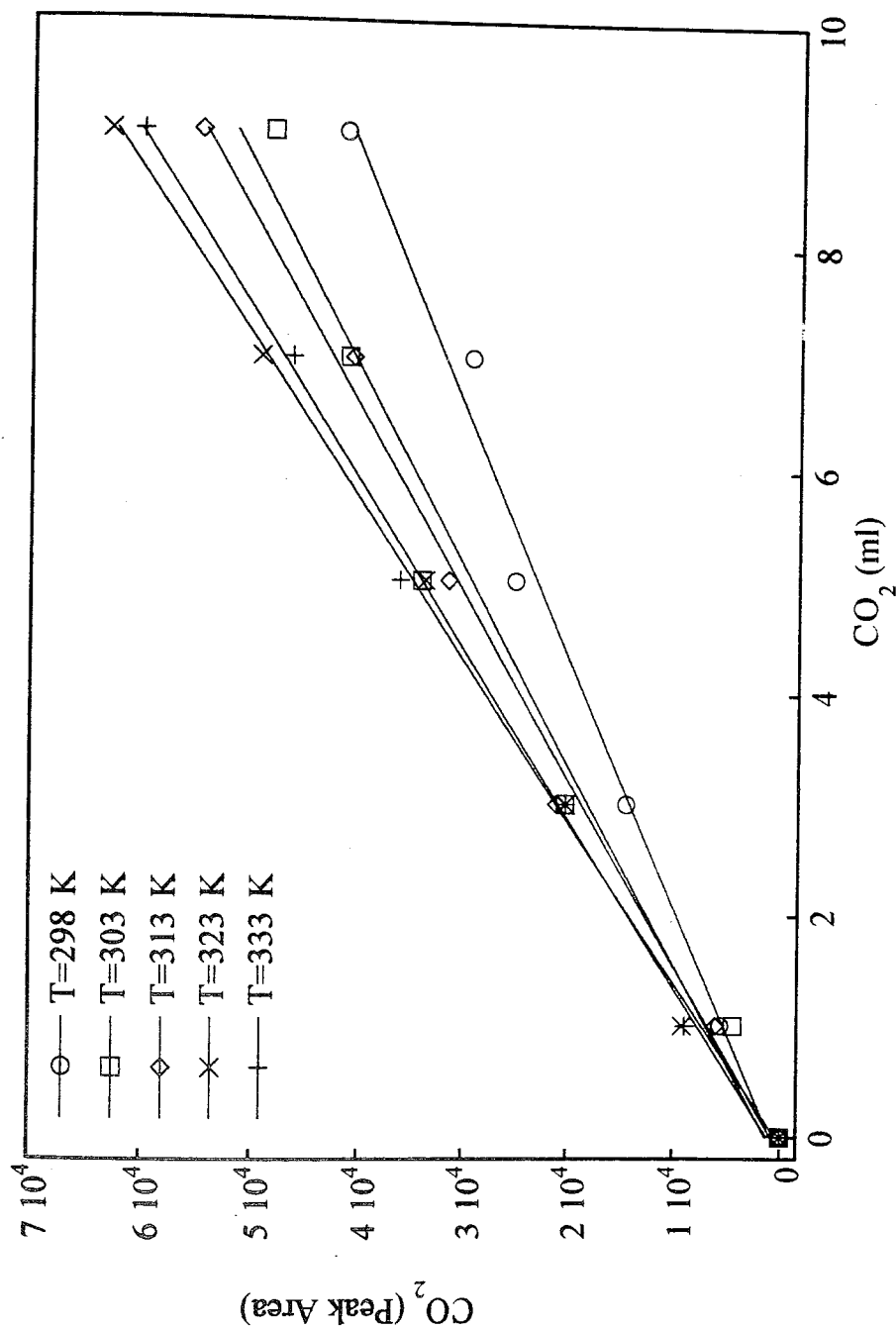
Figure A.3. Temperature calibration of 1,3-DHB in GC.

Table A.3. Temperature calibration of 1,3-DHB in GC.

CO$_2$ (ml)	T=298 K	T=303 K	T=313 K	T=323 K	T=333 K
1	5629	4446	6047	9122	8902
3	14499	20258	21080	20210	20192
5	25098	34053	31448	33689	36118
7	29216	40936	40549	49212	46314
9	41254	48136	54805	63007	60080
y = Peak Area x = CO$_2$ ml	y=902.7+4411.2x R=0.994	y=1398+5577.6x R=0.987	y=843.6+5954.7x R=0.997	y=468.5+6897.2x R=0.999	y=1206+6574.7x R=0.998
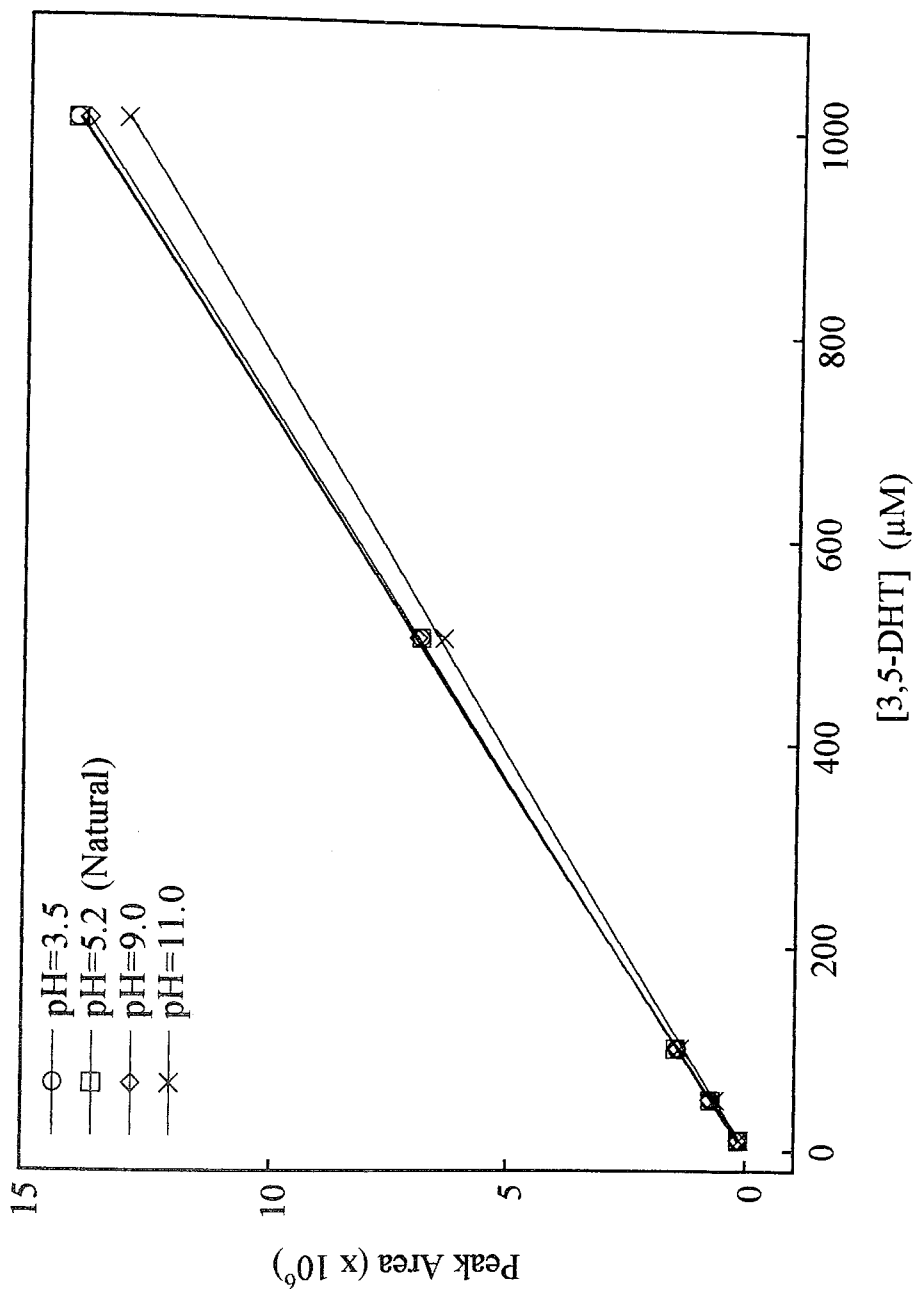
Figure A.4. pH calibration of 3,5-DHT in HPLC.

Table A.4. pH calibration of 3,5-DHT in HPLC.

[3,5-DHT] (μM)	pH=3.5	pH=5.2	pH=9.0	pH=11.0
1000	14.07	14.06	13.84	13.06
500	6.894	6.885	6.951	6.396
100	1.418	1.442	1.416	1.359
50	0.735	0.723	0.745	0.625
10	0.144	0.142	0.152	0.131
y = Peak Area ($\times 10^6$) x = [3,5-DHT] (μM)	y=-0.002+0.014x R=0.999	y=0.001+0.014x R=0.999	y=0.036+0.013x R=0.999	y=-0.089+0.013x R=0.999
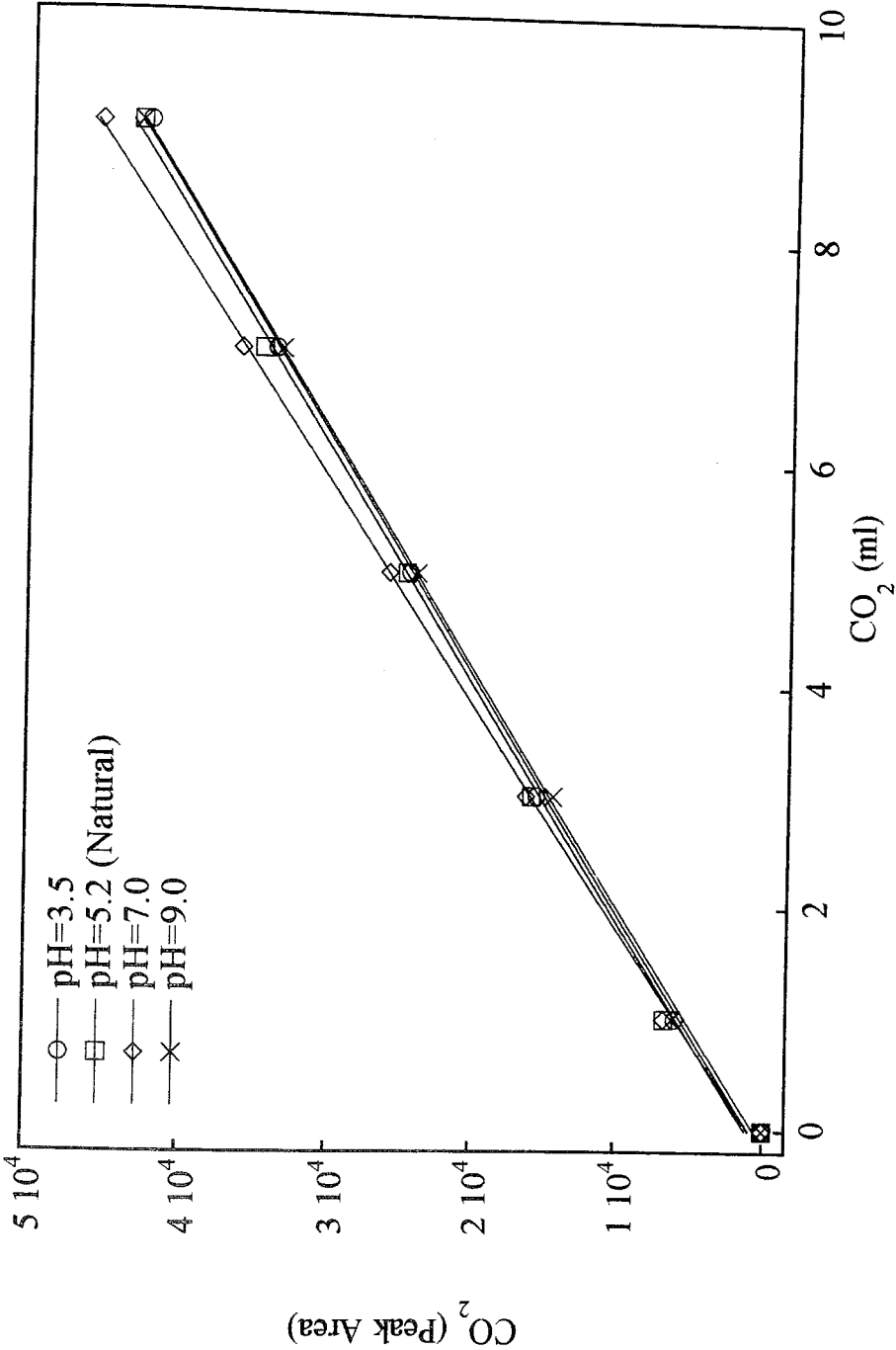
Figure A.5. pH calibration of 3,5-DHT in GC.

Table A.5. pH calibration of 3,5-DHT in GC.

| CO_2 (ml)	pH=3.5	pH=5.2	pH=7.0	pH=9.0
1	5973	6662	6701	6147
3	15506	15878	16205	14384
5	24492	24691	25882	23946
7	33794	34627	36106	33335
9	42377	42893	45552	42896
y = Peak Area x = CO_2 ml	y=906.5+4668.1x R=0.999	y=1176+4707.6x R=0.998	y=925.2+4995.8x R=0.999	y=564.1+4693.1x R=0.999
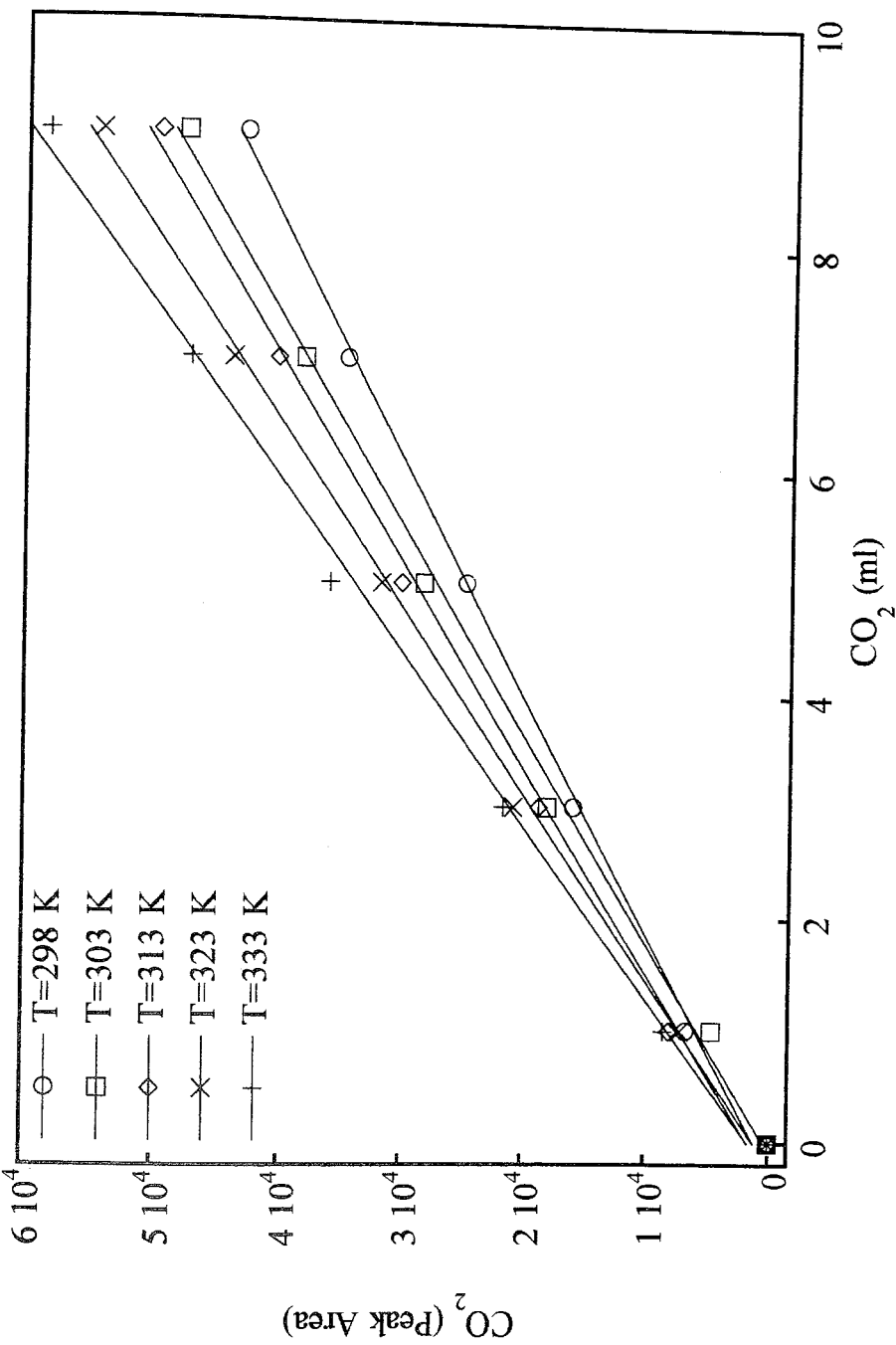
Figure A.6. Temperature calibration of 3,5-DHT in GC.

Table A.6. Temperature calibration of 3,5-DHT in GC.

CO$_2$ (ml)	T=298 K	T=303 K	T=313 K	T=323 K	T=333 K
1	6662	4564	8007	7127	8455
3	15878	17927	18634	20692	21559
5	24691	28238	30039	31722	35959
7	34627	38087	40234	43876	47191
9	42893	47620	49681	54273	58394
y = Peak Area x = CO$_2$ ml	y=1176+4707.6x R=0.998	y=394.1+5362.9x R=0.998	y=1688+5458.5x R=0.998	y=1188+6022.4x R=0.999	y=1608+6476.5x R=0.998
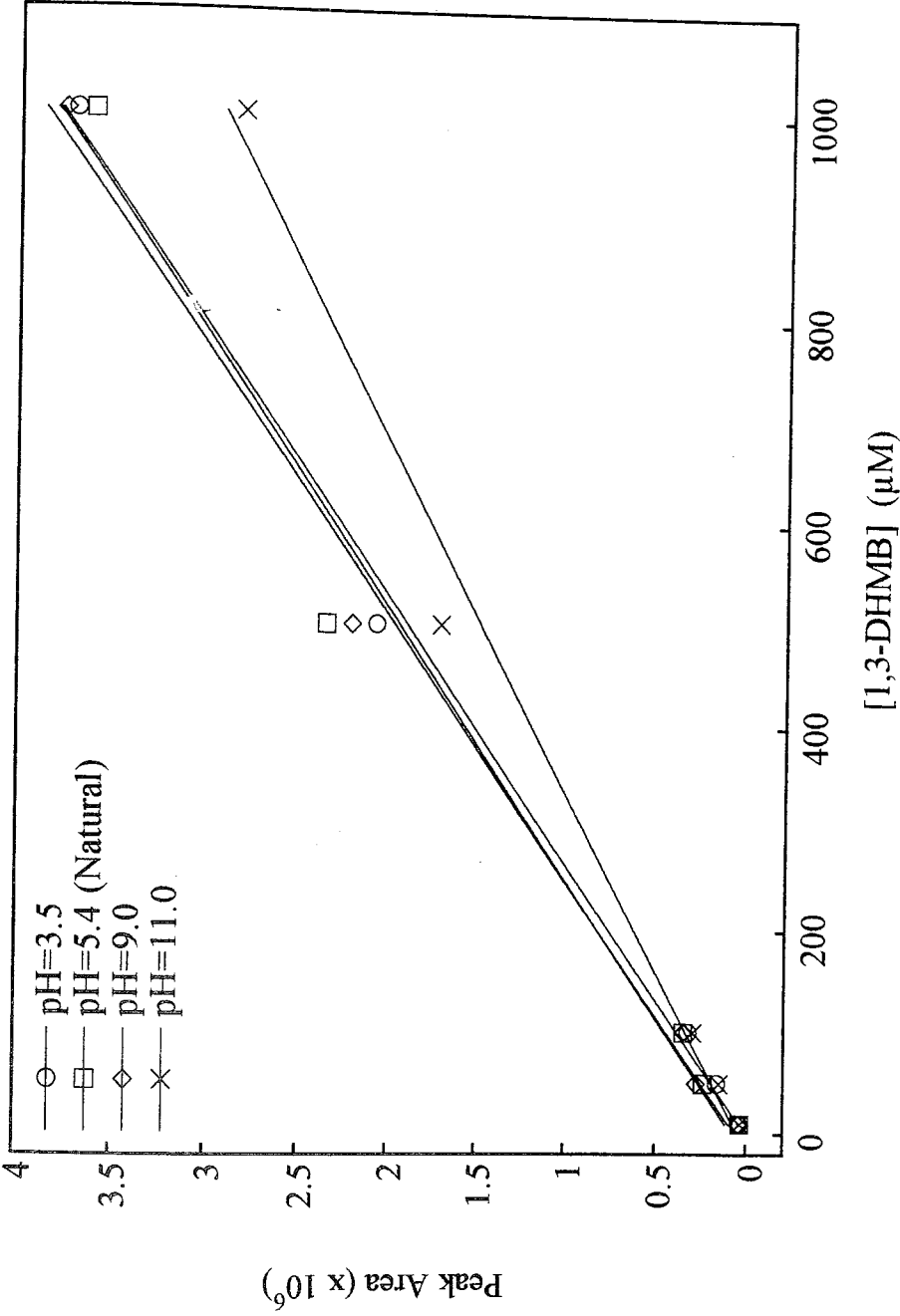
Figure A.7. pH calibration of 1,3-DHMB in HPLC.

241

Table A.7. pH calibration of 1,3-DHMB in HPLC.

[1,3-DHMB] (μM)	pH=3.5	pH=5.4	pH=9.0	pH=11.0
1000	3.712	3.617	3.765	2.812
500	2.068	2.346	2.204	1.706
100	0.320	0.345	0.343	0.293
50	0.163	0.238	0.274	0.149
10	0.041	0.034	0.041	0.035
y = Peak Area (x10^6) x = [1,3-DHMB] (μM)	y=0.004+0.0038x R=0.998	y=0.078+0.0037x R=0.989	y=0.058+0.0038x R=0.996	y=0.046+0.0029x R=0.994
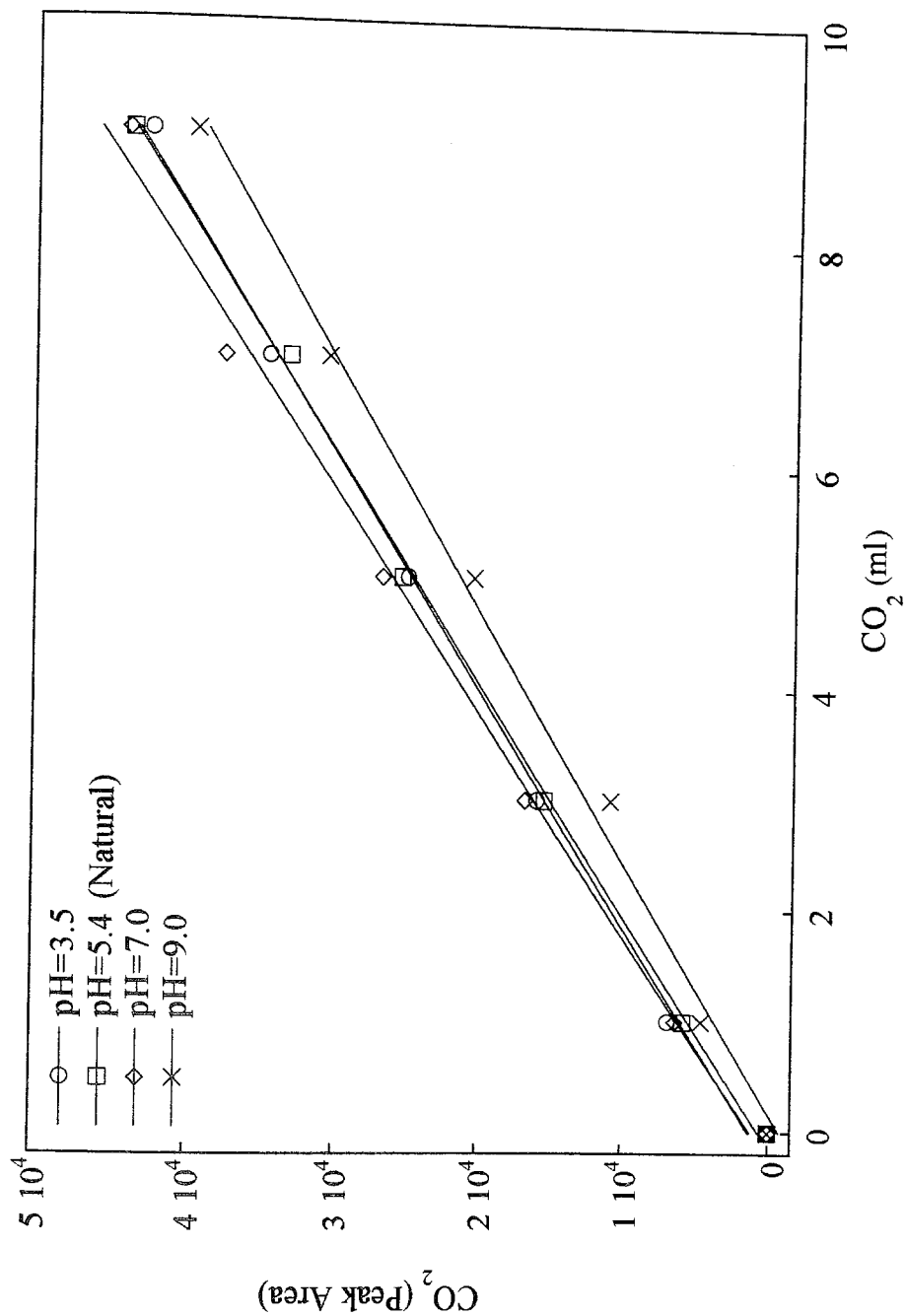
Figure A.8. pH calibration of 1,3-DHMB in GC.

Table A.8. pH calibration of 1,3-DHMB in GC.

| CO_2 (ml)	pH=3.5	pH=5.4	pH=7.0	pH=9.0
1	6853	5818	6330	4544
3	15925	15379	16698	10822
5	25025	25344	26721	20384
7	34616	33178	37578	30493
9	42651	43834	44087	39622
y = Peak Area	y=1338+4681.6x	y=686.5+4777.4x	y=1197+4969.3x	y=-703.4+4403.4x
x = CO_2 ml	R=0.998	R=0.999	R=0.997	R=0.998
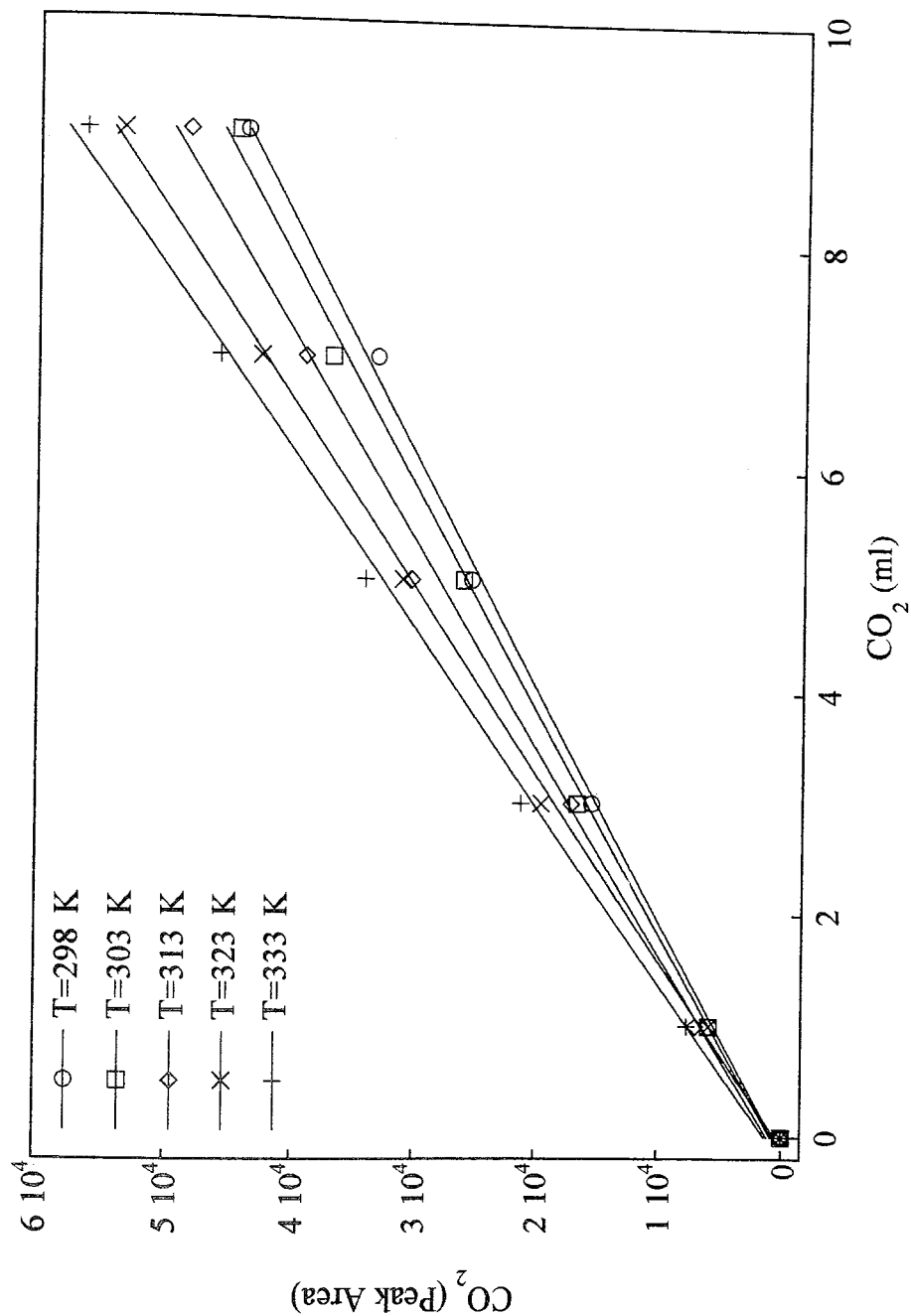
Figure A.9. Temperature calibration of 1,3-DHMB in GC.

Table A.9. Temperature calibration of 1,3-DHMB in GC.

CO_2 (ml)	T=298 K	T=303 K	T=313 K	T=323 K	T=333 K
1	5818	5814	6906	5809	7588
3	15379	16527	17015	19461	21152
5	25344	26002	30321	31038	34084
7	33178	36831	39047	42616	45892
9	43834	44492	48378	53560	56404
y = Peak Area x = CO_2 ml	y=686.5+4777.4x R=0.999	y=831.9+4987.1x R=0.999	y=1145+5391.9x R=0.998	y=456.2+5989.9x R=0.999	y=1332+6285.1x R=0.998
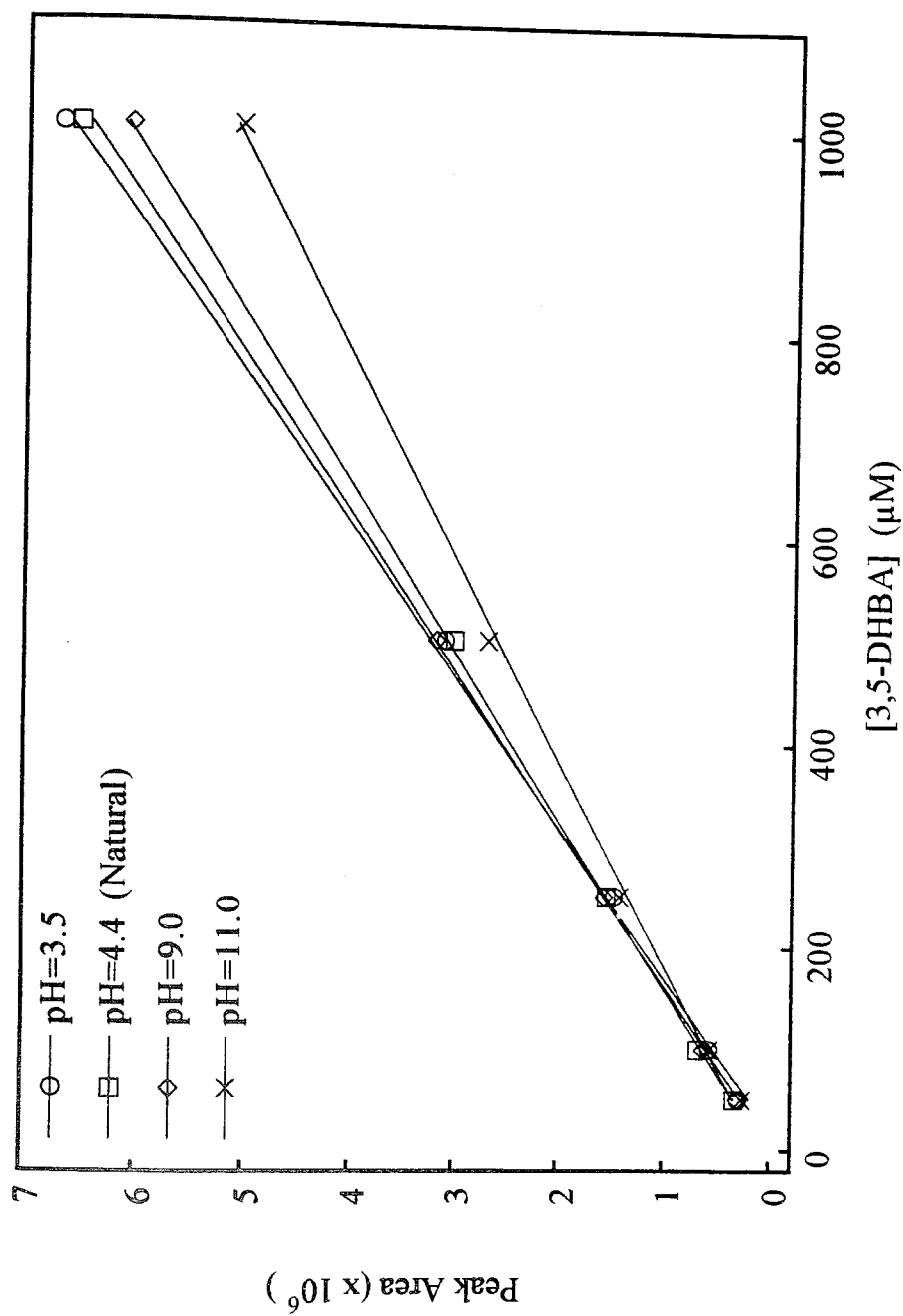
Figure A.10. pH calibration of 3,5-DHBA in HPLC.

Table A.10. Calibration of 3,5-DHBA in HPLC.

[3,5-DHBA] (μM)	pH=3.5	pH=4.4	pH=9.0	pH=11.0
1000	6.698	6.535	6.062	5.036
500	3.091	2.994	3.168	2.672
250	1.462	1.530	1.553	1.410
100	0.559	0.661	0.613	0.557
50	0.289	0.320	0.290	0.254
y = Peak Area (x10^6)	y=-0.152+0.0068x	y=-0.062+0.0065x	y=0.025+0.0061x	y=0.083+0.0051x
x = [3,5-DHBA] (μM)	R=0.998	R=0.999	R=0.996	R=0.994
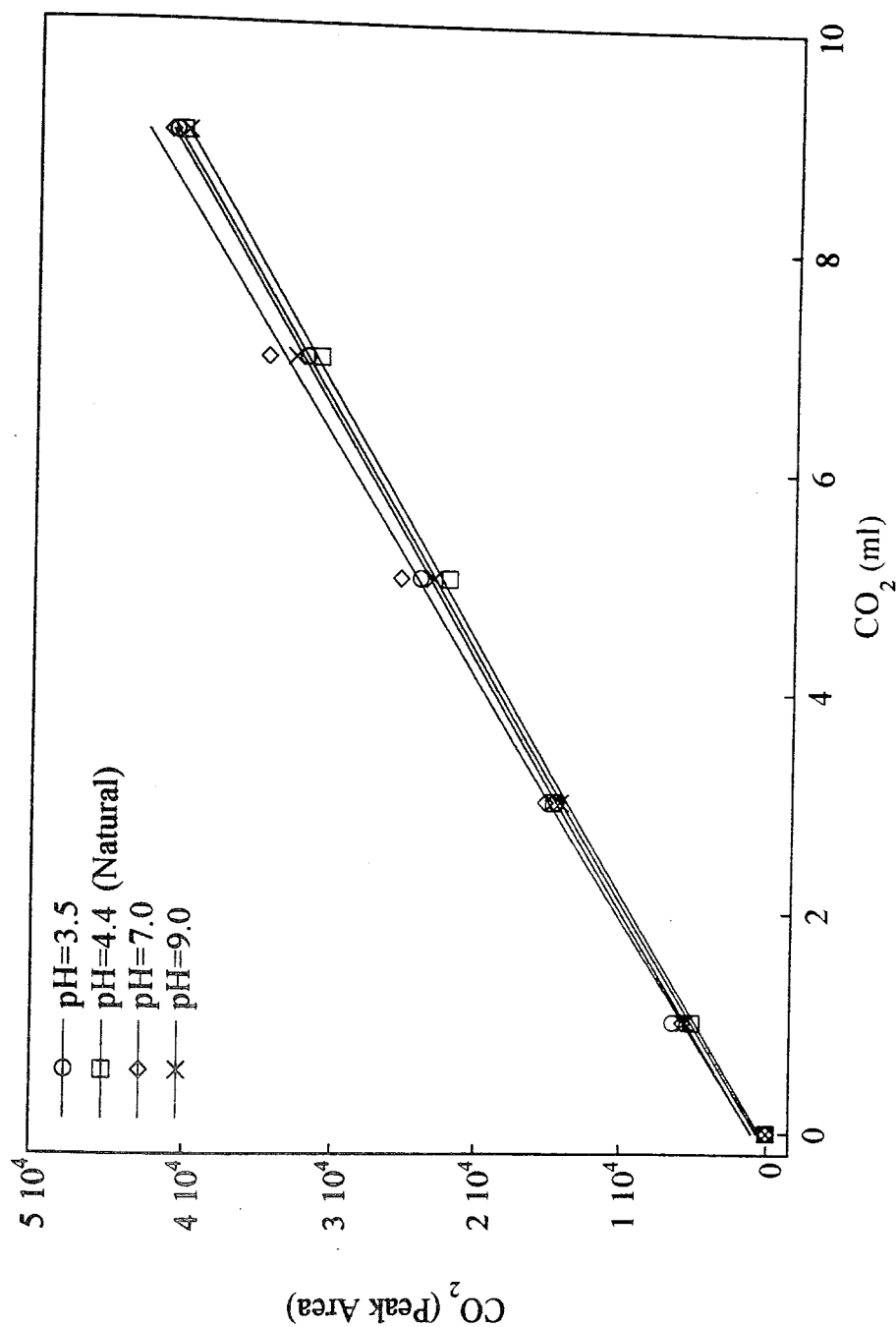
Figure A.11. pH calibration of 3,5-DHBA in GC.

Table A.11. pH calibration for 3,5-DHBA in GC.

CO$_2$ (ml)	pH=3.5	pH=4.4	pH=7.0	pH=9.0
1	6403	5074	5699	5548
3	14467	14635	15203	14160
5	24144	22066	25485	23174
7	32035	31080	34701	32793
9	41107	40584	41382	40281s
y = Peak Area	y=1034+4478.1x	y=450.2+4429.5x	y=974.3+4665.1x	y=639.2+4484.8x
x = CO$_2$ ml	R=0.998	R=0.999	R=0.997	R=0.999
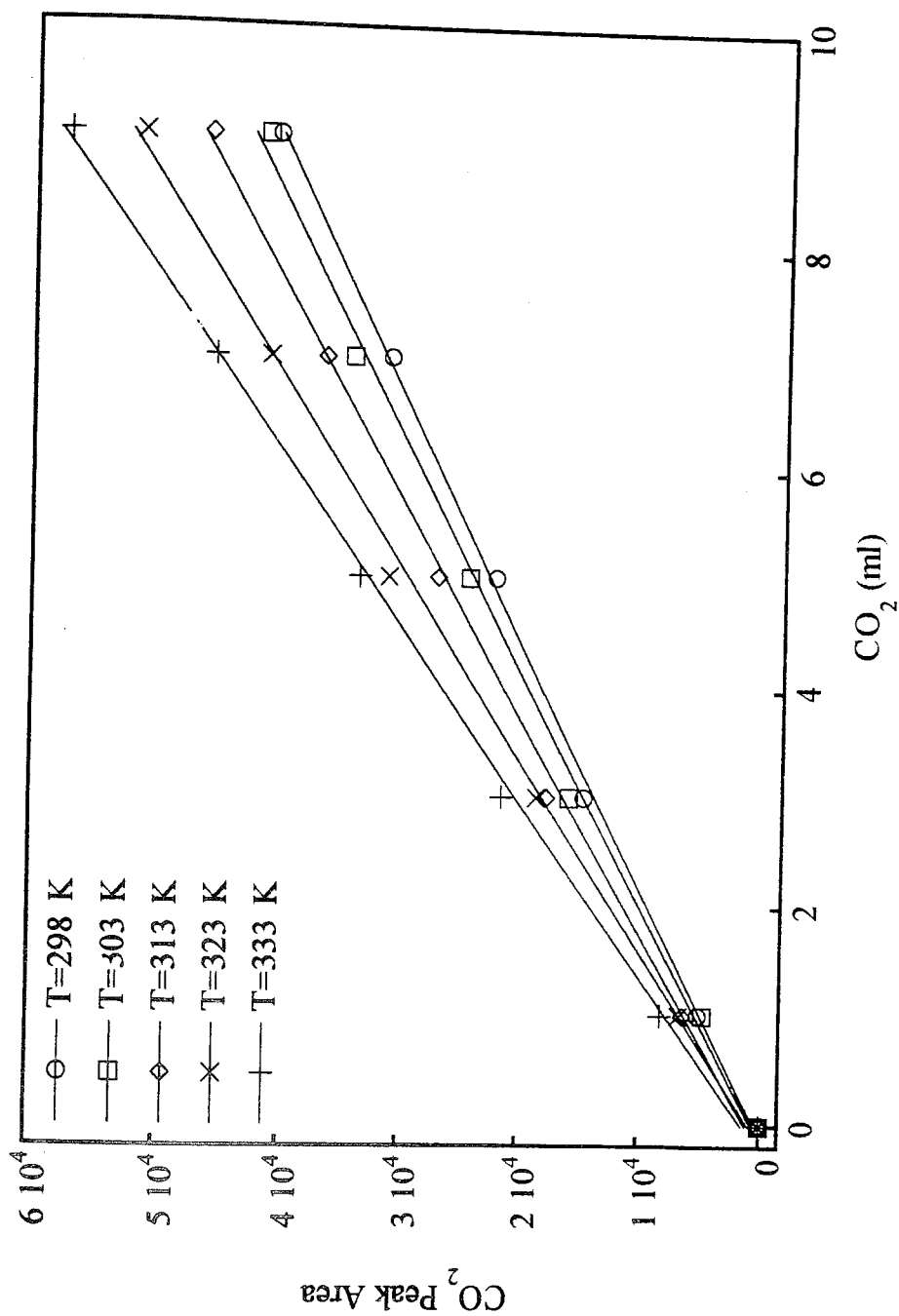
Figure A.12. Temperature calibration of 3,5-DHBA in GC.

Table A.12. Temperature calibration for 3,5-DHBA in GC.

CO_2 (ml)	T=298 K	T=303 K	T=313 K	T=323 K	T=333 K
1	5074	4688	6311	6604	8171
3	14635	15833	17716	18527	21448
5	22066	24329	26989	31141	33573
7	31080	34208	36493	41106	45582
9	40584	41408	46113	51532	57390
y = Peak Area	y=450.2+4429.5x	y=624.4+4668.8x	y=1166+5064.9x	y=916.8+5736.4x	y=1419+6306.1x
x = CO_2 ml	R=0.999	R=0.998	R=0.999	R=0.999	R=0.999

APPENDIX B
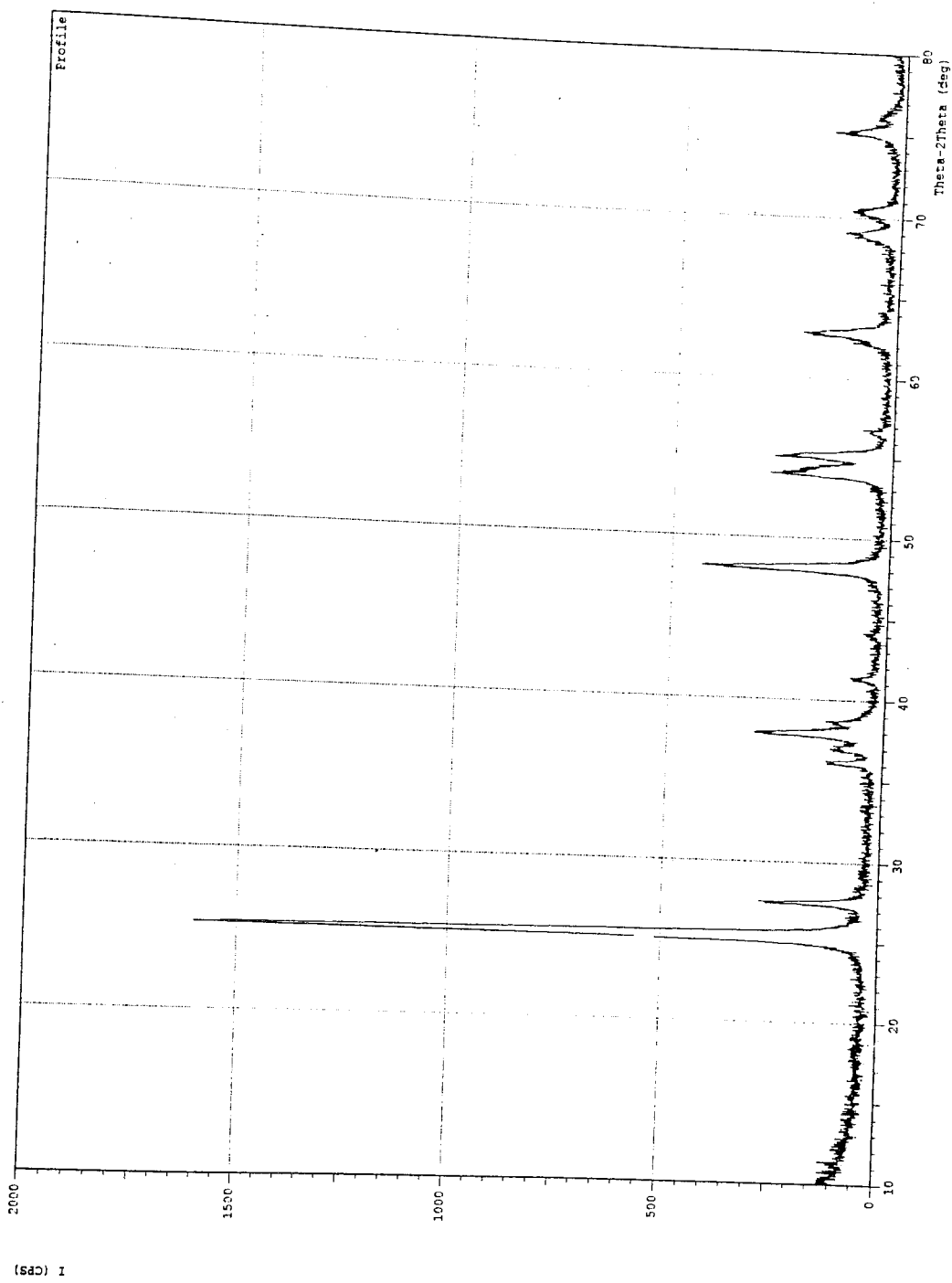
Figure B.1. X-ray diffraction analysis for undeposited TiO_2.
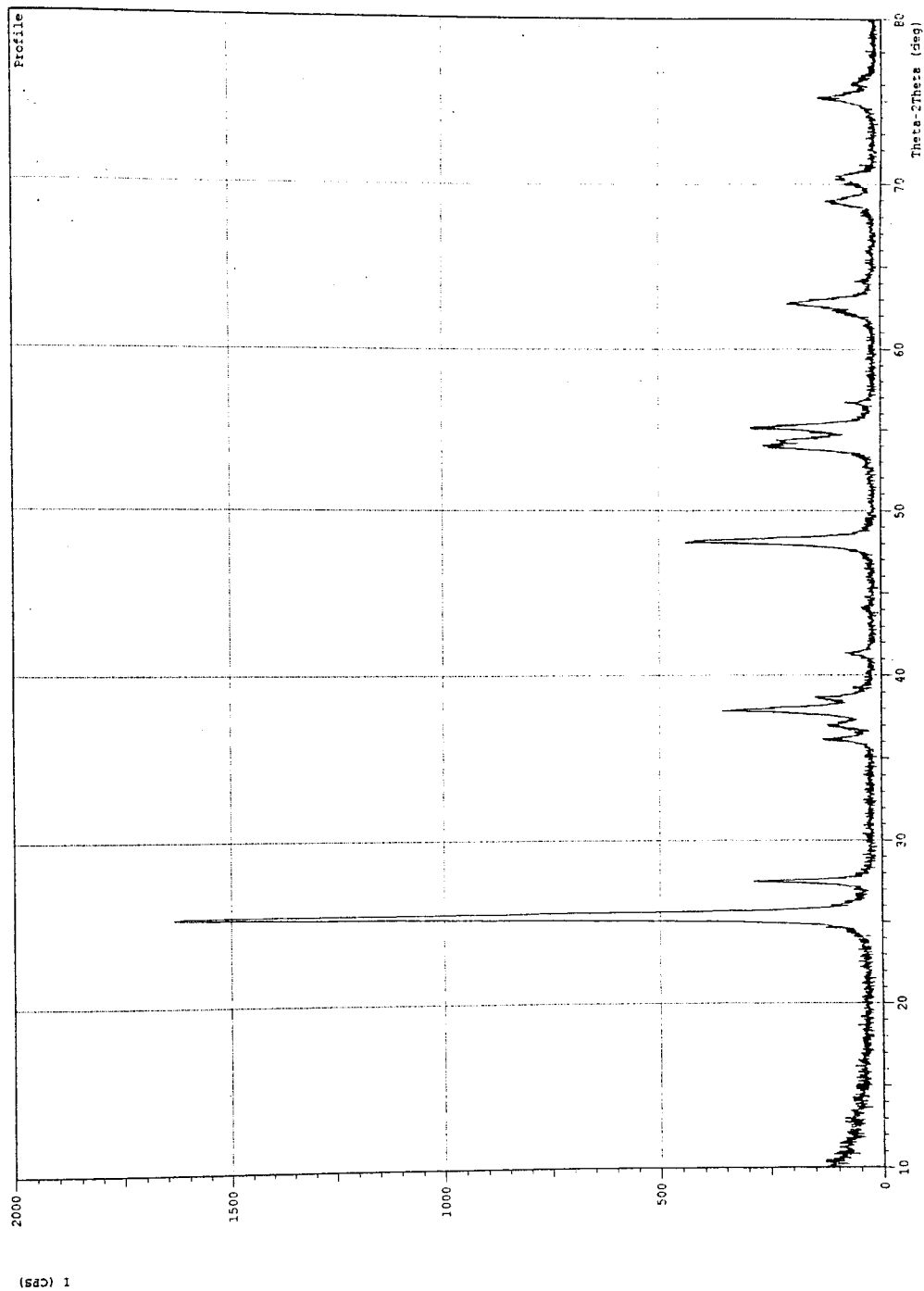
Figure B.2. X-ray diffraction analysis for V deposited TiO$_2$ without methanol.
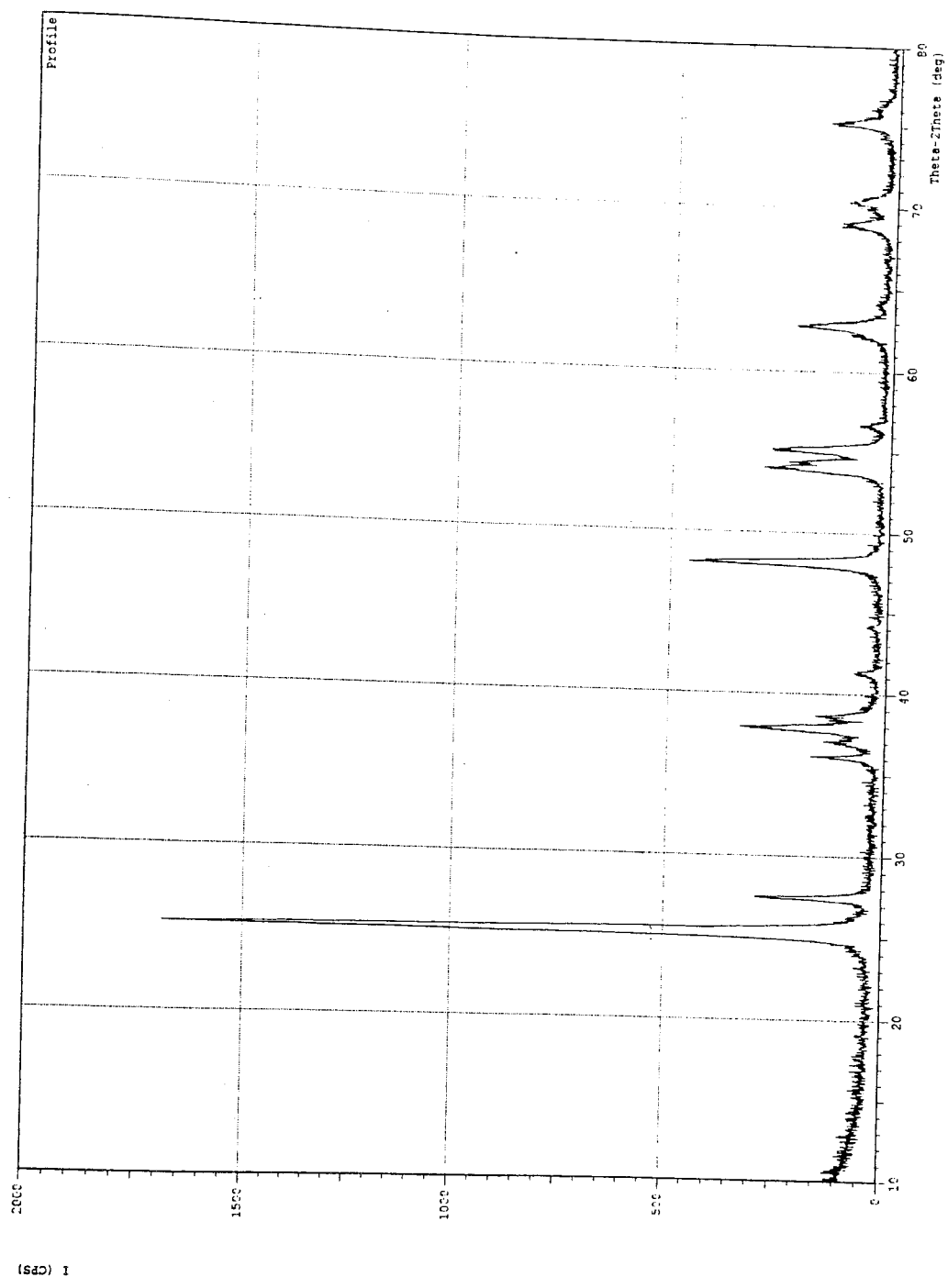
Figure B.3. X-ray diffraction analysis for V deposited TiO$_2$ with methanol.
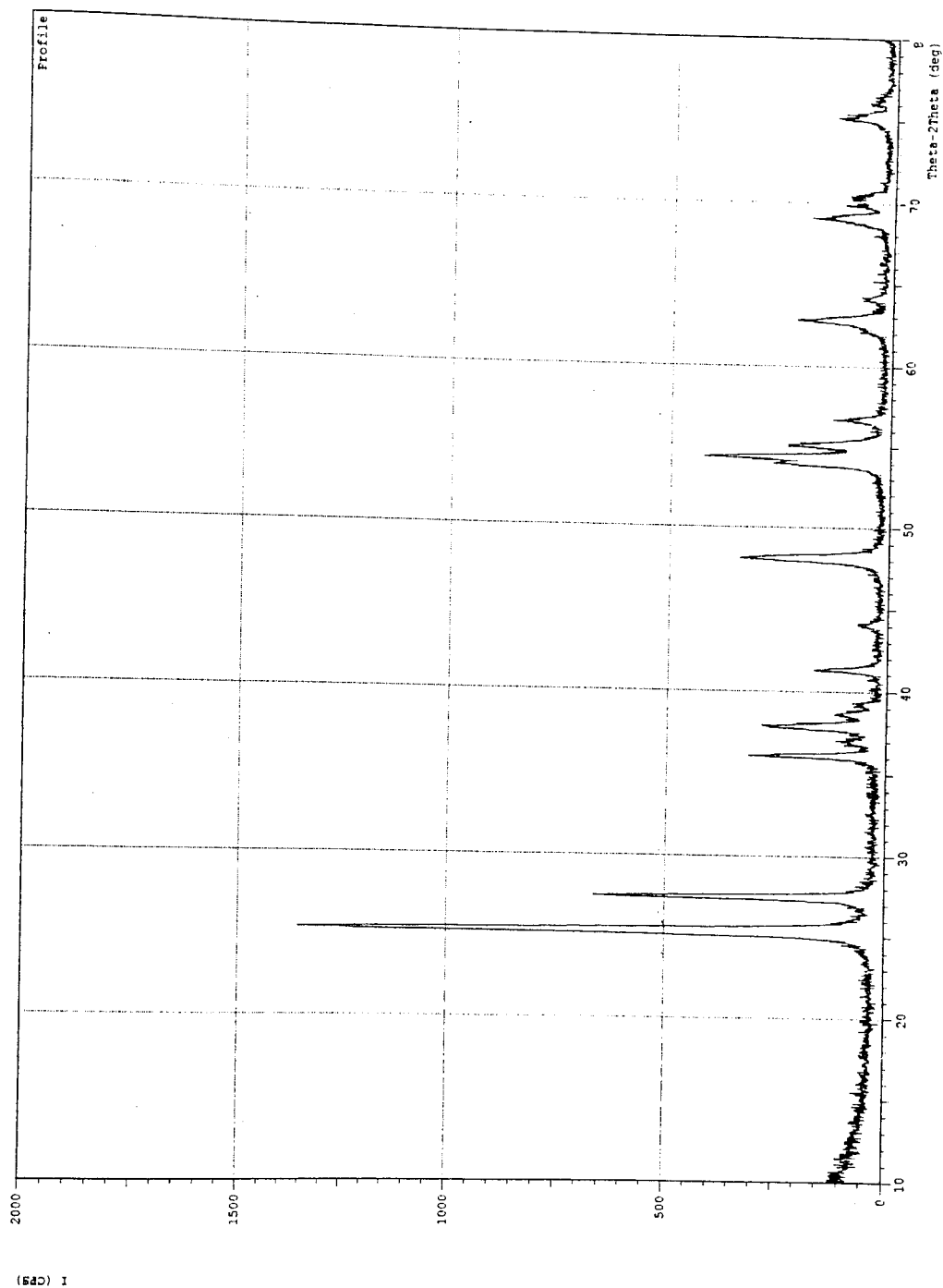
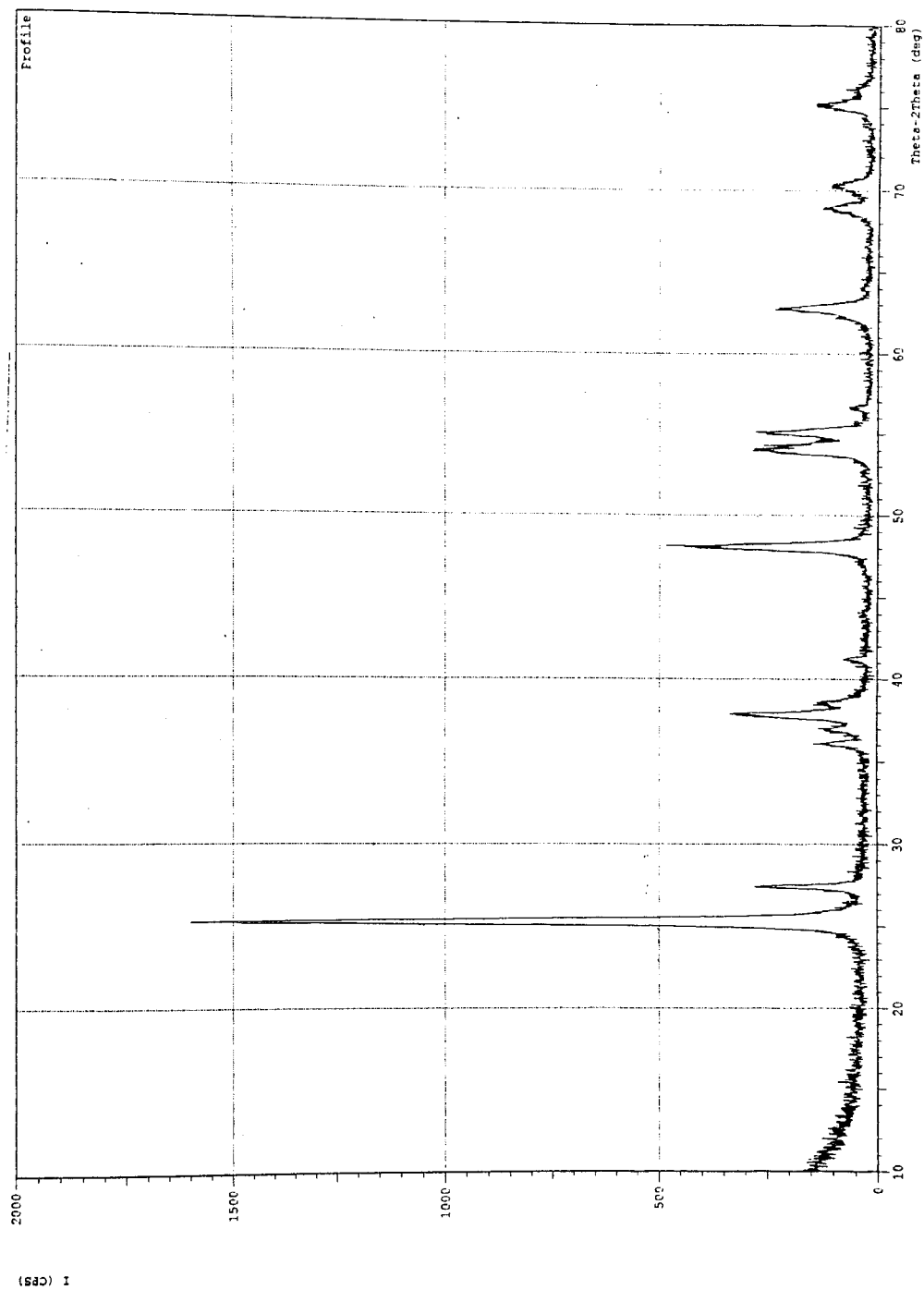Figure B.4. X-ray diffraction analysis for Cr deposited TiO$_2$ without methanol.

Figure B.5. X-ray diffraction analysis for Cr deposited TiO$_2$ with methanol.
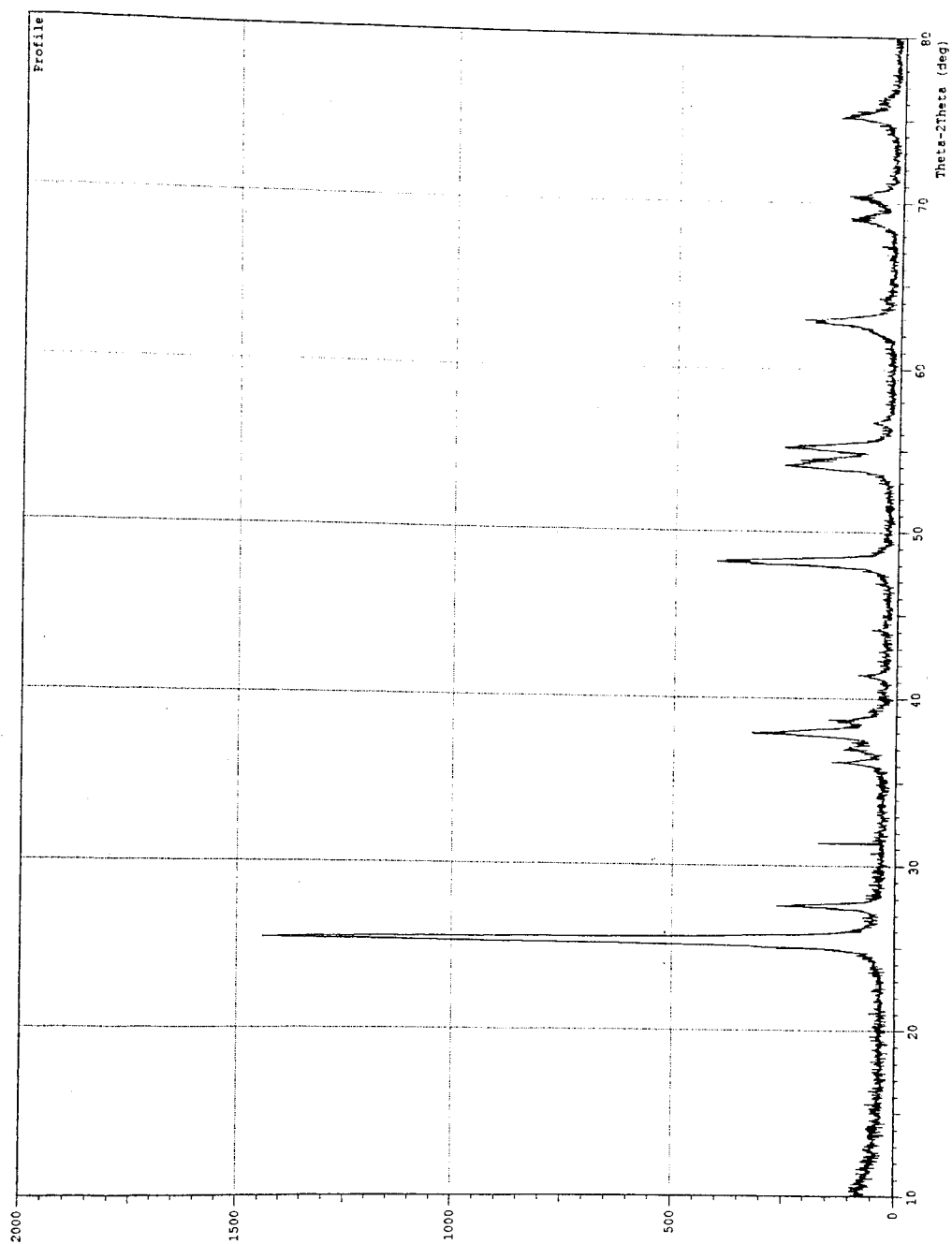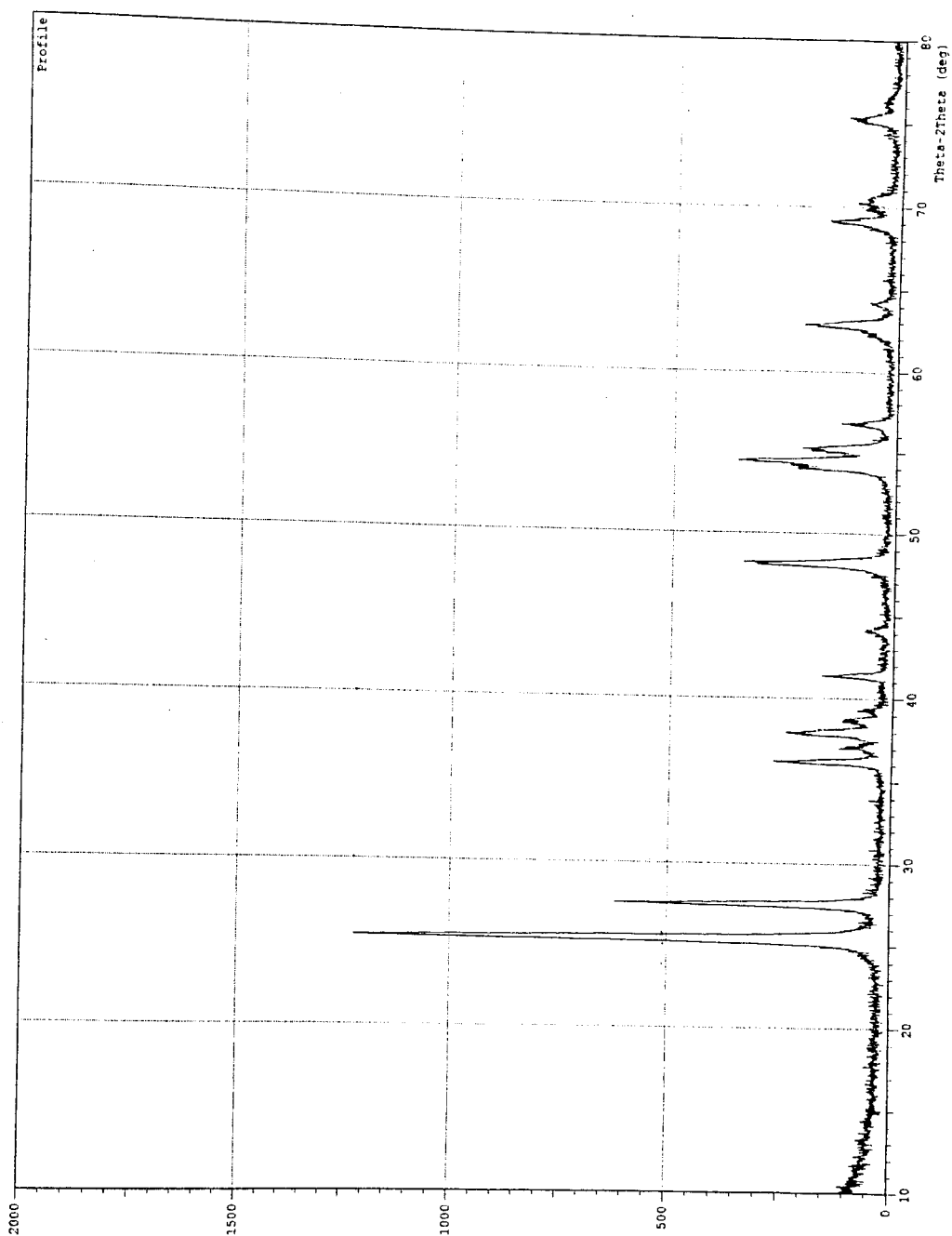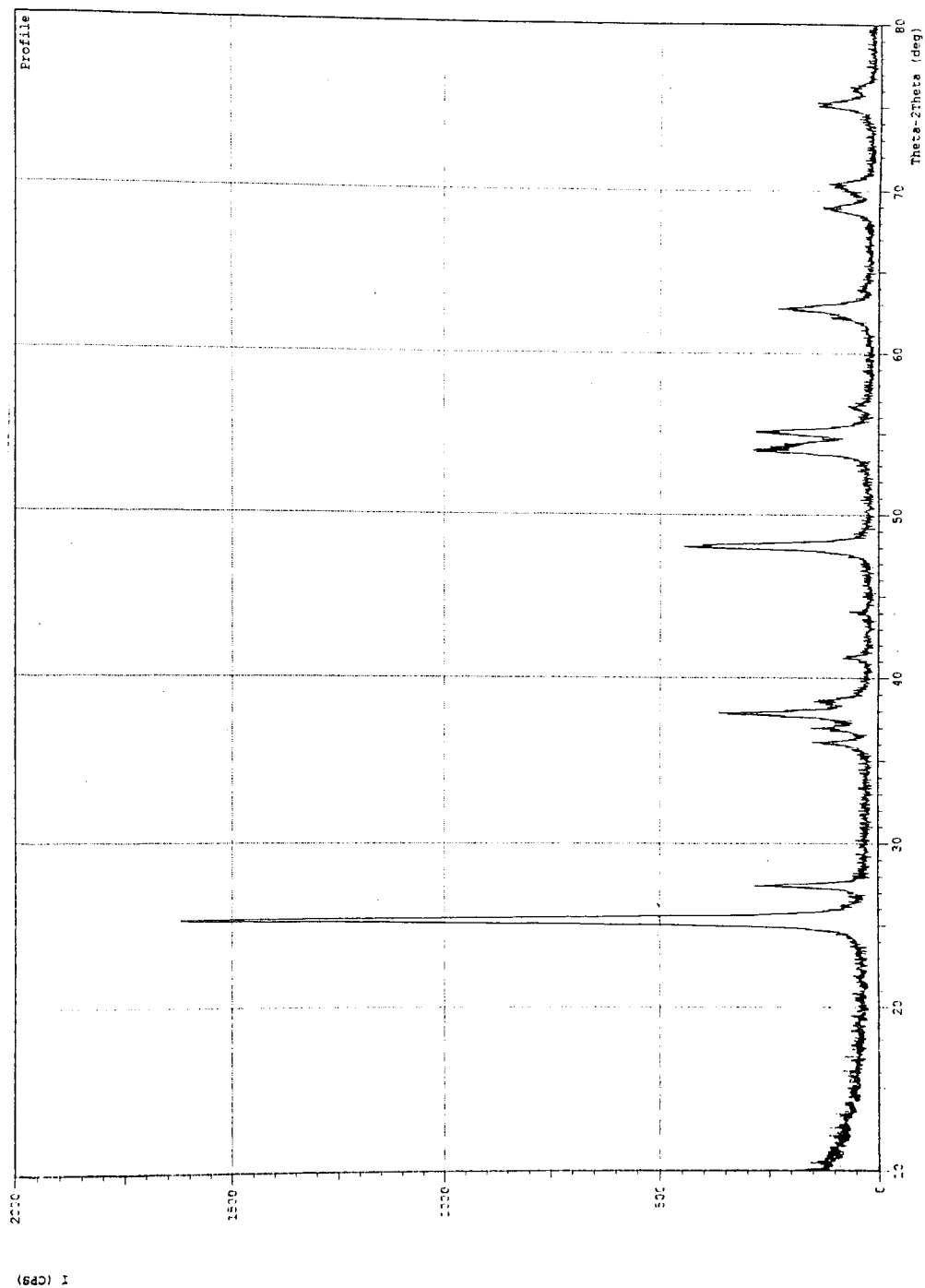
Figure B.6. X-ray diffraction analysis for Mn deposited TiO_2 without methanol.

Figure B.7. X-ray diffraction analysis for Mn deposited TiO_2 with methanol.

Figure B.8. X-ray diffraction analysis for Fe deposited TiO_2 without methanol.
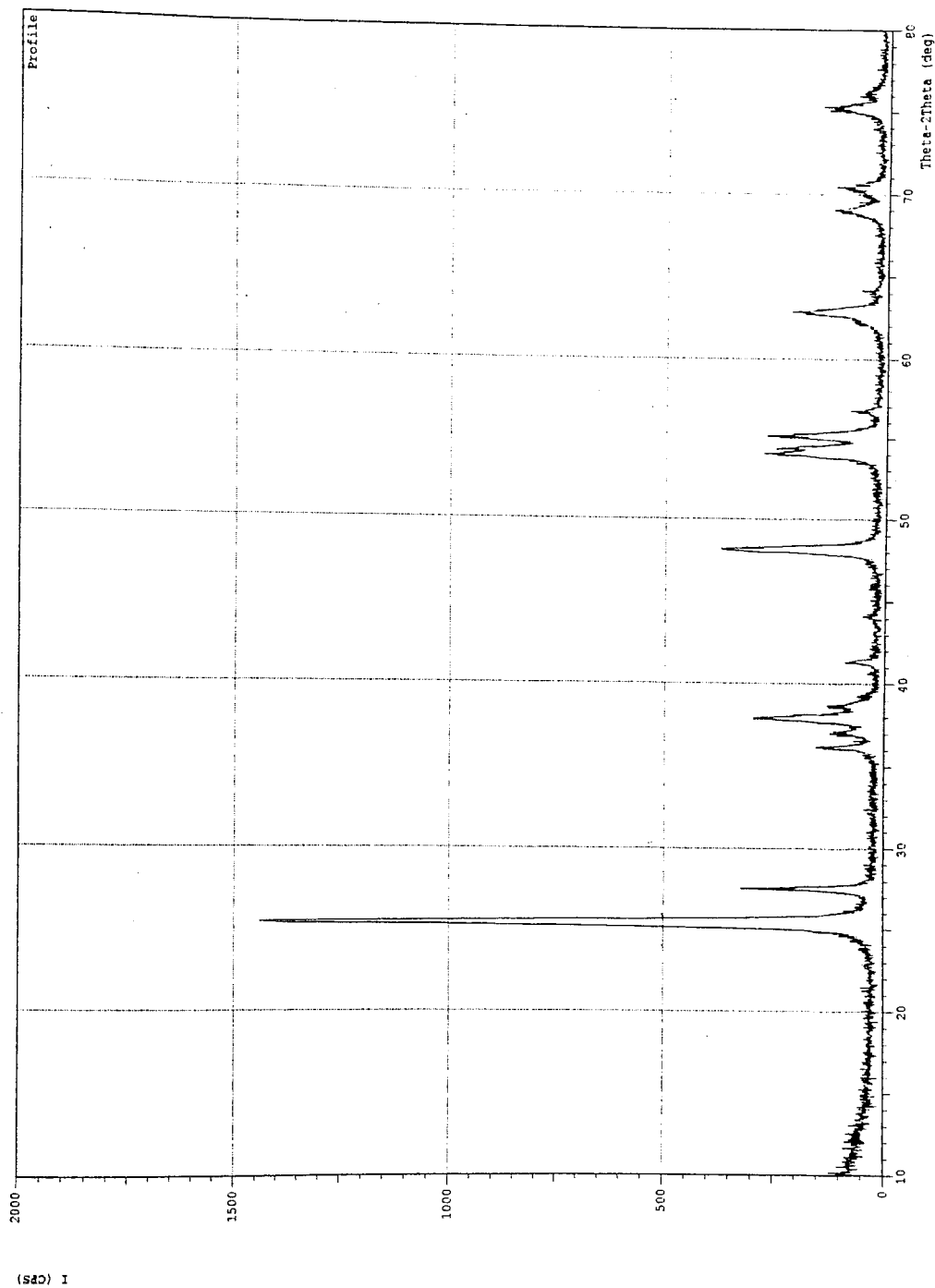
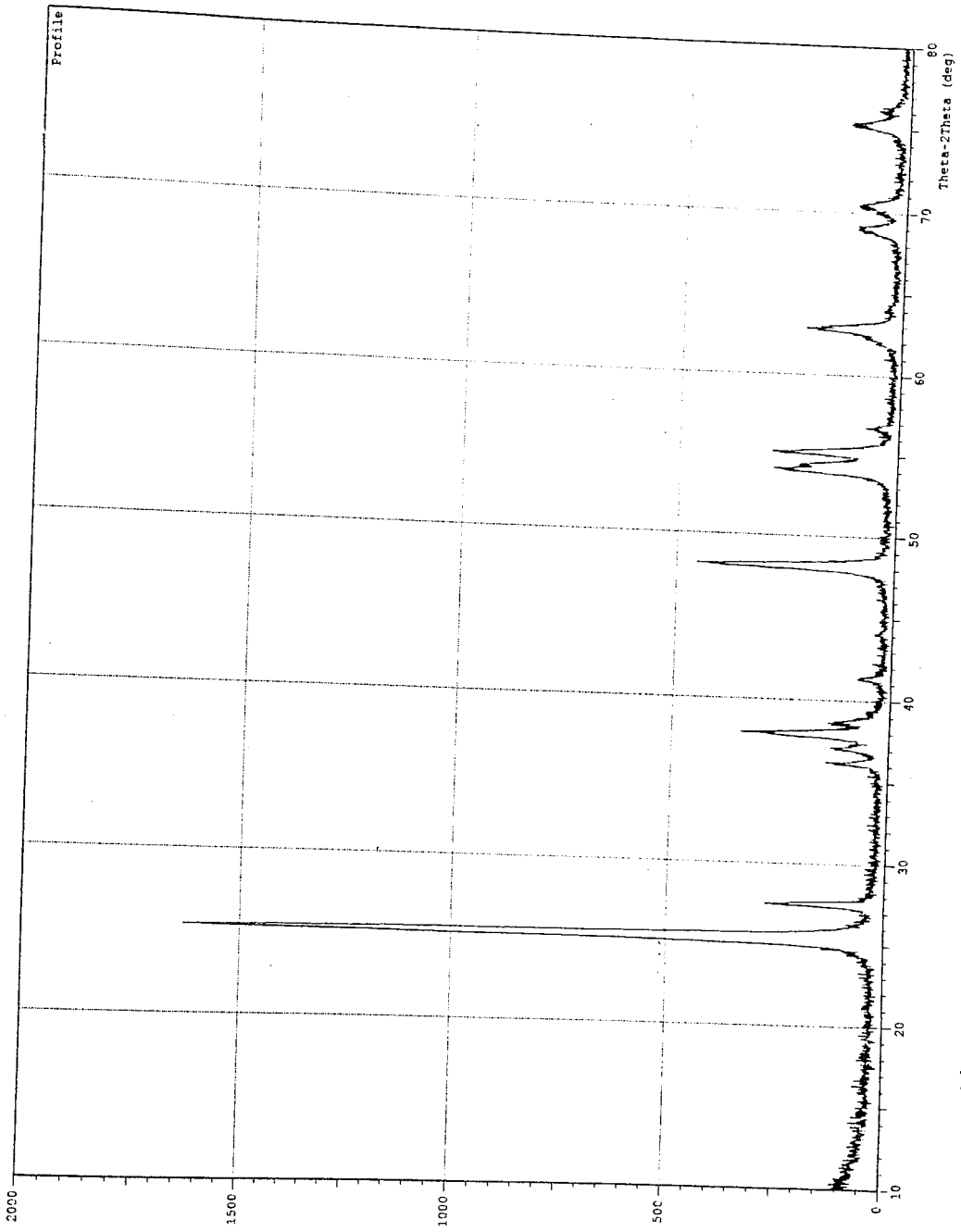Figure B.9. X-ray diffraction analysis for Fe deposited TiO_2 with methanol.

Figure B.10. X-ray diffraction analysis for Co deposited TiO₂ without methanol.
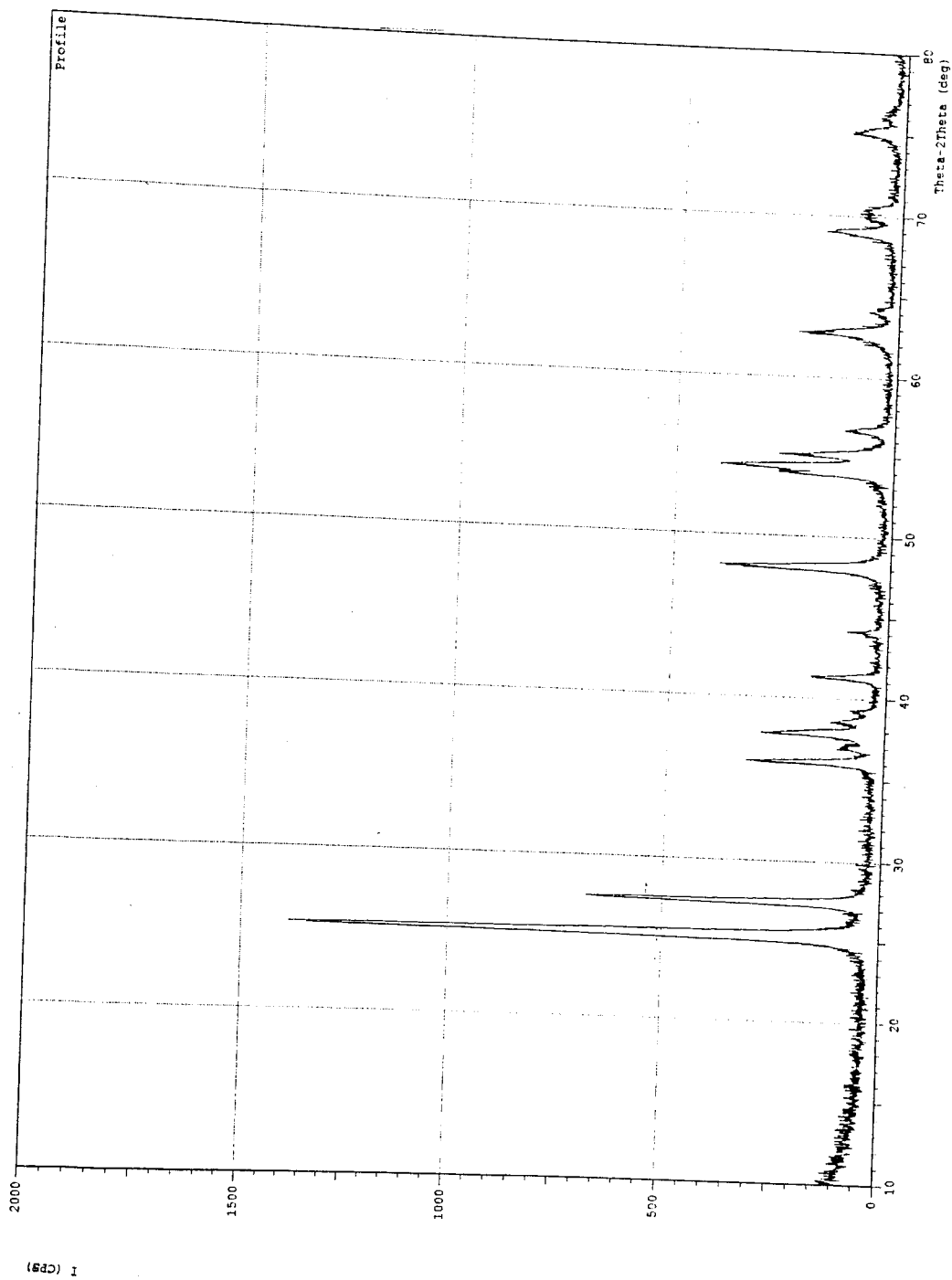
Figure B.11. X-ray diffraction analysis for Co deposited TiO$_2$ with methanol.

Figure B.12. X-ray diffraction analysis for Ni deposited TiO_2 without methanol.

Figure B.13. X-ray diffraction analysis for Ni deposited TiO_2 with methanol.

Figure B.14. X-ray diffraction analysis for Zn deposited TiO$_2$ without methanol.

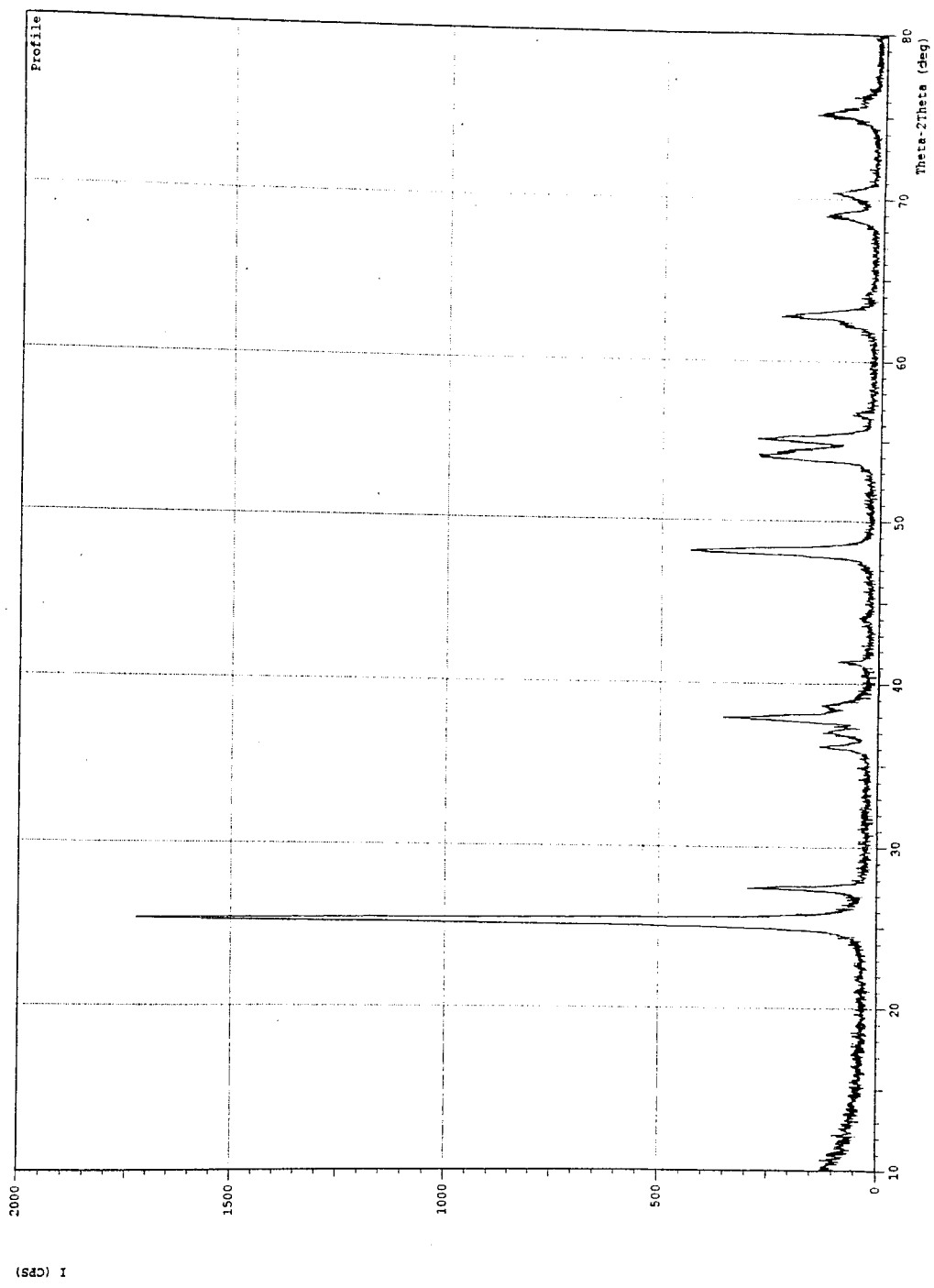Figure B.15. X-ray diffraction analysis for Zn deposited TiO$_2$ with methanol.

Figure B.16. X-ray diffraction analysis for Nb deposited TiO$_2$ without methanol.
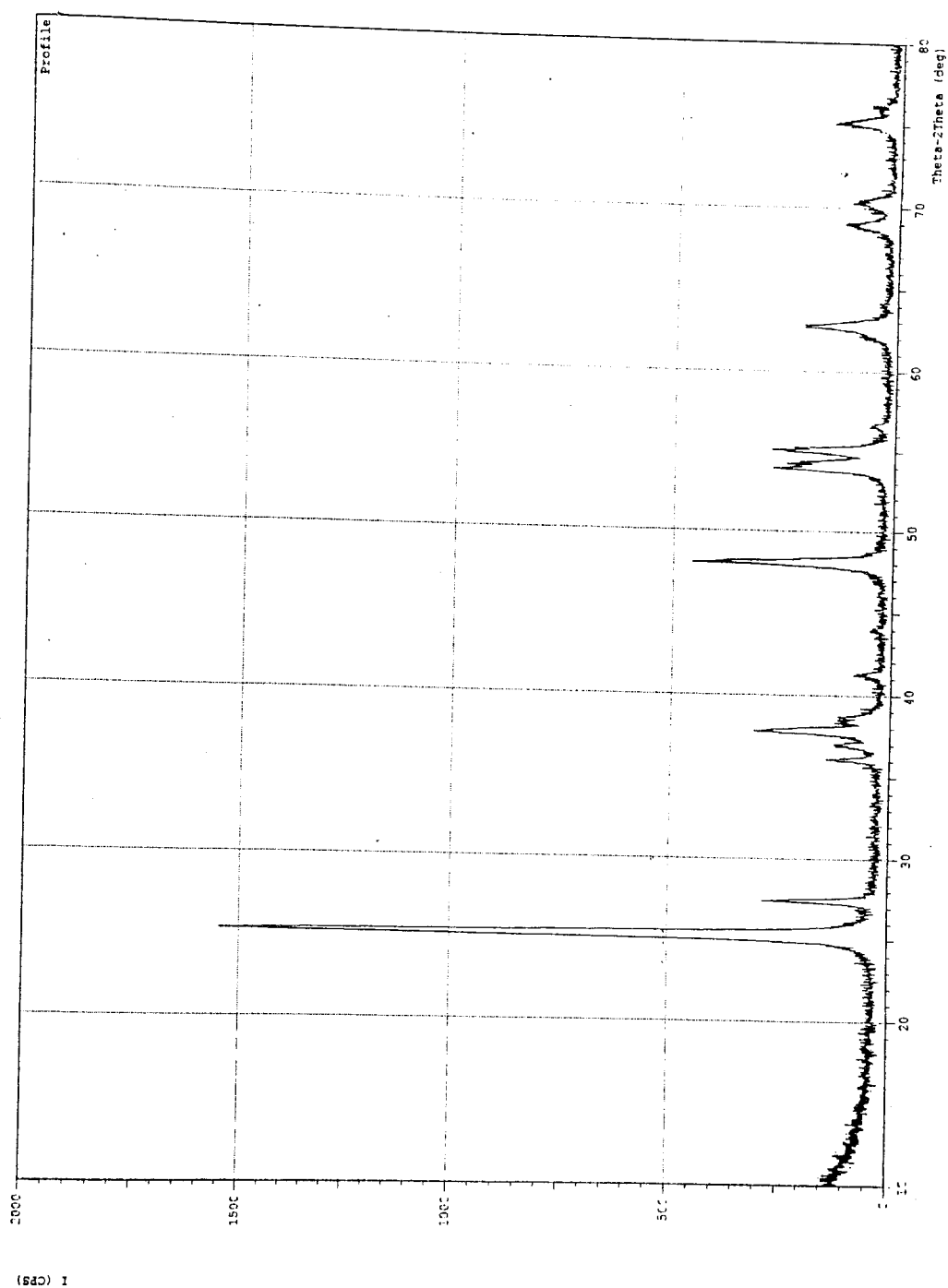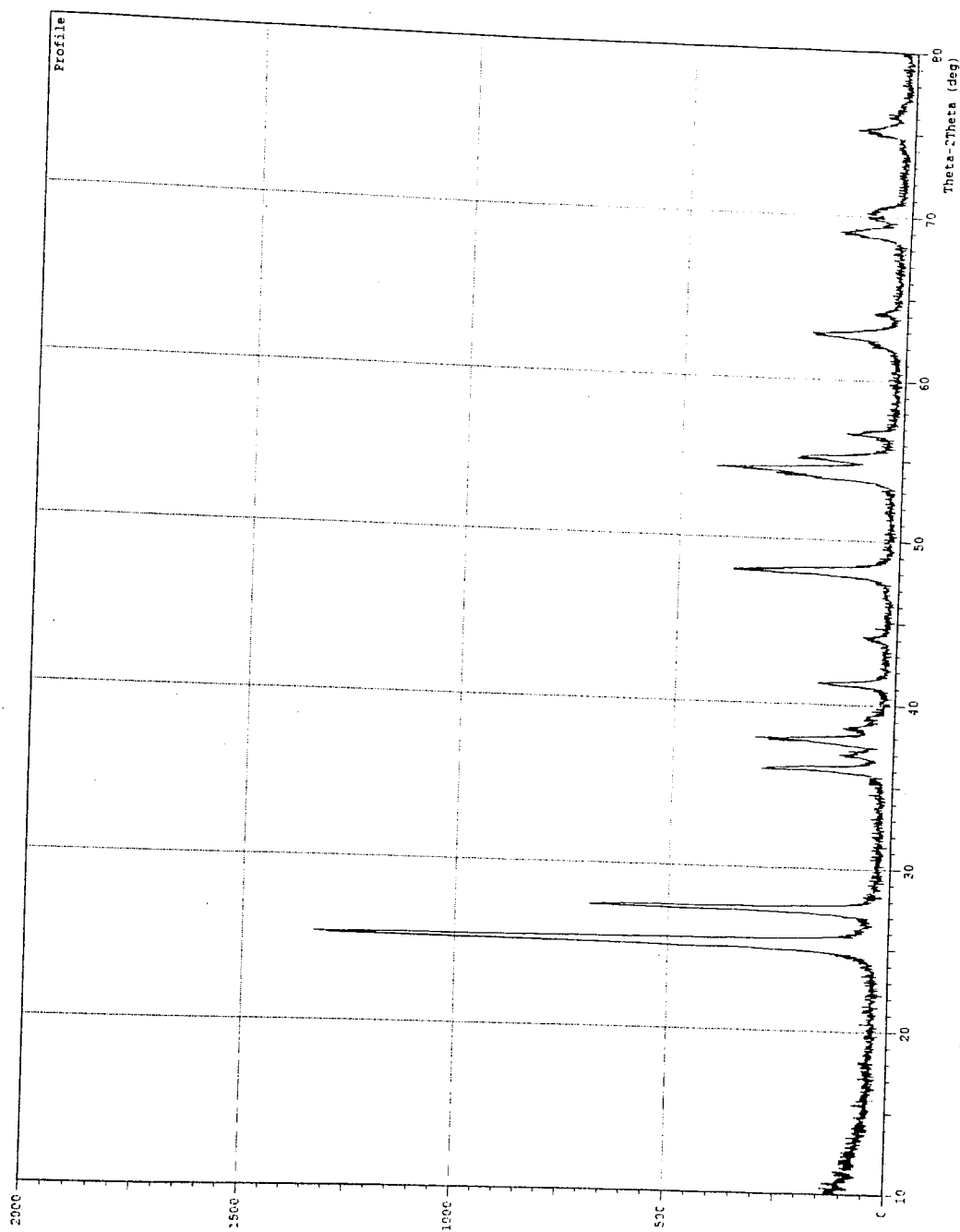
Figure B.17. X-ray diffraction analysis for Nb deposited TiO$_2$ with methanol.
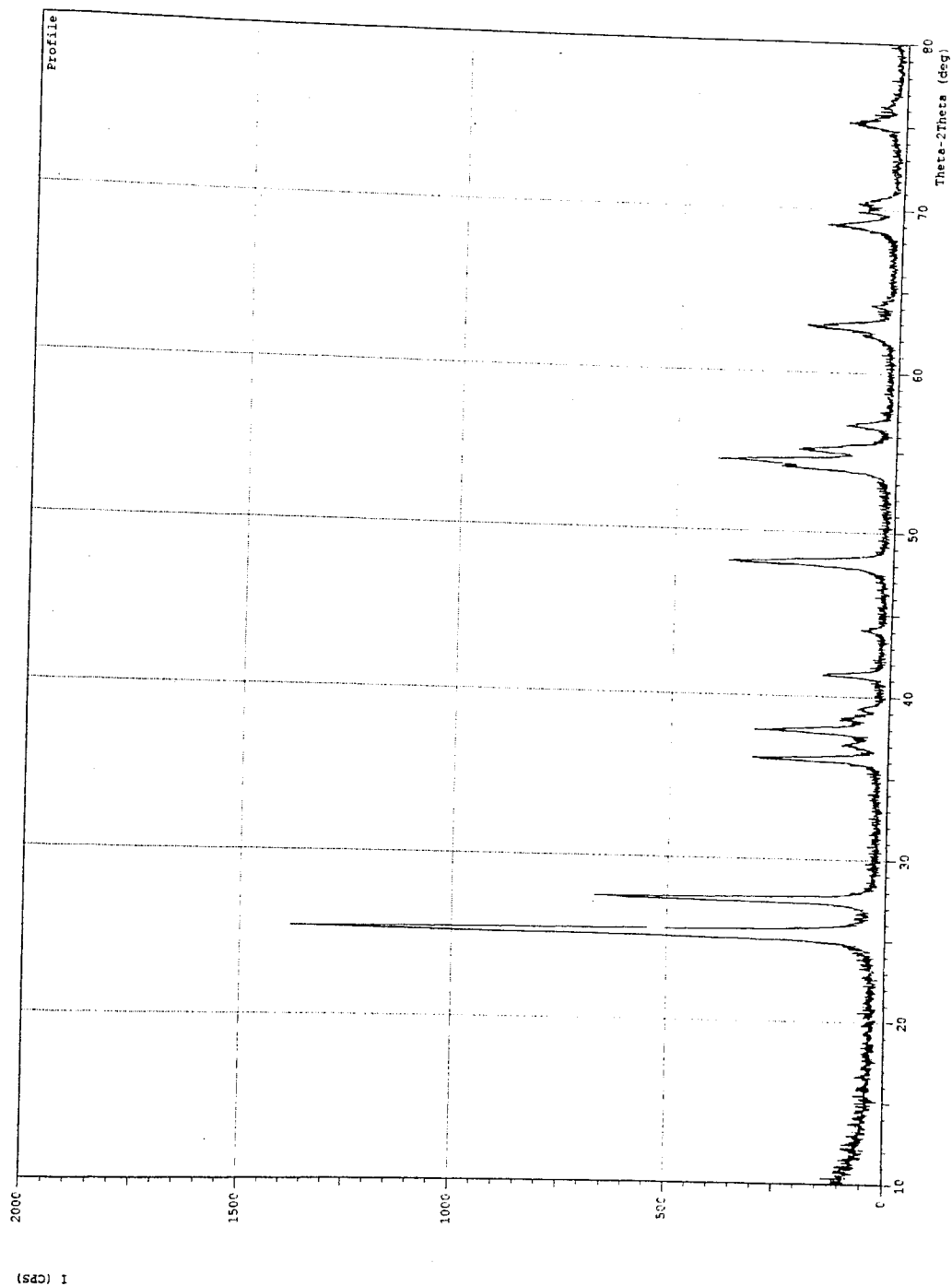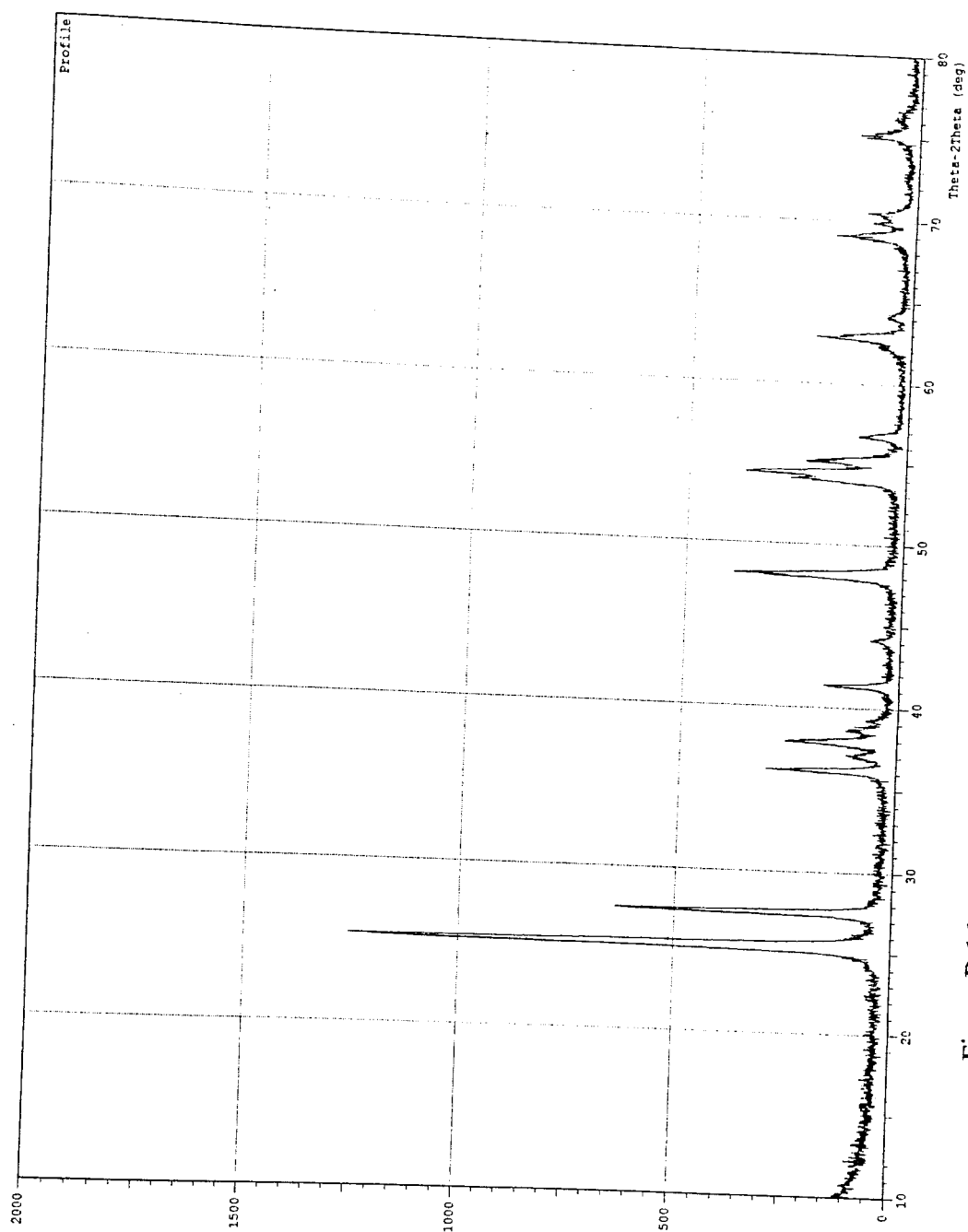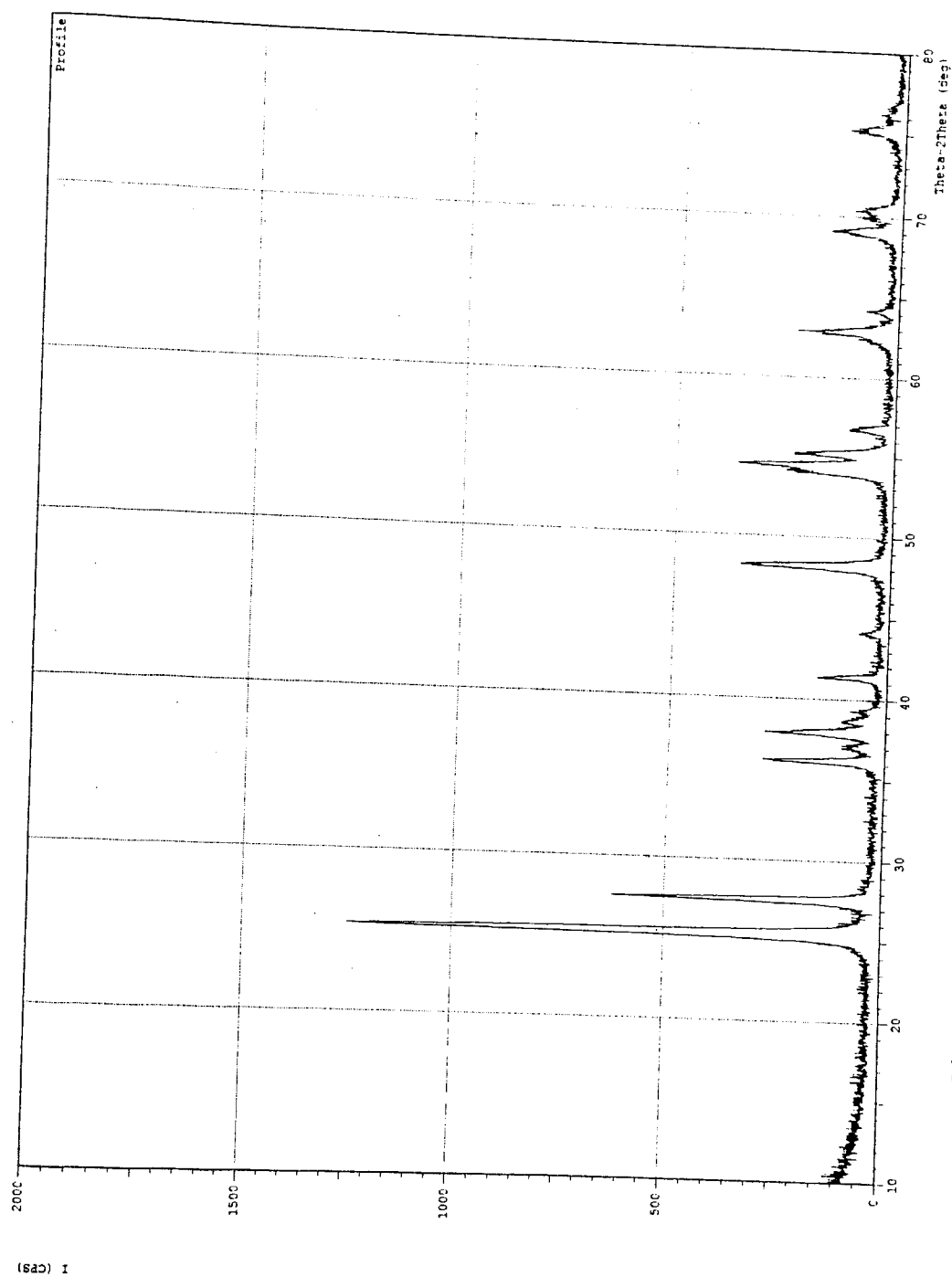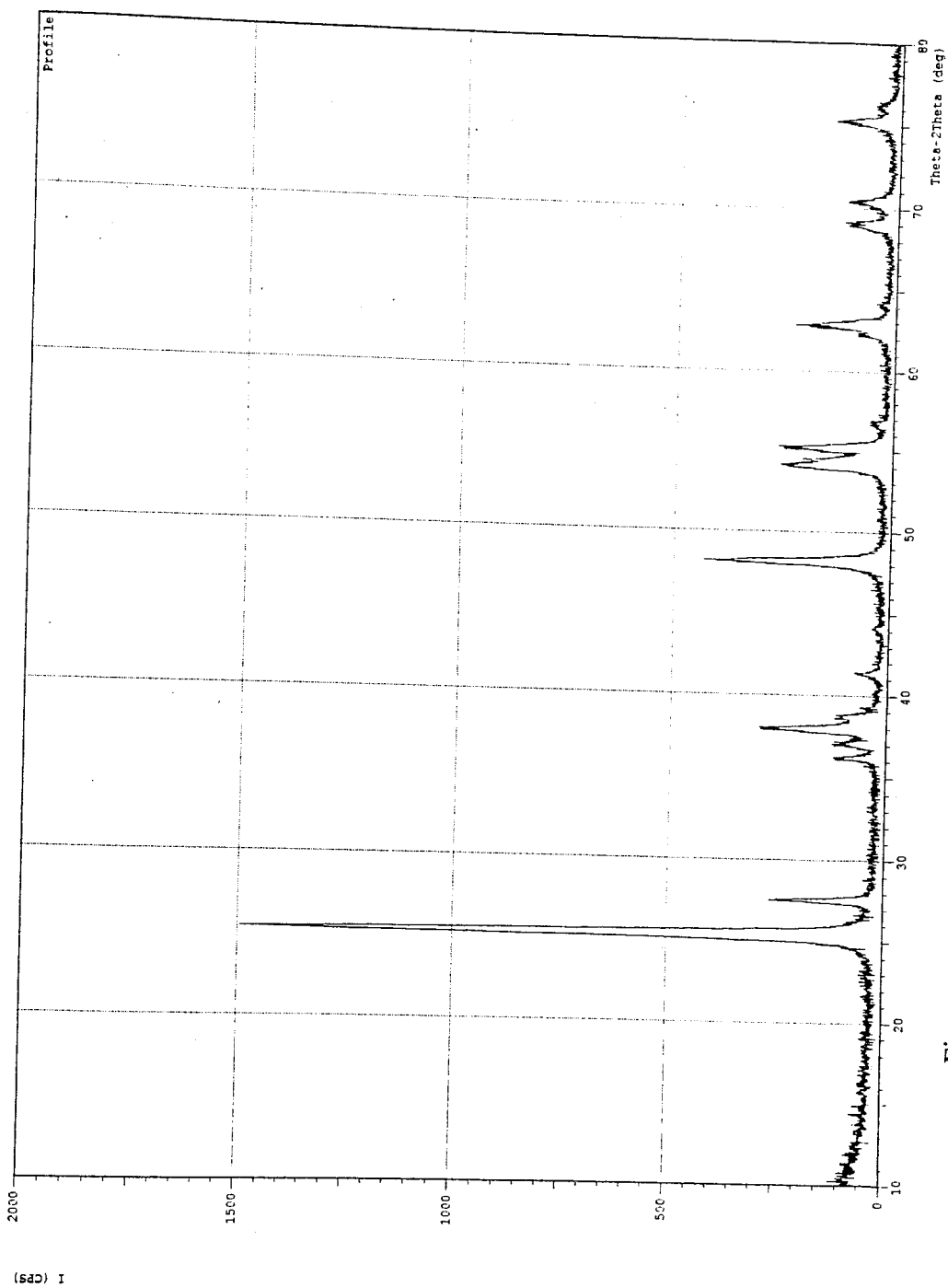
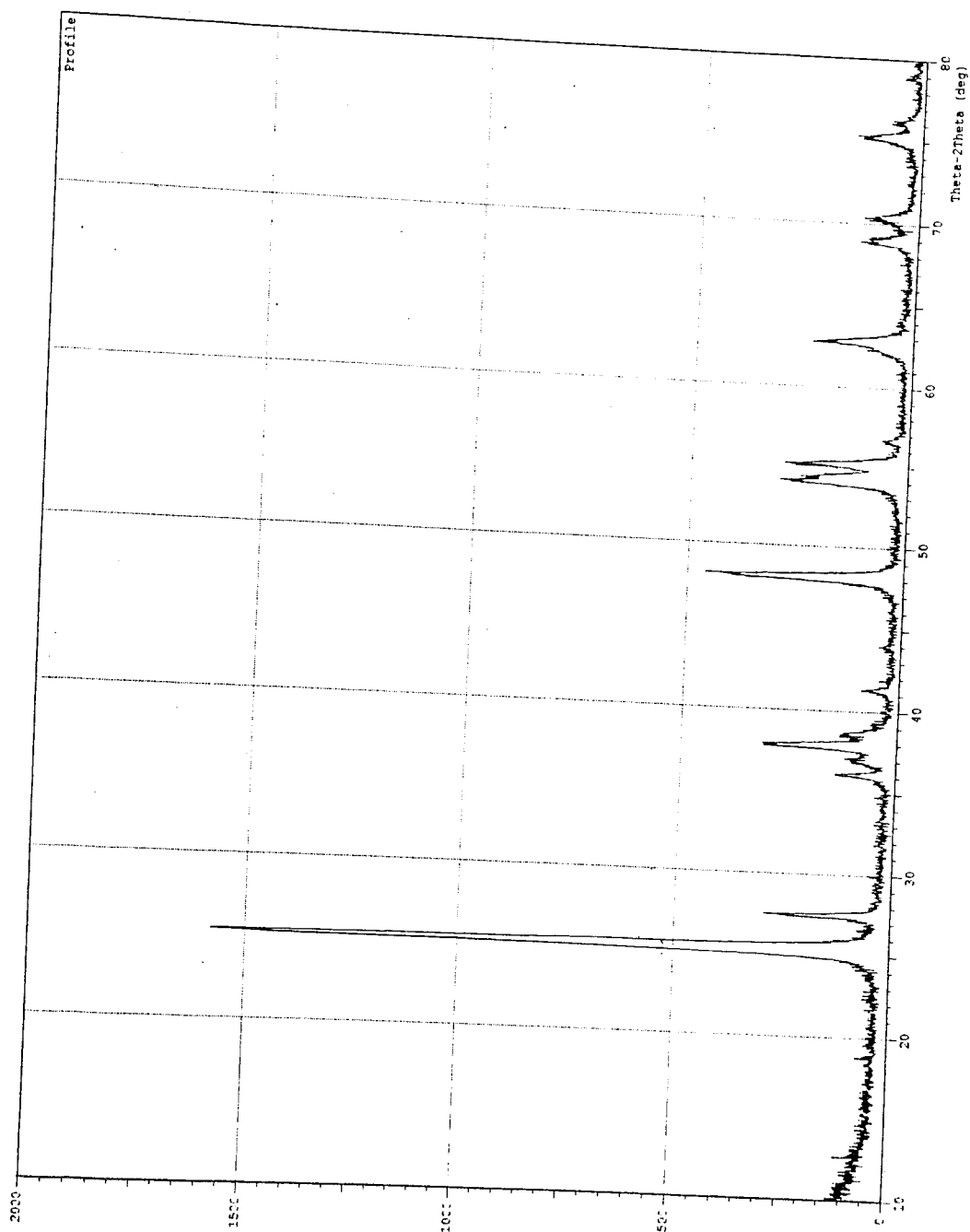Figure B.18. X-ray diffraction analysis for Ta deposited TiO$_2$ without methanol.

Figure B.19. X-ray diffraction analysis for Ta deposited TiO$_2$ with methanol.

REFERENCES

1. Ollis, D. F., and H. Al-Ekabi (editors), *Photocatalytic Purification and Treatment of Water and Air*, Elsevier, Amsterdam, 1993.

2. Fox, M. A. and T. Dulay, "Heterogenous Phtocatalysis," *Chemical Review*, Vol. 93, pp. 341-357, 1993.

3. Legrini, O., Oliveros, E., and A. M. Braun, "Photochemical Processes For Water Treatment," *Chemical Review*, Vol. 93, pp. 671-698, 1993.

4. Hoffman, M. R., Martin, S. T., Choi, W., and D. W. Bahnemann, "Environmental Applications of Semiconductor Photocatalysis," *Chemical Review*, Vol. 95, pp. 69-96, 1995.

5. Mills, A., and S. Le Hunte, "An Overview of Semiconductor Photocatalysis," *Journal of Photochemistry and Photobiology A: Chemistry*, Vol. 108, pp. 1-35, 1997.

6. Castrantas, H. M., and R. D. Gibilisco, "UV Destruction of Phenolic Compounds under Alkaline Conditions," *ACS Symposium Series*, Vol. 422, pp. 77-79, 1990.

7. Lipczynska-Kochany, E., and J. R. Bolton, "Flash-Photolysis HPLC Applications. 2. Direct Photolysis versus Hydrogen-Peroxide Mediated Photodegradation of 4-

Chlorophenol as Studied by a Flash-Photolysis HPLC Technique," *Environmental Science and Technology*, Vol. 26, pp. 259-262, 1992.

8. Peyton, G. R., and W. H. Glaze, "Destruction of Pollutants in Water with Ozone in Combination with Ultraviolet Radiation. 3. Photolysis of Aqueous Ozone," *Environmental Science and Technology*, Vol. 22, pp. 761-767, 1988.

9. Gurol, M. D., and R. Vatistas, "Oxidation of Phenolic-Compounds by Ozone and Ozone-UV-Radiation A Comparative-Study," *Water Research*, Vol. 21, pp. 895-900, 1987.

10. Takahashi, N., "Ozonation of Several Organic-Compounds Having Low Molecular-Weight Under Ultraviolet-Irradiation," *Ozone-Science and Engineering*, Vol. 12, pp. 1-18, 1990.

11. Ollis, D. F., Pelizetti, E., N. Serpone (editors), *Heterogeneous Photocatalysis in the Environment: Application to Water Purification*, New York: John Wiley, 1989.

12. Boehm, H. P., "Acidic and Basic Properties of Hydroxylated Metal Oxide Surfaces," *Faraday Society*, Vol. 52, pp. 264-275, 1971.

13. Bard, A. J., "Photoelectrochemistry and Heterogenous Photocatalysis at Semiconductors," *Journal of Photochemistry*, Vol. 10, pp. 59-75, 1979.

14. Moser, J., Gratzel, M., and R. Gallay, "Inhibition of Electron-Hole Recombination in Substitutionally Doped Colloidal Semiconductor Crystallites," *Helvetica Chimica Acta*, Vol. 70, pp. 1596-1604, 1987.

15. Rosenberg, I., Brock, J. R., and A. Heller, "Collection Optics of TiO_2 Photocatalyst on Hollow Glass Microbeads Floating on Oil Slicks," *Journal of Physical Chemistry*, Vol. 96, pp. 3423-3428, 1992.

16. Serpone, N., "Relative Photonic Efficiencies and Quantum Yields in Heterogeneous Photocatalysis," *Journal of Advanced Oxidation Technology*, Vol. 2, pp. 203-216, 1997.

17. Serpone, N., Sauve, G., Koch R., Tahiri H., Pichat, P., Piccinini, P,. Pelizetti, E., and H. Hidaka, "Standardization protocol of process efficiencies and activation parameters in heterogeneous photocatalysis: relative photonic efficiencies ζ_r," *Journal of Photochemistry and Photobiology A: Chemistry*, Vol. 94, pp. 191-203, 1996.

18. Borgarello, E., "Light induced Reduction of Rh(III), Pd(II), on TiO_2 Dispersions and Selective Photochemical Separation and Recovery of Au(III), Pt(IV), and Rh(III) in Chloride Media," *Inorganic Chemistry*, Vol. 25, pp. 4499-4503, 1986.

19. Abdullah, M., Low, K. C., and R. W. Matthews, "Effects of Common Inorganic Anions on Rates of Photocatalytic Oxidation of Organic Carbon over Illuminated Titanium Dioxide," *Journal of Physical Chemistry*, Vol. 94, pp. 6820-6825, 1990.

20. Okamoto, K., Yamamoto, Y., Tanaka, H., Tanaka, M., and A. Itaya, "Heterogenous Photocatalytic Decomposition of Phenol over TiO_2 Powder," *Bulletin Chemical Society Japan*, Vol. 58, pp. 2015-2023, 1985.

21. Okamoto, K., Yamamoto, Y., Tanaka, H., and A. Itaya, "Kinetcs of Heterogenous Photocatalytic Decomposition of Phenol over Anatase TiO_2 Powder," *Bulletin Chemical Society Japan*, Vol.58, pp. 2023-2028, 1985.

22. Matthevs, R. W., "An Adsorption Water Purifier with in Situ Photocatalytic Regeneration," *Journal of Catalysis*, Vol. 113, pp. 549-555, 1988.

23. Matthews, R. W., and S. R. McEvoy, "Photocatalytic Degradation of Phenol in the Presence of Near-UV Illuminated Titanium Dioxide," *Journal of Photochemistry and Photobiology A: Chemistry*, Vol. 64, pp. 231-246, 1992.

24. Trillas, M., Peral, J., and X. Domenech, "Photocatalyzed Degradation of Phenol, 2, 4-Dichlorophenol, Phenoxyacetic Acid Over Supported TiO_2 in a Flow System," *Journal of Chemical Technology and Biotechnology*, Vol. 67, pp.237-242, 1996.

25. Byrne, J. A., Eggins, B. R., Brown, N. M. D., McKinney, B., and M. Rouse, "Immobilisation of TiO_2 powder For the Treatment of Pollluted Water," *Applied Catalysis B: Environmental*, Vol. 17, pp. 25-36, 1998.

26. Auguliaro, V., Davi, E., Palmisano, L., Schiavello, M., and A. Sclafani, "Influence of Hydrogen Peroxide on the Kinetics of Phenol Photodegradation in Aqueous Titanium Dioxide Dispersion," *Applied Catalysis*, Vol. 65, pp. 101-116, 1990.

27. Wei, T. Y., and C. C. Wan, "Kinetics of Photocatalytic Oxidation of Phenol on TiO_2 Surface," *Journal of Photochemistry and Photobiology A: Chemistry*, Vol. 69, pp. 241-249, 1992.

28. Wei, T. Y., Wang, Y. Y., and C. C. Wan, "Photocatalytic Oxidation of Phenol In the Presence of Hydrogen Peroxide and Titanium Dioxide Particles," *Journal of Photochemistry and Photobiology A:Chemistry*, Vol. 55, pp. 115-126, 1990.

29. Wei, T. Y., and C. C. Wan, "Heterogeneous Photocatalytic Oxidation of Phenol with Titanium Dioxide Powders," *Industrial Engineering Chemical Research*, Vol. 30, pp. 1293-1300, 1991.

30. Sclafani, A., Palmisano, L., and E. Davi, "Photocatalytic Degradation of Phenol in Aqueous Polycrystalline TiO_2 Dispersions: The Influence of Fe^{3+}, Fe^{2+} and Ag^+ on the Reaction Rate," *Journal of Photochemistry and Photobiology A: Chemistry*, Vol. 56, pp. 113-123, 1991.

31. Trillas, M., Pujol, M., and X. Domenech, "Phenol Photodegradation over Titanium Dioxide," *Journal of Chemical Technology and Biotechnology*, Vol. 55, pp. 85-90, 1992.

32. Palmisano, L., Schiavello, M., Sclafani, A., Martra, G., Borello, E., and S. Coluccia, "Photocatalytic Oxidation of Phenol on TiO_2 Powders. A Fourier Transform Infrared Study," *Applied Catalysis B: Environmental*, Vol. 3, pp. 117-132, 1994.

33. Al-Sayyed, G., D'Oliveria, J. C., and P. Pichat, "Semiconductor Sensitized Photodegradation of 4-Chlorophenol in Water," *Journal of Photochemistry and Photobiology A: Chemistry*, Vol. 58, pp. 99-114, 1991.

34. Mills, A., and S. Morris, "Photomineralization of 4-Chlorophenol Sensitized by Titanium Dioxide: A Study of the Initial Kinetics of CO_2 Photogeneration," *Journal of Photochemistry and Photobiology A: Chemistry*, Vol. 71, pp. 75-83, 1993.

35. Akmehmet Balcıoğlu, I., and Y. İnel, "Photocatalytic Degradation of 4-Chlorophenol in Aqueous TiO_2 Suspensions: The Influence of H_2O_2 on the Photocatalytic Mineralization Rate," *Doğa-Turkish Journal of Chemistry*, Vol. 17, pp. 125-132, 1993.

36. Mills, A., Morris, S., and R. Davies, "Photomineralization of 4-Chlorophenol Sensitized by Titanium Dioxide: A Study of Intermediates," *Journal of Photochemistry and Photobiology A: Chemistry*, Vol. 70, pp. 183-191, 1993.

37. Mills, A., and S. Morris, "Photomineralization of 4-Chlorophenol Sensitized by Titanium Dioxide: A Study of the Effect of Annealing The Photocatalyst At Different Temperatures," *Journal of Photochemistry and Photobiology A: Chemistry*, Vol. 71, pp. 285-289, 1993.

38. Akmehmet Balcıoğlu, I., and Y. İnel, "Photocatalytic Degradation of Organic Contaminants in Semiconductor Suspensions with added H_2O_2," *Journal of Environmental Science and Health*, Vol. A31 (1), pp. 123-138, 1996.

39. Stafford, U., Gray, K., and P. Kamat, "Photocatalytic Degradation of 4-Chlorophenol: The Effects of Varying TiO₂ Concentration and Light Wavelength," *Journal of Catalysis*, Vol. 167, pp. 25-32, 1997.

40. D'Oliveira, J. C., Al-Sayyed, G., and P. Pichat, "Photodegradation of 2- and 3-Chlorophenol in TiO₂ Aquequs Suspensions," *Environmental Science and Technology*, Vol. 24, pp. 990-996, 1990.

41. Matthews, R. W., "Purification of Water with Near-UV Illuminated Suspensions of Titanium Dioxide," *Water Research*, Vol. 24, No. 5, pp. 653-660, 1990.

42. Barbeni, M., Pramauro, E., Pelizetti, E., Borgarello, E., and N. Serpone, "Photodegradation of Pentachlorophenol Catalyzed By Semiconductor Particles," *Chemosphere*, Vol. 14, No. 2, pp. 195-208, 1985.

43. Matthews, R. W., "Photooxidation of Organic Material In Aqueous Suspensions of TiO₂," *Water Research*, Vol. 20, No. 5, pp. 569-578, 1986.

44. Matthews, R. W., "Photooxidation of Organic Impurities in Water Using Thin Films of Titanium Dioxide," *Journal of Physical Chemistry*, Vol. 91, pp. 3328-3333, 1987.

45. Matthews, R. W., "Kinetics of Photocatalytic Oxidation of Organic Solutes over Titanium Dioxide," *Journal of Catalysis*, Vol. 111, pp. 264-272, 1988.

46. Guardia, M., Khalaf, K. D., Hasan, B. A., Rubio, A., and V. Carbonell, "In-Line, Titanium Dioxide Catalysed, Ultraviolet Mineralization of Toxic Aromatic Compounds in the Waste Stream From a Flow Injection Based Resorcinol," *Analyst*, Vol.120, pp. 231-235, 1995.

47. Guardia Othmer, D. F., *Encyclopedia of Chemical Technology*, New York: John Wiley, 1984.

48. İnel, Y., and A. N. Ökte, "Photocatalytic Degradation of Malonic Acid in Aqueous Suspensions of Titanium Dioxide: An Initial Kinetic Investigation of CO_2 Photogeneration," *Journal of Photochemistry and Photobiology A: Chemistry*, Vol. 96, pp. 175-180, 1996.

49. Ökte, A. N., "Photocatalytic Degradation of Phthalic Anhydride and Dicarboxylic Acids," MS. Thesis, Boğaziçi University, 1994.

50. Ertek, D., "Heterogeneous Photocatalytic Elimination of Metal Ions," Ph.D. Dissertation, Boğaziçi University, 1989.

51. Deljouie, P., "Heterogeneous Photocatalytic Activity of Transition-Metal Cation Impregnated TiO_2," MS. Thesis, Boğaziçi University, 1993.

52. Butler, N. J. and D. R. Cogley (editors), *Ionic Equilibrium Solubility and pH Calculations*, New York: John Wiley, 1998.

53. Sun, L., and J. R. Bolton, "Determination of the Quantum Yield for the Photochemical Generation of Hydroxyl Radicals in TiO_2 Suspensions," *Journal of Physical Chemistry*, Vol. 100, pp. 4127-4134, 1996.

54. Calvert, J. G., and J. N. Pitts, *Photochemistry*, New York: John Wiley, 1966.

55. Martin ,S. T., Morrison, C. L., and M. R. Hoffmann, "Photochemical Mechanism of Size-Quantized Vanadium-Doped TiO_2 Particles," *Journal of Physical Chemistry*, Vol. 98, pp. 13695-13704, 1994.

56. Choi,W., Termin, A., and M. R. Hoffmann,"Effects of Metal-Ion Dopants on the Photocatalytic Reactivity in Quantum-Sized TiO_2 Particles," *Angewandte Chemie International Edition In English*, Vol. 1994, No. 10, pp. 1091-1092, 1994.

57. Cotton, A., Wilkinson, G. and P. Gaus (editors), *Basic Inorganic Chemistry*, New York: John Wiley, 1995.

58. Cotton, A., and G. Wilkinson (editors), *Advanced Inorganic Chemistry A Comprehensive Text*, New York: John Wiley, 1972.

59. Atkins, P. W., *Physical Chemistry*, Oxford, Oxford University Press, 1994.

60. Litter, M. I., and J. A. Navio, "Photocatalytic Droperties of Iron-Doped Titania Semiconductors," *Journal of Photochemistry and Photobiology A:Chemistry*, Vol. 98, pp. 171-181, 1996.

61. Palmisano, L., Augugliaro, V., Sclafani, A., and M. Schiavello, "Activity of Chromium-Ion-Doped Tiatnia for the Dinitrogen Photoreduction to Ammonia and for the Phenol Photodegradation," *Journal of Physical Chemistry*, Vol. 92, pp. 6710-6713, 1988.

62. Martin ,S. T., Morrison, C. L., and M. R. Hoffmann, "Photochemical Mechanism of Size-Quantized Vanadium-Doped TiO_2 Particles," *Journal of Physical Chemistry*, Vol. 98, pp. 13695-13704, 1994.

63. Mizushima, K., Tanaka, M., and S. Iida, "Energy Levels of Iron Group Impurities in TiO_2," *Journal of The Physical Society of Japan*, Vol. 32, No. 6, pp. 1519-1524, 1972.

64. Mizushima, K., Tanaka, M.,A., Asai, Iida, S.,and J. B. Goodenough, "Impurity Levels of Iron-Group Ions in TiO_2 II," *Journal of Physical Chemistry of Solids*, Vol. 40, pp.1129-1140, 1979.